Méthode de modélisation et de commande des systèmes de positionnement multi-actionnés de type axe en Gantry

Ivan Mauricio Garciaherreros

2012–ENAM–0015

École doctorale n° 432 : Sciences et Métiers de l'Ingénieur

Doctorat ParisTech

T H È S E

pour obtenir le grade de docteur délivré par

l'École Nationale Supérieure d'Arts et Métiers

Spécialité " Automatique "

présentée et soutenue publiquement par

Iván Mauricio GARCÍA–HERREROS LANDAZÁBAL

le 23 mai 2012

Méthode de Modélisation et de Commande des Systèmes de Positionnement Multi-actionnés de Type Axe en Gantry

Directeur de thèse : **Pierre-Jean BARRE**
Co-encadrement de la thèse : **Xavier KESTELYN**

Jury

M. Pascal RAY, Professeur, IFMA, Institut Français de Mécanique Avancée	Président
M. Pierre SICARD, Professeur, GÉGI, Université du Québec à Trois Rivières	Rapporteur
M. Nacer M'SIRDI, Professeur, LSIS, Ecole Polytechnique Universitaire de Marseille	Rapporteur
M. Gabriel ABBA, Professeur, LCFC, Ecole National d'Ingénieurs de Metz	Examinateur
M. Pierre-Jean BARRE, Professeur, LSIS, Arts et Métiers ParisTech	Examinateur
M. Xavier KESTELYN, Maître de Conférences, L2EP, Arts et Métiers ParisTech	Examinateur
M. Ralph COLEMAN, Ingénieur, Senior Researcher, ETEL	Invité
M. Samir BOUABDALLAH, Docteur, Research Manager, ETEL	Invité

T H È S E

Arts et Métiers ParisTech - Centre de Lille
Laboratoire d'Electrotechnique et d'Electronique de Puissance de Lille (L2EP)

Remerciements

Ce travail a été réalisé au sein de l'équipe commande de Laboratoire d'Electronique et Electronique de Puissance de Lille (L2EP) en collaboration avec la société ETEL SA (Convention CIFRE)

Je tiens à remercier Monsieur le professeur Pascal RAY d'avoir accepté de présider mon jury de thèse. Je remercie également le professeur Gabriel ABBA d'avoir accepté de participer au jury de thèse en qualité d'examinateur.

Je souhaiterai remercier ensuite les professeurs Nacer M'SIRDI et Pierre SICARD d'avoir accepté de rapporter cette thèse ; vos observations et conseils m'ont beaucoup aidé, non-seulement pour ce document mais également au niveau professionnel. Je remercie également Messieurs Ralph COLEMAN et Samir BOUABDALLAH d'avoir accepté de participer au jury en tant qu'invités. J'espère que notre collaboration durera encore pour des nombreuses années.

Je tiens à remercier mon encadrant industriel, M. Ralph Coleman de la société ETEL pour m'avoir donné l'opportunité de réaliser ces travaux, pour sa disponibilité, et pour partager son expérience avec notre équipe. Je remercie également M. Denis PIAGET, directeur de la société ETEL, pour avoir rendu ce projet possible.

Je voudrais exprimer toute ma reconnaissance à mon directeur de thèse, M. Pierre-Jean BARRE, professeur à Arts et Métiers ParisTech, pour sa patience et ses conseils qui m'ont beaucoup aidé à grandir personnellement et professionnellement. Tes mots d'encouragement avant la soutenance ont été une grande source de force. Je remercie mon co-directeur de thèse, M. Xavier KESTELYN, maître de conférences à Arts et Métiers ParisTech, pour sa patience, sa disponibilité (malgré ses nombreuses occupations) et son implication totale dans ce travail. Tes conseils, ton amitié, ton objectivité et ta force m'ont poussé à aller toujours plus loin. Je remercie également Julien GOMAND, maître de conférences à Arts et Métiers ParisTech pour m'avoir accueilli et m'avoir guidé dans mes premiers pas dans le monde de la recherche. Je remercie mon encadrant de Master, M. Alain BOUSCAYROL, professeur à l'Université Lille Nord de France, qui m'a appris le sens de la rigueur scientifique et qui est resté très disponible lors du déroulement de ma thèse.

Enfin, je ne peux que remercier tous et chacun des membres de notre laboratoire ; ceux qui y sont, ceux qui sont déjà partis et ceux qui vont venir. Continuons à faire grandir notre laboratoire. Continuons à créer la bonne ambiance qui rend notre laboratoire si spécial. Continuons simplement à être fiers de faire partie de la grande famille du L2EP.

Enfin et surtout, merci à Valérie, ma compagne pour son soutien et pour m'avoir supporté pendant déjà trois ans. Je remercie également sa famille pour m'avoir accueilli comme l'un des leurs. Pour finir, je remercie ma grand-mère, Trudy, qui est partie depuis quelques temps déjà, mais qui a mis en route la série d'évènements qui m'a menée à écrire ces remerciements. Je remercie mes parents, mes frères, ma cousine Adriana, ma tante Consuelo et Joël, votre support inconditionnel m'a mené plus loin que ce que je pouvais imaginer il y a 10 ans. Merci de m'apprendre l'importance de l'honnêteté et du travail dur. Ce document est à votre honneur.

Sommaire

Liste des Figures vi

Liste des Tableaux ix

Liste de symboles / List of symbols x

Glossaire / Glossary ix

Introduction Générale 1

1. Contexte 3

1.1 Positionnement de ce projet de recherche 3

1.2 Les systèmes de positionnement dans l'industrie 6

1.3 L'axe en gantry (problématique du dispositif support de l'étude) 11

1.4 Conclusion 14

2. Etat de l'art de la commande des axes en gantry 15

2.1 Commande des axes en gantry dans la littérature 16

2.1.1 *Commande d'axes en gantry mono–actionnés* 16

2.1.2 *Commande d'axes en gantry bi–actionnés* 17

2.1.3 *Conclusion sur la commande d'axes en gantry* 21

2.2 Modélisation des axes en gantry dans la littérature 22

2.2.1 *Modélisation des axes en gantry mono–actionnés dans la littérature* 22

2.2.2 *Modélisation des axes en gantry bi–actionnés dans la littérature* 23

2.2.3 *Conclusion sur les modélisations des axes en gantry* 26

2.3 Eléments bibliographiques additionnels 27

2.4 Commande d'un axe en gantry bi–actionné rigide basée sur une modélisation physique causale (Gomand, 2008) 28

2.5 Approche proposée pour l'étude 29

3. Proposed methodology for modeling and controlling gantry stages 30

3.1 Physical modeling of gantry stages 32

3.1.1 *Analyzing gantry stages* 32

3.1.2 *Proposing a general model of the gantry stage* 35

3.1.3 *Kinematics of the gantry stage* 39

3.1.4 *Kinetics of the gantry stage* 44

3.2 Modeling the gantry stage 47

3.2.1 *Modeling hypotheses* 47

3.2.2 *Dynamic model of the gantry stage* 48

3.2.3 *Identification of the model's parameters* 56

3.3 Controlling the gantry stage 62

3.3.1 *Inversion–based control of (electro)mechanical systems using causal graphical representations* 62

3.3.2 *Causal Ordering Graph of the gantry stage* 65
3.3.3 *Energetic Macroscopic Representation of the gantry stage* 68
3.3.4 *Maximum Control Structure of the gantry stage* 72
3.3.5 *Practical Control Structure of the gantry stage* 72
3.4 Conclusion 75
4. Application of the proposed methodology to the modeling and control of gantry stage industrial systems 77
4.1 Application to « rigid » gantry stages 78
4.1.1 *Experimental set–up* (*Application Example* No.1) 78
4.1.2 *Dynamic Modeling* (*Application Example* No.1) 79
4.1.3 *Control on a decoupling basis* (*Application Example* No.1) 82
4.1.4 *Experimental set–up* (*Application Example* No.2) 91
4.1.5 *Dynamic Modeling* (*Application Example* No.2) 92
4.1.6 *Control on a decoupling basis* (*Application Example* No.2) 97
4.2 Application to a « flexible » gantry 100
4.2.1 *Experimental set–up* 100
4.2.2 *Dynamic Modeling* 101
4.2.3 *Control on a decoupling basis* 108
4.2.4 *Improving the positioning performance of the flexible gantry stage: Trajectory planning techniques* 114
4.2.5 *Comparison between the rigid and the flexible gantry* 118
4.3 Conclusion 119
5. Conclusions Générales et Perspectives 121
5.1 Synthèse des travaux réalisés et résultats marquants 121
5.2 Perspectives 121
5.2.1 *Perspectives à court terme* 125
5.2.2 *Perspectives à moyen terme* 125
Appendix A: Theoretical background 126
A.1: Euler–Bernoulli Beam Theory (EBBT) 126
A.2: Flexure of an Euler–Bernoulli Beam (Mounted in gantry) 127
A.2.1: *Dynamic Model* 127
A.2.2: *Comments on the Boundary Conditions of a beam mounted in gantry* 130
Appendix B: Closed–form solution method 132
B.1. Motion Equation of the headless gantry 132
B.2. The free–vibration problem 132
B.2.1 *Separation of variables* 132
B.2.2. *Eigenvalues, Eigenvectors and Eigenfunctions* 134

Appendix C: The Ritz method 139
C.1 Time–dependent boundary conditions 139
C.1.1 *Evaluation of the time–dependent boundary conditions of the gantry* 140
C.2 The Ritz method for a beam in flexure 140
Références Bibliographiques 143

Liste des Figures

Chapitre 1

Figure 1 – 1 : *Différents systèmes de positionnement multi–actionnés du type « axe en gantry »* 3
Figure 1 – 2 : *Eléments fondamentaux d'un système de positionnement* 6
Figure 1 – 3 : *Bloc–moteur et piston d'un moteur à combustion interne* 7
Figure 1 – 4 : *Placement de composants sur un circuit imprimé* [source : *www.enaelectronics.ca*] ... 7
Figure 1 – 5 : *Différents types de systèmes de positionnement ;* 8
Figure 1 – 6 : *Architecture du système de positionnement en série* 9
Figure 1 – 7 : *Architecture du système de positionnement en parallèle* 9
Figure 1 – 8 : *Différents systèmes de positionnement en série* 9
Figure 1 – 9 : *Différents systèmes de positionnement en parallèle* 10
Figure 1 – 10 : *Différentes structures dites « en gantry »* 11
Figure 1 – 11 : *Axe en gantry en série ou mono–actionné* (*a*); *et hybride ou bi–actionné avec liaisons rigides* (*b*) 11
Figure 1 – 12 : *Déformation de l'axe en gantry mono–actionné à cause des forces inertielles* 12
Figure 1 – 13 : *Déformation de l'axe en gantry bi–actionné avec des liaisons rigides* 12
Figure 1 – 14 : *Déformation de l'axe en gantry bi–actionné avec des liaisons flexibles* 13
Figure 1 – 15 : *Quand la poutre reliant les actionneurs est très rigide, celle–ci sert à les coupler mécaniquement.* 13
Figure 1 – 16 : *Quand la poutre reliant les actionneurs est très flexible, les actionneurs sont virtuellement découplés l'un de l'autre* (*a*). *Cependant, l'amplitude des oscillations de la poutre est importante* (*b*). 14

Chapitre 2

Figure 2 – 1 : *Modèle dynamique du gantry mono–actionné* 16
Figure 2 – 2 : *Commande maître–maître pour un gantry bi–actionné* (Tan, et al., 2004) 17
Figure 2 – 3 : *Structure de commande dans le repère fictif* $X - \Theta$ (Tanquary, et al., 2000) 18
Figure 2 – 4 : *Commande synchronisante LQR* (Chu, et al., 2004) 18
Figure 2 – 5 : *Commande synchronisante à logique floue* (Wang, et al., 2009) 19
Figure 2 – 6 : *Modèle du gantry bi–actionné et découplage par retour d'état* (Yu, et al., 2003) 20
Figure 2 – 7 : *Compensation du couplage mécanique par retour d'état* (Yu, et al., 2003) 20
Figure 2 – 8 : *modèle dynamique du gantry mono–actionné* 22
Figure 2 – 9 : *modèle chariot – poutre flexible – masse mobile* (Park, et al., 1999) 22
Figure 2 – 10 : *modèle d'un robot cartésien.* (*a*) *représentation schématique* (*b*) *modèle à paramètres distribués* (*c*) *modèle à paramétrés localisés avec prise en compte du non–minimum de phase* (*d*) *modèle souple classique* 23
Figure 2 – 11 : *modèle d'axe en gantry à deux actionneurs indépendants.* 24
Figure 2 – 12 : *modèle d'axe en gantry avec prise en compte du couplage mécanique* 24
Figure 2 – 13 : *modèle d'axe en gantry avec prise en compte du couplage mécanique* (Teo, et al., 2007) 25
Figure 2 – 14 : *modèle d'axe en gantry bi–actionné flexible* (Park, et al., 2001) 25
Figure 2 – 15 : *modèle d'axe en gantry bi–actionné flexible* (Stöppler, et al., 2008) 25
Figure 2 – 16 : *modèles d'axe en gantry avec prise en compte du couplage mécanique* (Gomand, 2008) 28
Figure 2 – 17 : *Compensation du couplage mécanique par anticipation* 28

Chapitre 3

Figure 3 – 1 : *A gantry stage* 32
Figure 3 – 2 : *Schematic representation of a gantry stage with pivot joints.* 32
Figure 3 – 3 : *A flexible plate joint* 33
Figure 3 – 4 : *The cross–arm is attached to the actuators at its ends via flexible plate joints (www.etel.ch)* 34
Figure 3 – 5 : *The cross–arm is attached to the actuators at intermediate positions* 34
Figure 3 – 6 : *A lumped–parameter model for the gantry stage* 35
Figure 3 – 7 : *Lumped parameter model of the gantry stage including the elastic cross–arm* 36
Figure 3 – 8 : *Displacement field $u(y, t)$ of the flexible cross–arm* 37
Figure 3 – 9 : *General model of the gantry stage* 39
Figure 3 – 10 : *Kinematics of the gantry stage* 40
Figure 3 – 11 : *Reference frames of the gantry stage* 40
Figure 3 – 12 : *Kinematics of the gantry stage* 41
Figure 3 – 13 : *Kinematics of the flexible gantry stage based on the coordinates $X(t)$, $\Theta(t)$, $Y(t)$, and $u_{Ritz}(y,t)$* 41
Figure 3 – 14 : *Kinetics of the linear actuator X_1* 44
Figure 3 – 15 : *Kinetics of the linear actuator X_2* 45
Figure 3 – 16 : *Kinetics of the linear actuator Y* 45
Figure 3 – 17 : *Kinetics of the cross–arm.* 46
Figure 3 – 18 : *General lumped–distributed parameters model of the gantry stage* 48
Figure 3 – 19 : *Single degree–of–freedom system* 59
Figure 3 – 20 : *Measured forces F_1 and F_2, and tracking errors of linear actuators X_1 and X_2 of a flexible gantry stage. Motion from $X = -0.15$ m to $X = 0.15$ m at an acceleration of 10 m/s² and a velocity of 0.75 m/s.* 60
Figure 3 – 21 : *Variation of the 1st resonance frequency of the cross–arm in function of the position of the payload. Test realized for two different payload masses.* 60
Figure 3 – 22 : *Dimensionless mode shape $\psi_1(Y)$ of the 1st flexible mode of the gantry stage's cross–arm for two different payload masses.* 61
Figure 3 – 23 : *COG with rigid* (a) *and causal* (b) *relationships* 62
Figure 3 – 24 : *EMR elements: (a) source, (b) accumulation, (c) conversion, and (d) coupling* 63
Figure 3 – 25 : *The inversion principle* 63
Figure 3 – 26 : *Basic inversions depicted using the COG description* 64
Figure 3 – 27 : *The inversion principle applied to the derivation of a feedforward and a feedback control structure* 64
Figure 3 – 28 : *Control sub–systems depicted using the EMR description.* 65
Figure 3 – 29 : *COG of the flexible gantry stage including N–flexible modes.* 67
Figure 3 – 30 : *Energetic Macroscopic Representation of the flexible gantry* 71
Figure 3 – 31 : *Maximum Control Structure of the flexible gantry (Feedback and Feedforward)* 73
Figure 3 – 32 : *Practical Control Structure of the flexible gantry (Feedback and Feedforward)* 74

Chapitre 4

Figure 4 – 1 : *Dual–drive gantry stage* "Phoenix 2004" *provided by ETEL* 78
Figure 4 – 2 : *Dynamic model of the rigid gantry stage* 79
Figure 4 – 3 : *Experimental and simulation responses of a) Motion references X_1 and X_2; b) Synchronization Error; Position Error of c) X_1 axis, d) X_2 axis; e) Motion references Y; and f)*

position error of Y axis. Test realized using independent axis control for a displacement of – 0.2 m *to* 0.2 m *for all axes, at a maximum speed of* 2 m/s, *and a maximum acceleration of* 20 m/s². 81

Figure 4 – 4 : *Feedback–feedforward decoupling basis control structure*..... 85

Figure 4 – 5 : *Feedback–feedforward decoupling basis control structure.*..... 86

Figure 4 – 6 : *Independent axis control vs. decoupling basis control, point–to–point* X_1 *and* X_2 *synchronized motions* (*from* –0.2 *to* +0.2 m) *at a maximum velocity of* 2 m/s *and a maximum acceleration of* 20 m/s²*; the position of the payload is kept at* 0.2 m (*i.e. maximum unbalance*)..... 87

Figure 4 – 7 : *Independent axis control vs. decoupling basis control, point–to–point diagonal movement* (X_1, X_2, *and Y from* –0.2 *to* +0.2 m) *at a maximum velocity of* 2 m/s *and a maximum acceleration of* 20 m/s². 88

Figure 4 – 8 : *Independent axis control vs. cross–coupling control vs. decoupling basis control. Ballbar tests realized with three* 100 mm *radius circles at a maximum tangential velocity of* 1.3 m/s *and acceleration of* 16 m/s². 90

Figure 4 – 9 : *Dual–drive gantry stage "Andromeda" provided by ETEL*..... 91

Figure 4 – 10 : *Acceleration measurements taken at actuator* X_1, *actuator* X_2, *and middle of the cross–arm for a displacement from* –0.15 m *to* +0.15 m. *Maximum velocity,* 0.75 m/s. *Maximum acceleration,* 7.5 m/s². 91

Figure 4 – 11 : *Dynamic model of the rigid gantry stage "Andromeda"* 92

Figure 4 – 12 : *Experimental and simulation responses. Test realized using independent axis control. Displacement from* – 0.15 m *to* + 0.15 m *for all axes at a maximum velocity,* 0.75 m/s *and a maximum acceleration,* 7.5 m/s²..... 94

Figure 4 – 13 : *Corrected Dynamic model of the rigid gantry stage "Andromeda"*..... 95

Figure 4 – 14 : *Experimental and simulation responses* (*corrected model*). *Test realized using independent axis control. Displacement from* – 0.15 m *to* + 0.15 m *for all axes at a maximum velocity,* 0.75 m/s *and a maximum acceleration,* 7.5 m/s²..... 96

Figure 4 – 15 : *Independent axis control vs. decoupling basis control, point–to–point* X_1 *and* X_2 *synchronized motions* (*from* +0.15 *to* –0.15 m) *at a maximum velocity of* 0.75 m/s *and a maximum acceleration of* 7.5 m/s²*; the position of the payload is kept at* 1.2 m (*i.e. maximum unbalance*).... 98

Figure 4 – 16 : *Independent axis control vs. decoupling basis control, point–to–point diagonal movement* (X_1, X_2, *and Y from* +0.15 *to* –0.15 m) *at a maximum velocity of* 0.75 m/s *and a maximum acceleration of* 7.50 m/s²..... 98

Figure 4 – 17 : *Independent axis control vs. decoupling basis control. Ballbar tests realized with three* 100 mm *radius circles at a maximum tangential velocity of* 0.8 m/s *and acceleration of* 6 m/s². 99

Figure 4 – 18 : *Independent axis control vs. decoupling basis control with compensation of the static friction of actuators* X_1, X_2, *and Y. Ballbar tests realized with three* 100 mm *radius circles at a maximum tangential velocity of* 0.8 m/s *and acceleration of* 6 m/s²..... 99

Figure 4 – 19 : *Modified dual–drive gantry stage*.....100

Figure 4 – 20 : *influence of the flexibility of the cross–arm on the reaction forces and tracking errors of actuators* X_1 *and* X_2. 100

Figure 4 – 21 : *Dynamic model of the flexible gantry stage*.....101

Figure 4 – 22 : *Experimental vs. Simulation. Acceleration* 2.5 m/s²; *Velocity* 0.25 m/s; *Y*=–1.1 m.104

Figure 4 – 23 : *Experimental vs. Simulation. Acceleration* 7.5 m/s²; *Velocity* 0.50 m/s; *Y*=–0.7 m.104

Figure 4 – 24 : *Experimental vs. Simulation. Acceleration* 10.0 m/s²; *Velocity* 0.75 m/s; *Y*=–0.1 m.105

Figure 4 – 25 : *Experimental vs. Simulation. Acceleration* 10.0 m/s², *Velocity* 1.00 m/s, *Y*=0.0 m.105

Figure 4 – 26 : *Experimental vs. Simulation. Acceleration* 5.0 m/s²; *Velocity* 1.00 m/s; *Y*=0.3. ...106

Figure 4 – 27 : *Experimental vs. Simulation. Acceleration* 2.5 m/s²; *Velocity* 0.75 m/s; *Y*=0.5 m.106

Figure 4 – 28 : *Experimental vs. Simulation. Acceleration* 5.0 m/s²; *Velocity* 1.00 m/s; ; *Y*=0.5 m.107

Figure 4 – 29 : *Experimental vs. Simulation. Acceleration* 10.0 m/s², *Velocity* 0.5 m/s, $Y = 1.3$ m107

Figure 4 – 30 : *Independent Axis vs. Decoupling Basis Control. Acceleration* 6.6 m/s², *Velocity* 0.85 m/s, *position* –0.15 m to +0.15 m. $Y = 0.3$ m. 113

Figure 4 – 31 : *Independent Axis vs. Decoupling Basis Control with Jerk. Acceleration* 6.6 m/s², *Velocity* 0.85 m/s, *position* –0.15 m to +0.15 m. $Y = 0.3$ m.....113

Figure 4 – 32 : *Two impulses input shaping command* (Singhose, 1997). *The* A_2 *response cancels the vibration of the* A_1 *response.*.....114

Figure 4 – 33 : *Variable Jerk motion Law*.....114

Figure 4 – 34 : *Single Jerk vs. double jerk trajectory planner. Simulation results for*: *Acceleration max* 6.6 m/s², *Velocity* 1.00 m/s, *Position* $X = 0.0$ to +1.0 m. *Position* $Y = -1.1$ to –0.3 m. *Top*, *Forces* F_1 and F_2 , *middle*, *Tracking error of actuators* X_1 *and* X_2, *bottom*, *Displacement* q_1 *at the middle of the cross–arm.*.....117

Figure 4 – 35 : *Single Jerk vs. double jerk trajectory planner.* 117

Figure 4 – 36 : *Rigid vs. flexible gantry. Decoupling Basis Control with Jerk; Acceleration* 5.6 m/s², *Velocity* 0.85 m/s, *position* –0.15 m to +0.15 m. $Y = 0.3$ m.....118

Liste des Tableaux

TABLEAU I : AVANTAGES ET INCONVENIENTS SYSTEMES DE POSITIONNEMENT EN SERIE ET PARALLELES..... 10

TABLE II : PHYSICAL PARAMETERS OF THE GANTRY STAGE "PHOENIX 2004"..... 80

TABLE III : PHYSICAL PARAMETERS OF THE GANTRY STAGE "ANDROMEDA" 93

TABLE IV : PHYSICAL PARAMETERS OF THE "FLEXIBLE" GANTRY STAGE..... 103

TABLE A–1 : BOUNDARY CONDITIONS OF AN EULER–BERNOULLI BEAM..... 103

TABLE A–2 : DIFFERENT BOUNDARY CONDITIONS FOR AN EULER–BERNOULLI BEAM 103

TABLE B–1 : EVOLUTION OF THE EIGENVALUES OF THE HEADLESS GANTRY WHEN $\beta_1 = \beta_2$..... 103

TABLE B–2 : EVOLUTION OF THE EIGENVALUES OF THE HEADLESS GANTRY WHEN $\beta_1 \neq 0$ AND $\beta_2 = 0$..... 103

Liste de symboles / List of symbols

V	Energie potentielle / Potential Energy
T	Energie Cinétique / Kinetic energy
$\mathcal{L}$	Lagrangien d'un système / Lagrangian of a system $\mathcal{L} = T - V$
δW	Travail virtuel des efforts sans potentiel / Virtual work done by potential–less forces
E	Module de Young / Young's modulus
A	Aire de section de la poutre en gantry / Gantry stage's cross–arm's cross sectional area
I	Moment Inertie de l'aire transversale de la poutre / Inertia moment of the beam's cross–section
u	Fonction de déplacement parallèle à l'axe x / Displacement function parallel to the x axis
v	Fonction de déplacement parallèle à l'axe y / Displacement function parallel to the y axis
w	Fonction de déplacement parallèle à l'axe z / Displacement function parallel to the z axis
$\boldsymbol{\delta}$	Symbole de Kronecker / Kronecker delta
δ	Operateur variational / Variational operator
L_b	Longueur de la poutre / Beam span
σ	Effort par unité de surface / Stress
ε	Déformation unitaire / Strain
J	Inertie de rotation / Rotational Inertia
M	Matrice de masse / Mass matrix
H	Matrice d'accélérations de coriolis et centripètes / Coriolis and Centripetal terms matrix
C	Matrice d'amortissement / Damping matrix
K	Matrice de raideur / Stiffness matrix
F	Vecteur des forces généralisées / vector of generalized forces
q	Vecteur des cordonnées généralisées / vector of generalized coordinates

Glossaire / Glossary

BBJ	Bang–Bang Jerk
BC	Boundary Condition
BVP	Boundary Value Problem
CAD	Computer Aided Design
DOF	Degree of Freedom
EBBT	Euler–Bernoulli Beam Theory
REM/EMR	Representation Énergétique Macroscopique / Energetic Macroscopic Representation
EVP	Eigenvalue Problem
FEMA	Finite Element Modal Analysis
IC	Initial Condition
SMC/MCS	Structure Maximale de Commande / Maximum Control Structure
MIMO	Multiple Inputs Multiple Outputs
ODE	Ordinary Differential equation
PCS	Practical Control Structure
PDE	Partial Differential Equation
PMLSM	Permanent Magnet Linear Synchronous Machine
SISO	Single Input Single Output
TBT	Timoshenko Beam Theory

Introduction Générale

Ce mémoire s'intéresse aux systèmes de positionnement multi–actionnés du type « axe en gantry ». Ce type de dispositifs de positionnement est utilisé dans l'industrie électronique et des semi–conducteurs pour des applications requérant une très haute précision, un très large espace de travail et une dynamique élevée (due aux cadences requises). Parmi les applications, on trouve le placement des composants électroniques, la fabrication et l'inspection des écrans plats ou encore la photolithographie sur substrat de silicium. Selon l'évolution des marchés des hautes technologies, les critères de performance pour ces applications (en termes de précision, répétabilité, et vitesse d'exécution) sont de plus en plus exigeants. L'objectif final de ce projet de recherche est donc d'améliorer, par la commande, les performances de positionnement des axes en gantry afin d'assurer ces critères.

Ce projet de recherche a été lancé par la société ETEL (www.etel.ch) avec deux objectifs principaux. Le premier, à court terme, consiste à vérifier s'il est possible d'améliorer par la commande les performances d'un système en gantry de grande dimension. En effet, dans le cas particulier des systèmes de positionnement dont le ratio espace de travail/précision devient trop important, des hypothèses telles que la rigidité structurelle ne sont plus valables. De ce fait, de simples modèles rigides ne suffisent plus à décrire le comportement du système et il devient alors difficile de proposer des stratégies adaptées à leur commande. Le deuxième objectif, à plus long terme, consiste à capitaliser les connaissances dans la conception et la commande des systèmes multi–actionnés avec prise en compte des flexibilités structurelles.

Cette thèse cherche donc à développer un outil méthodologique qui soit adapté à la modélisation et à la commande des systèmes de positionnement multi–actionnés de type « axe en gantry » pour maîtriser *in fine* le point « outil » dans l'espace de travail lors de déplacements à grande dynamique.

Ce mémoire est organisé en cinq chapitres.

Le premier chapitre sert de mise en contexte et à expliquer l'historique de la collaboration entre la société ETEL et le laboratoire L2EP. De plus, les systèmes de positionnement, leurs types et leurs applications industrielles seront présentés à divers niveaux de précision. La problématique des axes en gantry est présentée en fonction de l'évolution du besoin industriel.

Le deuxième chapitre propose un état de l'art des approches existantes pour la modélisation et la commande de tels dispositifs. Face à ce type de systèmes, relativement complexes à aborder, la littérature propose essentiellement des algorithmes de commande très élaborés, par exemple de type H–infini ou faisant appel à la logique floue, en raison d'un manque de connaissances du comportement physique de l'axe. En effet, pour les axes en gantry avec prise en compte des flexibilités, il n'existe pas d'approche de modélisation qui soit adaptée pour reproduire le comportement du système réel. Les modèles qui sont proposés dans l'état de l'art ne correspondent pas à la réalité ou, ils modélisent le comportement de l'axe en gantry de façon incomplète.

L'outil méthodologique que l'on cherche à développer doit pouvoir favoriser les allers/retours entre la conception mécanique et l'élaboration d'une commande. Il doit également être suffisamment générique pour être facilement transposable à toute la gamme d'axes en gantry fabriquée par la société ETEL.

Afin de répondre à ces exigences, l'approche choisie se doit d'être « universelle » et facilement transposable aux domaines de la conception mécanique et de la commande. De ce fait, dans le troisième chapitre, nous proposons une modélisation physique détaillée de l'axe en gantry. Comme les axes en gantry partagent certaines caractéristiques fondamentales, il est donc possible de produire un modèle unique qui soit valable pour toute la gamme d'axes en gantry. Alors, avec une modélisation physique détaillée et sa représentation à l'aide des formalismes de modélisation et de

commande graphique causale, il est possible de produire un outil de travail utilisable par les concepteurs de structures électromécaniques et de commande.

Pour valider la démarche proposée, dans le quatrième chapitre, nous présentons l'application expérimentale de la méthodologie de modélisation et de commande à trois types d'axes en gantry différents.

Enfin, le dernier chapitre propose une synthèse des principales conclusions issues des travaux menés, ainsi que les principales perspectives ouvertes par cette étude.

1. Contexte

1.1 Positionnement de ce projet de recherche

Un axe en gantry est un type de manipulateur cartésien consistant en un portique à un (ou plusieurs) actionneurs poussant une structure transversale, assimilable à une poutre. Sur cette dernière, selon l'application, un actionneur sert à déplacer la charge, la pointe–outil ou un autre dispositif d'actionnement, voir **Figure 1 – 1**. Ses applications sont nombreuses: dans le domaine de la machine–outil pour l'Usinage à Grande Vitesse (UGV); dans le domaine de la micro–électronique et des semi–conducteurs pour le placement des composants électroniques, la fabrication et l'inspection des écrans plats ou encore la photolithographie sur substrat de silicium. Enfin, là où il est nécessaire d'effectuer des mouvements de grande amplitude, de haute précision et à dynamique élevée, c'est le principe qui est retenu.

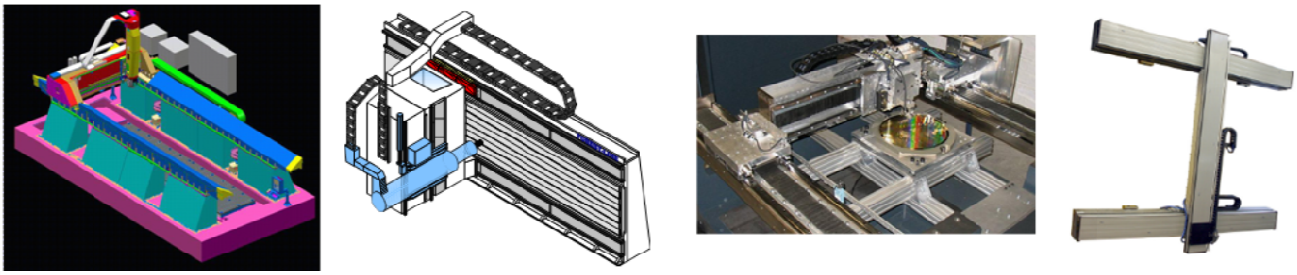

(*a*) (*b*) (*c*) (*d*)

Figure 1 – 1 : *Différents systèmes de positionnement multi–actionnés du type « axe en gantry » Machines d'Usinage Grand Vitesse de la société Forest line* (*a*) *et* (*b*)*. Machine de placement de composants électroniques* (*c*) *et machine de fabrication et inspection des écrans plats* (*d*) *de la société ETEL.*

Ce projet de recherche a été lancé par la société ETEL (www.etel.ch) afin d'étudier une problématique industrielle d'actualité. En effet, les machines de production deviennent de plus en plus rapides grâce aux progrès des technologies d'actionnement (Corsi, et al., 2007). Toutefois, cette rapidité a un coût énergétique conséquent qui, pour être compensé, implique une réduction de masses embarquées. Ce "mélange" dynamique élevée – masses réduites entraîne l'apparition de souplesses et flexibilités qui engendrent un niveau de vibrations tel que, dans de nombreux cas, la machine ne peut pas être utilisée à son niveau de performances optimal. Actuellement, pour améliorer les performances de positionnement, la solution industrielle est de conserver les éléments rigides (et lourds) malgré le coût énergétique induit.

D'autres solutions à cette problématique existent. L'une d'entre elles est l'utilisation de matériaux composites afin d'avoir une structure à la fois rigide et légère. Cette solution reste cependant peu démocratisée en raison du coût du procédé et des difficultés de fabrication, notamment l'ajout d'inserts métalliques – nécessaires à la fixation et à la traction – dans le composite. Une étude concernant cette solution a été menée dans le cadre du projet de fin d'études intitulé « Conception d'un Bras de Robot en Matériau Composite » de l'Ecole Nationale Supérieure d'Arts et Métiers (Parent, 2009). Une autre solution est d'utiliser des capteurs supplémentaires afin de mesurer le phénomène vibratoire et pouvoir agir sur ce dernier "au bon endroit". Cependant, la piste choisie dans ce mémoire, étant la moins coûteuse et donc industriellement la plus viable, consiste à trouver un compromis entre rigidité et légèreté avec des matériaux conventionnels et de gérer les problématiques associées par la commande.

L'objectif d'ETEL, à l'issue de cette étude, est de réaliser une réduction importante de poids dans l'ensemble de leurs systèmes de type « axe en gantry » et de maîtriser les problématiques associées par la commande.

Cet objectif, aussi simple qu'il paraît, cache un cahier des charges extrêmement exigeant. En effet, la commande de systèmes multi–actionnés du type « axe en gantry » avec prise en compte de la flexibilité présente deux problématiques principales très complexes :

- Problématique associée à la commande des systèmes multi–actionnés
    - Coordination des divers entraînements afin d'assurer une coopération des actionneurs par rapport à une fonctionnalité globale, sachant que les actionneurs se perturbent entre eux, ce qui peut occasionner des dysfonctionnements, voire des détériorations.
- Problématiques associées à la commande des systèmes flexibles
    - Complexité de modélisation
    - Systèmes non–stationnaires

De plus, le cahier des charges impose que la commande soit suffisamment générique pour permettre :

- Un échange entre les concepteurs des structures électromécaniques et ceux de la commande;
- Une transposition facile à toute la gamme d'axes en gantry fabriquée par la société ETEL ;
- Une "transparence" pour l'utilisateur final. Par exemple, si ce dernier doit faire un changement d'outil. Il doit seulement introduire le poids de l'outil pour régler à nouveau les paramètres de la commande et non relancer toute une série de calculs et d'identifications pour le faire. Dans l'industrie, un arrêt ou un déréglage de machine dans une ligne de production aurait de fortes retombées économiques.

Une telle généricité requiert une compréhension profonde de la technologie et du comportement du système étudié, ce qui passe nécessairement par une modélisation ayant un sens physique.

Pour ETEL, l'approche de commande basée sur une modélisation physique causale, et ses formalismes associés : GIC (Graphe Informationnel Causale) et REM (Représentation Energétique Macroscopique), développés au sein de l'équipe commande du L2EP, répondaient à cette attente. De plus, cette équipe avait déjà les compétences nécessaires pour traiter les problématiques associées à la commande des systèmes flexibles :

– Commande et entraînement des machines–outils à dynamique élevée : Formalismes et applications. (Habilitation à Diriger des Recherches) (Barre, 2004);
– Prise en compte des phénomènes vibratoires dans la génération de la commande des machines–outils à dynamique élevée (Thèse) (Béarée, 2005)
– Synthèse et réglage de lois de commande adaptées aux axes souples en translation (Thèse) (Colas, 2006)

Et les compétences pour traiter les problématiques associées à la commande des systèmes multi–actionnés :

– Formalismes de représentation et de commande appliqués aux systèmes électromécaniques multi–machines multi–convertisseurs (Habilitation à Diriger des Recherches) (Bouscayrol, 2003)
– Modélisation vectorielle multi–machines pour la commande des ensembles convertisseurs–machines polyphasés (Thèse) (Kestelyn, 2003)

Le challenge consistait maintenant à transposer ces compétences à la commande des systèmes multi–actionnés de type axe en gantry avec prise en compte de la flexibilité. Ainsi, une thèse CIFRE entre la société ETEL et le L2EP a été lancée

La collaboration ETEL/L2EP est née avec la thèse de Ghislain REMY (Remy, 2007). Ses travaux portaient sur la minimisation des forces perturbatrices générées par des actionneurs linéaires lors de la transformation électromécanique. Celles–ci pouvant provoquer des vibrations de la structure attachée à l'actionneur et donc dégrader les performances de positionnement. Dans sa thèse, il a proposé une modélisation très détaillée des moteurs linéaires d'actionnement, laquelle a été représentée à l'aide du formalisme GIC. Cette représentation a ensuite été utilisée pour définir de façon systématique des structures de commande adaptées à la commande de l'actionneur pour la suppression des vibrations mécaniques.

En parallèle, Julien GOMAND (Gomand, 2008) travaillait dans sa thèse sur les propriétés graphiques du formalisme GIC (commandabilité, observabilité, etc.). Il a pris comme cas d'étude un axe en gantry de petite taille[1]. Pour ce type de système, les problématiques associées à la commande des systèmes multi–actionnés sont les principaux facteurs dégradant les performances de positionnement. La commande qu'il a reproduit à partir de la représentation GIC du modèle dynamique de l'axe en gantry a permis d'améliorer la précision de 30% et la vitesse d'exécution de 10% par rapport à la commande industrielle initiale.

A l'issue de ces deux projets, les résultats obtenus étaient encourageants. La suite naturelle était de lancer cette nouvelle thèse, afin de prendre en compte non seulement les aspects associés à la commande des systèmes multi–actionnés, mais aussi ceux associés à la commande des systèmes flexibles.

[1] Le terme *petite taille* est utilisé ici pour définir un système de positionnement dont le comportement vibratoire est négligeable (par rapport au cahier de charges).

1.2 Les systèmes de positionnement dans l'industrie

On peut définir un système de positionnement comme « tout système (électro)mécanique où il y a déplacement spatial de pièces ou d'éléments du système et qui implique un contrôle de position d'un type ou d'un autre ».

Indépendamment de leur application, tous les systèmes de positionnement partagent les mêmes caractéristiques techniques fondamentales :

- Temps d'exécution du mouvement
- Exactitude (en mouvement point–à–point et en suivi de trajectoire)
- Répétabilité (en mouvement point–à–point et en suivi de trajectoire)
- Consommation énergétique
- Espace/volume de travail
- Type d'actionnement (mécanique, pneumatique, hydraulique, électromagnétique, etc.)
- Ergonomie (Facilité d'accès et d'opération)
- Facilité d'adaptation à des tâches variées
- Facilité d'installation
- Temps de stabilisation en fin de mouvement dans une tolérance donnée (Ex : $\pm$ 1µm)

De la même façon qu'avec les caractéristiques fondamentales ci–dessus, les systèmes de positionnement peuvent se représenter avec trois éléments fondamentaux, voir **Figure 1 – 2**

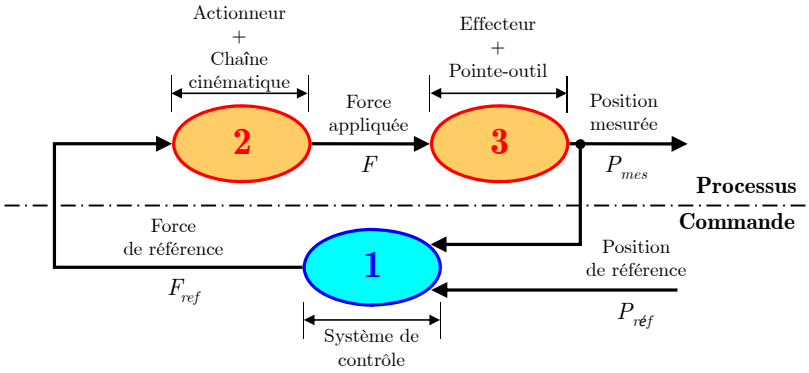

Figure 1 – 2 : *Eléments fondamentaux d'un système de positionnement*

Afin de modifier une ou plusieurs des caractéristiques techniques d'un système de positionnement, il est possible d'agir sur un des trois éléments basiques qui le composent. A savoir :

Effecteur et pointe–outil : concerne la pointe–outil et les éléments servant à la supporter ainsi que le capteur de position.

Actionneur(s) et chaîne(s) cinématique(s) : concerne les actionneurs et les mécanismes de transmission de la puissance (Ex : Moteur linéaire, système de transformation vis/écrou, etc.).

Système(s) de contrôle : concerne l'asservissement des actionneurs – en force et en position – et éventuellement la compensation des erreurs liées à la transmission de la puissance.

Dans un système asservi quelconque, la partie commande est la plus facile à modifier car la moins coûteuse. Par exemple : pour modifier les performances d'un système, il suffit de changer le type/structure du contrôleur, ou d'en modifier ses gains. Il n'y a pas de modifications physiques à apporter.

En outre, les actionneurs et les éléments à déplacer (avec la charge) présentent des limitations qui ne peuvent être compensées que par la commande (forces de cogging dans les actionneurs,

défauts géométriques dans la chaîne cinématique, vibrations de la charge, etc.). De ce fait, et afin d'améliorer les performances d'un système de positionnement, une grande quantité des projets de R&D se concentre sur ce point. Dans notre cas, l'objectif est de développer des algorithmes de commande basés sur un modèle physique. Cette approche offre une grande flexibilité vis–à–vis de l'implémentation industrielle. En effet, comme la commande est basée sur les paramètres physiques du système, l'algorithme de commande est très simple à implémenter, régler et adapter à des systèmes semblables.

Dans le cadre de la production industrielle, les systèmes de positionnement jouent un rôle essentiel. Ils interviennent quasiment dans toutes les étapes du processus d'industrialisation, de la fabrication jusqu'à l'inspection. Prenons comme exemple deux applications complètement différentes, appartenant à deux secteurs également différents. Dans l'industrie automobile, prenons la fabrication des blocs–cylindres. Ils sont fabriqués en fonte ou en alliage d'aluminium. Ainsi, en début de chaîne, nous avons un brut de fonderie dont les *surfaces fonctionnelles*[2] ne sont pas encore définies. Pour les obtenir, le brut de fonderie est usiné, voir **Figure 1 – 3**. Ces opérations sont exécutées par des machines–outils qui ne sont finalement que des systèmes de positionnement portant une broche et un outil de coupe. De la même façon, pour les opérations de contrôle, des machines de métrologie (équipées d'un système de positionnement) sont utilisées.

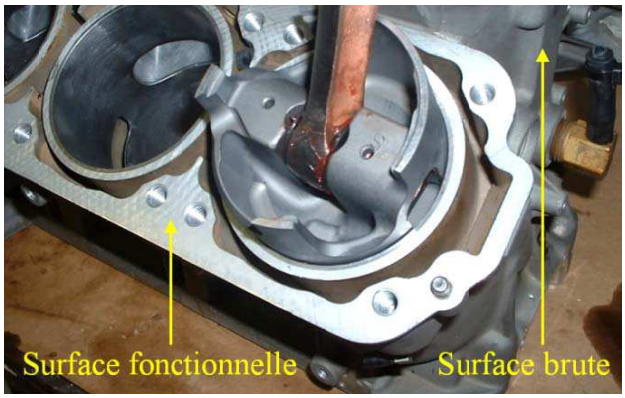

Figure 1 – 3 : *Bloc–moteur et piston d'un moteur à combustion interne*

Le deuxième exemple concerne l'industrie électronique de grande consommation comme la fabrication des téléphones portables, ordinateurs, etc. La pose des composants électroniques sur des circuits imprimés est aussi réalisée à l'aide de systèmes de positionnement, voir **Figure 1 – 4**

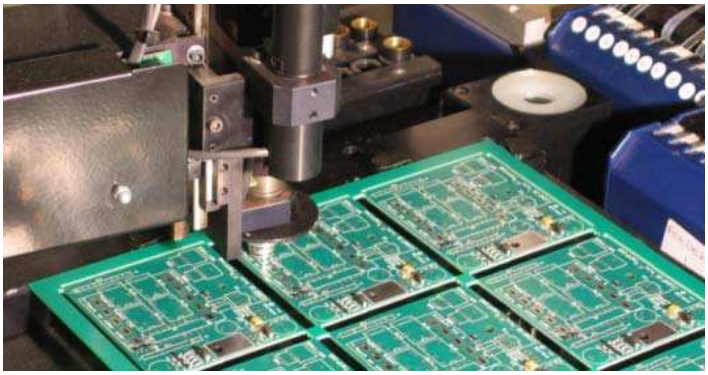

Figure 1 – 4 : *Placement de composants sur un circuit imprimé* [source : *www.enaelectronics.ca*]

Dans ces deux cas, les caractéristiques techniques souhaitées pour le système de positionnement sont la vitesse d'exécution, la précision, la répétabilité, le volume de travail, etc. Cependant, même si à première vue les caractéristiques souhaitées semblent être les mêmes, les ordres de grandeur ne le sont pas.

[2] *Surfaces fonctionnelles* du bloc–moteur: Surfaces de connexion avec la culasse et autres pièces du moteur, et les cylindres de logement des chemises – ou chambres à pistons.

Les causes de dégradation des performances d'un système de positionnement multi–actionné peuvent se classer en quatre catégories principales.

1. *Défauts géométriques* : Cette problématique concerne tous les aspects liés à la géométrie du système de positionnement. Dans ce cadre, on peut inclure les dérives thermiques et les défauts des mécanismes de transmission de la puissance.
2. *Couplage entre actionneurs* : Cette problématique concerne tous les aspects liés à la dynamique du système de positionnement et les mouvements relatifs entre ses composants.
3. *Comportement vibratoire* : La recherche des performances toujours plus élevées conduit les systèmes à la limite de leurs possibilités technologiques et structurelles, invalidant de ce fait l'hypothèse classiquement retenue d'une dynamique d'ensemble assimilable à celle d'un corps rigide (Barre, et al., 2006). Il s'ensuit que dans le domaine des systèmes de positionnement rapide, les phénomènes vibratoires ne puissent plus être sous–estimés.
4. *Bruit électrique* : Cette problématique est particulièrement associée à la transformation électromécanique des actionneurs et au système de contrôle. Dans ce cadre, on peut inclure le bruit (de mesure des capteurs, de l'amplificateur, de quantification, et de conversion AD/DA).

Il faut prendre en compte que tous les systèmes de positionnement – et en général tous les systèmes (électro)mécaniques – présentent dans une certaine mesure une combinaison de ces problématiques. Cependant, suivant l'application, une d'entre elles sera prédominante.

Pour répondre à ces problématiques, un grand nombre de configurations de système de positionnement existe pour toutes les applications et pour toutes les échelles de précision, voir **Figure 1 – 5** .

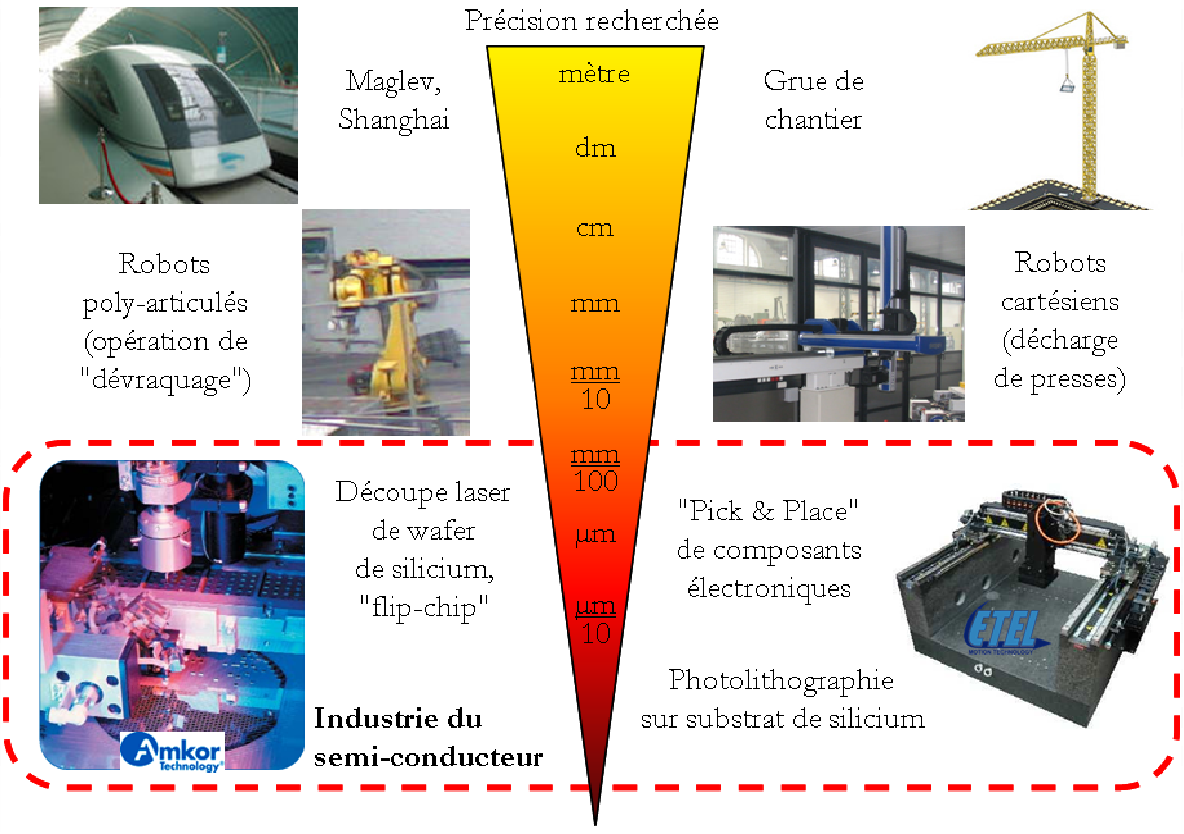

Figure 1 – 5 : *Différents types de systèmes de positionnement ; Applications et échelles de précision* **(Gomand, 2008)**

Une grande majorité des configurations de la **Figure 1 – 5** a été proposée pour des applications spécifiques (machine de photolithographie, grue de chantier, etc.). D'autres ont été proposées pour des applications plus génériques (*Ex* : manipulateur anthropomorphe, manipulateur cartésien, etc.). Indépendamment de toutes ces configurations différentes, les systèmes de positionnement peuvent se classifier en deux catégories fondamentales : série et parallèle.

Ces deux appellations font référence à la façon dont les éléments qui transmettent la puissance sont connectés à partir d'un repère donné jusqu'à la charge ou la pointe–outil. Ainsi, dans une configuration en série, l'ensemble actionneur–charge 1 déplace les ensembles 2 à N, l'ensemble 2 déplace les ensembles 3 à N, et ainsi de suite jusqu'à l'ensemble N ; N étant la pointe–outil, voir **Figure 1 – 6** .

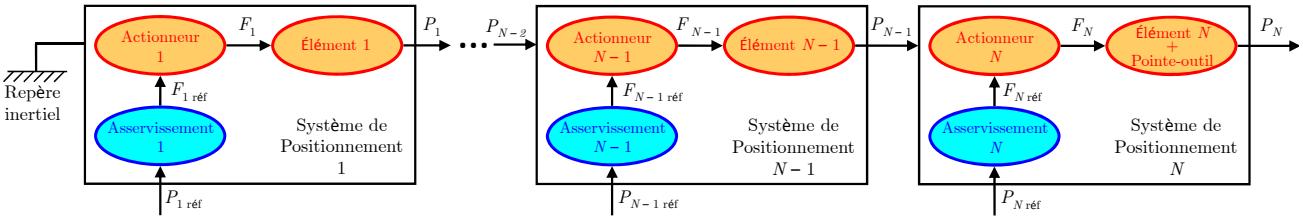

Figure 1 – 6 : *Architecture du système de positionnement en série*

Dans une configuration en parallèle, deux ou plusieurs éléments transmettent en tandem la puissance (depuis un repère inertiel donné) vers la pointe outil, voir **Figure 1 – 7** .

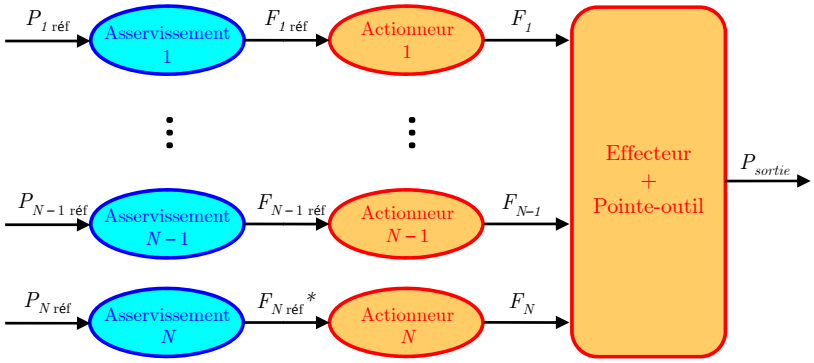

Figure 1 – 7 : *Architecture du système de positionnement en parallèle*

D'autres configurations, dites hybrides, peuvent être construites à partir des configurations en série et en parallèle.

Parmi les configurations en série, on peut aller facilement de dispositifs simples, comme des systèmes de positionnement linéaires ou rotatifs, à des systèmes beaucoup plus complexes comme des manipulateurs anthropomorphes, ou cartésiens ; qui ne sont finalement qu'un ensemble de systèmes de positionnement plus basiques, voir **Figure 1 – 8** .

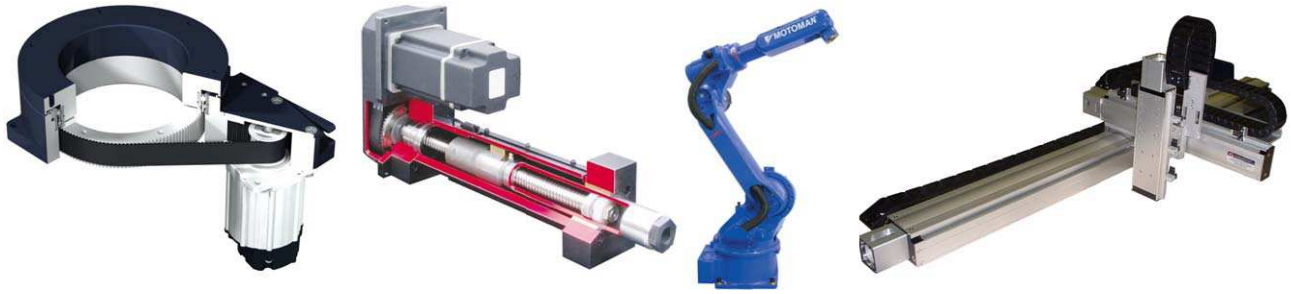

(*a*) (*b*) (*c*) (*d*)

Figure 1 – 8 : *Différents systèmes de positionnement en série*
Rotary assembly [*www.bell–evermannews.com*] (*a*)*; ball–screw mechanism* [*www.torquewrenchdetails.info*] (b)*; anthropomorphous robot* [*www.ferret.com.au*] (c); – *XYZ table* [*www.intellidrives.com*] (d)

Ces derniers sont le résultat d'une connexion en série des systèmes de positionnement plus simples. Ils sont moins précis et leurs performances sont vite limitées à cause de cette configuration. Par exemple, pour les manipulateurs anthropomorphes, l'erreur de précision de sortie est l'erreur accumulée par chaque élément connecté en série.

Les dispositifs de positionnement parallèles impliquent une mise en collaboration des actionneurs dans le but commun de déplacer un axe ou une plateforme portant la pointe–outil dans l'espace de travail, voir **Figure 1 – 9** . Dans ce type de systèmes, la précision est limitée du fait qu'on ne mesure pas directement la position de la pointe-outil, mais celle des actionneurs qui sont à l'autre extrémité de la chaîne cinématique. Alors, pour assurer une bonne précision, les systèmes parallèles sont en général fabriqués très rigides. Ce qui sert à créer des effets de couplage entre les actionneurs portant la charge.

Figure 1 – 9 : *Différents systèmes de positionnement en parallèle*

Le **TABLEAU I** présente un récapitulatif des principaux avantages et inconvénients des configurations en série et parallèles.

TABLEAU I
AVANTAGES ET INCONVENIENTS DES SYSTEMES DE POSITIONNEMENT SERIE ET PARALLELES

	Configuration en série	**Configuration parallèle**
Avantages	• Volume de travail important • Bas prix (technologie maîtrisée) • Applications diverses • Modélisation simple • Accessibilité	• Rigidité structurelle élevée • Dynamique élevée • Précision élevée • Répartition de la puissance • Cadences élevées
Inconvénients	• Accumulation des défauts • Souplesse structurelle • Cadence réduite • Couplage mécanique	• Espace de travail réduit • Prix élevé • Modélisation complexe • Mécanique complexe • Couplage mécanique

Pour l'industrie de la micro–électronique et des semi–conducteurs, les systèmes de positionnement parallèles et hybrides (série+parallèle) sont favorisés par rapport aux systèmes en série grâce à leurs avantages. Parmi les configurations hybrides, il y a l'axe en gantry. Il est compact, a une mécanique simple, un excellent rapport précision/volume de travail ainsi qu'un excellent rapport force/taille. Ses performances sont remarquables. Cependant, elles peuvent être améliorées grâce à la compréhension des problématiques associées à ce type de structure. Celles–ci seront présentées dans la section suivante.

1.3 L'axe en gantry (problématique du dispositif support de l'étude)

Le terme gantry, désigne une structure mécanique en portique, voir **Figure 1 – 10** . Dans le cadre des systèmes de positionnement, nous restreignons son usage à la description d'axes formés par une poutre guidée par translation à ses deux extrémités, tel que celui de la **Figure 1 – 10 (d)**

(*a*) (*b*) (*c*) (*d*)

Figure 1 – 10 : *Différentes structures dites « en gantry »*
portique d'atelier (*a*); *portique de port* (*b*); *gantry médical* (*c*); *gantry de positionnement* (*d*)

Afin de suivre l'évolution de l'industrie, les axes en gantry ont fortement évolué. Structurellement, ils sont passés d'une configuration en série (ou mono–actionnée) à une configuration hybride (ou bi–actionnée), voir **Figure 1 – 11** . Dans le premier cas, la poutre est actionnée à une de ses extrémités, l'autre est soit guidée, soit en porte–à–faux. Dans le deuxième cas, la poutre est actionnée à ses deux extrémités. De la même façon, des actionneurs du type machine tournante et mécanisme vis/écrou (pour transformer le mouvement) ont cédé leur place à des entraînements directs du type Machines Linéaires Synchrones à Aimants Permanents (MLSAP) avec ou sans fer.

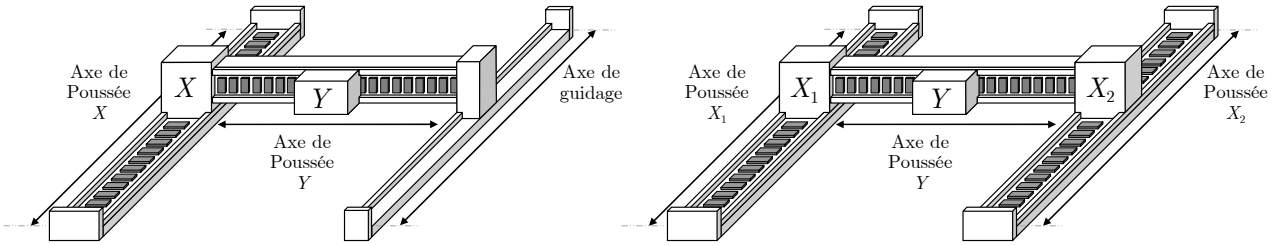

(*a*) (*b*)

Figure 1 – 11 : *Axe en gantry série ou mono–actionné* (*a*); *et hybride ou bi–actionné avec liaisons rigides* (*b*)

Dans l'industrie de la micro–électronique et du semi–conducteur, la transition entre mono et bi–actionné n'a pas été immédiate. Les premiers axes en gantry mono–actionnés sont apparus vers la fin des années 80, avec pour application principale, la dépose de composants électroniques sur des circuits imprimés. L'objectif des axes en gantry mono–actionnés était donc d'assurer les cadences et précisions imposées par le marché de l'électronique de grande consommation. Cependant, le gantry mono–actionné n'était ni assez rapide ni assez précis pour suivre l'évolution de l'industrie électronique, ce qui était dû à deux facteurs :

(1) A cause de l'inertie, la poutre avait tendance à tourner sur l'axe de poussée. Ceci à son tour générait de la torsion sur les axes de guidage, entraînant donc l'usure des axes de guidage et une augmentation de la consommation énergétique due à une augmentation des frottements, voir **Figure 1 – 12** (*a*).

(2) Le gantry mono–actionné peut s'assimiler à une poutre en porte–à–faux en translation. De toutes les configurations de poutre possibles, la poutre en porte–à–faux est celle possédant la plus faible fréquence fondamentale de vibration (Han, et al., 1999). La bande passante du contrôleur en position était alors limitée par cette fréquence, ce qui se traduisait en une vitesse de déplacement limitée pour éviter des déformations élastiques importantes, voir **Figure 1 – 12** (*b*).

Ainsi, entre deux opérations de dépose de composants, il y a une période d'attente afin de laisser la pointe–outil se stabiliser à la position souhaitée. Dans la littérature, les travaux cherchant à résoudre ces problèmes se concentrent essentiellement sur la modification des trajectoires de référence pour la prise en compte des déformations élastiques (Yoshikawa, et al., 1993) et la commande optimale de type H_∞ (Rieber, et al., 2001).

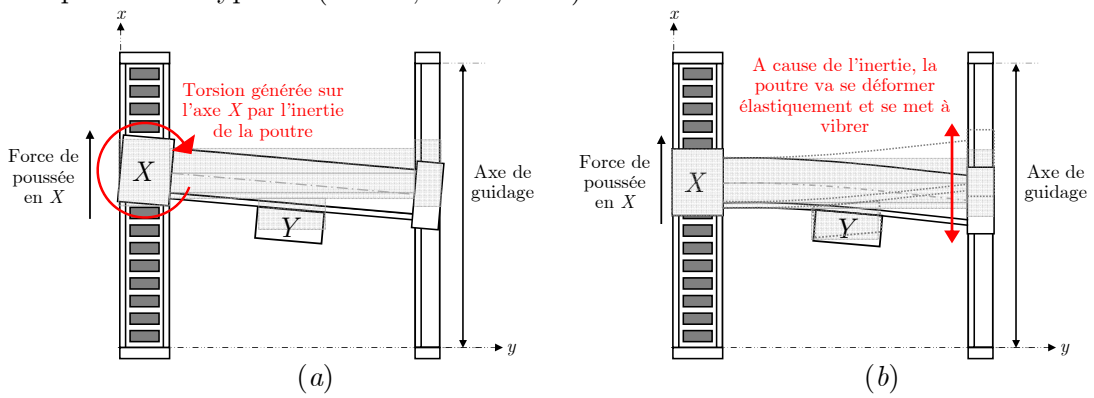

Figure 1 – 12 : *Déformation de l'axe en gantry mono–actionné à cause des forces inertielles. Deux situations sont possibles : la poutre ne se déforme pas et génère de la torsion autour de l'axe de pousse* (a) *; la poutre se déforme élastiquement* (b)*. Dans la réalité, on trouve un mélange des situations* (a) *et* (b)*.*

Afin d'augmenter les cadences de production au niveau industriel, la solution la plus naturelle a été d'ajouter un actionneur supplémentaire. Ainsi, la puissance d'actionnement est doublée et la fréquence fondamentale de vibration de la poutre est naturellement augmentée (Han, et al., 1999). Cependant, cette modification structurelle n'a pas que des avantages, elle introduit aussi les inconvénients inhérents des systèmes multi–actionnés :

- Synchronisation entre les actionneurs afin d'éviter toute rotation de la poutre autour d'elle–même.
- Les actionneurs se perturbent entre eux à cause de la répartition inégale de la charge entre les deux actionneurs. Ce déséquilibre est occasionné par le mouvement de la tête tout au long de la poutre et les différences entre les axes de poussée 1 et 2 (différences de masse, de frottements, de temps de réponse des boucles de contrôle en force et en position, etc.). Ce déséquilibre est le principal facteur de désynchronisation entre les axes en collaboration.

Dans les premiers modèles d'axe en gantry bi–actionné, la synchronisation était forcée par des liaisons poutre/actionneur rigides. De ce fait, la désynchronisation entre les axes de poussée, bien que limitée, occasionnait de fortes contraintes dans les liaisons poutre/actionneur et une usure importante des axes de guidage, voir **Figure 1 – 13** .

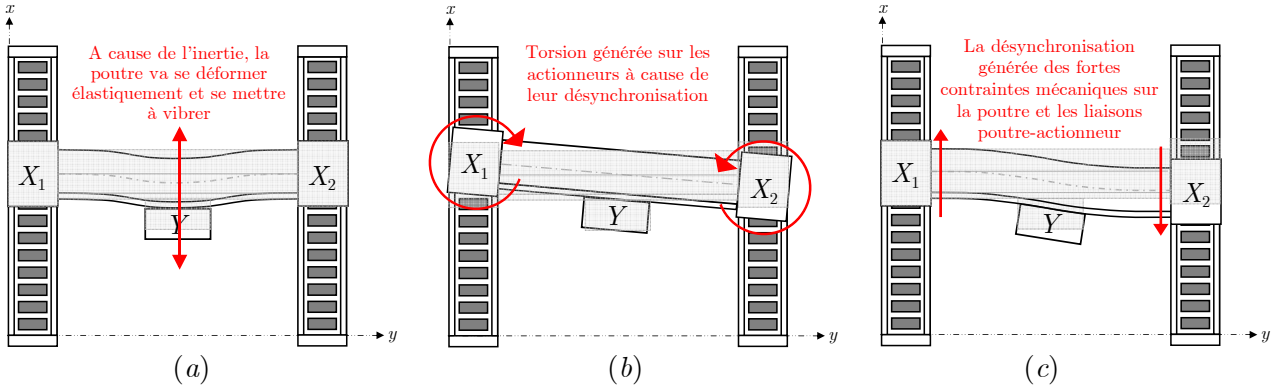

Figure 1 – 13 : *Déformation de l'axe en gantry bi–actionné avec des liaisons rigides. Trois situations sont possibles : à cause de l'inertie, la poutre se déforme élastiquement et se met à vibrer* (a) *; les actionneurs sont désynchronisés, la poutre ne se déforme pas et génère de la torsion sur les actionneurs* (b) *; les actionneurs sont désynchronisés, la poutre se déforme subissant des fortes contraintes mécaniques* (c)*. Dans la réalité, on trouve un mélange des situations* (a)*,* (b) *et* (c)*.*

La solution au problème du gantry bi–actionné avec des liaisons rigides a été simplement de remplacer les liaisons rigides par des liaisons flexibles. La fréquence fondamentale de vibration de la poutre est légèrement abaissée, mais une désynchronisation est maintenant permise. Ainsi, la force de torsion associée à cette désynchronisation est absorbée par les liaisons flexibles, voir **Figure 1 – 14 .**

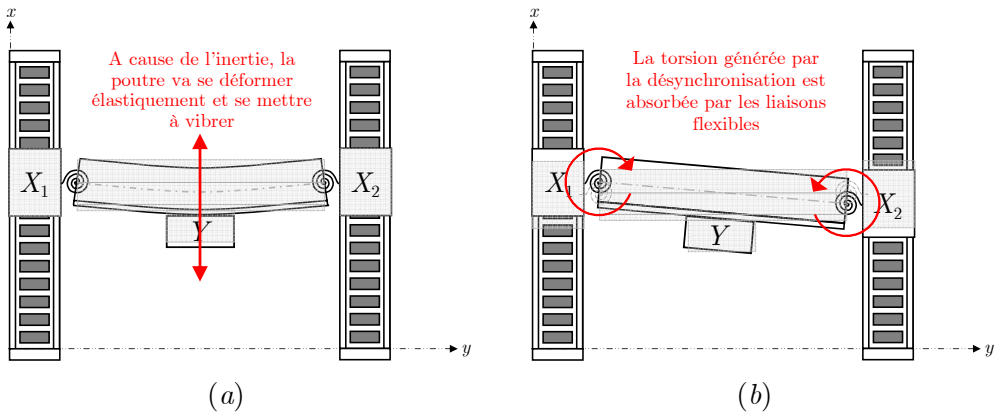

(a) (b)

Figure 1 – 14 : *Déformation de l'axe en gantry bi–actionné avec des liaisons flexibles. Deux situations sont possibles : à cause de l'inertie, la poutre se déforme élastiquement et se met à vibrer* (a) *; les actionneurs sont désynchronisés, la poutre ne se déforme pas et génère de la torsion sur les liaisons flexibles* (b)*. Dans la réalité, on trouve un mélange des situations* (a) *et* (b)*.*

L'axe en gantry bi–actionné avec des liaisons flexibles pose deux problèmes spécifiques qui dégradent ses performances en positionnement :

(1) Le couplage mécanique entre les actionneurs;

(2) la flexibilité de la poutre.

Ces deux problématiques couvrent un large spectre :

Si la poutre est très rigide, les performances de positionnement seront dégradées par le couplage mécanique entre les actionneurs. En effet, la répartition inégale de la charge entre les actionneurs mis en collaboration est vue comme une perturbation induite par un actionneur sur l'autre et vice–versa par le biais de la poutre rigide, voir **Figure 1 – 15**. De plus, une poutre rigide est généralement synonyme de masse importante. Par conséquent, le coût énergétique de chaque opération est considérable. Pour certains axes en gantry, la masse de la poutre et des actionneurs utilisés pour porter des composants qui ne font que quelques grammes peut atteindre facilement 200 kilogrammes.

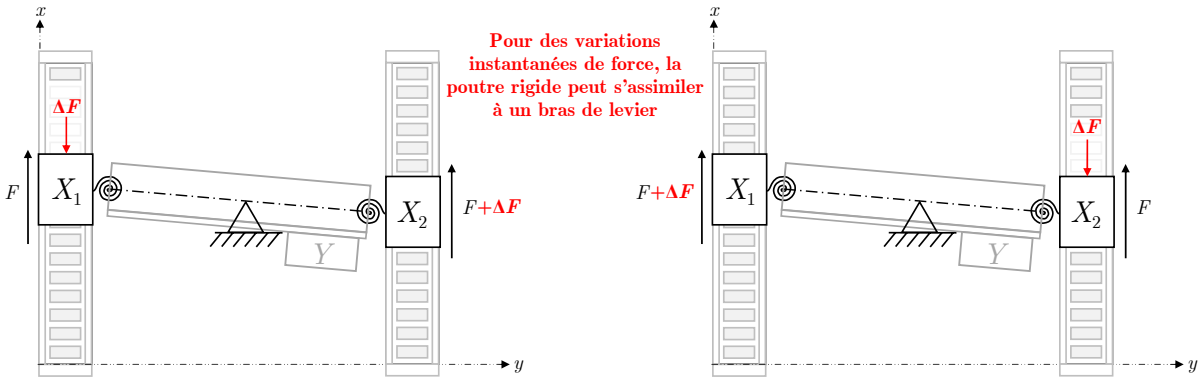

Figure 1 – 15 : *Quand la poutre reliant les actionneurs est très rigide, celle–ci sert à les coupler mécaniquement.*

Si la poutre est choisie très légère, et donc plus flexible, l'énergie consommée et le couplage mécanique se verront réduits considérablement, voir **Figure 1 – 16**. Cependant, les vibrations de la poutre auront un impact plus important sur la performance de positionnement. De plus, les

fréquences de vibration de la poutre vont varier en fonction de la position de l'axe Y sur la poutre, ce qui rend très difficile la commande en position de la pointe–outil.

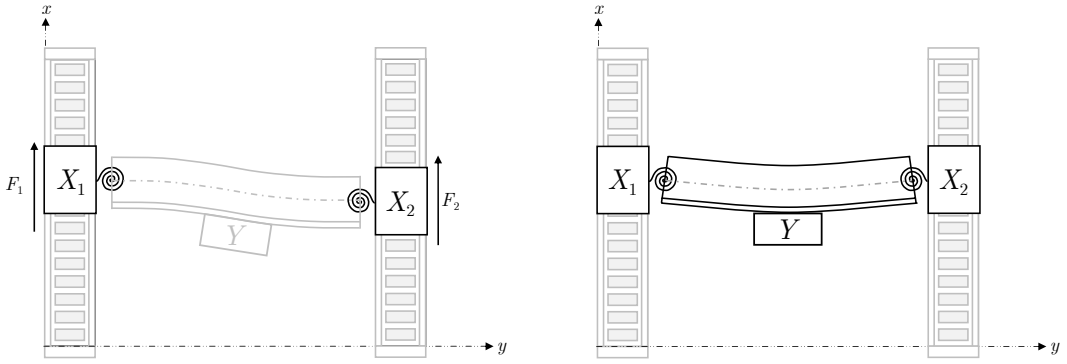

(a) (b)

Figure 1 – 16 : *Quand la poutre reliant les actionneurs est très flexible, les actionneurs sont virtuellement découplés l'un de l'autre* (a). *Cependant, l'amplitude des oscillations de la poutre est importante* (b).

Il est évident que des poutres parfaitement rigides ou flexibles sont des cas idéaux. Dans la pratique, on trouve un mélange des deux situations et les facteurs affectant la performance en positionnement de la pointe–outil peuvent être déterminés en fonction de la souplesse de la poutre. Dans (§1.1), on explique qu'une solution pour rendre la poutre à la fois rigide et légère est l'utilisation de matériaux composites. Cependant, les développements de cette technologie font de celle–ci une solution encore coûteuse. Pour l'instant, la solution la plus intéressante est de trouver un compromis entre rigidité et légèreté avec des matériaux conventionnels et de gérer les problématiques associées par la commande.

1.4 Conclusion

Dans les systèmes de positionnement, lorsque le rapport "espace de travail/précision" est trop élevé, le comportement vibratoire devient critique et les techniques de commande trouvent leurs limites car elles ne permettent plus d'assurer la précision demandée. Il est donc nécessaire d'introduire de nouveaux types de structures de type parallèle ou hybride qui rigidifient la structure mécanique tout en introduisant des degrés de liberté supplémentaires. Dans le cas de l'axe en gantry, passer d'une structure (série) mono–actionnée à une structure (hybride) bi–actionnée apporte de la rapidité et de la rigidité (de l'axe transversale) pour un encombrement et un coût quasiment identiques.

Cependant, les techniques actuelles de conception et de commande de ces systèmes multi–actionnés ne permettent pas de déterminer a priori la nature et la rigidité des liaisons entre les éléments, le respect de contraintes en termes d'échauffement des matériels, consommation énergétique ou maîtrise de la pointe–outil.

Ces difficultés se traduisent aujourd'hui par un verrou technologique comportant deux volets :

- Le besoin de nouvelles stratégies de commande capables de limiter les vibrations de la pointe–outil tout en gérant au mieux les degrés de liberté supplémentaires.
- Le besoin de modélisation et de formalismes de représentation adaptés permettant d'utiliser une approche de conception intégrant la dynamique des structures et capable de déterminer le nombre et la nature des degrés de libertés complémentaires.

Dans le chapitre suivant, nous évaluerons les approches proposées dans l'état de l'art pour la commande des systèmes du type axe en gantry.

2. Etat de l'art de la commande des axes en gantry

Notre objectif est d'établir un outil méthodologique adapté à la modélisation et à la commande des systèmes de positionnement multi–actionnés de type « axe en gantry ».

Pour y parvenir, il est indispensable de comprendre les problématiques associées à la commande d'une structure flexible multi–actionnée, à savoir :

- Problématiques associées à la commande des systèmes flexibles
- Problématiques associées à la commande des systèmes multi–actionnés

Dans le chapitre précédent (§ 1.3), quelques aspects concernant ces problématiques et comment elles affectent la performance en positionnement des axes en gantry ont été discutés.

L'objectif de ce chapitre est de présenter la façon dont ces problématiques sont abordées dans la littérature scientifique et industrielle. Il est organisé de la façon suivante :

(§ 2.1) ***Commande des axes en gantry dans la littérature***

Dans cette partie, nous discuterons uniquement et rapidement des aspects associés à la commande des axes en gantry mono– et bi–actionnés sans développer les aspects liés à la modélisation. En effet, le modèle étant au cœur de la méthodologie proposée dans ce mémoire, une analyse détaillée des différentes stratégies de modélisation des axes en gantry sera proposée dans les parties (§ 2.2) à (§ 2.5).

(§ 2.2) ***Modélisation des axes en gantry dans la littérature***

Dans cette partie, une revue des modèles d'axe en gantry disponibles dans la littérature est faite. Elle montre l'absence de modélisations physiques détaillées pour la commande.

(§ 2.3) ***Eléments bibliographiques additionnels***

Un des objectifs principaux de ce mémoire est de prendre en compte les phénomènes vibratoires associés à la flexibilité structurelle de l'axe en gantry dans sa modélisation, et par extension, dans sa commande. Dans la bibliographie concernant les axes en gantry, les auteurs qui ont pris en compte ces phénomènes sont rares. Aussi, nous explorerons donc dans la littérature générale les méthodes de modélisation et de commande existantes pour des systèmes flexibles.

(§ 2.4) ***Commande d'un axe en gantry bi–actionné rigide basée sur une modélisation physique causale***

Ce travail de recherche est la troisième collaboration entre la société ETEL et le laboratoire L2EP. La collaboration précédente, faite dans le cadre de la thèse de J. GOMAND (Gomand, 2008) se portait sur l'étude des propriétés graphiques du formalisme GIC. Afin de valider la démarche proposée, J. Gomand propose la commande d'un axe en gantry pour des applications de pose–dépose de composants électroniques avec des résultats très encourageants. Cette démarche a en effet servi comme première étape au développement d'outils méthodologiques de modélisation et commande pour les axes en gantry. Première étape car les travaux de J. Gomand ne prennent pas en compte la dynamique de l'actionneur Y de l'axe en gantry ni la flexibilité de la poutre connectant les actionneurs parallèles.

(§ 2.5) ***Approche proposée pour l'étude***

L'approche adoptée dans notre étude est basée sur une modélisation physique détaillée de l'axe en gantry. Cette modélisation, associée à des formalismes de représentation graphique causale et des méthodes d'identification expérimentale permettra de développer des structures de commande adaptées aux problématiques spécifiques des axes en gantry.

2.1 Commande des axes en gantry dans la littérature

2.1.1 Commande d'axes en gantry mono–actionnés

Dans les premières étapes du développement des axes en gantry mono–actionnés, les actions pour améliorer leurs performances de positionnement n'ont pas été effectuées sur la commande mais sur la structure mécanique. En effet, une des premières approches a été de rendre la poutre et la liaison poutre–actionneur très rigide.

En réponse à cette rigidification – et alourdissement – du gantry mono–actionné, (Yoshikawa, et al., 1993) proposa qu'au lieu de renforcer la poutre et la liaison poutre–actionneur, une approche plus efficiente serait d'appliquer une loi de commande capable de prendre en compte les déplacements élastiques de la poutre et de la liaison poutre–actionneur. Dans ce but, il propose de modéliser la poutre comme étant rigide et de rapporter toute la flexibilité au niveau de la liaison poutre–actionneur, voir **Figure 2 – 1** (*a*). Afin d'appliquer la théorie de la commande optimale, les équations de mouvement du modèle sont linéarisées autour du point de fonctionnement souhaité (déplacement de la poutre sans déformation élastique de la jonction poutre–actionneur).

Deux types de loi de commande sont alors proposés : un contrôle de mouvement point–à–point et un contrôle de mouvement en trajectoire. Dans le premier cas, le problème est formulé comme un problème de commande en temps minimal. Il faut aller d'un point A vers un point B le plus rapidement possible tout en minimisant l'erreur de positionnement (ou les déformations élastiques) et la consommation énergétique. Dans le deuxième cas, le problème est formulé comme un problème de commande de trajectoire optimale. La trajectoire de référence est modifiée de façon à ce que la déformation élastique soit prise en compte et contrée lors de déplacements passant par une trajectoire prédéfinie. Afin de réaliser une commande sans capteur, un observateur d'ordre minimal est proposé pour estimer les déformations élastiques de la jonction poutre–actionneur.

Une approche similaire est proposée par (Rieber, et al., 2001); la modélisation de l'axe en gantry est donnée par le modèle à paramètres distribués de la **Figure 2 – 1** (*b*). Mathématiquement, la poutre est modélisée comme un corps flexible ayant un mode rigide (translation en x) et une infinité de modes flexibles (vibrations en x à des fréquences de résonance données). Ces vibrations sont excitées par la force de poussée générée par l'actionneur X et leurs fréquences de résonance vont varier en fonction de la position du chariot Y au long de la poutre. Afin d'appliquer la théorie de la commande optimale, ce modèle est linéarisé autour du point de fonctionnement souhaité (déplacement de la poutre sans déformations élastiques). Ensuite, un critère de performance cherchant à minimiser la déformation élastique de la poutre pendant le mouvement est utilisé pour programmer les gains de la commande en retour d'état.

Dans les deux cas, les auteurs proposent uniquement des résultats de simulation. Néanmoins, la conclusion des deux études est qu'une amélioration de la performance de positionnement par la commande est une solution économiquement plus viable en termes de productivité et du poids total du manipulateur.

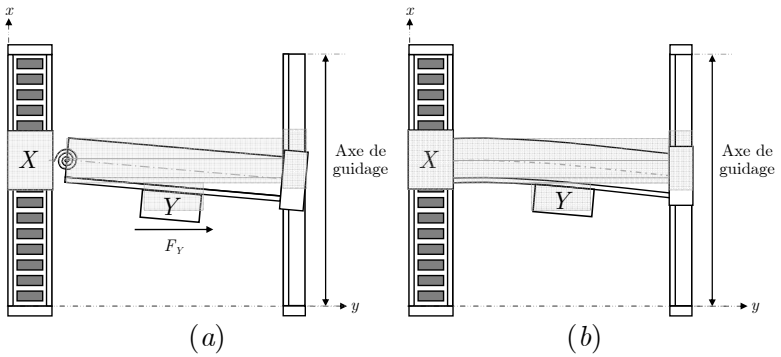

Figure 2 – 1 : *Modèle dynamique du gantry mono–actionné*
(*a*) *à paramètres localisées* (Yoshikawa, et al., 1993)
(*b*) *à paramètres distribués* (Rieber, et al., 2001)

2.1.2 Commande d'axes en gantry bi–actionnés

Malgré l'efficacité des commandes proposées pour les axes en gantry mono–actionnés (en termes de réduction des vibrations de la pointe–outil), ceux–ci étaient toujours pénalisés par une mauvaise répartition de la charge par rapport à l'axe de poussée, voir **Figure 1 – 12** (*a*). Ce qui limitait la dynamique de déplacement de l'axe. L'évolution vers la configuration bi–actionnée était, en effet, inévitable.

Avec l'évolution du gantry vers la configuration bi–actionnée, l'intérêt pour le contrôle des vibrations de la pointe–outil a diminué très rapidement. En effet, l'ajout d'un actionneur supplémentaire sert à rigidifier la poutre (Park, et al., 2001). La dégradation de la performance de positionnement de la pointe–outil, attribuée auparavant à la flexibilité de la poutre, est à présent liée à sa rigidité et donc à la compensation de l'erreur de synchronisme entre les actionneurs parallèles.

Dans l'industrie, l'approche favorisée est de contrôler chaque actionneur indépendamment. Les signaux de référence sont alors identiques et le couplage mécanique entre les actionneurs est ignoré, voir **Figure 2 – 2**. Ceci induit des erreurs de synchronisation entre les axes parallèles. Spécifiquement, ces erreurs sont liées à une répartition inégale de la masse à transporter entre les deux moteurs (y compris la charge) et la différence entre les forces de friction des deux moteurs. En effet, les ensembles contrôleur–actionneur en parallèle sont généralement réglés avec les mêmes paramètres une fois pour toutes. Ils ont donc des constantes de temps similaires; alors, cette répartition inégale de charges induit des perturbations d'un actionneur à l'autre qui sont difficiles à compenser de façon efficace.

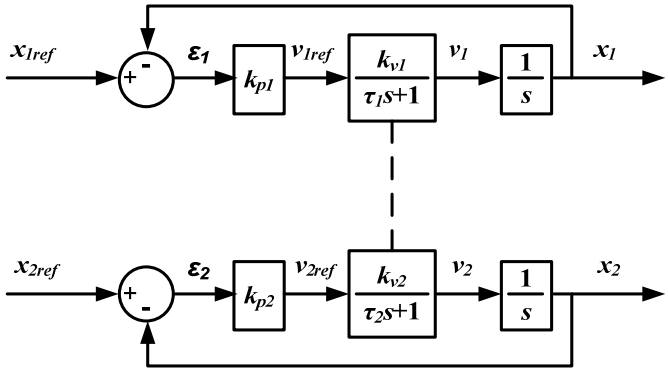

Figure 2 – 2 : *Structure de commande maître–maître pour un gantry bi–actionné* (Tan, et al., 2004)

Afin d'améliorer les performances de ce type de commande, (Teo, et al., 2007) propose un réglage adaptatif des gains des contrôleurs indépendants ayant comme critère de minimisation l'erreur de synchronisation entre les axes. Cette méthode a l'avantage particulier de ne pas requérir une identification précise des paramètres du système.

Il existe une approche plus efficace pour conserver des contrôleurs indépendants et dissocier les constantes de temps associées aux ensembles contrôleur–actionneur : commander la machine dans un repère fictif $X - \Theta$ comme proposé dans le brevet industriel (Tanquary, et al., 2000) et dont la structure de commande est présentée dans la **Figure 2 – 3**. Le réglage de ce type de commande, comme la plupart des commandes de type industriel, est fait par une approche très pragmatique, liée au respect d'un cahier des charges donné.

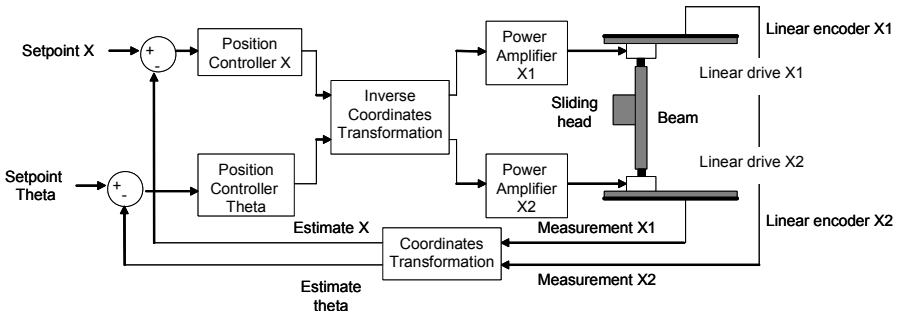

Figure 2 – 3 : *Structure de commande dans le repère fictif X – Θ* (Tanquary, et al., 2000)

A part cette commande un peu particulière, la grande majorité des commandes que l'on trouve dans la littérature ont comme structure de départ la commande à axes indépendants de la **Figure 2 – 2** à laquelle on vient ajouter un contrôleur supplémentaire. Celui–ci peut être soit du type commande synchronisante, soit du type compensation du couplage. Structurellement, la ligne de distinction entre ces deux commandes peut sembler très mince. Cependant, l'objectif de commande n'est pas le même. Les commandes synchronisantes cherchent avant tout à forcer la synchronisation entre les deux actionneurs sans prendre en compte le couplage. Les commandes du type compensation du couplage cherchent à minimiser les effets du couplage entre les actionneurs parallèles afin de simplifier la tâche aux contrôleurs indépendants.

2.1.2.1 Commandes synchronisantes

Les commandes synchronisantes sont associées à la commande à axes indépendants afin de forcer la synchronisation entre les actionneurs parallèles. Elles sont caractérisées par l'absence d'informations sur le phénomène de couplage ou de son origine.

(Chu, et al., 2004) propose une commande synchronisante basée sur la formulation de la commande optimale. Les actionneurs parallèles sont modélisés indépendamment en utilisant l'approximation de premier ordre en vitesse, voir **Figure 2 – 4**. L'index de performance J à minimiser (2.1) inclut l'erreur de synchronisation $\Delta X = X_1 - X_2$, les efforts de synchronisation u_1 et u_2, et des coefficients de pondération r_1 et r_2.

$$J = \sum_{k=0}^{\infty} \left\{ r_1 \left[\Delta X(k) \right]^2 + r_2 \left[u_1^2(k) + u_2^2(k) \right] \right\} \tag{2.1}$$

Les coefficients de pondération r_1 et r_2 sont à choisir par l'automaticien. En effet, le choix de ces critères de pondération est plutôt arbitraire. Par exemple, si les facteurs de pondération sont choisis $r_1 = 1$ et $r_2 = 0$, cela veut dire que l'objectif de la commande est de minimiser l'erreur de synchronisation quel que soit le coût énergétique. Inversement, si $r_1 = 0$ et $r_2 = 1$, on se passe entièrement de la commande synchronisante, ce qui nous laisse avec la commande à axes indépendants de base. Les auteurs ne délivrent pas de commentaires ou d'indications supplémentaires sur le choix des coefficients r_1 et r_2, ce qui rend difficile le réglage des asservissements, sinon à utiliser une méthode heuristique.

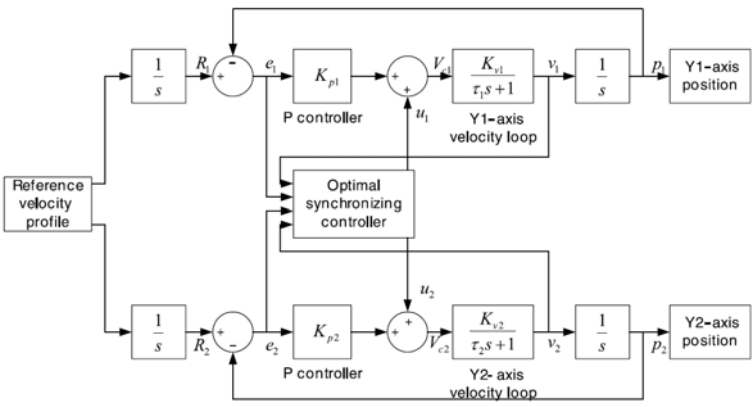

Figure 2 – 4 : *Commande synchronisante LQR* (Chu, et al., 2004)

Un tout autre type de commande synchronisante est proposé par (Wang, et al., 2009). Ce dernier propose une commande synchronisante à logique floue, voir **Figure 2 – 5**. Dans ce type de contrôleur, les variables conventionnellement numériques sont remplacées par des variables linguistiques. Dans ce contexte, l'erreur de synchronisation est linguistiquement représentée comme étant presque nulle, petite, moyenne, ou grande; et positive ou négative. Avec cette information, le moteur d'inférence (le contrôleur) va générer une sortie appropriée. Par exemple, si l'erreur de synchronisation est grande et positive, le moteur d'inférence va recommander soit d'augmenter la force F_1, soit de réduire la force F_2, soit de les moyenner. Ceci est fait selon le réglage, qui, dans le cas de (Wang, et al., 2009), est fait à l'aide d'algorithmes génétiques. Ensuite, la phase de « defuzzyfication » permet de traduire ces recommandations dans des signaux numériques. Ce type de contrôleur, avec son réglage par algorithmes génétiques, fait penser à la commande optimale présentée précédemment. Une approche similaire, mais cette fois–ci en utilisant des réseaux de neurones, peut être trouvée dans (Lin, et al., 2011).

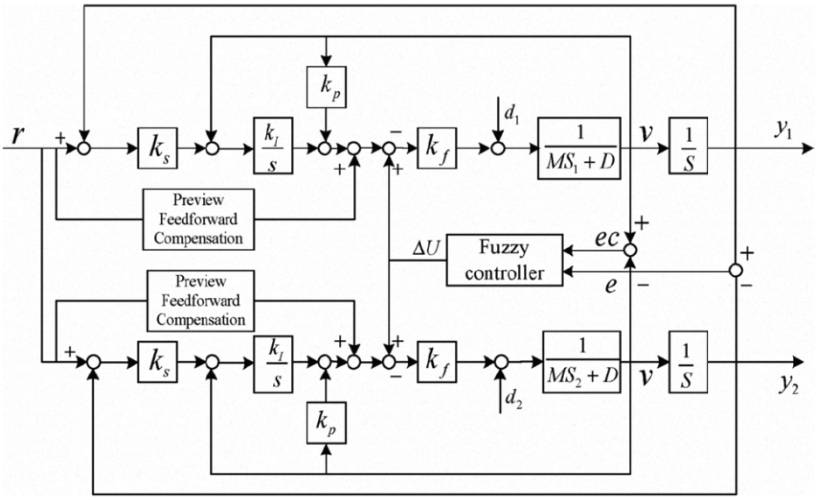

Figure 2 – 5 : *Commande synchronisante à logique floue* (Wang, et al., 2009)

Un des grands inconvénients de ce type de commande est que cet asservissement supplémentaire de la synchronisation s'insère dans une structure qui comporte déjà un asservissement de position et de vitesse pour chaque moteur. Il ne peut donc agir de manière indépendante sur des variables d'état du système qui ne sont pas indépendantes de celles déjà contrôlées. De plus, l'objectif des asservissements de position et de vitesse des deux moteurs comprend déjà l'objectif de synchronisation car les deux axes disposent de deux trajectoires de référence identiques. L'action de l'asservissement de l'erreur de synchronisme est cependant différente : lorsque les asservissements de position et de vitesse tendent à synchroniser les deux moteurs par un suivi de la même trajectoire, celui de synchronisation exerce une action opposée sur les deux axes en accélérant le moteur le plus en retard et en ralentissant le second, s'opposant ainsi à l'action de son asservissement de position. Si cette action peut améliorer la synchronisation des deux moteurs, elle dégrade nécessairement les performances énergétiques de l'axe en gantry.

2.1.2.2 Commandes par compensation du couplage

Les commandes par compensation du couplage cherchent avant tout à minimiser les effets du couplage mécanique sur les actionneurs parallèles. Ainsi, il est plus facile pour les contrôleurs indépendants de synchroniser les actionneurs parallèles. Souvent, à cette compensation du couplage, on associe une commande robuste des boucles indépendantes de façon à ce que ces derniers soient insensibles aux variations des paramètres associés aux mouvements de la charge tout au long de la poutre et aux effets résiduels du couplage mécanique. Une telle structure est proposée par (Yu, et al., 2003) : le modèle initial du gantry est proposé dans l'espace d'état sous la forme de la **Figure 2 – 6**.

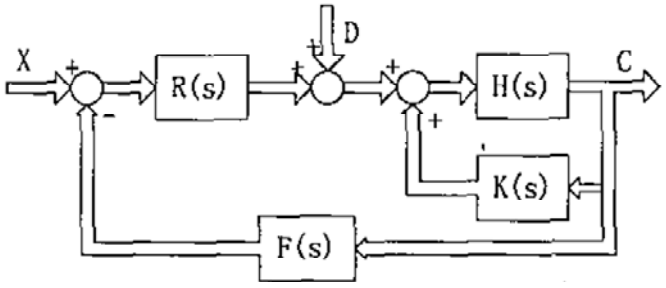

Figure 2 – 6 : *Modèle du gantry bi–actionné et découplage par retour d'état* (Yu, et al., 2003)

Où,

$\boldsymbol{X}$ est le vecteur d'entrée (positions de référence : $X_{1\ réf}$ et $X_{2\ réf}$)
$\boldsymbol{C}$ est le vecteur de sortie (positions mesurées : $X_{1\ mes}$ et $X_{2\ mes}$)
$\boldsymbol{R}$ sont les contrôleurs indépendants
$\boldsymbol{H}$ sont les actionneurs parallèles
$\boldsymbol{K}$ est le couplage entre les actionneurs
$\boldsymbol{F}$ est la matrice de découplage (retour d'état à déterminer)

La sortie $\boldsymbol{C}$ du système de la **Figure 2 – 6** est donnée par (2.2)

$$\boldsymbol{C} = \left[\boldsymbol{I} + \boldsymbol{H}\left(\boldsymbol{RF} - \boldsymbol{K}\right)\right]^{-1}\left(\boldsymbol{HRX} + \boldsymbol{HD}\right) \tag{2.2}$$

Pour avoir un système qui est découplé dans le sens des entrées $\boldsymbol{X}$ et des perturbations $\boldsymbol{D}$, les produits matriciels $[\boldsymbol{I}+\boldsymbol{H}(\boldsymbol{RF} - \boldsymbol{K})]^{-1}\boldsymbol{HRX}$ et $[\boldsymbol{I}+\boldsymbol{H}(\boldsymbol{RF} - \boldsymbol{K})]^{-1}\boldsymbol{HD}$ doivent produire des matrices diagonales. Ce qui se réduit à rendre l'expression $(\boldsymbol{RF} - \boldsymbol{K})$ diagonale étant donné que les matrices $\boldsymbol{H}$ et $\boldsymbol{R}$ sont déjà diagonales. La matrice $\boldsymbol{F}$ qui remplie cette condition est donnée par (2.3)

$$\boldsymbol{F} = \boldsymbol{R}^{-1}\left(\boldsymbol{K} + \boldsymbol{I}\right) = \begin{bmatrix} 1 & V_{12}/R_{11} \\ V_{21}/R_{22} & 1 \end{bmatrix} = \begin{bmatrix} 1 & f_{12} \\ f_{21} & 1 \end{bmatrix} \tag{2.3}$$

Ce qui produit la structure de commande suivante, **Figure 2 – 7**.

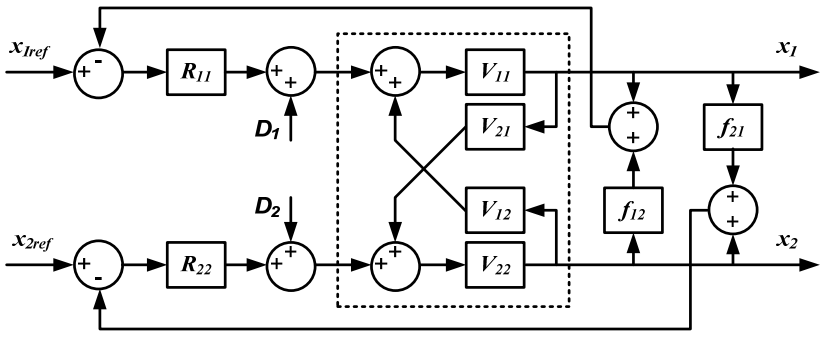

Figure 2 – 7 : *Compensation du couplage mécanique par retour d'état* (Yu, et al., 2003)

L'inconvénient majeur de cette approche est que le couplage est considéré invariant et présenté d'une façon qui est difficilement généralisable à des paramètres physiques de la machine (fonction de transfert). Ce couplage invariant peut s'interpréter comme le cas particulier où la charge est placée au milieu de la poutre (position $Y = 0$) ou dans le cas où sa masse est négligeable par rapport à la masse de la poutre. Dans ce cas, ce qui est identifié est le couplage dû aux différences de masse et des coefficients de friction entre les actionneurs parallèles. C'est apparemment ce que les auteurs compensent par le biais de la matrice de découplage $\boldsymbol{F}$. Le couplage induit par le mouvement de la charge au long de la poutre est interprété comme une variation des paramètres associés aux actionneurs parallèles. Pour compenser cette "variation" des paramètres, l'auteur propose une commande robuste des boucles de position indépendantes, l'objectif étant de rendre la commande en position la moins sensible aux variations des paramètres.

Une approche similaire est proposée dans (Ximei, et al., 2006). Cette fois–ci, le couplage dynamique est modélisé et compensé par le biais d'un observateur d'état.

2.1.2.3 Prise en compte des vibrations de la pointe–outil dans la commande des axes en gantry bi–actionnés

A notre connaissance, peu d'auteurs se sont intéressés à la prise en compte de la flexibilité de l'axe en gantry bi–actionné dans la commande. (Stöppler, et al., 2008) propose de contrôler activement les vibrations de la pointe–outil à l'aide d'un actionneur piézo–électrique. Il faut noter que cet auteur ne fait aucune référence à la commande des actionneurs parallèles. Dans cette application particulière, les positions mesurées des actionneurs parallèles et la mesure d'accélération de la pointe–outil sont injectées dans un modèle à trois masses–deux ressorts afin d'obtenir une estimation de l'erreur de positionnement de la pointe–outil.

Malheureusement, le modèle choisi ne permet de simuler qu'une seule fréquence de résonance de valeur fixe. Alors que dans la pratique, la poutre en gantry, selon sa flexibilité, peut présenter plusieurs fréquences de résonance. De plus, ces dernières vont varier non–linéairement en fonction de la position de la charge au long de la poutre. Alors, pour prendre en compte ces phénomènes dans la compensation des oscillations, l'auteur décide de remplacer son modèle physique par une structure d'observateur classique. Dans un sens purement mathématique, cet observateur permet d'estimer ces phénomènes et donc de réduire les oscillations de la pointe–outil. L'inconvénient dans ce cas est que cet observateur est réglé pour des conditions de travail prédéfinies; si elles changent, l'observateur doit être réglé à nouveau. Ce qui requiert l'intervention d'un automaticien expérimenté et des outils de mesure souvent coûteux – interféromètre laser dans le cas de (Stöppler, et al., 2008) –, ce qui à son tour freine dramatiquement l'applicabilité industrielle. Un modèle physique assez détaillé aurait conféré l'avantage d'une prise en compte rapide et naturelle des modifications.

2.1.3 Conclusion sur la commande d'axes en gantry

Dans la mesure où elles exécutent l'objectif de commande établi, les commandes présentées précédemment sont, en effet, très performantes.

Nonobstant, des critères de performance plus subjectifs (tels que la facilité d'implémentation, la simplicité algorithmique, ou même la consommation énergétique) sont ternis par l'absence de compréhension de la technologie et du comportement du système. Dans la plupart des cas, cette compréhension se trouve remplacée par des méthodes permettant de se passer de la connaissance du processus physique. Ce manque de compréhension du problème mène à ce que les résultats obtenus ne soient pas toujours réalistes ou appropriés à un travail pratique (contrôleurs structurellement complexes, complexité de réglage, contresens physiques, difficultés d'identification, etc.). Les commandes synchronisantes correspondent à un exemple d'incompréhension. Elles cherchent à contrôler indépendamment des variables qui ne sont pas indépendantes car contrôlées par ailleurs. Certes la synchronisation est améliorée, mais au détriment des performances énergétiques.

En effet, la réalisation d'une bonne commande est étroitement liée à la compréhension du comportement du système et donc à la qualité de sa modélisation et aux hypothèses simplificatrices qui lui sont associées. De plus, l'identification des paramètres du modèle est une phase importante pour définir la qualité du modèle (Borne, et al., 1992). Dans cette modélisation (généralement mathématique), il est avantageux d'apporter le plus grand nombre de simplifications car ainsi la complexité du modèle final sera diminuée. Cependant, si une telle simplification est poussée trop loin, le modèle résultant ne tiendra plus compte de la réalité. C'est alors en revenant sur ces simplifications de modèle et sur la précision d'identification que l'on pourra améliorer les performances de la commande (Bouscayrol, 2003).

Alors, afin de pallier ce manque de compréhension des phénomènes physiques existants au sein du système, la suite du chapitre se concentre sur les approches de modélisation existantes pour les axes en gantry.

2.2 Modélisation des axes en gantry dans la littérature

2.2.1 Modélisation des axes en gantry mono–actionnés dans la littérature

Pour la prise en compte des déformations élastiques de la poutre en porte–à–faux, deux approches sont favorisées dans la littérature.

La première approche consiste à reporter/transférer la flexibilité de la poutre et celle de la liaison poutre–actionneur vers une unique raideur torsionnelle localisée à la place de la liaison poutre–actionneur, voir **Figure 2 – 8** (a). Dans (Yoshikawa, et al., 1993), les équations de mouvement d'un tel système sont dérivées en utilisant le formalisme de Lagrange–Euler.

La deuxième approche, plus proche de la physique du système, consiste à considérer la liaison poutre–actionneur rigide et à considérer la poutre flexible. Cette modélisation à paramètres distribués de la **Figure 2 – 8** (b) est proposée par (Rieber, et al., 2001). La poutre est modélisée selon le modèle d'Euler–Bernoulli (voir Annexe A.1) et transformée par la suite en un système de n–équations différentielles découplées à l'aide de la méthode de Galerkin (Reddy, 2002).

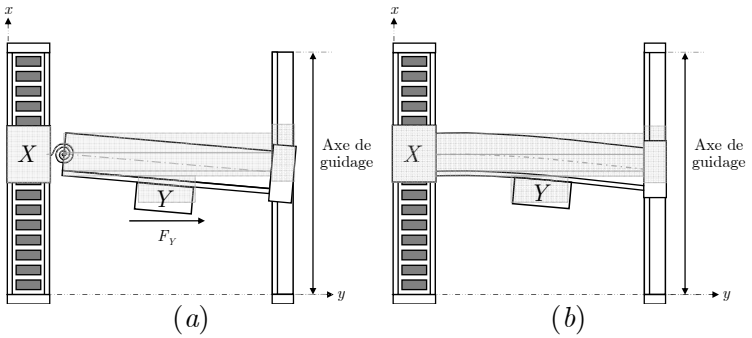

Figure 2 – 8 : *Modèle dynamique du gantry mono–actionné à paramètres localisées* (a) *et à paramètres distribués* (b)

Des modélisations semblables, mais pas spécifiques au gantry mono–actionné, peuvent être trouvées dans (Park, et al., 1999) et dans (Colas, 2006).

(Park, et al., 1999) propose le modèle chariot–poutre–masse mobile de la **Figure 2 – 9**. Ce modèle n'est lié à aucune application spécifique. L'auteur propose cette modélisation – très détaillée – comme une alternative aux modèles « poutre fixe – charge mobile » proposés dans la littérature dans le cadre de l'analyse vibratoire de ponts, de chemins de fer, ou d'axes de guidage (Frýba, 1999).

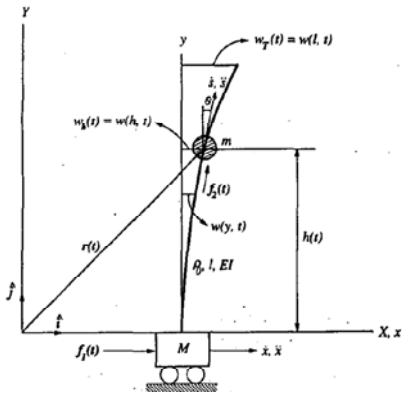

Figure 2 – 9 : *Modèle chariot – poutre flexible – masse mobile* (Park, et al., 1999)

(Colas, 2006) propose pour un manipulateur cartésien, **Figure 2 – 10** (a), trois approches différentes de modélisation (b), (c) et (d). Il montre ainsi, comment pour un même système, on peut produire soit un modèle très général – ou à constantes réparties, **Figure 2 – 10** (b) –, soit un modèle plus local – ou à paramètres localisés, **Figure 2 – 10** (d). Il est évident que le domaine de validité et le degré de complexité de chaque modèle ne sont pas du tout les mêmes.

Cet exemple est très intéressant parce que son comportement est en tout point semblable à celui du gantry mono–actionné. Les deux systèmes ont une partie en mouvement dont le comportement est assimilable à celui d'un corps rigide en translation. De plus, ils ont tous les deux une partie dont le comportement est assimilable à celui d'un corps flexible. Les vibrations de ce corps dit "flexible" ont des fréquences de résonance qui vont être variables. Dans le cas du manipulateur cartésien, cette variation sera due à la longueur variable du bras Z mobile, **Figure 2 – 10** (a), alors que pour le gantry mono–actionné, cette variation sera due à la position variable de la charge tout au long de la poutre.

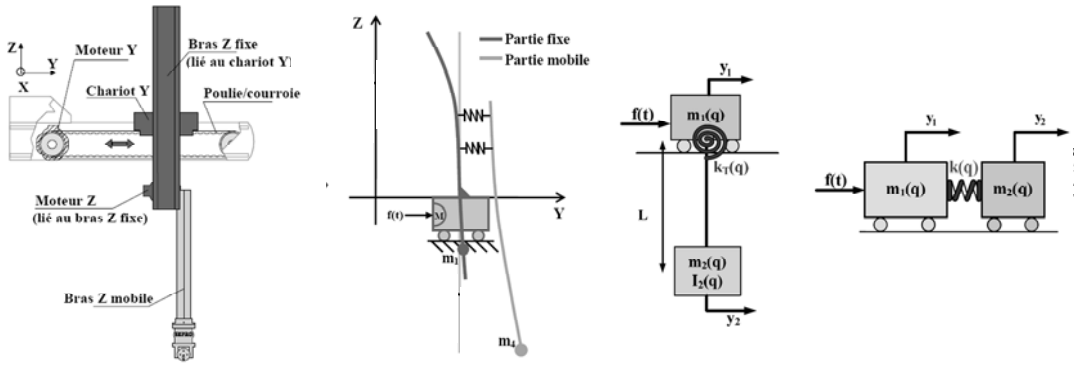

(a) (b) (c) (d)

Figure 2 – 10 : *Modèle d'un robot cartésien.* (*a*) *représentation schématique* (*b*) *modèle à paramètres distribués* (*c*) *modèle à paramétrés localisés avec prise en compte du non–minimum de phase* (*d*) *modèle souple classique*

Pour la commande du robot cartésien; (Colas, 2006) a utilisé le modèle deux masses–ressort, **Figure 2 – 10** (*d*). Ce modèle représente le mode rigide (translation de l'ensemble chariot Y et bras Z) et le mode de vibration dominant de la poutre – ou au moins le déplacement du point–outil dû à celui–ci –. Ce déplacement du point–outil dû à la flexibilité de la poutre est à maîtriser par la commande. Pour prendre en compte la variation en fréquence du mode de vibration dominant due à la longueur variable du bras Z mobile, (Colas, 2006) a estimé les paramètres $m_1(q)$, $m_2(q)$ et $k(q)$ en fonction de cette longueur. Ainsi, ce modèle local est valable pour tout l'espace de travail. Finalement, il a comparé différentes techniques de commande (boucles en cascade, placement de pôles, commande optimale, logique floue, etc.) et a déterminé la plus adaptée pour la suppression des ondulations de la charge dans le cadre d'une implémentation industrielle (facilité d'implémentation, réglage simple, etc.). Une conclusion intéressante d'une telle étude est que les commandes qui ont le mieux fonctionné sont celles basées sur une modélisation physique préalable avec des incertitudes structurées (la performance de base a été définie comme celle de la commande industrielle d'origine). Il faut noter que ces commandes sont tout à fait transposables à la commande du gantry mono–actionné.

2.2.2 Modélisation des axes en gantry bi–actionnés dans la littérature

Avec l'apparition du gantry bi–actionné, les effets les plus gênants vis–à–vis de la performance en positionnement ne sont plus associés uniquement à la déformation élastique de la poutre mais aussi à la synchronisation des axes parallèles. En effet, le fait de placer un actionneur de chaque côté de la poutre sert à la rigidifier (modification des conditions aux limites) et à répartir la masse en translation plus uniformément. Ce qui se traduit par une bande passante en positionnement plus élevée et donc un système plus rapide et plus précis. Cependant, cette rigidité sert aussi à transmettre les perturbations d'un actionneur à l'autre et donc à les coupler.

Malgré l'existence évidente de ce couplage, dans la littérature, peu d'auteurs le prennent en compte. Dans la plupart des cas, les actionneurs parallèles sont modélisés comme deux actionneurs indépendants et le couplage mécanique est considéré comme une perturbation extérieure, voir

Figure 2 – 11. On trouve par exemple ce type de modèle dans (Kim, et al., 2003), (Chu, et al., 2004), (Tan, et al., 2004) et (Yu, et al., 2006).

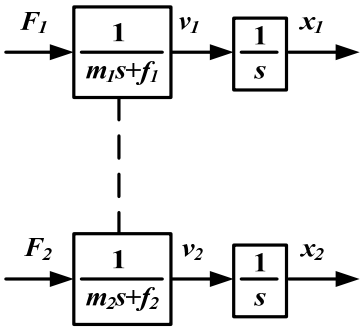

Figure 2 – 11 : *Modèle d'axe en gantry à deux actionneurs indépendants*

D'autres modèles, un peu plus complets modélisent le couplage avec deux fonctions de transfert croisées $(V_1/F_2)_{\mathrm{F1}=0}$ et $(V_2/F_1)_{\mathrm{F2}=0}$ associées à deux fonctions de transfert des actionneurs indépendants $(V_1/F_1)_{\mathrm{F2}=0}$ et $(V_2/F_2)_{\mathrm{F1}=0}$ (Yang, et al., 2003). Dans cette représentation mathématique, les vitesses V_1 et V_2 sont obtenues par superposition des sources d'effort F_1 et F_2, **Figure 2 – 12** (a). Un modèle mathématique plus proche de la physique est proposé dans (Yu, et al., 2003). En effet, le couplage entre les moteurs est représenté par des fonctions de transfert force/position, ce qui permet d'éviter une somme algébrique des positions (ou des vitesses) en faisant apparaître des efforts de couplage qui s'ajoutent aux efforts fournis par les actionneurs, **Figure 2 – 12** (b).

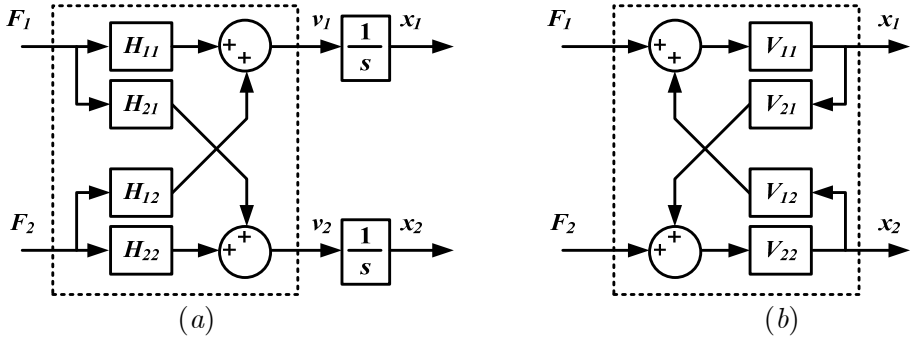

(a) (b)

Figure 2 – 12 : *Modèle d'axe en gantry avec prise en compte du couplage mécanique*
(a) *Par deux fonctions de transfert mécaniques croisées* (Yang, et al., 2003)
(b) *Par deux fonctions de transfert force/position* (Yu, et al., 2003)

Ces modèles mathématiques d'axes en gantry peuvent être plus ou moins précis selon l'ordre des fonctions de transfert utilisées. Evidement, le nombre de paramètres et, par conséquent, la difficulté de l'identification expérimentale augmentent avec l'ordre du modèle. L'inconvénient majeur de ce type de modélisation est que les paramètres des fonctions de transfert ne peuvent être associés d'une manière simple à des éléments physiques constituant l'axe, ce qui implique une perte de généralité de la modélisation.

(Teo, et al., 2007) propose un modèle simple et physique qui permet de quantifier le couplage mécanique généré par la poutre et la charge, voir **Figure 2 – 13**. Ce modèle est composé d'une poutre de masse m_b et d'une charge de masse m_h qui se déplace tout au long de la poutre. Ce modèle permet de prendre en compte l'asymétrie d'inertie induite par la charge. Ce modèle propose également le changement de repère des positions mesurées (X_1, X_2, Y) aux coordonnées relatives (X, Θ, Y) liées au centre géométrique de la poutre. Ce changement de repère permet d'écrire les équations de mouvement d'une façon plus synthétique et de mettre en évidence l'effet de l'asymétrie de masse sur l'erreur de synchronisation.

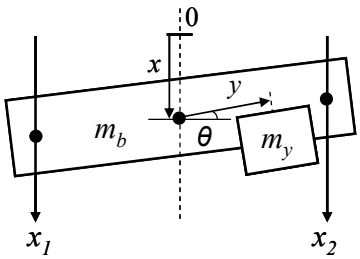

Figure 2 – 13 : *Modèle d'axe en gantry avec prise en compte du couplage mécanique* (Teo, et al., 2007)

Ce modèle est cependant limité au cas particulier des axes très rigides dont les effets dynamiques des actionneurs X_1 et X_2 peuvent être négligés par rapport à la poutre et à la charge, ce qui est le cas des gantry bi–actionnés qui utilisent des actionneurs sans fer.

Pour la prise en compte de la flexibilité de la poutre, peu d'études ont été menées dans le cadre d'une configuration en gantry bi–actionné. Par exemple, (Park, et al., 2001) donne l'équation d'une poutre de Timoshenko (Han, et al., 1999) avec des conditions aux limites définies par les raideurs torsionelles et linéaires k_θ et k_y, **Figure 2 – 14**. Aucune méthode de résolution n'est proposée. Des résultats de simulation montrant l'influence des raideurs k_θ et k_y sur le comportement vibratoire de la poutre sont présentés. La charge M est considérée immobile et fixe au centre de la poutre. Les actionneurs parallèles sont considérés parfaitement synchronisés voire fixes. Une étude beaucoup plus complète que celle–ci est présentée en annexe (Annexe B). Cette étude a été menée dans le cadre de la validation des hypothèses de modélisation des axes en gantry bi–actionnés flexibles proposées dans ce mémoire.

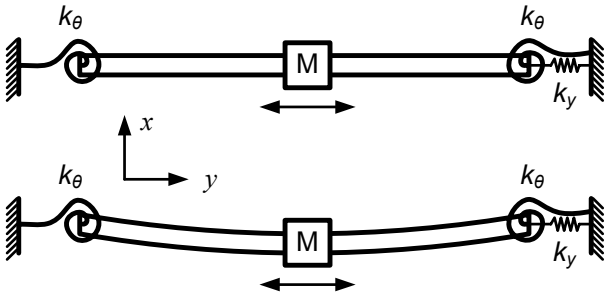

Figure 2 – 14 : *Modèle d'axe en gantry bi–actionné flexible* (Park, et al., 2001)

Ensuite, il y a le modèle de gantry à trois masses – deux ressorts proposé par (Stöppler, et al., 2008), **Figure 2 – 15**. Les masses m_l et m_r représentent celles des actionneurs parallèles. Les raideurs C_l et C_r représentent la raideur équivalente de la poutre ($C_l = C_r$), et, m_h est la masse équivalente combinée de la poutre et de la charge. L'objectif de ce modèle est d'estimer l'erreur de position de la pointe–outil à partir des positions mesurées des actionneurs parallèles et la mesure d'accélération de la pointe–outil.

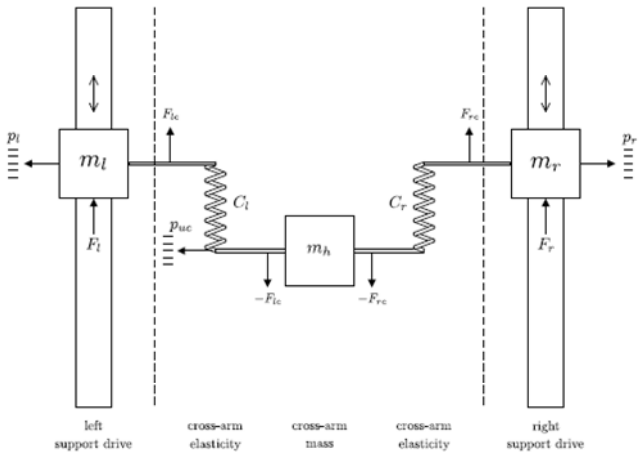

Figure 2 – 15 : *Modèle d'axe en gantry bi–actionné flexible* (Stöppler, et al., 2008)

Cependant, ce modèle est limité à un mode de vibration à fréquence fixe. Alors qu'en réalité, la poutre peut manifester plusieurs modes de vibration avec des fréquences de résonance variables, ces dernières variant non–linéairement en fonction de la position de la charge. Pour affiner son modèle, l'auteur a opté pour l'abandon de toute modélisation physique et décide d'estimer l'erreur de position de la pointe–outil à l'aide d'une structure d'observateur d'état. Une approche possible pour affiner le modèle aurait été d'identifier la variation des paramètres m_l, m_r, c_l, c_r, et m_h en fonction de la position de la charge; comme proposé par (Colas, 2006).

2.2.3 Conclusion sur les modélisations des axes en gantry

L'objectif d'une modélisation pour la commande est de mettre en évidence les variables du système sur lesquels on veut agir (les sorties), les variables qui génèrent une évolution de la sortie (les entrées), et le modèle de comportement (approximatif) décrivant la relation entre les entrées et les sorties.

L'accord entre la modélisation et le comportement observé du système se réalise par un processus d'itération. Ce processus, résultat d'une interprétation des phénomènes observés, s'arrête quand l'erreur induite par la représentation mathématique est suffisamment faible.

L'intérêt de ce processus d'itération est de caractériser d'une façon adéquate les propriétés du système étudié.

Cette caractérisation peut être de deux types :

- *Caractérisation par simplification* : Partir d'un modèle très complexe qui prend en compte tous les éléments du système et le simplifier. Cette approche est utilisée par (Colas, 2006) dans (§ 2.2.1)
- *Caractérisation par complexification* : Partir d'un modèle très simple et le faire évoluer en complexité afin de prendre en compte d'autres phénomènes.

L'objectif est de converger vers une solution ayant un sens physique. Cependant, la frontière entre un modèle qui ne rend pas compte de la réalité et celui qui est trop complexe est très difficile à percevoir. Trouver le juste milieu relève plus de l'expérience personnelle que des résultats théoriques.

Dans certains cas, le manque de réalisme d'un modèle est compensé en faisant appel à des méthodes plus génériques permettant de se passer complètement de la compréhension du comportement du système réel. Cependant, si ces méthodes permettent d'atteindre un objectif de performance spécifique, des critères de performances plus globales (consommation énergétique, simplicité algorithmique, facilité d'implémentation) sont ternies par ce manque de compréhension.

Pour les axes en gantry bi–actionnés avec prise en compte de la flexibilité, à présent, il n'existe pas d'approche de modélisation qui soit adaptée pour reproduire le comportement du système réel. Les modèles qui sont proposés dans l'état de l'art :

- Ne correspondent pas à la réalité,
  - Le couplage entre actionneurs n'est pas pris en compte (Kim, et al., 2003), (Chu, et al., 2004), (Tan, et al., 2004) et (Yu, et al., 2006)
  - Les actionneurs parallèles se déplacent en synchronisation parfaite (Park, et al., 2001)
- Ils modélisent le comportement de l'axe en gantry d'une façon incomplète,
  - Le couplage est modélisé comme invariant et difficilement généralisable aux paramètres physiques du système réel (Yang, et al., 2003), (Yu, et al., 2003)
  - Les paramètres associés aux actionneurs parallèles ne sont pas pris en compte (Teo, et al., 2007)

- Les variations de la fréquence de résonance de la poutre flexible en fonction de la position de la charge ne sont pas prises en compte (Stöppler, et al., 2008)
- Aucune modélisation prenant en compte les aspects rigides et flexibles d'un axe en gantry bi–actionné n'est proposée.

Pour la suite de ce chapitre, dans (§ 2.3), un état de l'art étendu à la modélisation et commande des systèmes flexibles en général est proposé. Dans (§ 2.4), la modélisation physique (*caractérisation par complexification*), la représentation causale et la commande basée sur le modèle d'un axe en gantry bi–actionné rigide sont présentées.

2.3 Eléments bibliographiques additionnels

Concernant la commande des systèmes flexibles en général, la bibliographie disponible est très large. Une excellente compilation à ce sujet peut être trouvée dans le rapport bibliographique « Robust Control of Flexible Motion Systems » (Verhoeven, 2009) de l'université technique d'Eindhoven (Pays–Bas), et dans les ouvrages Dynamics and Control of Structures (Meirovitch, 1990); Advanced Structural Dynamics and Active Control of Structures : A modal approach (Gawronski, 2004); et Vibration Control of Active Structures: An Introduction (Preumont, 2011). Cependant, ces ouvrages ne réunissent pas d'une façon satisfaisante modélisation et commande, soit ils proposent des modélisations très complexes et pas de commande, soit ils proposent des modèles très simples auxquels on associe des commandes très complexes dont les résultats obtenus ne sont pas toujours réalistes et appropriés à un travail pratique.

Les modélisations dites très complexes sont généralement définies par des équations différentielles partielles et des conditions aux limites, auxquelles on propose toute une série de méthodes de résolution approximatives. Parmi elles, on trouve les méthodes : de Ritz (voir Annexe C), de Galerkin, des modes assumés, d'analyse modale, des éléments finis, et autres. Cependant, au moment de transposer modélisation et commande, ces méthodes se voient limitées parce que, soit elles ne donnent pas d'informations utiles vis–à–vis de la commande, soit elles sont trop détaillées et induisent des temps de calcul incompatibles avec une application en temps réel. Par exemple, par la méthode des éléments finis, on obtient des informations par rapport aux déformations, forces, fréquences de résonance, etc., mais pas d'informations sur l'interaction entre les modes, ce qui les excite, etc. De plus, la plupart des structures flexibles étudiées dans la littérature sont de type soit statique (elles ne bougent pas), soit pseudo–statique (la dynamique du mouvement est très faible et donc négligeable).

Ainsi, pour la commande des systèmes flexibles, trois approches sont le plus souvent utilisées. Il y a la commande optimale, qui consiste à formuler le problème de la commande d'un système flexible comme un problème d'optimisation. Elle est basée sur un modèle linéarisé autour d'un point de fonctionnement souhaité de la structure flexible à commander et d'un critère de performance qui généralement inclut l'erreur de positionnement (ou la déformation élastique) et les efforts appliqués à la structure. La solution de ce problème d'optimisation est la valeur des gains du contrôleur permettant de minimiser les déformations élastiques et les efforts appliqués à la structure. Ensuite, il y a la commande modale, qui est presque exclusivement dédiée à des structures statiques ou pseudo statiques, celles–ci sont basées sur un modèle issu des techniques d'analyse modale. Elles permettent d'estimer les modes flexibles du système, et de proposer une commande active du système flexible. Finalement, il y a les commandes a priori, qui sont presque exclusivement destinées à des systèmes flexibles ayant des modes rigides (en général des machines outil), on identifie expérimentalement un ou plusieurs mode(s) flexible(s) dominant(s), et on génère une trajectoire destinée à minimiser leur excitation (Béarée, 2005).

2.4 Commande d'un axe en gantry bi–actionné rigide basée sur une modélisation physique causale (Gomand, 2008)

(Gomand, 2008) propose trois modélisations différentes pour l'axe en gantry, **Figure 2 – 16**. Les deux premières sont inspirées des modélisations proposées par (Colas, 2006) pour un manipulateur cartésien flexible. Ces modèles sont proposés dans la base des positions mesurées X_1, X_2 et Y. Le point de départ est un modèle local (avec un domaine de validité très limité) qui évolue vers un modèle global (très proche de la physique du système et donc avec un domaine de validité plus large). Ce dernier prend en compte la masse de la poutre m_b et de la charge m_h, ainsi que celle des actionneurs parallèles X_1 et X_2. Les paramètres de friction des axes parallèles sont également pris en compte. La raideur des liaisons poutre–actionneur est représentée par les raideurs torsionelles k_1 et k_2. Ce modèle permet de mettre en évidence le couplage mécanique entre les actionneurs parallèles et de les associer aux éléments physiques constituant le système.

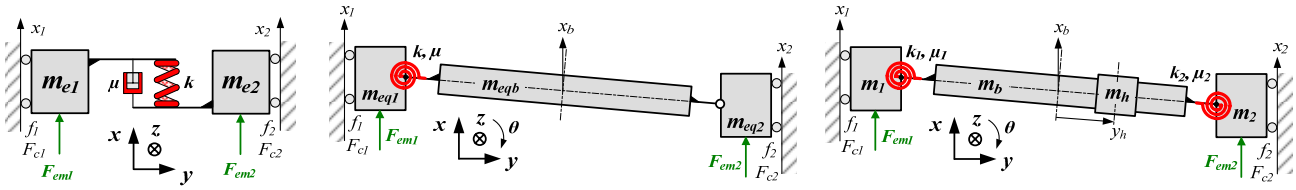

(a) (b) (c)

Figure 2 – 16 : *Modèles d'axe en gantry avec prise en compte du couplage mécanique* (Gomand, 2008)
(a) *Modèle deux masses ressort adapté à la prise en compte du couplage mécanique*
(b) *Evolution vers la prise en compte des effets inertiels équivalents de la poutre et de la charge*
(c) *Modèle détaillé d'un axe en gantry bi–actionné*

La **Figure 2 – 17** présente (en orange) le Graphe Informationnel Causal (GIC) du modèle d'axe en gantry de la **Figure 2 – 16** (c). Sa commande (en bleue) et ses compensations par anticipation (en violet) ont été obtenues selon le principe d'inversion (Barre, 2004).

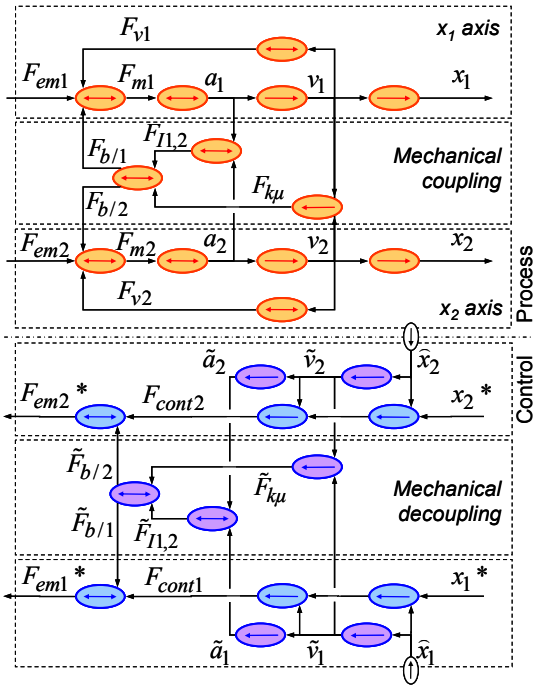

Figure 2 – 17 : *Compensation du couplage mécanique par anticipation de sa dynamique* (Gomand, 2008)

La structure de commande de la **Figure 2 – 17** fonctionne comme une commande à axes indépendants conventionnelle et le couplage mécanique est compensé par anticipation de termes. Le modèle proposé par (Gomand, 2008) fonctionne alors comme un observateur dont le réglage est effectué par l'identification des paramètres physiques de l'axe en gantry. Il faut noter que cette méthode de commande est à l'origine du brevet industriel (Gomand, et al., 2009)

2.5 Approche proposée pour l'étude

L'objectif final de ce travail de recherche est d'établir un outil méthodologique adapté à la modélisation et à la commande des systèmes de positionnement multi–actionnés de type « axe en gantry » pour maîtriser *in fine* le point « outil » dans l'espace de travail lors de déplacements à grande dynamique.

Cet outil méthodologique doit :

- favoriser les échanges entre les concepteurs mécaniques et les automaticiens qui mettent en place la commande
- être suffisamment générique pour être facilement transposable à toute la gamme d'axes en gantry multi–actionnés fabriqués par la société ETEL.

Cet outil méthodologique doit permettre également de lever le verrou technologique à deux volets freinant le développement des lois de commande adaptées aux systèmes flexibles multi–actionnés.

Ce verrou technologique est défini par :

- L'absence d'algorithme de commande réellement adapté pour pouvoir maîtriser les déformations d'une structure flexible multi–actionnée.
- Le manque de formalisme de représentation et d'analyse permettant de prendre en compte le couplage parmi les facteurs les plus influents et d'en déduire des solutions adéquates en termes de mécanique, de choix du nombre des degrés de liberté (actionneurs) et d'algorithmes de commande.

Afin de garantir le développement d'un outil méthodologique répondant à toutes ces exigences, nous devons partir d'une approche qui soit universelle et facilement transposable aux domaines de la conception mécanique et de la commande. De ce fait, nous décidons de passer par une modélisation physique détaillée de l'axe en gantry (un modèle qui soit aussi parlant pour l'un que pour l'autre). Comme les axes en gantry partagent une série de caractéristiques fondamentales, il est donc possible de produire un modèle unique qui soit extensible à toute la gamme d'axes en gantry. Ainsi, avec une modélisation physique détaillée, il est possible de produire un outil de travail sur lequel les spécialistes de la conception et de la commande peuvent travailler.

Pour lever les deux volets du verrou technologique, nous utiliserons les approches de la commande basée sur une modélisation physique causale proposées par le L2EP. Nous les adapterons à la représentation des systèmes flexibles multi–actionnés et des structures de commande adaptées seront déduites grâce au principe d'inversion.

3. Proposed methodology for modeling and controlling gantry stages

The objective of this thesis is to build a control system of the gantry stage that is capable of controlling simultaneously the mechanical coupling between the linear actuators X_1, X_2, and Y; and the vibrations of the cross–arm along the x – direction.

The project specifications impose that this control system has to be generic enough to allow:

- An exchange between the "design" and the "control" people
- An application to all the gantry stages build by ETEL

This conjunction of objectives suggests that the development of a control structure for the gantry stage should be based on a physical modeling of the system. To structure such development, the methodology that is proposed in this chapter is divided in two major steps: the physical modeling of the gantry stage, and the control structure that is derived from such modeling.

(§ 3.1) *Physical modeling of gantry stages*

The objective of the modeling section is to produce a physical model of the gantry stage that is capable of emulating the coupling between actuators X_1, X_2, and Y; and the vibrations of the cross–arm along the x – direction. Besides that, such model has to be generic enough to be applicable to all gantry stages that are built by ETEL.

To add a little challenge, it has been decided that the developed model shall not only be applicable to all ETEL's gantry stages but to most gantry stages that are found in industry.

The modeling section is organized as follows:

(§ 3.1.1) *Types of gantry stages*: the objective here is to study common features between gantry stages, such as the number and position of actuators, or the type of joints connecting the cross–arm to the actuators.

(§ 3.1.2) *General model of the gantry stage*: Based on the common features between gantry stages, it is possible to propose an initial model of the gantry stage including all of them.

(§ 3.1.3) *Kinematics of the gantry stage*: The laws of physics are only valid with respect to an inertial frame. To this purpose, it is essential to define the motion of all elements appertaining to the gantry stage with respect to the origin (or inertial frame). One of the main features of this section is the introduction of the relative coordinates $X(t)$ and $\Theta(t)$ to replace the coordinates $X_1(t)$ and $X_2(t)$ corresponding to the measured position of the actuators X_1 and X_2. This single transformation allows avoiding close–kinematic chains into the modeling; and thus the use of recursive algorithms to deduce the motion equations.

(§ 3.1.4) *Kinetics of the gantry stage*: In this section, the forces acting on the gantry stage are defined.

(§ 3.1.5) *Modeling hypotheses*: At this point, a general analysis of the gantry stage configuration has lead to the development of the general model of the gantry stage. To develop such a model, several modeling hypothesis have been stated. In this section, we propose a review of such hypotheses and the statement of new modeling hypotheses.

(§ 3.1.5) *Dynamic model of the gantry stage*: In this section, we present the motion equations of the general model of the gantry stage. These motion equations will be obtained using the Lagrange–Euler formalism.

(§ 3.1.6) *Identification of the model's parameters*: A necessary step into the development of any model is the identification of the parameters defining it. In this section, a method to identify the parameters of the gantry stage is proposed.

(§ 3.2) *Control of gantry stages*

The objective of this section is to present two methods to develop a control structure based on the physical modeling of a system and to apply them to the control of gantry stages. Both methods are based on the principle of imposed integral causality, i.e. the evolution of the outputs can be defined only in terms of the integral of the inputs. This principle is the base of the causal graphical descriptions: Causal Ordering Graph (COG) and Energetic Macroscopic Representation (EMR).

The control section is organized as follows:

(§ 3.2.1) *Causal Ordering Graph of the gantry stage*: By using the principle of cause and effect, the COG allows organizing the way the inputs will interact between them; with the elements of the system; and how they will evolve into the outputs. Representing a system using the COG formalisms has two major advantages. First, it allows making a zoom into the elements constituting the gantry stage and its internal interaction as well as their interactions with other elements. Second, by inversion of this representation a control structure with measurements, compensations, and controllers can be obtained.

(§ 3.2.2) *Energetic Macroscopic Representation of gantry stages*: The COG description provides, as commented before, a very detailed representation of the system and the opportunity of building very stable simulation models. Nevertheless, as a system grows large or it involves a multi–actuated structure, obtaining a control structure by inversion becomes unpractical because of the number of measurements, compensations, and controllers that are obtained. Indeed, this large number of measurements, compensations, and controllers means larger calculation times for real–time applications. To avoid such difficulties, it is decided to move to the Energetic Macroscopic Representation (EMR) description. As its counterpart, the COG formalism, the EMR formalism is also based on the principle of integral causality; but this time, the elements constituting the system are connected by action reaction variables.

Because of this advantage, the EMR formalism will be used to develop a control structure for the gantry stage.

The development of a control structure using either the COG or the EMR formalisms happens in two stages:

(§ 3.2.3) *Maximum Control Structure of the gantry stage*: It consists in deriving a control structure by step–by–step inversion of the system represented by either the COG or EMR formalisms. All variables are considered measurable and controllable. At this stage, the control structure requires a maximum of controllers and measurements, hence the name Maximum Control Structure.

(§ 3.2.4) *Practical Control Structure of the gantry stage*: Since not all elements within the system are controllable or measureable, the Maximum Control Structure is reduced in order to keep only what it can be measured and controlled. This is the control structure that is possible to implement in real–time.

3.1 Physical modeling of gantry stages

3.1.1 Analyzing gantry stages

A gantry stage consists of a cross–arm, which is mounted on two linear actuators (X_1 – and X_2 – axes) spatially installed in parallel. This cross–arm serves as a support for a third linear actuator (Y – axis) carrying a payload. This payload can be an additional actuator (Z – axis); a wafer table as described in (Kwan, 2006); or any other device.

Ignoring the payload, the overall gantry stage provides a two degree–of–freedom positioning system, as in **Figure 3 – 1**.

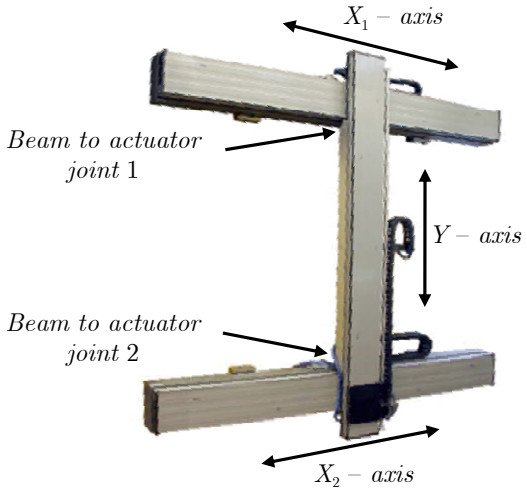

Figure 3 – 1 : *A gantry stage* (www.etel.ch)

The connections between the cross–arm and the moving parts of actuators X_1 and X_2 are provided by mechanical joints. For the gantry stage, an optimal combination of joints is one that:

- Guarantees a fixed connection between, either actuator X_1 or X_2, and the cross–arm so that the exact position of the Y – axis moving part is known with respect to the actuator it is attached to;
- Avoids indeterminate static equilibrium of the cross–arm and/or lateral forces on actuators X_1 and X_2 due to length variations of the cross–arm associated to temperature variations;
- Allows yaw motions of the cross–arm.

Generally, three types of joints are used:

– *Pivot joint*: this type of joint allows yaw motions of the cross–arm, see **Figure 3 – 2** (a); and guarantees a fixed connection between the cross–arm and one actuator, see **Figure 3 – 2** (b).

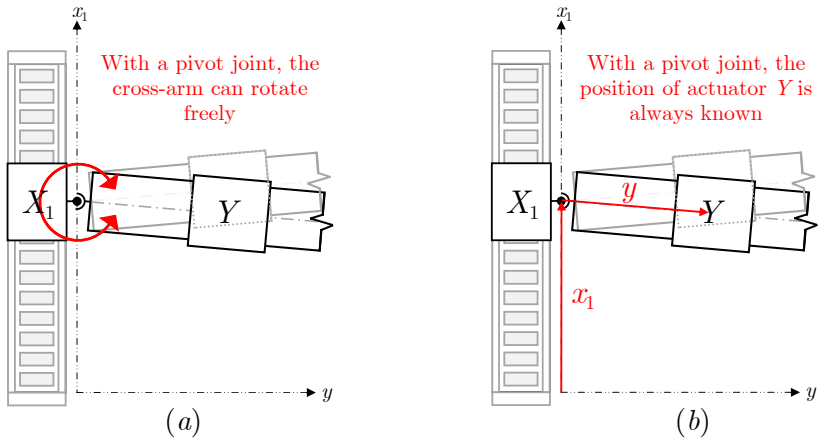

Figure 3 – 2 *: Schematic representation of a gantry stage with pivot joints.*
(a) Yaw (rotation) motions of the cross–arm are allowed
(b) The position of the Y–axis is always known with respect to an inertial frame

– *Flexible plate joint*: This type of joint allows yaw motions of the cross–arm, see **Figure 3 – 3** (a); and allows small lateral displacements of the cross–arm. This way, indeterminate static equilibrium of the cross–arm and/or lateral forces on actuators X_1 and X_2 are avoided. See **Figure 3 – 3** (b)

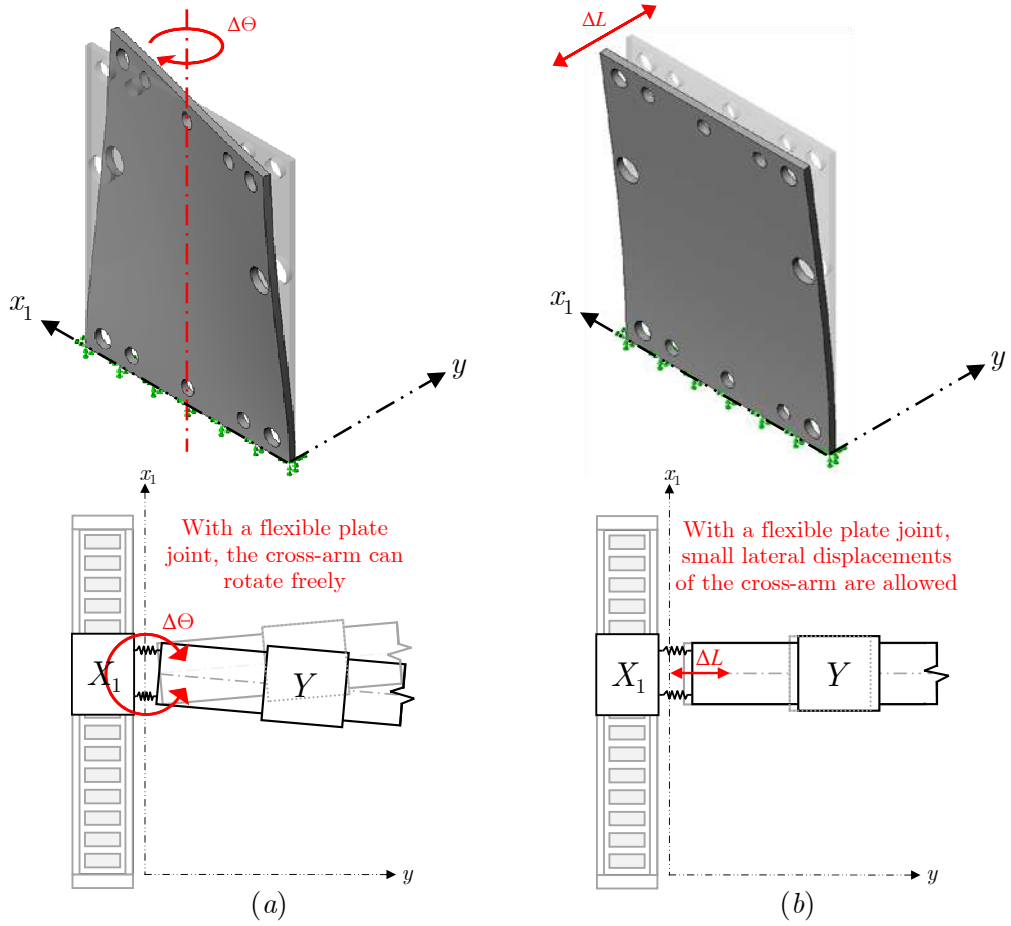

Figure 3 – 3 *: A flexible plate joint*
(a) Yaw (rotation) motions of the cross–arm
(b) Displacement of the cross–arm along its longitudinal direction

– *Rigid joint*: A rigid joint means that the cross–arm is fastened to the actuator. This type of connection is usually found in large size configurations, such as gantry cranes, since fastening the cross–arm to the actuator is mechanically simpler and cheaper than adding additional pieces. Thanks to the size factor, the cross–arm is slender enough to withstand safely the deformation associated to the desynchronization of the parallel actuators. Moreover, for obvious safety reasons, the dynamics of large size systems are low; therefore, the coupling and the subsequent desynchronization between the parallel actuators is negligible.

For high–precision gantry stages, rigid junctions become less and less common due to the drawbacks that they entail, see (§ 1.3). Nevertheless, they will be considered in the development of a general model of the gantry stage as they are still used on some gantry stages, and gantry–like systems.

When rigid joints are used to connect both sides of the cross–arm to the actuators, they are associated to a sliding joint to avoid indeterminate static equilibrium on the cross–arm and/or lateral forces on actuators X_1 and X_2.

For the cross–arm, two mounting configurations exist:

– *The cross–arm is attached to the actuators at its ends*: In the example, see **Figure 3 – 4**, the cross–arm is attached to the actuators via two flexible plates. As commented before, the optimal attachment configuration is one that: allows yaw motions of the cross–arm; a fixed connection between the cross–arm and one of the parallel actuators; and avoids lateral forces on the parallel actuators and/or indeterminate static equilibrium of the cross–arm. Thus, one of the plates is constrained to restrict cross–arm displacements along the longitudinal direction; this plate works then as a pivot joint with torsional stiffness. The other plate is free to displace and to rotate.

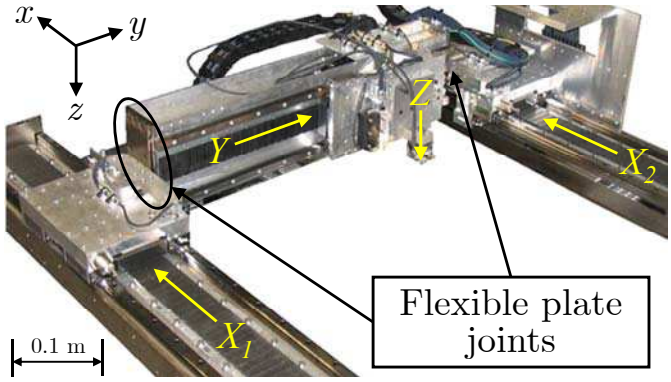

Figure 3 – 4 *: The cross–arm is attached to the actuators at its ends via flexible plate joints*

– *The cross–arm is attached to the actuators at intermediate positions*: In the example, see **Figure 3 – 5**, the cross–arm is attached to the actuators via a flexible plate joint (top) and a pivot joint (bottom). The pivot joint provides a rigid connection between one of the actuators and the cross–arm. The flexible plate joint allows the cross–arm to displace and to rotate.

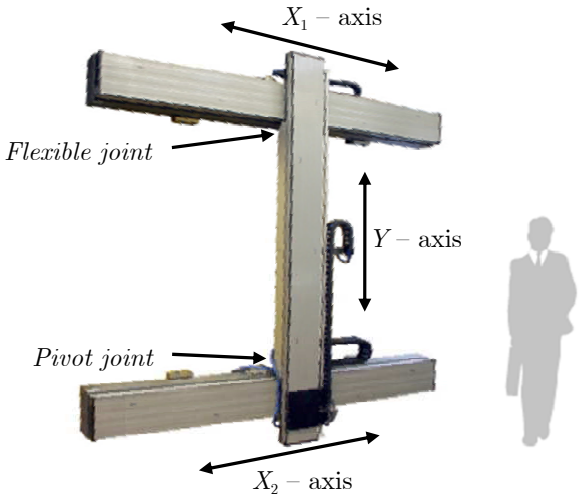

Figure 3 – 5 *: The cross–arm is attached to the actuators at intermediate positions*

An additional element that differs from one gantry stage to the other is the type (or types) of actuators that are used to constitute it. Since, the objective of this research project is to establish a methodological tool of modeling and control that is adapted to most types of gantry stages; it is assumed that these actuators generate a linear force and present the classical opposing forces due to their inertia and due to the static and viscous frictions of their guiding mechanisms. Detailed information on the modeling and control of linear electrical machines can be found in (Remy, 2007).

Concerning their installation, gantry stages can be mounted on different types of bases (or supporting structures). The typical base types are welded, die–cast, and granite or marble for very high–precision applications.

3.1.2 Proposing a general model of the gantry stage

3.1.2.1 A general rigid model of the gantry stage

To propose a general model of the gantry stage, it is necessary to consider three elements,

(1) Gantry stages are composed of:

- Three actuators (X_1, X_2, and Y)
  - Two actuators (X_1 and X_2), which carry the cross–arm along the x–direction;
  - One actuator (Y) which is mounted on the cross–arm and carries the payload along the y–direction.
- A cross–arm
- Two mechanical joints that connect the cross–arm to the actuators X_1 and X_2. They can be of type: pivot, flexible, or rigid joint.
- A payload

(2) There are two types of gantry stages:

– Gantry stages whose cross–arm is attached to the actuators at its ends,

– Gantry stages whose cross–arm is attached to the actuators at an intermediate positions.

(3) The deformation of the gantry stage along the z–axis is supposed negligible.

Based on elements (1) to (3), the following model is proposed:

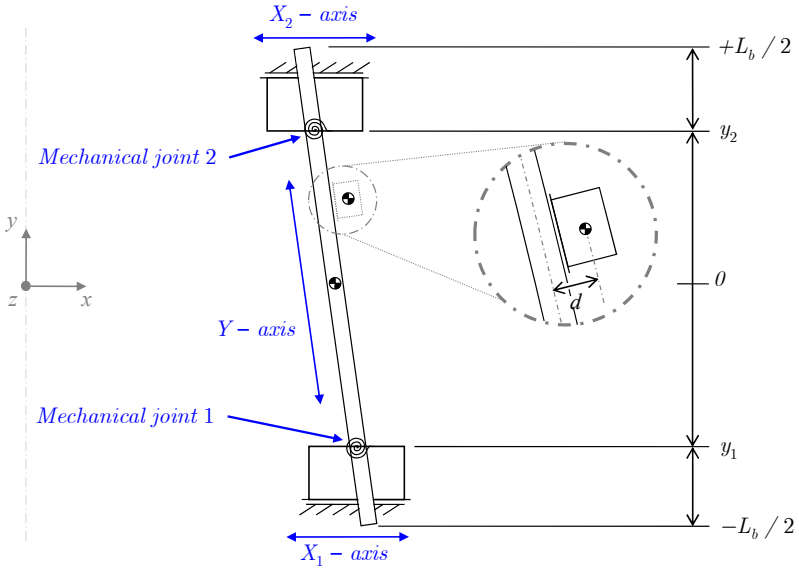

Figure 3 – 6 *: A lumped–parameter model for the gantry stage*

Where,

L_b is the length of the cross–arm;

y_1 is the location of the cross–arm to actuator joint No.1

y_2 is the location of the cross–arm to actuator joint No.2

d is the distance between the centers of mass of the cross–arm and of the payload

Note that on **Figure 3 – 6**, the mechanical joints are depicted as torsional stiffnesses. This is the result of two simplifying hypotheses:

– *The length variations of the cross–arm are considered negligible*: This hypothesis is verified if one considers that the ratio $\Delta L_b / L_b$ is usually smaller than the position measurement error and the backlash of the mechanical installation of the cross–arm.

– *All mechanical joints used on the gantry stage behave as torsional stiffnesses*: This hypothesis can be verified if one considers that a pivot joint can be modeled as a torsional spring with zero stiffness and a rigid joint as a torsional spring with infinite stiffness.

The next step to develop a general model of the gantry stage is to take into account the elasticity of the elements constituting it.

3.1.2.2 Introduction of the elasticity into the general model of the gantry stage

Before introducing the elasticity of the system into the modeling, it is important to consider the following simplifying hypothesis.

– *The actuators are considered as rigid bodies:* Indeed, the elastic deformation of the actuators is supposed negligible in comparison to the deformation of the cross–arm and those of the mechanical joints.

– *The elasticity of the supporting structure is not considered into the modeling:* The motion of actuators X_1, X_2 along the x–direction; and of actuator Y along the y–direction can excite flexible modes of the supporting structure in which the gantry stage is mounted. This phenomenon is not taken into account in the modeling of the gantry stage as its effects can be easily compensated by using either trajectory planning techniques (Béarée, 2005) or by active vibration compensation.

To model the elasticity at a macroscopic level, two approaches can be found in the literature:

- To model the elasticity using a lumped–parameter model (mass–spring models)
- To model the elasticity using a distributed–parameter model

Modeling the elasticity of a system using a lumped–parameter model provides good engineering approximations. Nevertheless, when it comes to model complex flexible systems, such as the gantry stage, this methodology reaches its limits quickly. Take, for example, the flexible model of the gantry stage proposed by (Stöppler, et al., 2008), see **Figure 2 – 15**. This mass–spring model, developed to estimate the cross–arm's elastic deformation, estimates one single vibration of fixed frequency. Not a very accurate model considering that, in reality, the cross–arm deforms at several vibration frequencies, and the value of these frequencies changes in function of the payload's position. Hence, if a similar approach is adopted, similar problems shall be encountered; see **Figure 3 – 7**,

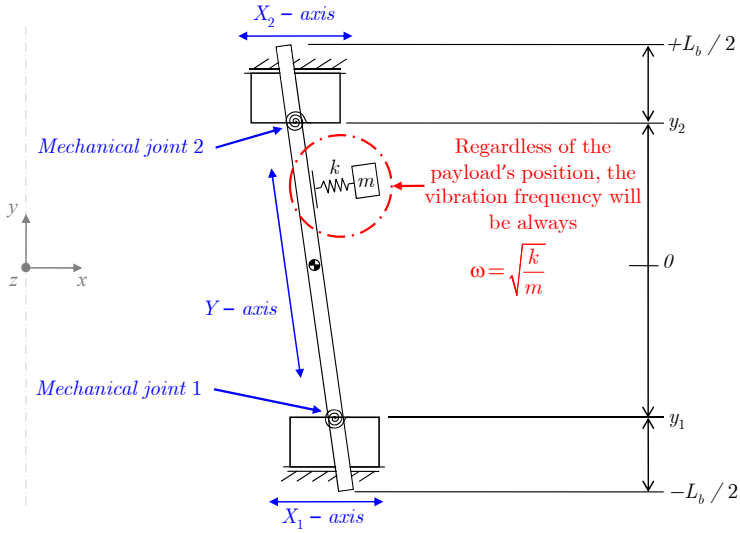

Figure 3 – 7 *: Lumped parameter model of the gantry stage including the elasticity of the cross–arm*

One alternative to refine the model on **Figure 3 – 7** would be to identify the variation of modal stiffness k in function of the payload's position as proposed by (Colas, 2006) for a flexible cartesian robot. Even then, the model would be bound to estimate one single vibration, but at least its frequency variation would be known.

Modeling the elasticity of the cross–arm using a distributed–parameter model has the benefit of being close to the physics of the system. In this approach, the elastic deformation of the cross–arm is defined as the displacement field $u(y, t)$, which describes the deformation of the cross–arm at any point y and at any time $t > 0$ with respect to an un–deformed configuration, see **Figure 3 – 8**. This displacement field, which is caused by the motion of the gantry stage along the x – direction, can be related to physical parameters of the cross–arm by means of the theory of beams.

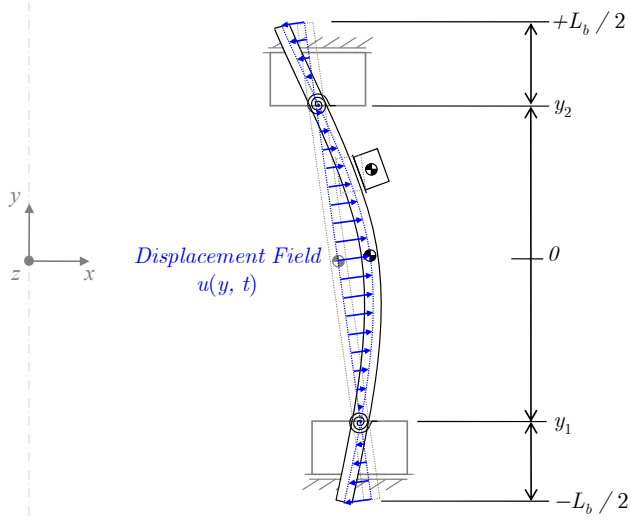

Figure 3 – 8 *: Displacement field $u(y, t)$ of the flexible cross–arm*

Indeed, by comparing the cross–arm to a flexible beam and by modeling it using one of the many available beam theories [*Euler–Bernoulli*, *Rayleigh*, *Timoshenko*, etc., see (Wang, et al., 2000)]; it is possible to obtain a mathematical description of the cross–arm that is based on its physical parameters.

It is important to take into consideration that this mathematical description is given by a Partial Differential Equation (PDE) with Boundary Conditions (BCs).

For example, the equation of motion (3.1) is known as the *Euler–Bernoulli beam model*. The term μ is the linear density; $u_{,tt}$ is the acceleration of an infinitesimal slice of the cross–arm; the term $EIu_{,yyyy}$ is usually referred to as the *flexure term*, where EI is called the *flexural stiffness*[3]; and $p(y, t)$ is the external transverse force density.

$$\mu \frac{\partial^2 u(y,t)}{\partial t^2} + EI \frac{\partial^4 u(y,t)}{\partial y^4} = p(y,t) \tag{3.1}$$

It is observed that the equation of motion (3.1) is a fourth–order partial differential equation in space and second order in time. Thus, to solve it, four boundary conditions and two initial conditions are necessary. See **Appendix A** for details on the modeling of continuous beams using the *Euler–Bernoulli beam model*.

[3] E is the Young's Modulus and I is the second moment of area of cross–section of the beam (or cross–arm) about the *neutral axis*. The neutral axis is the line of intersection of the plane of the neutral fibers, and the plane of the cross–section of the beam. (Hagedorn, et al., 2007)

Two sets of methods exist to solve a problem defined by a PDE with BCs:

- Closed–form or exact solution method
- Approximate solution method

In the case of the beam equation (3.1), the *exact solution method* consists in posing the solution $u(y,\ t)$ as the infinite series of spatial and time functions (3.2). The spatial functions $\phi_i(y)$ are defined as a superposition of trigonometric and hyperbolic functions (Han, et al., 1999). Each spatial function represents the deformation shape of the cross–arm for a given resonance frequency. Both the deformation shapes and the resonance frequencies are dictated by the boundary conditions and the physical parameters of the cross–arm. Then, based on the principle of *orthogonality of functions* and the *expansion theorem* (Hayek, 2001), it is possible to represent the response of the cross–arm as a series of independent ordinary differential Equations (ODEs). The time functions $q_i(t)$ are then the solutions to each of these independent equations[4].

$$u(y,t)=\sum_{i=1}^{\infty}\phi_i(y)\,q_i(t) \tag{3.2}$$

The exact solution method is devoted to distributed–parameter systems admitting exact solutions. This type of solution is characteristic of systems having uniformly distributed parameters and homogeneous (or time invariant) boundary conditions. However, in real life, systems having these characteristics are quite rare. Hence, one must content with approximate solutions.

The *approximate solution methods* have the advantage of being adapted to take into consideration non–homogeneous boundary conditions, intermediate loads acting on the continuum, and complex geometries. Among these methods, one can name:

- Discretization by lumping
- Myklestad's method for bending vibration
- Ritz method
- Rayleigh–Ritz method
- Assumed modes method
- Galerkin's method
- Finite Element Method (FEM)

Further information regarding such methods can be obtained, for example, from (Reddy, 2002), or from any book on structural and mechanical vibrations.

To model the gantry stage, the Ritz method has been chosen because it allows including easily elements such as the mechanical joints and the payload into the modeling of the flexible cross–arm[5]. Indeed, this method consists in posing the solution $u_{Ritz}(y,\ t)$ as the finite series of spatial and time functions (3.3).

$$u_{Ritz}(y,t)=\sum_{k=1}^{N}\psi_k(y)\,q_k(t) \tag{3.3}$$

Where, N is the number of flexible modes to take into consideration. The spatial $\psi_k(y)$ and time $q_k(t)$ functions can be measured experimentally using experimental modal analysis for example.

[4] The exact solution method and its application to an *Euler–Bernoulli* beam mounted in gantry are presented in detail on *Appendix B*.

[5] See *Appendix C* for a detailed explanation of the modeling of a beam in flexure using the Ritz method.

Based on the previous assumptions, the following general model of the gantry stage is obtained,

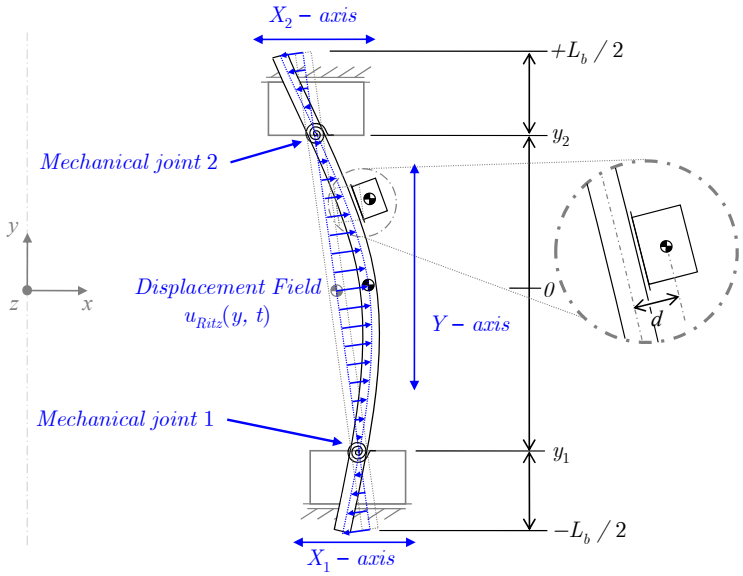

Figure 3 – 9 *: General model of the gantry stage*

The next step in the development of a model–based control structure of the gantry stage is to determine its motion equations. To this purpose, it is necessary to:

- Determine the kinematics of the gantry stage (§ 3.1.3).
- Determine the kinetics of the gantry stage (§ 3.1.4).

3.1.3 Kinematics of the gantry stage

Kinematics (from Greek κινεῖν, *kinein*, to move) is the branch of classical mechanics that describes the motion of bodies (objects) and systems (groups of objects) without consideration of the forces that cause the motion (Whittaker, et al., 1988).

The *first step* to determine the kinematics of a system is to determine a set of reference frames in which to observe its motion.

Reference frames are classified as either inertial or non–inertial:

- An *inertial* or *Newtonian* reference frame is one whose points are either absolutely fixed in space or at most translate relative to an absolutely fixed set of points with the same constant velocity.
- A *non–inertial* or *non–Newtonian* reference frame is one whose points accelerate with time.

"It is an axiom of Newtonian mechanics that inertial reference frames exist and that the laws of mechanics are valid only in an inertial reference frame" (Rao, 2006).

The *second step* to determine the kinematics of a system is to assign a set of coordinates to the chosen reference frames (Cartesian, Polar, Spherical, Cylindrical, Trajectory, etc.).

The *third step* to determine the kinematics of a system is to determine the position, velocity, and acceleration of each part of the system.

The gantry stage kinematics is defined upon the model on **Figure 3 – 10**. The position of the payload, which is the position of interest, is the result of four coupled motions:

- The motion $X_1(t)$ imposed by the X_1–axis
- The motion $X_2(t)$ imposed by the X_2–axis
- The motion $Y(t)$ imposed by the Y–axis
- The motion of the cross–arm $u_{Ritz}(y, t)$ imposed by the X_1– and X_2– axes

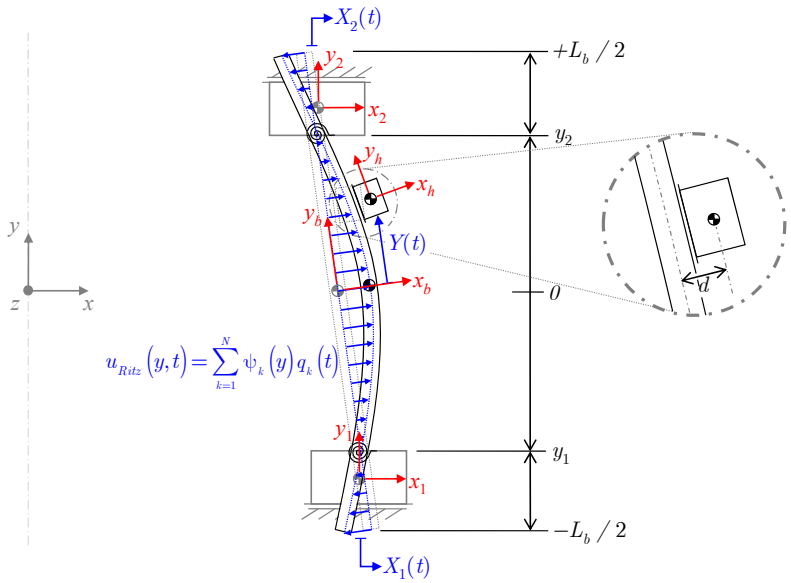

Figure 3 – 10 *: Kinematics of the gantry stage*

On **Figure 3 – 10**, the *inertial reference frame* is given by the origin (x, y, z); the *non–inertial reference frames* are located at the center of mass of each rigid body constituting the gantry stage. (x_1, y_1) and (x_2, y_2) for the linear actuators X_1 and X_2; (x_b, y_b) for the un-deformed cross–arm; and (x_h, y_h) for the payload.

To simplify the definition of the gantry stage's kinematics, let's consider for a moment that the cross–arm behaves as a **rigid body**, as in **Figure 3 – 11**.

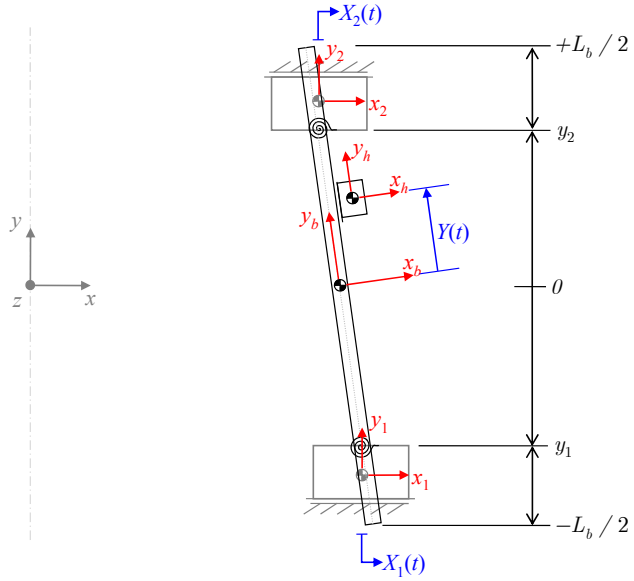

Figure 3 – 11 *: Reference frames of the gantry stage*

In order to formulate the position, velocity, and acceleration of each particle of the gantry stage, it is necessary to define kinematic chains connecting each *non–inertial* reference frame to the origin (x, y, z).

When defining the kinematic chains linking the motion of the payload and of the cross–arm to the origin, one common approach is to define them in terms of the measured position $X_1(t)$, $X_2(t)$, and $Y(t)$ of the X_1–, X_2–, and Y–axes. Nevertheless, as it can be appreciated on **Figure 3 – 12** (a), this approach introduces interdependent closed kinematic chains into the modeling (cross–arm's and payload's positions seen from either X_1– or X_2– axis); making the subsequent kinetic analysis and derivation of the motion equations quite laborious.

To avoid such difficulties, one may consider modeling using open–kinematic chains by referencing all the motions to the center of the cross–arm, as in **Figure 3 – 12** (b). $X(t)$ is the translation of the center of mass of the cross–arm. $\Theta(t)$ is the yaw angle of the cross–arm.

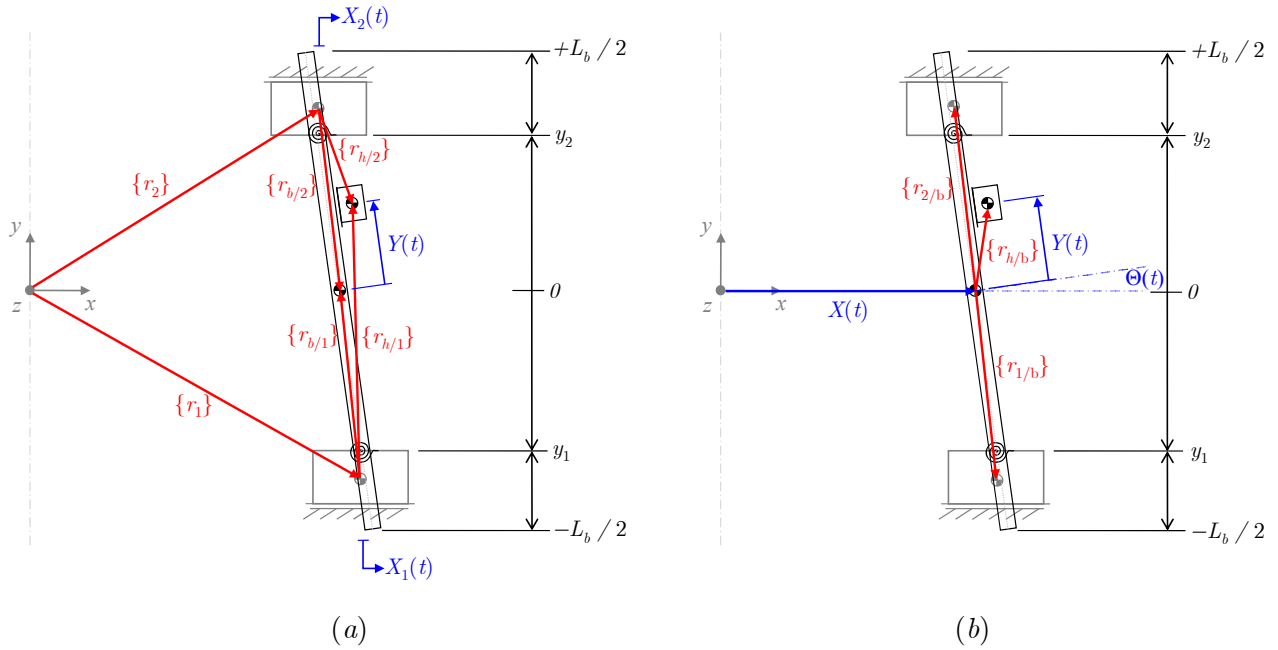

(a) (b)

Figure 3 – 12 *: Kinematics of the gantry stage*
(a) based on the coordinates $X_1(t)$, $X_2(t)$, and $Y(t)$
(b) based on the coordinates $X(t)$ (cross–arm's translation), $\Theta(t)$ (cross–arm's yaw angle), and $Y(t)$

The new coordinates $X(t)$ and $\Theta(t)$ are defined, respectively, by (3.4) and (3.5),

$$X(t) = \left[X_1(t) + X_2(t)\right]/2\,; \qquad \Theta(t) = \tan^{-1}\left\{\left[X_1(t) - X_2(t)\right]/\left(y_2 - y_1\right)\right\} \tag{3.4), (3.5}$$

Then, the general model of the gantry stage can be defined as,

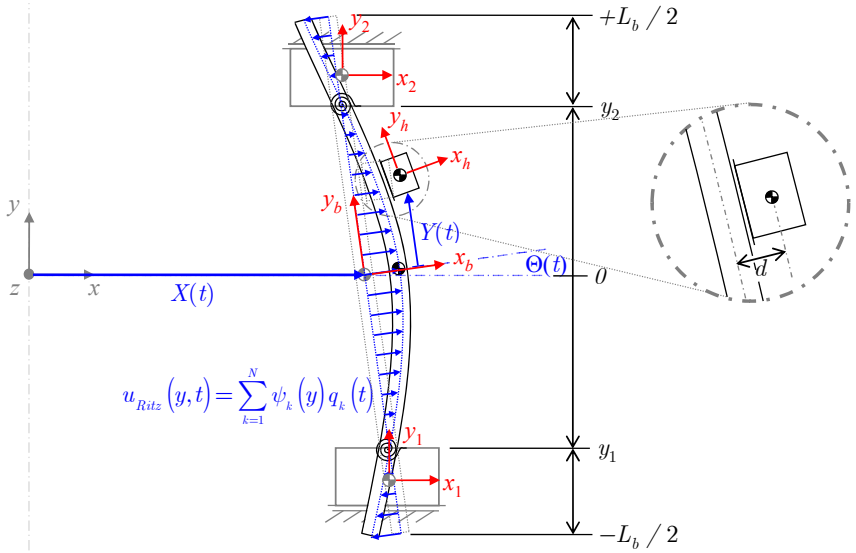

Figure 3 – 13 *: Kinematics of the flexible gantry stage based on the coordinates $X(t)$, $\Theta(t)$, $Y(t)$, and $u_{Ritz}(y,t)$*

By using homogeneous transformation matrices (Fu, 1987), the position of any point within the system can be defined using (3.6).

$$\{{}^0 r_i\} = \left[{}^0 A_i\right] \{{}^i r_i\} \tag{3.6}$$

Where,

$\{{}^0 r_i\}$ is the position vector, i.e. $\{{}^0 r_i\}=\{{}^0 x_i,\ {}^0 y_i,\ {}^0 z_i,\ 1\}^{\mathrm{T}}$, that defines the position of any point of the i – th element of the system with respect to the origin. The index i defines the label of the element under scrutiny.

In the case of the general model of the gantry stage presented on **Figure 3 – 13**, when

$i = b$ defines the cross–arm;

$i = h$ defines the payload (which includes the linear actuator Y);

$i = J_1$ defines the mechanical joint No. 1 (not shown in **Figure 3 – 13**);

$i = J_2$ defines the mechanical joint No. 2 (not shown in **Figure 3 – 13**);

$i = 1$ defines the linear actuator X_1;

$i = 2$ defines the linear actuator X_2.

A coordinate defined in terms of the vector $\{{}^0 r_i\}$ is known as an *absolute position.*

$\{{}^i r_i\}$ is the position vector, i.e. $\{{}^i r_i\}=\{{}^i x_i,\ {}^i y_i,\ {}^i z_i,\ 1\}^{\mathrm{T}}$, that defines the position of any point of the i – th element of the system with respect to non–inertial frame i.

A coordinate defined in terms of the vector $\{{}^i r_i\}$ is known as a *relative position.*

$[{}^0 A_i]$ is the homogeneous transformation matrix i to 0. It allows transforming a relative position, i.e. the position of a point defined with respect to non–inertial frame i, to an absolute position, i.e. the position of point defined with respect to the origin.

Now, the velocity of any point within the system is defined by (3.7),

$$\{{}^0 v_i\} = \frac{d\{{}^0 r_i\}}{dt} = \frac{d[{}^0 A_i]}{dt}\{{}^i r_i\} + [{}^0 A_i]\ \frac{d\{{}^i r_i\}}{dt} \tag{3.7}$$

<u>*Remarks*</u>: the ${}^i x_i$, ${}^i y_i$, ${}^i z_i$ terms are written as x_i, y_i, z_i to simplify the writing.

After all these considerations, it is now possible to define the kinematics of the gantry stage.

a) Kinematics of the cross–arm

The position of any point of the cross–arm as seen from the origin is defined by (3.8)

$$\{{}^0 r_b\}=[{}^0 \mathrm{A}_b]\{{}^b r_b\}=\begin{bmatrix}\cos(\Theta) & -\sin(\Theta) & 0 & X\\ \sin(\Theta) & \cos(\Theta) & 0 & 0\\ 0 & 0 & 1 & 0\\ 0 & 0 & 0 & 1\end{bmatrix}\begin{Bmatrix}x_b\\ y_b\\ z_b\\ 1\end{Bmatrix}\ \therefore\ x_b=\sum_{k=1}^{N}\psi_k(y)q_k(t) \tag{3.8}$$

Where,

$\{{}^0 r_b\}$ is the absolute position of any point of the cross–arm.

$\{{}^b r_b\}$ is the position of any point of the cross–arm with respect non–inertial frame b, i.e. $\{{}^b r_b\} = \{x_b,\ y_b,\ z_b,\ 1\}^{\mathrm{T}}$. x_b is the Ritz series (3.3) accounting the deformation of the cross–arm.

$[{}^0 A_b]$ is the homogeneous transformation matrix b to 0. It transforms the coordinates of any point of the cross–arm, relative to non–inertial frame b, to the reference frame.

b) Kinematics of the payload

The position of any point of the payload as seen from the origin is defined by (3.9)

$$\{{}^{0}r_{h}\}=[{}^{0}\mathrm{A}_{h}]\{{}^{h}r_{h}\}=\begin{bmatrix}\cos(\Lambda) & -\sin(\Lambda) & 0 & X-\sin(\Theta)Y+\cos(\Theta)[d+\sum_{k=1}^{N}\psi_{k}(Y)q_{k}(t)]\\ \sin(\Lambda) & \cos(\Lambda) & 0 & \cos(\Theta)Y+\sin(\Theta)[d+\sum_{k=1}^{N}\psi_{k}(Y)q_{k}(t)]\\ 0 & 0 & 1 & 0\\ 0 & 0 & 0 & 1\end{bmatrix}\begin{Bmatrix}x_{h}\\ y_{h}\\ z_{h}\\ 1\end{Bmatrix} \therefore \Lambda(t)=\Theta(t)+\sum_{k=1}^{N}\psi_{k}'[Y(t)]q_{k}(t) \quad (3.9)$$

Where,

$\{{}^{0}r_{h}\}$ is the absolute position of any point of the payload.

$\{{}^{h}r_{h}\}$ is the position of any point of the payload with respect to non–inertial frame h, i.e. $\{{}^{h}r_{h}\}=\{x_{h},\ y_{h},\ z_{h},\ 1\}^{\mathrm{T}}$.

$[{}^{0}A_{h}]$ is the homogeneous transformation matrix h to 0. It transforms the coordinates of any point of the payload, relative to non–inertial frame h, to the reference frame.

$\Lambda(t)$ is the yaw angle of the payload. It is defined as the superposition of the yaw angle $\Theta(t)$, corresponding to the rigid rotation of the cross–arm, and the slope of the deformation of the cross–arm. $\psi_{k}'[Y(t)]$ is the derivative of the k^{th} mode shape with respect to y evaluated at the position $Y(t)$ of the payload.

c) Kinematics of the mechanical joints

The position of the mechanical joints as seen from the origin is defined by (3.10). With $n=1$ for the joint J_1 located at y_1; and $n=2$ for the joint J_2 located at y_2. See **Figure 3 – 13**.

$$\{{}^{0}r_{Jn}\}=[{}^{0}\mathrm{A}_{Jn}]\{{}^{Jn}r_{Jn}\}=\begin{bmatrix}\cos(\mathrm{K}_{n}) & -\sin(\mathrm{K}_{n}) & 0 & X-y_{n}\sin(\Theta)+\sum_{k=1}^{N}\psi_{k}(y_{n})q_{k}(t)\\ \sin(\mathrm{K}_{n}) & \cos(\mathrm{K}_{n}) & 0 & y_{n}\cos(\Theta)\\ 0 & 0 & 1 & 0\\ 0 & 0 & 0 & 1\end{bmatrix}\begin{Bmatrix}x_{Jn}\\ y_{Jn}\\ z_{Jn}\\ 1\end{Bmatrix} \therefore \mathrm{K}_{n}(t)=\Theta(t)+\sum_{k=1}^{N}\psi_{k}'(y_{n})q_{k}(t) \quad (3.10)$$

Where,

$\{{}^{0}r_{Jn}\}$ is the absolute position of any point of the mechanical joint n.

$\{{}^{Jn}r_{Jn}\}$ is the position of any point of the mechanical joint n with respect to non–inertial frame Jn, i.e. $\{{}^{Jn}r_{Jn}\}=\{x_{Jn},\ y_{Jn},\ z_{Jn},\ 1\}^{\mathrm{T}}$.

$[{}^{0}A_{Jn}]$ is the homogeneous transformation matrix Jn to 0. It transforms the coordinates of any point of the mechanical joint n, relative to non–inertial frame Jn, to the reference frame.

$\mathrm{K}_{n}(t)$ is the yaw angle of the mechanical joint n. It is defined as the superposition of the yaw angle $\Theta(t)$, corresponding to the rigid rotation of the cross–arm, and the slope of the deformation of the cross–arm at the position y_n of the n – th mechanical joint.

d) Kinematics of the X_1– and X_2– axes

The positions of the X_1– *and* X_2– *axes* as seen from the reference frame $\{x,\ y,\ z,\ 1\}^{\mathrm{T}}$ are defined by (3.11). With $n=1$ for the X_1 – axis; and $n=2$ for the X_2 – axis.

$$\{{}^{0}r_{Xn}\}=[{}^{0}\mathrm{A}_{Xn}]\{{}^{Xn}r_{Xn}\}=\begin{bmatrix}1 & 0 & 0 & X-y_{n}\sin(\Theta)\\ 0 & 1 & 0 & y_{n}\cos(\Theta)\\ 0 & 0 & 1 & 0\\ 0 & 0 & 0 & 1\end{bmatrix}\begin{Bmatrix}x_{Xn}\\ y_{Xn}\\ z_{Xn}\\ 1\end{Bmatrix} \quad (3.11)$$

Where,

$\{{}^{0}r_{Xn}\}$ is the absolute position of any point of the X_n– axis.

$\{{}^{Xn}r_{Xn}\}$ is the position of any point of the X_n – axis with reference to non–inertial frame n, i.e. $\{{}^{Xn}r_{Xn}\}=\{x_{Xn},\ y_{Xn},\ z_{Xn},\ 1\}^{\mathrm{T}}$.

$[{}^{0}A_{Xn}]$ is the homogeneous transformation matrix Xn to 0. It transforms the coordinates of any point of the mechanical joint n, relative to non–inertial frame Xn, to the reference frame.

3.1.4 Kinetics of the gantry stage

Kinetics (From Ancient Greek: κίνησις, kinesis, *movement* or *to move*) is a term for the branch of classical mechanics that is concerned with the relationship between the motion of bodies and its causes, namely forces and torques (Whittaker, et al., 1988).

The objective of kinetics is threefold:

(1) To describe quantitatively the forces that act on a particle

(2) To determine the motion that results from the application of these forces using postulated laws of physics

(3) To analyze the motion

In mechanics, the kinetics is deduced from the kinematics by the introduction of the concept of mass.

On the kinematics section (§ 3.2.1), it was determined that the position of the payload is the result of four coupled motions:

- The motion $X_1(t)$ imposed by the X_1- axis
- The motion $X_2(t)$ imposed by the X_2- axis
- The motion $Y(t)$ imposed by the $Y-$ axis
- The motion of the cross–arm $u_{Ritz}(y,\ t)$ imposed by the X_1- and X_2- axes

Now, let's take a particular interest on each of these motions

a) Motion $X_1(t)$

This motion is imposed by the linear actuator X_1. This actuator can be a rotary actuator and a ball–screw mechanism or a direct drive of type Permanent Magnet Linear Synchronous Machine (PMLSM) or other. This linear actuator can be modeled as,

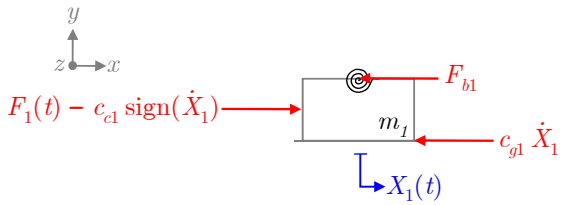

Figure 3 – 14 *: Kinetics of the linear actuator X_1*

Where,

m_1 is the mass of the linear actuator X_1. The actuator is considered as a rigid body.

$F_1(t)$ is the linear force generated by the linear actuator X_1. The (electro)mechanical transformation is considered perfect.

c_{c1} is the force corresponding to the static friction of the linear actuator X_1. Although this force varies slightly along the actuator's stroke, only its mean value will be considered.

c_{g1} is the viscous friction of the linear actuator X_1. Only its mean value is considered[6].

F_{b1} is the force coming from the cross–arm. This coupling force is a combination of the inertial forces induced by the cross–arm and the payload, as well as the force induced by the linear actuator X_2.

[6] A generic static plus viscous friction model is used here as it can be easily adapted to most linear actuators. However, if necessary, more elaborated friction models can be used without affecting the general outline of the methodology developed in this chapter. A good compilation of the most common friction models can be found in (Lampaert, et al., 2004)

Providing that X_2– and Y– axes are also linear actuators, the same modeling hypotheses are applicable for them.

b) Motion $X_2(t)$

The X_2– axis is a *linear actuator* that can be modeled as,

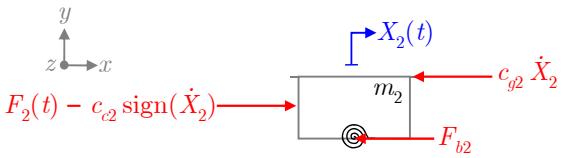

Figure 3 – 15 *: Kinetics of the linear actuator X_2*

Where,

m_2	is the mass of the linear actuator X_2
$F_2(t)$	is the linear force generated by the linear actuator X_2
c_{c2}	is the force corresponding to the static friction of the linear actuator X_2
c_{g2}	is the viscous friction of the linear actuator X_2
F_{b2}	is the force coming from the cross–arm.

c) Motion $Y(t)$

The Y– axis is a *linear actuator* that can be modeled as,

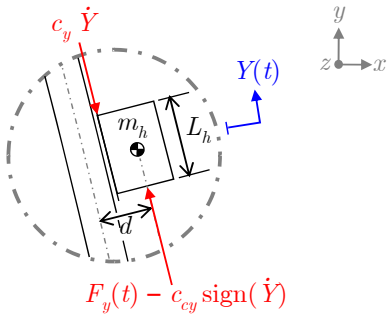

Figure 3 – 16 *: Kinetics of the linear actuator Y*

Where,

m_h	is the mass of the payload
L_h	is the length of the payload
d	is the distance between the centers of mass of the payload and of the cross–arm.
$F_y(t)$	is the linear force generated by the linear actuator Y
c_{cy}	is the force corresponding to the static friction of the linear actuator Y
c_y	is the viscous friction of the linear actuator Y

d) Motion $u_{Ritz}(y, t)$

The motion $u_{Ritz}(y, t)$ describes the motion of the cross–arm,

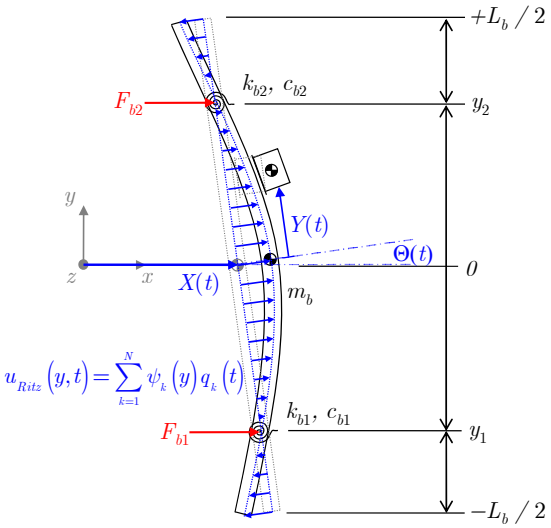

Figure 3 – 17 *: Kinetics of the cross–arm*

Where,

m_b	is the mass of the cross–arm
L_b	is the length of the cross–arm
y_1, y_2	are the locations of the mechanical joints connecting the actuators X_1 and X_2 to the cross–arm.
k_{b1}, k_{b2}	are the rotary stiffnesses of the mechanical joints 1 and 2.
c_{b1}, c_{b2}	are the viscous frictions of the mechanical joints 1 and 2.
F_{b1}, F_{b2}	are the equivalent forces imposed by the actuators X_1 and X_2 to the cross–arm.

3.2 Modeling the gantry stage

The objective of this section is twofold:

- To use the mechanical analysis proposed on the previous section to obtain the motion equations of the general model of the gantry stage.
- To represent such equations in a causal way so that an adapted control structure can be obtained by model inversion.

To this purpose, this section is divided as follows:

(§ 3.2.1) Recall of the modeling hypotheses that made possible the development of the general model of the gantry stage and statement of additional modeling hypotheses

(§ 3.2.2) Dynamical model of the gantry stage; the motion equations will be obtained using the Lagrange–Euler formalism.

(§ 3.2.3) Presentation of a method to identify the parameters of the proposed model.

3.2.1 Modeling hypotheses

3.2.1.1 Modeling hypotheses derived from the mechanical analysis presented on (§ 3.1)

- The length variations of the cross–arm are considered negligible.
- There is no displacement of the beam along the transverse direction.
- The mechanical joints are considered as discrete torsion stiffnesses with proportional damping.
- The mechanical joints are considered massless. Indeed, their mass is negligible when compared to those of the cross–arm, the actuators, or the payload.
- The actuators X_1, X_2, and Y are considered as rigid bodies.
- The cross–arm can be assimilated to a flexible beam. Thus; it can be modeled using one of the many beam models available.
- All the motions are referred to the geometric center of the cross–arm, i.e. the motions $X_1(t)$ and $X_2(t)$ are replaced by the equivalent motions $X(t)$ and $\Theta(t)$. This transformation allows avoiding closed–kinematic chains into the modeling.
- The (electro)mechanical transformation of the actuators X_1, X_2, and Y is considered perfect, i.e. $F = F_{ref}$.

3.2.1.2 Additional modeling hypotheses

- The cross–arm will be modeled using the Euler–Bernoulli beam model, i.e. the rotary inertia of the infinitesimal section is neglected. This hypothesis is justified if one considers that more advanced beam models, such as *Timoshenko beam model*, reveal that the rotary inertia is unimportant for low–frequency vibrations. A full study of this is presented on (Han, et al., 1999).
- The elasticity of the cross–arm and those of the mechanical joints are decoupled. See **Appendix B** for justification.

3.2.2 Dynamic model of the gantry stage

The lumped–distributed parameter model presented on **Figure 3 – 18** is based on the mechanical analysis proposed on the previous section. It can be described using fourteen physical parameters:

- Four masses m_b, m_h, m_1 and m_2 corresponding, respectively, to the mass of the cross–arm, the payload, and the parallel actuators X_1 and X_2.
- Five friction coefficients c_{g1}, c_{g2}, c_y, c_{b1} and c_{b2} corresponding to the viscous friction of actuators X_1, X_2, and Y, and to those of the mechanical joints.
- Three forces c_{c1}, c_{c2}, and c_{cy} corresponding to the static friction of actuators X_1, X_2, and Y.
- Two stiffness coefficients k_{b1} and k_{b2} of the mechanical joints 1 and 2.

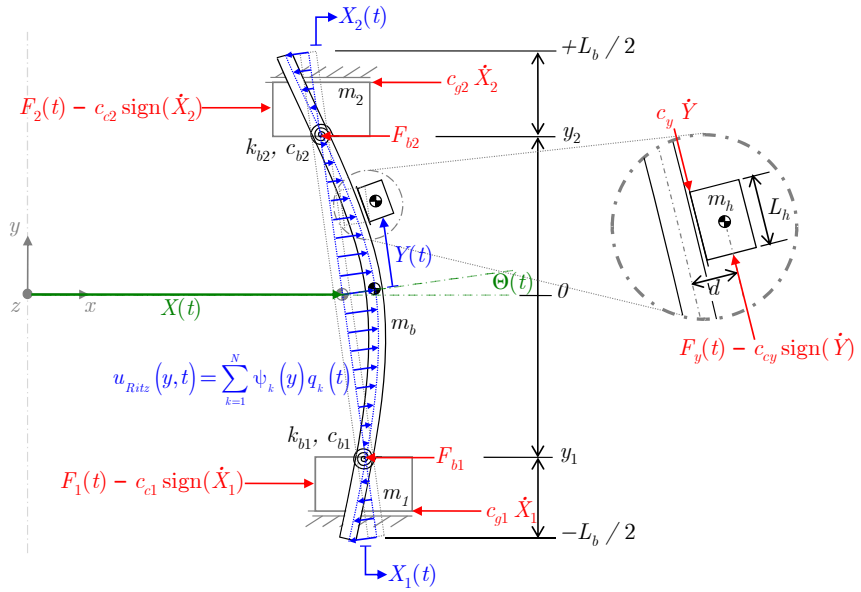

Figure 3 – 18 *: General lumped–distributed parameters model of the gantry stage*

As a recall, the cross–arm and the payload have lengths L_b and L_h. The position of the payload is measured from the geometric center of the cross–arm and it is denoted by $Y(t)$ and d. $X(t)$ denotes the linear position of the geometric center of the cross–arm, $\Theta(t)$ denotes the yaw angle of the cross–arm, and the $u_{Ritz}(y, t)$ denotes the deformation of the cross–arm along the x – direction. In $u_{Ritz}(y, t)$, N defines the number of flexible modes to take into account on the model.

X(t) and $\Theta(t)$ are defined as functions of the measured positions of the linear actuators X_1 and X_2, see (3.4) and (3.5). The mode shapes $\psi_k(y)$ are assumed to be known as they can be estimated experimentally.

Based on the general model of the gantry stage, presented on **Figure 3 – 18**, the motion equations of the gantry stage are to be obtained using the Lagrange–Euler formalism

$$\frac{\partial L}{\partial q_i} - \frac{d}{dt}\left(\frac{\partial L}{\partial \dot{q}_i}\right) - \frac{\partial D}{\partial \dot{q}_i} + Q_i = 0 \tag{3.12}$$

Where,

$L = T - V$ is the Lagrangian of the system. T and V are, respectively, the kinetic and potential energies of the gantry stage.

D is the dissipative energy of the gantry stage.

q_i is the set of generalized coordinates[7] of the system defined by $q_i = X(t)$, $\Theta(t)$, $Y(t)$, $q_1(t),\ldots q_N(t)$.

Q_i is the set of generalized forces acting on the generalized coordinates q_i.

[7] A set of generalized coordinates is one in which each coordinate is independent and the number of coordinates is just sufficient to specify completely the configuration of a system. Generally, the number of generalized coordinates is equal to the number of Degrees Of Freedom (DOFs) of a system.

3.2.2.1 Kinetic Energy T of the Gantry stage

The general expressions for the kinetic energy are all given in (3.13). *Note*: The operator Tr[ ] is the trace of a matrix.

$$T=\frac{1}{2}mv^2=\frac{1}{2}\{v\}^{\mathrm{T}}m\{v\}=\frac{1}{2}\mathrm{Tr}\left[\{v\}m\{v\}^{\mathrm{T}}\right] \tag{3.13}$$

By replacing (3.7) into (3.13) the kinetic energy of the i – th element of the gantry stage is obtained,

$$\begin{aligned}T_i&=\left(1/2\right)\mathrm{Tr}\left[\{{}^0v_i\}m\{{}^0v_i\}^{\mathrm{T}}\right]\\&=\left(1/2\right)\mathrm{Tr}\left[\left\{[{}^0\dot{\mathrm{A}}_i]\{{}^ir_i\}+[{}^0\mathrm{A}_i]\{{}^i\dot{r}_i\}\right\}m\left\{[{}^0\dot{\mathrm{A}}_i]\{{}^ir_i\}+[{}^0\mathrm{A}_i]\{{}^i\dot{r}_i\}\right\}^{\mathrm{T}}\right]\\&=\left(1/2\right)\mathrm{Tr}\left[[{}^0\dot{\mathrm{A}}_i]\{{}^ir_i\}m\{{}^ir_i\}^{\mathrm{T}}[{}^0\dot{\mathrm{A}}_i]^{\mathrm{T}}+[{}^0\dot{\mathrm{A}}_i]\{{}^ir_i\}m\{{}^i\dot{r}_i\}^{\mathrm{T}}[{}^0\mathrm{A}_i]^{\mathrm{T}}+[{}^0\mathrm{A}_i]\{{}^i\dot{r}_i\}m\{{}^ir_i\}^{\mathrm{T}}[{}^0\dot{\mathrm{A}}_i]^{\mathrm{T}}+[{}^0\mathrm{A}_i]\{{}^i\dot{r}_i\}m\{{}^i\dot{r}_i\}^{\mathrm{T}}[{}^0\mathrm{A}_i]^{\mathrm{T}}\right]\end{aligned} \tag{3.14}$$

Now, if we calculate the differential of the kinetic energy and then we integrate, we obtain the general expression of the kinetic energy of the i – th element of the gantry stage in terms of the contribution of its rigid, coupled (rigid–flexible) and flexible modes.

$$\int dT_i=\frac{1}{2}\mathrm{Tr}\left[[{}^0\dot{\mathrm{A}}_i][J_{iR}][{}^0\dot{\mathrm{A}}_i]^{\mathrm{T}}+[{}^0\dot{\mathrm{A}}_i][J_{iC}][{}^0\mathrm{A}_i]^{\mathrm{T}}+[{}^0\mathrm{A}_i][J_{iC}]^{\mathrm{T}}[{}^0\dot{\mathrm{A}}_i]^{\mathrm{T}}+[{}^0\mathrm{A}_i][J_{iF}][{}^0\mathrm{A}_i]^{\mathrm{T}}\right]\ \therefore\ \begin{aligned}[J_{iR}]&=\int\{{}^ir_i\}dm\{{}^ir_i\}^{\mathrm{T}}\\[J_{iC}]&=\int\{{}^ir_i\}dm\{{}^i\dot{r}_i\}^{\mathrm{T}}\\[J_{iF}]&=\int\{{}^i\dot{r}_i\}dm\{{}^i\dot{r}_i\}^{\mathrm{T}}\end{aligned} \tag{3.15}$$

The integral terms in (3.15) are the rigid $[J_{iR}]$ (3.16); coupled (rigid–flexible) $[J_{iC}]$ (3.17); and flexible $[J_{iF}]$ (3.18)inertial matrices of the i – th element of the system.

$$[J_{iR}]=\begin{bmatrix}\int x_i^2dm & \int x_iy_idm & \int x_iz_idm & \int x_idm\\ \int x_iy_idm & \int y_i^2dm & \int y_iz_idm & \int y_idm\\ \int x_iz_idm & \int y_iz_idm & \int z_i^2dm & \int z_idm\\ \int x_idm & \int y_idm & \int z_idm & \int dm\end{bmatrix}=\begin{bmatrix}\left(-I_{xx}+I_{yy}+I_{zz}\right)/2 & I_{xy} & I_{xz} & m_i\overline{x}_i\\ I_{xy} & \left(I_{xx}-I_{yy}+I_{zz}\right)/2 & I_{yz} & m_i\overline{y}_i\\ I_{xz} & I_{yz} & \left(I_{xx}+I_{yy}-I_{zz}\right)/2 & m_i\overline{z}_i\\ m_i\overline{x}_i & m_i\overline{y}_i & m_i\overline{z}_i & m_i\end{bmatrix} \tag{3.16}$$

$$[J_{iC}]=\begin{bmatrix}\int x_i\dot{x}_idm & \int x_i\dot{y}_idm & \int x_i\dot{z}_idm & 0\\ \int y_i\dot{x}_idm & \int y_i\dot{y}_idm & \int y_i\dot{z}_idm & 0\\ \int z_i\dot{x}_idm & \int z_i\dot{y}_idm & \int z_i\dot{z}_idm & 0\\ \int \dot{x}_idm & \int \dot{y}_idm & \int \dot{z}_idm & 0\end{bmatrix};\quad [J_{iF}]=\begin{bmatrix}\int \dot{x}_i^2dm & \int \dot{x}_i\dot{y}_idm & \int \dot{x}_i\dot{z}_idm & 0\\ \int \dot{x}_i\dot{y}_idm & \int \dot{y}_i^2dm & \int \dot{y}_i\dot{z}_idm & 0\\ \int \dot{x}_i\dot{z}_idm & \int \dot{y}_i\dot{z}_idm & \int \dot{z}_i^2dm & 0\\ 0 & 0 & 0 & 0\end{bmatrix} \tag{3.17), (3.18}$$

Based on this definition of the kinetic energy of an elastic body, the kinetic energy expressions for each element of the gantry are presented next.

a) Kinetic energy of the cross–arm

The kinetic energy of the cross–arm is calculated using (3.15). The kinematics of the cross–arm, i.e. the expressions for $[{}^0\mathrm{A}_b]$ and $\{{}^br_b\}$, is defined by (3.8).

$$T_b=\frac{1}{2}Tr\left[[{}^0\dot{\mathrm{A}}_b][J_{bR}][{}^0\dot{\mathrm{A}}_b]^{\mathrm{T}}+[{}^0\dot{\mathrm{A}}_b][J_{bC}][{}^0\mathrm{A}_b]^{\mathrm{T}}+[{}^0\mathrm{A}_b][J_{bC}]^{\mathrm{T}}[{}^0\dot{\mathrm{A}}_b]^{\mathrm{T}}+[{}^0\mathrm{A}_b][J_{bF}][{}^0\mathrm{A}_b]^{\mathrm{T}}\right]\ \therefore\ \begin{aligned}[J_{bR}]&=\int\{{}^br_b\}dm\{{}^br_b\}^{\mathrm{T}}\\[J_{bC}]&=\int\{{}^br_b\}dm\{{}^b\dot{r}_b\}^{\mathrm{T}}\\[J_{bF}]&=\int\{{}^b\dot{r}_b\}dm\{{}^b\dot{r}_b\}^{\mathrm{T}}\end{aligned} \tag{3.19}$$

b) Kinetic energy of the payload

The payload is considered as behaving as a rigid body; therefore, the general expression for the kinetic energy (3.15) is simplified since the coupling rigid–flexible and flexible inertia matrices become zero,

$$T_h=\frac{1}{2}Tr\left[[{}^0\dot{\mathrm{A}}_h][J_{hR}][{}^0\dot{\mathrm{A}}_h]^{\mathrm{T}}\right]\ \therefore\quad [J_{hR}]=\int\{{}^hr_h\}dm\{{}^hr_h\}^{\mathrm{T}};\quad [J_{hC}]=0;\quad [J_{hF}]=0 \tag{3.20}$$

c) Total kinetic energy of the gantry stage

Finally, the total kinetic energy of the gantry stage is the result of the addition of the kinetic energy of each element,

$$T = T_b + T_h \tag{3.21}$$

Note that the kinetic energy of neither the mechanical joints nor the linear actuators X_1 and X_2 is being considered into expression (3.21). In the case of the mechanical joints this is completely normal as they're considered massless. Hence they don't have kinetic energy. The linear actuators on the other hand do have kinetic energy. However, they're not considered into expression (3.21) for simple convenience. Indeed, if the motion equations are defined in terms of the resulting forces F_{b1} and F_{b2} acting on the cross–arm, instead of the forces F_1 and F_2 generated by actuators X_1 and X_2, their writing and graphical representation will be greatly simplified. The dynamical properties of actuators X_1 and X_2 will be contained into the definition of F_{b1} and F_{b2}, as in (3.29)

3.2.2.2 Potential Energy *V* of the Gantry stage

The potential energy is a lot easier to determine. It is stored by the elements within the system deforming elastically, i.e. the mechanical joints and the cross–arm. The effects of gravity, which acts along the z – direction, on the system are considered negligible.

The stiffness of the mechanical joints 1 and 2 is modeled as the discrete rotary stiffnesses k_{b1} and k_{b2}. Their potential elastic energy is given by (3.22). Where, $\mathrm{K_n}$ (with n=1, 2.) is the rotation angle of the joint; see expression (3.10).

$$V_{mech.joints} = \frac{1}{2}\left(k_{b1}\,\mathrm{K}_1^2 + k_{b2}\,\mathrm{K}_2^2\right) \tag{3.22}$$

The potential elastic energy of an Euler–Bernoulli beam (Ginsberg, 2001) is given by,

$$V_{beam} = \frac{1}{2}\int_{-L_b/2}^{L_b/2} EI\left[\frac{\partial u(y,t)}{\partial y^2}\right]^2 dy \tag{3.23}$$

In the case of the cross–arm of the gantry stage, $u(y,\ t)$ is approximated by $u_{Ritz}(y,\ t)$, see (§ 3.1.2.2). Expression (3.23) becomes then,

$$V_{cross-arm} = \frac{1}{2}\int_{-L_b/2}^{L_b/2} EI\left[\frac{\partial u_{Ritz}(y,t)}{\partial y^2}\right]^2 dy = \frac{1}{2}\int_{-L_b/2}^{L_b/2} EI\left[\sum_{k=1}^{N}\psi_k''(y)q_k(t)\right]^2 dy \tag{3.24}$$

Decomposing,

$$V_{cross-arm} = \frac{1}{2}\sum_{\substack{j=1\\k=1}}^{N} k_{jk}\,q_j(t)q_k(t) \;\;\therefore\;\; k_{jk} = \int_{-L_b/2}^{L_b/2} EI\,\psi_j''(y)\psi_k''(y)dy \tag{3.25}$$

Finally, the total elastic potential energy of the gantry stage is given by (3.26)

$$V = V_{mech.joints} + V_{cross-arm} \tag{3.26}$$

3.2.2.3 Rayleigh's dissipative function *D*

The dissipative energy is proportional to the elastic potential energy. This is because, physically, the stiffnesses have an associated damping coefficient that is proportional to the deformation velocity. Physically, this phenomenon is known as viscoelasticity (Fung, 2001). An extra element having dissipation is the payload; we must therefore consider the viscous friction associated to this actuator. The expression for the total dissipative energy of the gantry stage is given by (3.27). γ is the viscous damping coefficient of the cross–arm.

$$D = \frac{1}{2}\left(c_{b1}\,\dot{\mathrm{K}}_1^2 + c_{b2}\,\dot{\mathrm{K}}_2^2\right) + \frac{1}{2}\sum_{\substack{j=1\\k=1}}^{N} c_{jk}\,\dot{q}_j(t)\dot{q}_k(t) + \frac{1}{2}c_y\dot{Y}^2 \;\;\therefore\;\; c_{jk} = \int_{-L_b/2}^{L_b/2}\gamma EI\,\psi_j''(y)\psi_k''(y)dy \tag{3.27}$$

Once more, it is important to note that the dissipative energy associated to actuators X_1 and X_2 is not taken into consideration. As commented before, this is done to simplify the writing of the motion equations and its graphical representation. The terms associated to the dissipative energy of actuators X_1 and X_2 will appear on the definition of forces F_{b1} and F_{b2}.

3.2.2.4 Generalized coordinates q_i and forces Q_i of the gantry stage

In the case of the gantry stage, there are two sets of generalized coordinates fully defining the configuration of the gantry stage. The first set is those of the measured positions of the linear actuators X_1, X_2, Y, and the deformation of the cross–arm given by the time functions of $u_{Ritz}(y,t)$, i.e. q_1, q_2,..., q_N. The second set is defined by the coordinates $X(t)$, $\Theta(t)$, $Y(t)$, $q_1(t)$,...,$q_N(t)$. the coordinates $X(t)$ and $\Theta(t)$ represent, respectively, the translation and the yaw angle of the cross–arm. As commented on (§ 3.1.3), the second set of coordinates is preferred as it allows modeling the motion of the gantry stage using open–kinematic chains; simplifying greatly the derivation of the motion equations.

A generalized force is one provoking the evolution of a generalized coordinate. The generalized forces of a mechanical system can be defined using the power balance method, see **Appendix C**, or by using the principle of virtual work (Reddy, 2002).

The generalized coordinates of the gantry stage are defined by (3.28), the generalized forces by (3.29).

$$q=\begin{bmatrix} X \\ \Theta \\ Y \\ q_1 \\ q_2 \\ \vdots \\ q_k \end{bmatrix};\quad Q=\begin{bmatrix} F_X \\ F_\Theta \\ F_Y \\ Q_1 \\ Q_2 \\ \vdots \\ Q_k \end{bmatrix}=\begin{bmatrix} F_{b1}+F_{b2} \\ \left(F_{b1}-F_{b2}\right)\cos\left(\Theta\right)\left(y_2-y_1\right)/2 \\ F_Y \\ F_{b1}\psi_1\left(y_1\right)+F_{b2}\psi_1\left(y_2\right) \\ F_{b1}\psi_2\left(y_1\right)+F_{b2}\psi_2\left(y_2\right) \\ \vdots \\ F_{b1}\psi_k\left(y_1\right)+F_{b2}\psi_k\left(y_2\right) \end{bmatrix} \quad \therefore \begin{array}{l} F_{b1}=F_1-m_1\ddot{X}_1-c_{g1}\dot{X}_1-c_{c1}\,\mathrm{sign}\left(\dot{X}_1\right) \\ F_{b2}=F_2-m_2\ddot{X}_2-c_{g2}\dot{X}_2-c_{c2}\,\mathrm{sign}\left(\dot{X}_2\right) \\ F_Y=F_y-c_{cy}\,\mathrm{sign}\left(\dot{Y}\right) \end{array} \tag{3.28), (3.29}$$

3.2.2.5 Motion equations of the gantry stage

With each term of the Lagrange–Euler formalism defined for the gantry stage, it is possible to obtain its motion equations, as follows:

a) Motion of the gantry stage along the generalized coordinate $X(t)$

The mathematical definition of the motion of the gantry stage along the generalized coordinate $X(t)$ is given by,

$$\frac{\partial L}{\partial X(t)}-\frac{d}{dt}\left(\frac{\partial L}{\partial \dot{X}(t)}\right)-\frac{\partial D}{\partial \dot{X}(t)}+F_X=0 \tag{3.30}$$

Or,

$$M_{XX}\ddot{X}+M_{X\Theta}\ddot{\Theta}+M_{XY}\ddot{Y}+M_{X1}\ddot{q}_1+M_{X2}\ddot{q}_2+\ldots+M_{Xk}\ddot{q}_k+\ldots+M_{XN}\ddot{q}_N+H_{X\Theta}\dot{\Theta}+H_{XY}\dot{Y}=F_X \tag{3.31}$$

Where,

M_{XX} is the combined mass of the cross–arm and of the payload. It is defined by (3.32)

$$M_{XX}=m_b+m_h \tag{3.32}$$

$M_{X\Theta}$ is the coupled inertia between the translation $X(t)$ and the rotation $\Theta(t)$ of the cross–arm. It is defined by (3.33). N is the number of flexible modes to take into consideration within the model.

$$M_{X\Theta}=-\mathrm{Sin}\left(\Theta\right)\left[\sum_{k=1}^{N}\left[\int_{-L_b/2}^{L_b/2}\mu\psi_k\left(y\right)dy\right]q_k+m_h\left[d+\sum_{k=1}^{N}q_k\psi_k\left(Y\right)\right]\right]-m_hY\mathrm{Cos}\left(\Theta\right)\ \therefore\ k=1,2,\ldots,N \tag{3.33}$$

M_{XY} is the coupled inertia between the translation $X(t)$ and the motion $Y(t)$ of the payload. It is defined by (3.34)

$$M_{XY} = m_h\left[\mathrm{Cos}(\Theta)\sum_{k=1}^{N} q_k \psi_k'(Y) - \mathrm{Sin}(\Theta)\right] \;\therefore\; k=1,2,\ldots,N \tag{3.34}$$

M_{Xk} is the coupled inertia between the translation $X(t)$ of the cross–arm and the vibrations of the cross–arm defined by the motion $q_k(t)$. It is defined by (3.35)

$$M_{Xk} = \mathrm{Cos}(\Theta)\left[m_h \psi_k(Y) + \int_{-L_b/2}^{L_b/2} \mu \psi_k(y)dy\right] \tag{3.35}$$

$H_{X\Theta}$ and H_{XY} are the centripetal and coriolis acceleration terms created by the motion of the payload, which is translating, rotating, and vibrating with respect to the motion $X(t)$ of the cross–arm. They are defined by (3.36) and (3.37),

$$H_{X\Theta} = -\left\{\begin{array}{l} 2\left(\mathrm{Sin}(\Theta)\left(\sum_{k=1}^{N}\left[\int_{-L_b/2}^{L_b/2}\mu\psi_k(y)dy\right]\dot{q}_k + m_h\frac{d}{dt}\left[\sum_{k=1}^{N} q_k\psi_k(Y)\right]\right) + \mathrm{Cos}(\Theta)m_h\dot{Y}\right) + \\ +\left(\mathrm{Cos}(\Theta)\left(\sum_{k=1}^{N}\left[\int_{-L_b/2}^{L_b/2}\mu\psi_k(y)dy\right]q_k + m_h\left[d+\sum_{k=1}^{N} q_k\psi_k(Y)\right]\right) - \mathrm{Sin}(\Theta)m_h Y\right)\dot{\Theta} \end{array}\right\} \;\therefore\; k=1,2,\ldots,N \tag{3.36}$$

$$H_{XY} = 2m_h\mathrm{Cos}(\Theta)\left[\sum_{k=1}^{N}\dot{q}_k\psi_k'(Y)\right] + m_h\mathrm{Cos}(\Theta)\left[\sum_{k=1}^{N} q_k\psi_k''(Y)\right]\dot{Y} \;\therefore\; k=1,2,\ldots,N \tag{3.37}$$

F_X is the equivalent force imposed by the actuators X_1 and X_2 to the cross–arm to produce the motion $X(t)$. It is defined by (3.38)

$$F_X = F_{b1} + F_{b2} \tag{3.38}$$

b) Rotation of the gantry stage with respect to the center of the cross–arm $\Theta(t)$

The mathematical definition of the motion of the gantry stage about the geometric center of the cross–arm $\Theta(t)$ is given by,

$$\frac{\partial L}{\partial \Theta(t)} - \frac{d}{dt}\left(\frac{\partial L}{\partial \dot{\Theta}(t)}\right) - \frac{\partial D}{\partial \dot{\Theta}(t)} + F_\Theta = 0 \tag{3.39}$$

Or,

$$\begin{array}{l} M_{X\Theta}\ddot{X} + M_{\Theta\Theta}\ddot{\Theta} + M_{\Theta Y}\ddot{Y} + M_{\Theta 1}\ddot{q}_1 + M_{\Theta 2}\ddot{q}_2 + \ldots + M_{\Theta k}\ddot{q}_k + \ldots + M_{\Theta N}\ddot{q}_N + C_{\Theta\Theta}\dot{\Theta} + C_{\Theta 1}\dot{q}_1 + C_{\Theta 2}\dot{q}_2 + \ldots + C_{\Theta k}\dot{q}_k + \ldots \\ \ldots + C_{\Theta N}\dot{q}_N + K_{\Theta\Theta}\Theta + K_{\Theta 1}q_1 + K_{\Theta 2}q_2 + \ldots + K_{\Theta k}q_k + \ldots + K_{\Theta N}q_N + H_{\Theta\Theta}\dot{\Theta} + H_{\Theta Y}\dot{Y} = F_\Theta \end{array} \tag{3.40}$$

Where,

$M_{X\Theta}$ is the coupled inertia between the translation $X(t)$ and the rotation $\Theta(t)$ of the cross–arm. It is defined by (3.33). Note that due to physical reasons, the coupling terms are symmetrical.

$M_{\Theta\Theta}$ is the rotary inertia of all the elements of the gantry stage with respect to the geometric center of the cross–arm. It is defined by (3.41),

$$M_{\Theta\Theta} = \int_{-L_b/2}^{L_b/2}\mu\left[\sum_{k=1}^{N}\psi_k(y)q_k\right]^2 dy + J_b + J_h + m_h Y^2 + m_h\left[d+\sum_{k=1}^{N}\psi_k(Y)q_k\right]^2 \;\therefore\; k=1,2,\ldots,N \tag{3.41}$$

Note that $M_{\Theta\Theta}$ has factors of $q_k(t)$. This is because the Θ–axis is deformed along with the deformation of the cross–arm.

$M_{\Theta Y}$ is the coupled inertia between the rotation $\Theta(t)$ and the motion $Y(t)$ of the payload. It is defined by (3.42)

$$M_{\Theta Y}=m_h\left[d+\sum_{k=1}^{N}\psi_k(Y)q_k\right]-Ym_h\left[\sum_{k=1}^{N}\psi'_k(Y)q_k\right]+J_h\left[\sum_{k=1}^{N}\psi''_k(Y)q_k\right]\ \therefore\ k=1,2,\ldots,N \tag{3.42}$$

$M_{\Theta k}$ is the coupled inertia between the rotation $\Theta(t)$ of the cross–arm and the vibrations of the cross–arm defined by the motion $q_k(t)$. It is defined by (3.43)

$$M_{\Theta k}=-Ym_h\psi_k(Y)+J_h\psi'_k(Y)-\left[\mu\int_{-L_b/2}^{L_b/2}y\psi_k(y)dy\right] \tag{3.43}$$

$C_{\Theta\Theta}$ is viscous friction opposing to the rotation $\Theta(t)$ of the cross–arm. It is defined by (3.44)

$$C_{\Theta\Theta}=c_{b1}+c_{b2} \tag{3.44}$$

$C_{\Theta k}$ is the coupling viscous friction between the rotation $\Theta(t)$ and the vibrations $q_k(t)$ of the cross–arm. It is defined by (3.45)

$$C_{\Theta k}=c_{b1}\psi'_k(y_1)+c_{b2}\psi'_k(y_2) \tag{3.45}$$

$K_{\Theta\Theta}$ is torsional stiffness opposing to the rotation $\Theta(t)$ of the cross–arm. It is defined by (3.46)

$$K_{\Theta\Theta}=k_{b1}+k_{b2} \tag{3.46}$$

$K_{\Theta k}$ is the coupling torsional stiffness between the rotation $\Theta(t)$ and the vibrations $q_k(t)$ of the cross–arm. It is defined by (3.47)

$$K_{\Theta k}=k_{b1}\psi'_k(y_1)+k_{b2}\psi'_k(y_2) \tag{3.47}$$

$H_{\Theta\Theta}$ and $H_{\Theta Y}$ are the centripetal and coriolis acceleration terms created by the motion of the payload, which is translating with respect to the rotation of the cross–arm $\Theta(t)$. They are defined by (3.48) and (3.49)

$$H_{\Theta\Theta}=2\left\{\int_{-L_b/2}^{L_b/2}\mu\left[\sum_{k=1}^{N}\psi_k(y)q_k\right]\left[\sum_{k=1}^{N}\psi_k(y)\dot{q}_k\right]dy+m_h\left[d+\sum_{k=1}^{N}\psi_k(Y)q_k\right]\left[\sum_{k=1}^{N}\psi_k(Y)\dot{q}_k\right]\right\}\ \therefore\ k=1,2,\ldots,N \tag{3.48}$$

$$H_{\Theta Y}=\left\{\begin{array}{l}\left\{-2Ym_h\left(\sum_{k=1}^{N}\psi'_k(Y)\dot{q}_k\right)+2\dot{\Theta}\left\{m_h\left[Y+\left(d+\sum_{k=1}^{N}\psi_k(Y)q_k\right)\left(\sum_{k=1}^{N}\psi'_k(Y)q_k\right)\right]\right\}+2J_h\left(\sum_{k=1}^{N}\psi''_k(Y)\dot{q}_k\right)\right\}+\\ +\dot{Y}\left[J_h\left(\sum_{k=1}^{N}\psi''_k(Y)q_k\right)-Ym_h\left(\sum_{k=1}^{N}\psi''_k(Y)q_k\right)\right]\end{array}\right\}\ \therefore\ k=1,2,\ldots,N \tag{3.49}$$

F_Θ is the equivalent force imposed by the actuators X_1 and X_2 to the cross–arm to produce the rotation $\Theta(t)$ of the cross–arm. It is defined by (3.50)

$$F_\Theta=(F_{b1}-F_{b2})\mathrm{Cos}(\Theta)(y_2-y_1)/2 \tag{3.50}$$

c) Motion $Y(t)$ of the payload

The mathematical definition of the motion $Y(t)$ of the payload is given by,

$$\frac{\partial L}{\partial Y(t)}-\frac{d}{dt}\left(\frac{\partial L}{\partial \dot{Y}(t)}\right)-\frac{\partial D}{\partial \dot{Y}(t)}+F_Y=0 \tag{3.51}$$

Or,

$$M_{XY}\ddot{X}+M_{\Theta Y}\ddot{\Theta}+M_{YY}\ddot{Y}+M_{Y1}\ddot{q}_1+M_{Y2}\ddot{q}_2+\ldots+M_{Yk}\ddot{q}_k+\ldots+M_{YN}\ddot{q}_N+C_{YY}\dot{Y}+H_{Y\Theta}\dot{\Theta}+H_{YY}\dot{Y}=F_Y \tag{3.52}$$

Where,

M_{XY} is the coupled inertia between the translation $X(t)$ and the motion $Y(t)$ of the payload. It is defined by (3.34)

$M_{\Theta Y}$ is the coupled inertia between the rotation $\Theta(t)$ and the motion $Y(t)$ of the payload. It is defined by (3.42)

M_{YY} is the inertia of the motion along the $Y(t)$ axis. It is defined by (3.53).

$$M_{YY} = m_h + m_h\left[\sum_{k=1}^{N}\psi_k'(Y)q_k\right]^2 + J_h\left[\sum_{k=1}^{N}\psi_k''(Y)q_k\right]^2 \quad \therefore\ k=1,2,\ldots,N \tag{3.53}$$

Note that M_{YY} has factors of $q_k(t)$. This is because the Y–axis is deformed along with the deformation of the cross–arm.

M_{Yk} is the coupled inertia between the motion of the payload $Y(t)$ and the vibrations of the cross–arm defined by the motion $q_k(t)$. It is defined by (3.54)

$$M_{Yk} = m_h\psi_k(Y)\left[\sum_{k=1}^{N}\psi_k'(Y)q_k\right] + J_h\psi_k'(Y)\left[\sum_{k=1}^{N}\psi_k''(Y)q_k\right] \quad \therefore\ k=1,2,\ldots,N \tag{3.54}$$

C_{YY} is viscous friction opposing to motion $Y(t)$ of the payload along the Y–axis. It is defined by (3.55)

$$C_{YY} = c_y \tag{3.55}$$

$H_{Y\Theta}$ and H_{YY} are the centripetal and coriolis acceleration terms created by the motion of the payload, which is translating with respect to the center of the cross–arm, which is translating $X(t)$ and rotating $\Theta(t)$. They are defined by (3.56) and (3.57)

$$H_{Y\Theta} = m_h\left\{2\left(\sum_{k=1}^{N}\psi_k(Y)\dot{q}_k\right) - \dot{\Theta}\left[Y + \left(d + \sum_{k=1}^{N}\psi_k(Y)q_k\right)\left(\sum_{k=1}^{N}\psi_k'(Y)q_k\right)\right]\right\} \quad \therefore\ k=1,2,\ldots,N \tag{3.56}$$

$$H_{YY} = \left\{\begin{array}{l} 2\left[m_h\left(\sum_{k=1}^{N}\psi_k'(Y)q_k\right)\left(\sum_{k=1}^{N}\psi_k'(Y)\dot{q}_k\right) + J_h\left(\sum_{k=1}^{N}\psi_k''(Y)q_k\right)\left(\sum_{k=1}^{N}\psi_k''(Y)\dot{q}_k\right)\right] + \\ +\dot{Y}\left(\sum_{k=1}^{N}\psi_k''(Y)q_k\right)\left[m_h\left(\sum_{k=1}^{N}\psi_k'(Y)q_k\right) + J_h\left(\sum_{k=1}^{N}\psi_k'''(Y)q_k\right)\right] \end{array}\right\} \quad \therefore\ k=1,2,\ldots,N \tag{3.57}$$

F_Y is the equivalent force imposed by the actuator Y to the payload. It is defined by (3.58)

$$F_Y = F_y - c_{cy}\,\mathrm{sign}(\dot{Y}) \tag{3.58}$$

d) Flexible motions $q_j(t)$ of the cross–arm

The mathematical definition of the flexible motion of the cross–arm $q_j(t)$ is given by (3.59). j is the number of the flexible motion that is being modeled.

$$\frac{\partial L}{\partial q_j(t)} - \frac{d}{dt}\left(\frac{\partial L}{\partial \dot{q}_j(t)}\right) - \frac{\partial D}{\partial \dot{q}_j(t)} + Q_j = 0 \tag{3.59}$$

Or,

$$\begin{array}{l} M_{jX}\ddot{X} + M_{j\Theta}\ddot{\Theta} + M_{jY}\ddot{Y} + M_{j1}\ddot{q}_1 + M_{j2}\ddot{q}_2 + \cdots + M_{jk}\ddot{q}_k + \cdots + M_{jN}\ddot{q}_N + C_{j\Theta}\dot{\Theta} + C_{j1}\dot{q}_1 + C_{j2}\dot{q}_2 + \cdots + C_{jk}\dot{q}_k + \cdots \\ \cdots + C_{jN}\dot{q}_N + K_{j\Theta}\Theta + K_{j1}q_1 + K_{j2}q_2 + \cdots + K_{jk}q_k + \cdots + K_{jN}q_N + H_{jY}\dot{Y} + H_{j\Theta}\dot{\Theta} = Q_j \end{array} \tag{3.60}$$

Where,

M_{jX} is the coupled inertia between the j – th vibrational motion $q_j(t)$ of the cross–arm and the translation $X(t)$ of the cross–arm. It is defined by (3.35), with $k = j$.

$M_{j\Theta}$ is the coupled inertia between the j – th vibrational motion $q_j(t)$ of the cross–arm and the rotation $\Theta(t)$ of the cross–arm. It is defined by (3.43), with $k = j$.

M_{jY} is the coupled inertia between the the j – th vibrational motion $q_j(t)$ of the cross–arm and the motion $Y(t)$ of the payload. It is defined by (3.54), with $k = j$ (excepting those inside the sums).

M_{jk} is the coupled inertia between the the j – th vibrational motion $q_j(t)$ and the k – th vibrational motion $q_k(t)$ of the cross–arm. It is defined by (3.61)

$$M_{jk} = m_h \psi_j(Y)\psi_k(Y) + J_h \psi'_j(Y)\psi'_k(Y) + m_{jk} \;\; \therefore \;\; m_{jk} = \int_{-L_b/2}^{L_b/2} \mu \psi_j(y)\psi_k(y)dy; \;\; k = 1,2,\ldots,N \tag{3.61}$$

Note that in M_{jk} the mass is also function of the payload's position (Y–axis).

$C_{j\Theta}$ is the coupling viscous friction between the j – th vibrational motion $q_j(t)$ and the rotation $\Theta(t)$ of the cross–arm. It is defined by (3.45), with $k = j$.

C_{jk} is the coupling viscous friction between the the j – th vibrational motion $q_j(t)$ and the k – th vibrational motion $q_k(t)$ of the cross–arm. It is defined by (3.62)

$$C_{jk} = c_{b1}\psi'_j(y_1)\psi'_k(y_1) + c_{b2}\psi'_j(y_2)\psi'_k(y_2) + c_{jk} \;\; \therefore \;\; c_{jk} = \int_{-L_b/2}^{L_b/2} \gamma EI \, \psi''_j(y)\psi''_k(y)dy \tag{3.62}$$

$K_{j\Theta}$ is the coupling torsional stiffness between the j – th vibrational motion $q_j(t)$ and the rotation $\Theta(t)$ of the cross–arm. It is defined by (3.45), with $k = j$.

K_{jk} is the coupling stiffness between the the j – th vibrational motion $q_j(t)$ and the k – th vibrational motion $q_k(t)$ of the cross–arm. It is defined by (3.63)

$$K_{jk} = k_{b1}\psi'_j(y_1)\psi'_k(y_1) + k_{b2}\psi'_j(y_2)\psi'_k(y_2) + k_{jk} \;\; \therefore \;\; k_{jk} = \int_{-L_b/2}^{L_b/2} EI \, \psi''_j(y)\psi''_k(y)dy \tag{3.63}$$

$H_{j\Theta}$ and H_{jY} are the centripetal and coriolis acceleration terms created by the j – th vibrating motion of the payload with respect to the center of the cross–arm, which is translating $X(t)$ and rotating $\Theta(t)$. They are defined by (3.64) and (3.65)

$$H_{k\Theta} = -\dot{\Theta}\left[\int_{-L_b/2}^{L_b/2} \mu \psi_k(y)\left(\sum_{k=1}^{N} \psi_k(y)q_k\right)dy + m_h \psi_k(Y)\left(d + \sum_{k=1}^{N} \psi_k(Y)q_k\right)\right] \;\; \therefore \;\; k = 1,2,\ldots,N \tag{3.64}$$

$$H_{kY} = 2\left\{m_h \psi_k(Y)\left[\left(\sum_{k=1}^{N} \psi'_k(Y)\dot{q}_k\right) - \dot{\Theta}\right] + J_h \psi'_k(Y)\left(\sum_{k=1}^{N} \psi''_k(Y)\dot{q}_k\right)\right\} + \dot{Y}\left[m_h \psi_k(Y)\left(\sum_{k=1}^{N} \psi''_k(Y)q_k\right) + J_h \psi'_k(Y)\left(\sum_{k=1}^{N} \psi'''_k(Y)q_k\right)\right] \tag{3.65}$$

Q_j is the force exciting the j – th flexible mode. It is defined by (3.66)

$$Q_j = F_{b1}\psi_j(y_1) + F_{b2}\psi_j(y_2) \tag{3.66}$$

Finally, the motion equations of the gantry stage taking into account the three rigid motions X(t), Θ(t), and Y(t); and N vibrational motions of the cross–arm can be defined by the matrix equation (3.67).

$$[M]\{\ddot{q}\} + [H]\{\dot{q}\} + [C]\{\dot{q}\} + [K]\{q\} = \{Q\} \tag{3.67}$$

Where, M, C and K are the inertia (3.68), damping (3.69), and stiffness (3.70) matrices. H is the coriolis and centripetal acceleration matrix (3.71),

$$M = \begin{bmatrix} M_{XX} & M_{X\Theta} & M_{XY} & M_{X1} & M_{X2} & \cdots & M_{Xk} & \cdots & M_{XN} \\ M_{X\Theta} & M_{\Theta\Theta} & M_{\Theta Y} & M_{\Theta 1} & M_{\Theta 2} & \cdots & M_{\Theta k} & \cdots & M_{\Theta N} \\ M_{XY} & M_{\Theta Y} & M_{YY} & M_{Y1} & M_{Y2} & \cdots & M_{Yk} & \cdots & M_{YN} \\ M_{X1} & M_{\Theta 1} & M_{Y1} & M_{11} & M_{12} & \cdots & M_{1k} & \cdots & M_{1N} \\ M_{X2} & M_{\Theta 2} & M_{Y2} & M_{12} & M_{22} & \cdots & M_{2k} & \cdots & M_{2N} \\ \vdots & \vdots & \vdots & \vdots & \vdots & \ddots & & & \vdots \\ M_{Xk} & M_{\Theta k} & M_{Yk} & M_{1k} & M_{2k} & & M_{kk} & & M_{kN} \\ \vdots & \vdots & \vdots & \vdots & \vdots & & & \ddots & \vdots \\ M_{XN} & M_{\Theta N} & M_{YN} & M_{1N} & M_{2N} & \cdots & M_{kN} & \cdots & M_{NN} \end{bmatrix}; \quad C = \begin{bmatrix} 0 & 0 & 0 & 0 & 0 & \cdots & 0 & \cdots & 0 \\ 0 & C_{\Theta\Theta} & 0 & C_{\Theta 1} & C_{\Theta 2} & \cdots & C_{\Theta k} & \cdots & C_{\Theta N} \\ 0 & 0 & C_{YY} & 0 & 0 & \cdots & 0 & \cdots & 0 \\ 0 & C_{\Theta 1} & 0 & C_{11} & C_{12} & \cdots & C_{1k} & \cdots & C_{1N} \\ 0 & C_{\Theta 2} & 0 & C_{12} & C_{22} & \cdots & C_{2k} & \cdots & C_{2N} \\ \vdots & \vdots & \vdots & \vdots & \vdots & \ddots & & & \vdots \\ 0 & C_{\Theta k} & 0 & C_{1k} & C_{2k} & & C_{kk} & & C_{kN} \\ \vdots & \vdots & \vdots & \vdots & \vdots & & & \ddots & \vdots \\ 0 & C_{\Theta N} & 0 & C_{1N} & C_{2N} & \cdots & C_{kN} & \cdots & C_{NN} \end{bmatrix} \tag{3.68), (3.69}$$

$$K=\begin{bmatrix} 0 & 0 & 0 & 0 & 0 & \cdots & 0 & \cdots & 0 \\ 0 & K_{\Theta\Theta} & 0 & K_{\Theta 1} & K_{\Theta 2} & \cdots & K_{\Theta k} & \cdots & K_{\Theta N} \\ 0 & 0 & 0 & 0 & 0 & \cdots & 0 & \cdots & 0 \\ 0 & K_{\Theta 1} & 0 & K_{11} & K_{12} & \cdots & K_{1k} & \cdots & K_{1N} \\ 0 & K_{\Theta 2} & 0 & K_{12} & K_{22} & \cdots & K_{2k} & \cdots & K_{2N} \\ \vdots & \vdots & \vdots & \vdots & \vdots & \ddots & & & \vdots \\ 0 & K_{\Theta k} & 0 & K_{1k} & K_{2k} & & K_{kk} & & K_{kN} \\ \vdots & \vdots & \vdots & \vdots & \vdots & & & \ddots & \vdots \\ 0 & K_{\Theta N} & 0 & K_{1N} & K_{2N} & \cdots & K_{kN} & \cdots & K_{NN} \end{bmatrix} ; \quad H=\begin{bmatrix} 0 & H_{X\Theta} & H_{XY} & 0 & 0 & \cdots & 0 & \cdots & 0 \\ 0 & H_{\Theta\Theta} & H_{\Theta Y} & 0 & 0 & \cdots & 0 & \cdots & 0 \\ 0 & H_{Y\Theta} & H_{YY} & 0 & 0 & \cdots & 0 & \cdots & 0 \\ 0 & H_{1\Theta} & H_{1Y} & 0 & 0 & \cdots & 0 & \cdots & 0 \\ 0 & H_{2\Theta} & H_{2Y} & 0 & 0 & \cdots & 0 & \cdots & 0 \\ \vdots & \vdots & \vdots & \vdots & \vdots & \ddots & & & \vdots \\ 0 & H_{k\Theta} & H_{kY} & 0 & 0 & & 0 & & 0 \\ \vdots & \vdots & \vdots & \vdots & \vdots & & & \ddots & \vdots \\ 0 & H_{N\Theta} & H_{NY} & 0 & 0 & \cdots & 0 & \cdots & 0 \end{bmatrix} \qquad (3.70),\ (3.71)$$

And there are, of course, the generalized coordinates (3.72), and the generalized forces (3.73),

$$q=\begin{bmatrix} X \\ \Theta \\ Y \\ q_1 \\ q_2 \\ \vdots \\ q_k \\ \vdots \\ q_N \end{bmatrix}; \quad Q=\begin{bmatrix} F_X \\ F_\Theta \\ F_Y \\ Q_1 \\ Q_2 \\ \vdots \\ Q_k \\ \vdots \\ Q_N \end{bmatrix}=\begin{bmatrix} F_{b1}+F_{b2} \\ \left(F_{b1}-F_{b2}\right)\cos\left(\Theta\right)\left(y_2-y_1\right)/2 \\ F_Y \\ F_{b1}\psi_1\left(y_1\right)+F_{b2}\psi_1\left(y_2\right) \\ F_{b1}\psi_2\left(y_1\right)+F_{b2}\psi_2\left(y_2\right) \\ \vdots \\ F_{b1}\psi_k\left(y_1\right)+F_{b2}\psi_k\left(y_2\right) \\ \vdots \\ F_{b1}\psi_N\left(y_1\right)+F_{b2}\psi_N\left(y_2\right) \end{bmatrix} \quad \therefore \quad \begin{aligned} F_{b1} &= F_1-m_1\ddot{X}_1-c_{g1}\dot{X}_1-c_{c1}\,\mathrm{sign}\left(\dot{X}_1\right) \\ F_{b2} &= F_2-m_2\ddot{X}_2-c_{g2}\dot{X}_2-c_{c2}\,\mathrm{sign}\left(\dot{X}_2\right) \\ F_Y &= F_y-c_{cy}\,\mathrm{sign}\left(\dot{Y}\right) \end{aligned} \qquad (3.72),\ (3.73)$$

3.2.3 Identification of the model's parameters

One of the greatest advantages of building a model that is based on the physical system is that it provides a deep understanding of the system's processes and of the interactions between the elements constituting it. Thanks to this understanding, the identification of the system's parameters can be done by organizing a series of simple experiments aiming to excite specific processes and interactions of the system. Moreover, these experiments can be executed using the built–in independent axis controllers that are provided with any industrial gantry stage.

For the sake of clarity, the identification process is divided in two parts. The first part concerns the identification of the parameters concerning the rigid motions X, Θ, and Y. The second part concerns the identification related to the flexible motions q_1, q_2…, q_N.

3.2.3.1 Identification of the parameters related to the rigid motions X, Θ, and Y

a) Identification of the parameters associated to the Y–axis

The identification starts with the simplest element of the gantry stage, the Y–axis. To avoid yaw motions, actuators X_1 and X_2 are set to a fixed position via its respective position controllers. As a result, $X(t) = constant$ and $\Theta(t) \approx 0$ rad. It is assumed that the motion of the payload does not induce vibrations to the cross–arm; therefore, $q_1 = q_2 = \ldots\ q_N = 0$. Under such conditions, the motion equations of the gantry stage (3.67) are reduced to,

$$m_h\ddot{Y}+c_y\dot{Y}+c_{cy}\,\mathrm{sign}\left(\dot{Y}\right)=F_y \qquad (3.74)$$

To estimate the static and viscous friction of the Y–axis, the payload is displaced back and forth along the actuator's stroke at various constant velocities. Under such conditions, the measured force F_y has two components:

$$c_y\dot{Y}_{ref}+c_{cy}\,\mathrm{sign}\left(\dot{Y}_{ref}\right)=F_y \qquad (3.75)$$

- one constant (corresponding to the static friction), i.e. $c_{cy}\,\mathrm{sign}\left(\dot{Y}\right)$
- one proportional to the velocity (corresponding to the viscous friction), i.e. $c_y\dot{Y}$

A similar experiment can be done to estimate the payload's mass m_h; this time by displacing it at constant acceleration cycles. The measured force F_y has then three components:

$$m_h \ddot{Y}_{ref} + c_y \dot{Y}_{ref} + c_{cy}\,\mathrm{sign}\left(\dot{Y}_{ref}\right) = F_y \quad \therefore \quad \dot{Y}_{ref} = \int \ddot{Y}_{ref}\,dt \tag{3.76}$$

- one constant (static friction), i.e. $c_{cy}\,\mathrm{sign}\left(\dot{Y}_{ref}\right)$
- one proportional to the linearly increasing velocity (viscous friction), i.e. $c_y \dot{Y}_{ref}$
- one constant (corresponding to the payload's mass m_h multiplied by the imposed constant acceleration), i.e. $m_h \ddot{Y}_{ref}$

The distance d between the centers of mass of the cross–arm and the payload can be estimated from the reaction forces F_1 and F_2 of the linear actuators X_1 and X_2 measured during the constant acceleration tests using,

$$d = -\left[\frac{\left(F_1 - F_2\right)\left(y_2 - y_1\right)}{2 m_h \ddot{Y}_{ref}}\right] \tag{3.77}$$

b) Identification of the parameters associated to the rigid motions $X(t)$ and $\Theta(t)$

The procedure to identify the parameters associated to the rigid motions $X(t)$ and $\Theta(t)$ is essentially the same that was used to identify the parameters of the Y–axis. We start by reducing the motion equations of the gantry stage. To do so, the payload is fixed in the middle of the cross–arm via its associate position controller, making $Y(t)$ and its derivatives are equal to zero. Then, to suppress the effects of the cross–arm vibrations, the measured forces $F_1(t)$ and $F_2(t)$ of the linear actuators X_1 and X_2 can be filtered in order to consider their mean value only.

To estimate the static and viscous friction of actuators X_1 and X_2, both actuators are displaced back and forth in synchronization along the x–direction at various constant velocities, i.e. $\dot{X}_1 = \dot{X}_2$. The measured forces F_1 and F_2 have two components each:

$$F_n = c_{gn} \dot{X}_{n\,ref} + c_{cn}\,\mathrm{sign}\left(\dot{X}_{n\,ref}\right) \quad \therefore \quad n = 1,2 \tag{3.78}$$

- one constant (corresponding to the static friction), i.e. $c_{cn}\,\mathrm{sign}\left(\dot{X}_{n\,ref}\right)$
- one proportional to the velocity (corresponding to the viscous friction), i.e. $c_{gn} \dot{X}_{n\,ref}$

By moving actuators X_1 and X_2 in synchronization at constant acceleration cycles, i.e. $\ddot{X}_1 = \ddot{X}_2$, the motion equations (3.67) can be reduced to expressions (3.79) and (3.80)

$$m_1 + m_2 + m_b + m_h = \left\{\left(F_1 + F_2\right) - \left[c_{c1}\,\mathrm{sign}\left(\dot{X}_{1ref}\right) + c_{c2}\,\mathrm{sign}\left(\dot{X}_{2ref}\right)\right] - \left(c_{g1} + c_{g2}\right)\dot{X}_{ref}\right\} \Big/ \ddot{X}_{ref} \quad \therefore \quad \begin{matrix} \dot{X}_{ref} = \int \ddot{X}_{ref}\,dt \\ \dot{X}_{1ref} = \dot{X}_{2ref} = \dot{X}_{ref} \end{matrix} \tag{3.79}$$

$$m_1 - m_2 = \left\{\left(F_1 - F_2\right) - \left[c_{c1}\,\mathrm{sign}\left(\dot{X}_{1ref}\right) - c_{c2}\,\mathrm{sign}\left(\dot{X}_{2ref}\right)\right] - \left(c_{g1} - c_{g2}\right)\dot{X}_{ref}\right\} \Big/ \ddot{X}_{ref} \tag{3.80}$$

Where,

$m_1+m_2+m_b+m_h$	is the total mass that is displaced by actuators X_1 and X_2.
$m_1 - m_2$	is the mass asymmetry of the gantry stage. The effect of the payload on the mass asymmetry has been eliminated by aligning its center of mass to those of the cross–arm along the x – direction.
F_1 and F_2	are the measured forces of actuators X_1 and X_2.
c_{g1}, c_{g2}, c_{c1}, and c_{c2}	are the viscous and static friction coefficients of actuators X_1 and X_2.
$\ddot{X}_{ref}$	is the imposed constant acceleration reference.

Expressions (3.79) and (3.80) represent a system with more unknowns, i.e. m_1, m_2, and m_b, than equations. To estimate each of these values, it is first necessary to calculate the parameters associated to the rotation of the cross–arm.

We start by identifying the torsional stiffness of the mechanical joints. To do so, the cross–arm is rotated to different fixed angles[8], e.g. –0.1 rad, –0.09 rad… +0.1 rad. Then, by measuring the forces F_1 and F_2 necessary to hold the cross–arm at each fixed angle, it is possible to calculate the value of the total rotary stiffness $k_{b1}+k_{b2}$ using (3.81). Remember that the cross–arm's and mechanical joint's stiffnesses are considered elastically decoupled, i.e. the cross–arm stiffness is a lot greater than the mechanical joints stiffness.

$$k_{b1}+k_{b2}=\left(F_1-F_2\right)\left(y_2-y_1\right)\Big/2\Theta_{ref} \tag{3.81}$$

To estimate the damping coefficient of the junctions, the cross–arm is rotated at various constant speeds, i.e. $\dot{X}_{1\,ref}=-\dot{X}_{2\,ref}$. Then, by measuring the forces F_1 and F_2, it is possible to calculate the value of the coefficients $c_{b1}+c_{b2}$ of the junctions using (3.82).

$$\begin{aligned} &c_{b1}+c_{b2}=\left\{\left[\left(F_1-F_2\right)-\left(c_{c1}\,\mathrm{sign}\left(\dot{X}_{1\,ref}\right)-c_{c2}\,\mathrm{sign}\left(\dot{X}_{2\,ref}\right)\right)\right]\left(y_2-y_1\right)\Big/2-\left(k_{b1}+k_{b2}\right)\Theta_{ref}\right\}\Big/\dot{\Theta}_{ref}-\left(c_{g1}+c_{g2}\right)\left(y_2-y_1\right)^2\Big/4 \\ &\therefore\quad \dot{\Theta}_{ref}\approx\left[\left(\dot{X}_{1\,ref}-\dot{X}_{2\,ref}\right)\Big/\left(y_2-y_1\right)\right];\quad \Theta_{ref}=\int\dot{\Theta}_{ref}dt \end{aligned} \tag{3.82}$$

Note that with respect to (3.5), the expression for $\dot{\Theta}_{ref}$ has been linearized using the small angle approximation, i.e. $\tan(\Theta) \approx \Theta$. This is possible because the yaw angle of the cross–arm is mechanically limited to less than 10°.

To estimate the rotary inertia of the gantry stage, the cross–arm is rotated at various constant angular accelerations, i.e. $\ddot{X}_{1\,ref}=-\ddot{X}_{2\,ref}$. Then, by measuring the forces F_1 and F_2, it is possible to calculate the rotary inertia of the gantry stage using (3.83). For convenience, the payload's position has been set to zero, i.e. $Y(t) = 0$.

$$\begin{aligned} &J_b+J_h+\left(m_1+m_2\right)\left(\frac{y_2-y_1}{2}\right)^2+m_h d^2= \\ &\frac{1}{\ddot{\Theta}_{ref}}\left\{\left\{\left(F_1-F_2\right)-\left[c_{c1}\,\mathrm{sign}\left(\dot{X}_{1\,ref}\right)-c_{c2}\,\mathrm{sign}\left(\dot{X}_{2\,ref}\right)\right]\right\}\left(\frac{y_2-y_1}{2}\right)-\left[c_{b1}+c_{b2}+\left(c_{g1}+c_{g2}\right)\left(\frac{y_2-y_1}{2}\right)^2\right]\dot{\Theta}_{ref}-\left(k_{b1}+k_{b2}\right)\Theta_{ref}\right\} \\ &\therefore\quad \ddot{\Theta}_{ref}\approx\left[\left(\ddot{X}_{1\,ref}-\ddot{X}_{2\,ref}\right)\Big/\left(y_2-y_1\right)\right];\quad \dot{\Theta}_{ref}=\int\ddot{\Theta}_{ref}dt;\quad \Theta_{ref}=\int\dot{\Theta}_{ref}dt \end{aligned} \tag{3.83}$$

Where,

J_b and J_h are, respectively, the rotary inertias of the cross–arm and of the payload.

Finally, to estimate the values of the masses of actuators, it is assumed that the rotary inertias of the cross–arm J_b and of the payload J_h can be approximated using (3.84), which is the definition of the rotary inertia of a bar about its centroid.

$$J_b=m_b L_b^2\Big/12;\quad J_h=m_h L_h^2\Big/12 \tag{3.84}$$

Then, providing that the parameters L_b, L_h, d, m_h, and the difference $(m_1–m_2)$ are known; with some algebraic manipulation of (3.79) and (3.83), it is possible to estimate the remaining unknown parameters m_1, m_2, and m_b associated to the rigid motions $X(t)$ and $\Theta(t)$ of the gantry stage.

One possible objection to this identification method is that, as the estimation of one parameter relies on the estimation of a previous parameter and so on, the risk of error propagation may be important.

[8] The yaw angle of most gantry stages, having flexible mechanical joints, is limited to about 0.1 rad (or 7°). Beyond this limit, the gantry stage may experience permanent mechanical damage. For gantries having rigid joints this limit is far lower. **The maximum yaw angle supported by the gantry stage is usually specified by the fabricant.**

3.2.3.2 Identification of the parameters associated to the flexible motions $q_1(t)$, $q_2(t)$, ..., $q_N(t)$

Remarks: It is important to take into account that on a physical application, usually the first – and possibly the second – flexible mode(s) have a significant influence on the overall system's performance. Higher–order flexible modes, unless excited, are of very small amplitude and are quickly damped.

The identification of the flexible modes is based on the modal–analysis identification technique (Harris, et al., 2002). It goes as follows:

The resonance frequency of a single degree–of–freedom system such as the one on **Figure 3 – 19** is defined by (3.85)

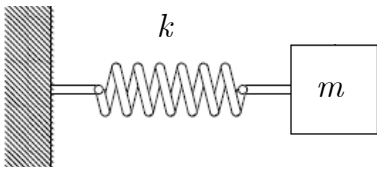

Figure 3 – 19 : *Single degree–of–freedom system*

$$\omega = \sqrt{k/m} \tag{3.85}$$

Now, based upon the model of the gantry machine (3.67), and more particularly on expressions M_{jk} (3.61) and K_{jk} (3.63), the $k^{\underline{th}}$ resonance frequency of the cross–arm can be defined as,

$$\omega_k\left[Y(t)\right] = \left(\sqrt{\frac{K_{jk}}{M_{jk}}}\right)_{j=k} = \sqrt{\frac{k_{b1}\psi_k'^2(y_1) + k_{b2}\psi_k'^2(y_2) + k_{kk}}{m_h\psi_k^2\left[Y(t)\right] + J_h\psi_k'^2\left[Y(t)\right] + m_{kk}}} \quad \therefore \quad \begin{matrix} k_{kk} = \int_{-L_b/2}^{L_b/2} EI\,\psi_k''^2(y)dy \\ m_{kk} = \int_{-L_b/2}^{L_b/2} \mu\,\psi_k^2(y)dy \end{matrix} \tag{3.86}$$

Where,

- k_{b1} and k_{b2} are the rotary stiffnesses of the mechanical joints 1 and 2.
- $\omega_k[Y(t)]$ is the $k^{\underline{th}}$ resonance frequency of the cross–arm in function of the payload's position.
- k_{kk} is the modal stiffness of the $k^{\underline{th}}$ flexible mode of the cross–arm without the payload
- m_{kk} is the modal mass of the $k^{\underline{th}}$ flexible mode of the cross–arm without the payload
- m_h is the payload's mass
- J_h is the payload's rotary inertia.
- $\psi_k[Y(t)]$ is the (non–dimensional) mode shape of the $k^{\underline{th}}$ flexible mode of the cross–arm in function of payload's position.
- $\psi_k'(y)$ is the derivative of the $k^{\underline{th}}$ mode shape with respect to y.

Assuming that,

$$k_{kk} \gg k_{b1}\psi_k'^2(y_1) + k_{b2}\psi_k'^2(y_2); \quad m_h\psi_k^2\left[Y(t)\right] + m_{kk} \gg J_h\psi_k'^2\left[Y(t)\right] \tag{3.87}$$

Then, the expression (3.86) of the $k^{\underline{th}}$ resonance frequency of the cross–arm can be simplified to,

$$\omega_k\left[Y(t)\right] = \sqrt{\frac{k_{kk}}{m_{kk} + m_h\psi_k^2\left[Y(t)\right]}} \tag{3.88}$$

To estimate the parameters k_{kk}, m_{kk}, and $\psi_k[Y(t)]$ of each flexible mode k; we have developed a method that is based on the measurement means provided by the gantry stage itself. Indeed, the resonance frequencies of the cross–arm can be extracted from either the measured forces F_1 and F_2, or from the tracking errors of actuators X_1 or X_2, as in **Figure 3 – 20**. This extraction can be done using a lot of different numerical methods such as the Fast Fourier Transform (FFT), correlation, and so on. Further information on such methods can be obtained, for example, from (Hayes, 1996).

It has to be noted that extracting the resonance frequencies from either the measured forces or tracking errors of actuators X_1 and X_2 requires some practical experience. The person executing the experiments has to be capable of distinguishing them from other sources of vibration or noise. These sources can be: switching noise, actuator's cogging forces, vibration of the supporting structure, mechanical backlash, and so on.

Additionally, it is important to note that in real applications, only very few flexible modes are excited. The example plots presented on **Figure 3 – 20** have been taken from a gantry stage whose cross–arm has been replaced with a very slender beam, see **Figure 3 – 5**. The objective of this modification was to have the cross–arm vibrating at the lowest possible eigenfrequencies and to excite as many of them as possible during the motion.

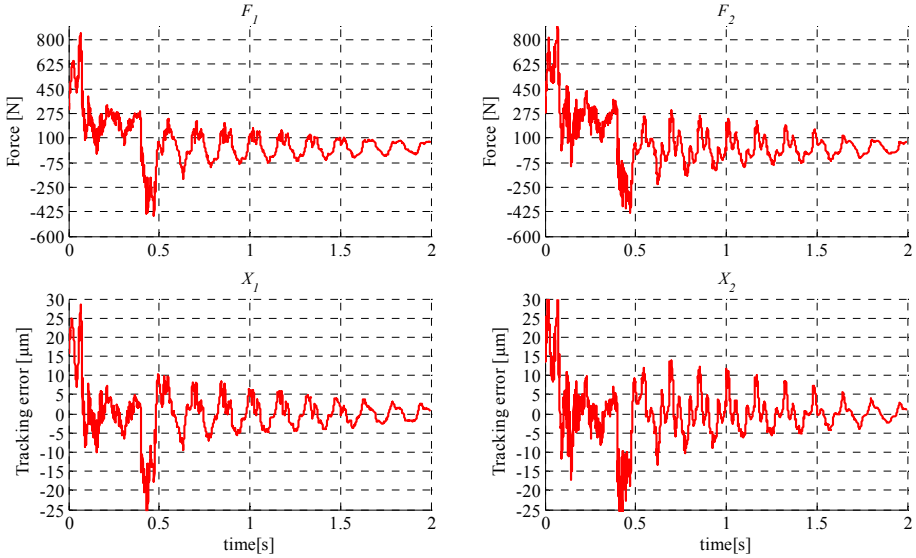

Figure 3 – 20 : *Measured forces F_1 and F_2, and tracking errors of linear actuators X_1 and X_2 of a flexible gantry stage. Motion from $X = -0.15$ m to $X = 0.15$ m. Max acceleration* 10 m/s²; *Max velocity* 0.75 m/s.

From the measurements with different dummy payloads, it has been found that the resonance frequencies of the cross–arm follow a pattern whose shape is independent of the payload's mass, see **Figure 3 – 21**.

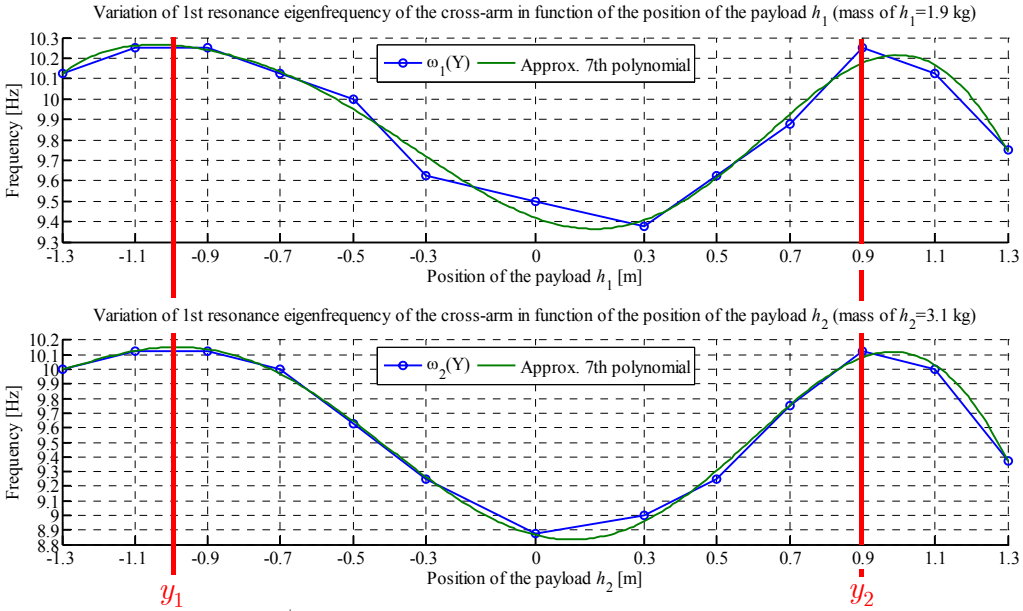

Figure 3 – 21 : *Variation of the* 1st *resonance frequency of the cross–arm in function of the position of the payload. Test realized for two different payload masses.*

Note that the highest resonance frequency occurs when the payload is aligned to either mechanical joint 1 or 2, i.e. positions y_1 or y_2 on **Figure 3 – 21**. Physically, this means that the payload is invisible[9] to the cross–arm since it is located at a node; therefore, (3.88) becomes (3.89).

$$\omega_k\left(y_1 \text{ or } y_2\right)=\sqrt{k_{kk}/m_{kk}} \tag{3.89}$$

At this point, it is possible to estimate the $k^{\underline{th}}$ modal stiffness k_{kk} and modal mass m_{kk} using modal decomposition, as described in (Harris, et al., 2002). Nevertheless, as the proposed method is aimed to use no measurement equipment other than the provided by the gantry stage itself, it is assumed that the value of the modal mass m_{kk} is half of the identified mass m_b of the cross–arm[10]. Then, the value of the $k^{\underline{th}}$ modal stiffness k_{kk} can be determined using,

$$k_{kk}=m_{kk}\omega_k^2\left(y_1\right)=m_{kk}\omega_k^2\left(y_2\right) \tag{3.90}$$

The remaining parameter to estimate is the mode shape $\psi_k(Y)$ of the cross–arm's $k^{\underline{th}}$ flexible mode. This parameter can be estimated from the measured variation of the eigenfrequency by re–organizing (3.88) into (3.91). Note that the value of ω_0 is the eigenfrequency of the cross–arm when the payload is located at either position y_1 or y_2. Note also that the sign of $\psi_k(Y)$ is chosen accordingly in order to make $\psi_k(Y)$ continuous over the cross-arm's span.

$$\psi_k\left(Y\right)=\pm\sqrt{\left(m_{kk}/m_h\right)\left\{\left[\omega_0/\omega_k\left(Y\right)\right]^2-1\right\}} \quad \therefore \quad \omega_0=\sqrt{k_{kk}/m_{kk}} \tag{3.91}$$

This way it is possible to identify the remaining unknown parameter of the model and to characterize the influence of the motion of the payload over the dynamical response of the system. See **Figure 3 – 22**.

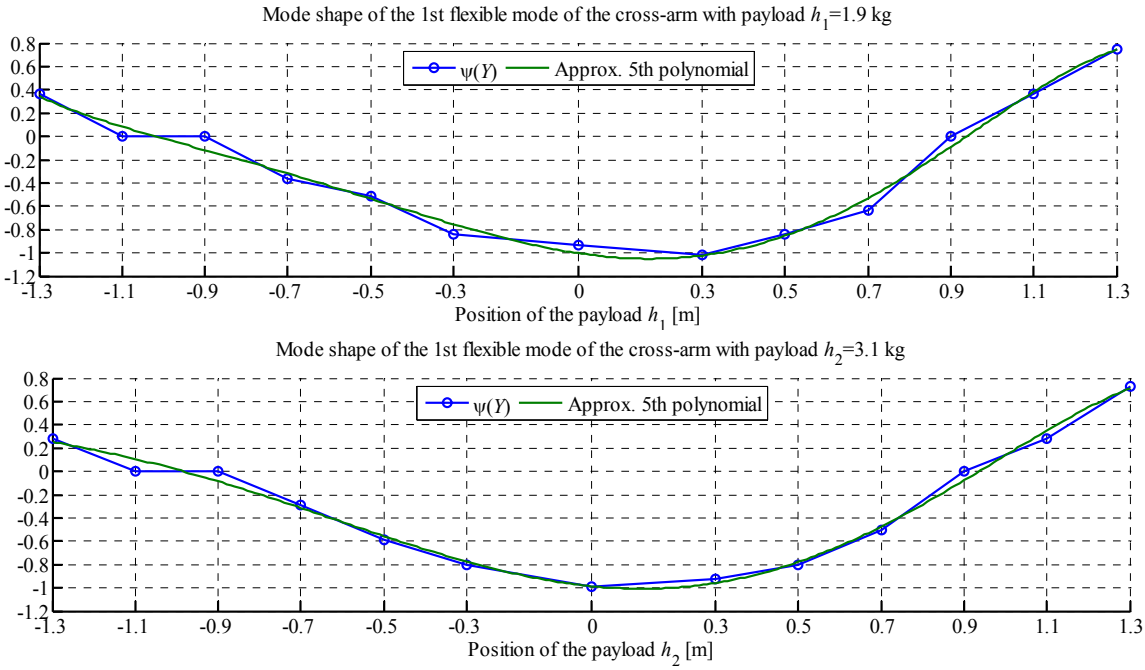

Figure 3 – 22 : *Dimensionless mode shape $\psi_1(Y)$ of the 1st flexible mode of the gantry stage's cross–arm for two different payload masses.*

3.2.3.3 Model validation

With the model's parameters identified, we may proceed to its validation. This will be presented in detail on Chapter 4 for three different gantry stages.

---

[9] Note that there is a slight difference between the maximum of the first eigenfrequency with each payload mass. This is because of the rotary inertia of the payload J_h, which for convenience has been ignored.

[10] This assumption is supported by the estimations of the modal mass m_{kk} made using the method presented on (Harris, et al., 2002)

3.3 Controlling the gantry stage

3.3.1 Inversion–based control of (electro)mechanical systems using causal graphical representations

3.3.1.1 A brief introduction to causal graphical representations

A System is composed of inputs and outputs. Its modeling consists in expressing outputs from inputs. (Electro)Mechanical systems can be decomposed into elementary interconnected elements, which manage energy dissipation, storage, and transformation. All sub–systems can be modeled using differential equations with state variables. These variables are associated with energy and are dependent on inputs and time according to integral causality. When inputs change, the state variables reach other steady states after transient states: outputs are always consequence of inputs. The natural causality is the integral causality because it respects the energy flowing considering the state variables as delayed from their inputs. Integral causal representation leads then to a more physical description (Barre, et al., 2006). Based on the principle of natural, or integral, causality; the Causal Ordering Graph (COG), and later the Energetic Macroscopic Representation (EMR), formalisms were built.

The COG was introduced by (Hautier, et al., 1996) to represent, using a causal graph of variables, power electronics and electrical machines models. Then, by using the inversion–based control methodology (see § 3.3.1.2), the inversion of such graphs yields one control structure of the system with measurements and controllers. By using the COG formalism, any system respecting the principle of integral causality, can be represented using two types of relationships: **Rigid** and **Causal**

Rigid relationships indicate that there is no time dependence between output and input. That is, a change on the input has an immediate effect on the output. A rigid relation is depicted by an orange ellipse with a double arrow inside, as in **Figure 3 – 23** (a).

Causal relationships indicate time dependence. Since integral causality is imposed, the output is then the integral of the input. A Causal relationship is depicted by an orange ellipse with a single arrow inside, as in **Figure 3 – 23** (b).

The COG representation has the advantage of depicting, in detail, a system's processes and the interactions between its elements.

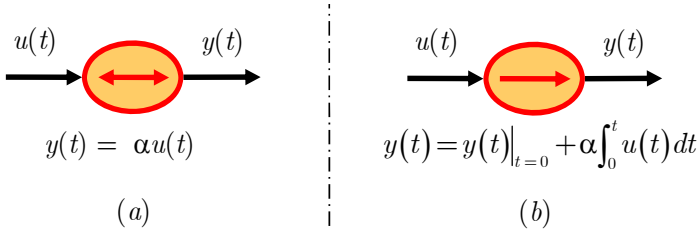

Figure 3 – 23 *: COG with rigid* (a) *and causal* (b) *relationships*

With a growing interest on multi–machine multi–converter systems, and confronted to the complexity of their modeling and control; the EMR was introduced as a complementary tool of the COG as it allows an even more synthetic representation of complex systems (Bouscayrol, 2003). The EMR is based on the action–reaction principle. All subsystems are connected by action–reaction variables and its product yields the exchanged power. As for the COG, internal descriptions of elements are defined according to internal causality. Therefore, the inversion–based control methodology is also applicable to this formalism. The EMR has also been recently extended to the study of multi–physical systems; see for example (Agbli, et al., 2011)

The EMR includes four types of elements: *source*, *accumulation*, *conversion*, and *coupling*. Source elements are terminal elements which deliver or receive energy; they are depicted by green oval pictograms, as in **Figure 3 – 24** (a). Accumulation elements store energy, e.g. a capacitor, a

flywheel, an inductance, etc.; they are depicted by orange rectangular pictograms with an oblique bar inside, **Figure 3 – 24** (*b*). Conversion elements transform energy without accumulating it, e.g. an inverter, a lever, a gearbox, etc.; they are depicted by an orange square for a mono–physical conversion, e.g. electrical–electrical; or by an orange circle if the conversion is multi–physical, e.g. electrical–mechanical; as in **Figure 3 – 24** (*c*). Finally, coupling elements allow distributing energy among subsystems; they are depicted by interleaved orange squares for a mono–physical coupling and by interleaved orange circles for a multi–physical coupling, see **Figure 3 – 24** (*d*).

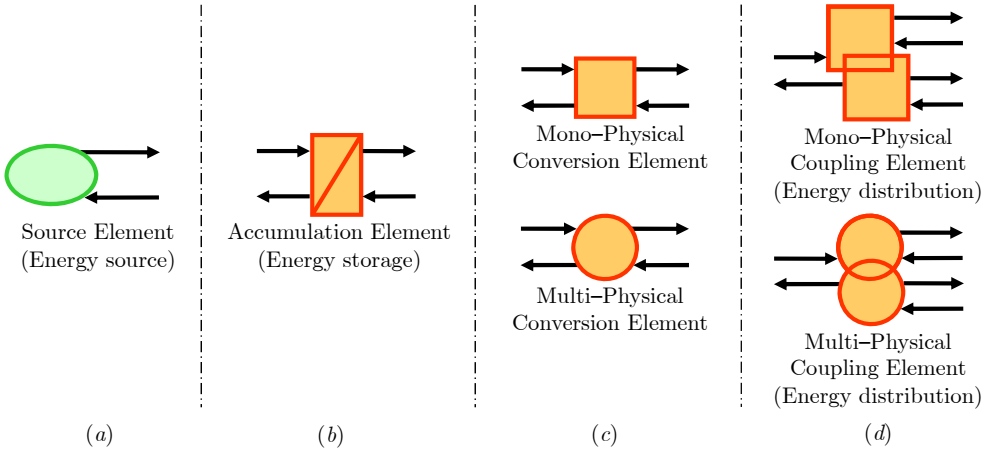

Figure 3 – 24 *: EMR elements:* (*a*) *source*, (*b*) *accumulation*, (*c*) *conversion, and* (*d*) *coupling*

3.3.1.2 Inversion–based control methodology

The objective of modeling a system is to put in evidence the variables of the system that we want to act upon (the outputs), the variables that generate an evolution of the output (the inputs), and the approximate behavior model describing the relationships between inputs and outputs.

The objective of a control structure is to define an adapted input so to produce the expected output, see **Figure 3 – 25**. In fact, the control has to express the tuning input $u_{tun}(t)$ as a function of the output set–point $y_{ref}(t)$. In consequence, the control can be defined as the inverse of the approximate behavior model describing the relationships between the inputs and outputs.

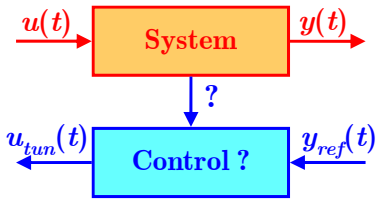

Figure 3 – 25 *: The inversion principle*

For the systems defined using the COG or EMR causal graphical descriptions, there are three basic inversion rules[11].

(1) *Single–input rigid relationships*

If the relation α is correctly estimated by $\tilde{\alpha}$, then, a direct inversion can be used,

$$y(t)=\alpha u(t) \;\rightarrow\; u_{tun}(t)=\frac{1}{\tilde{\alpha}}y(t) \tag{3.92}$$

This type of inversion requires neither measurement nor controller; see **Figure 3 – 26** (*a*)

[11] For further information on COG and EMR causal graphical descriptions and inversion–based control methodology see (Hautier, et al., 1996), (Bouscayrol, 2003), and (Barre, 2004).

(2) *Multi–input rigid relationships*

If it is chosen to act on one specific input to impose the output; then, the supplementary inputs are regarded as disturbances. These disturbances have to be either measured or estimated so that it is possible to define the tuning input $u_{tun}(t)$ from the output set point $y_{ref}(t)$, see **Figure 3 – 26** (b)

$$y(t)=u_1(t)+u_2(t) \;\rightarrow\; u_{1\,tun}(t)=y_{ref}(t)-u_{2\,mes}(t) \tag{3.93}$$

This type of inversion requires a controller if the disturbance inputs can be neither measured nor estimated.

(3) *Single–input causal relationships*

The direct inversion of such a relationship leads to a derivation, which has non–physical causality. To overcome this drawback, an indirect inversion is made by using a controller. That is, the tuning input $u_{tun}(t)$ is generated by the product of the controller function $\boldsymbol{C}$ and the comparison between the output set point $y_{ref}(t)$ and the output itself $y_{mes}(t)$, see (3.94). The objective of such comparison is to make the output $y_{mes}(t)$ converge towards the set point $y_{ref}(t)$. The controller function $\boldsymbol{C}$ determines the dynamics of such convergence.

$$y(t)=y(t)\Big|_{t=0}+\int u(t)dt \;\rightarrow\; u_{tun}(t)=\boldsymbol{C}\left[y_{ref}(t)-y_{mes}(t)\right] \tag{3.94}$$

As aforementioned, the inversion of this type of relationship requires the measurement of the output and a controller, see **Figure 3 – 26** (c).

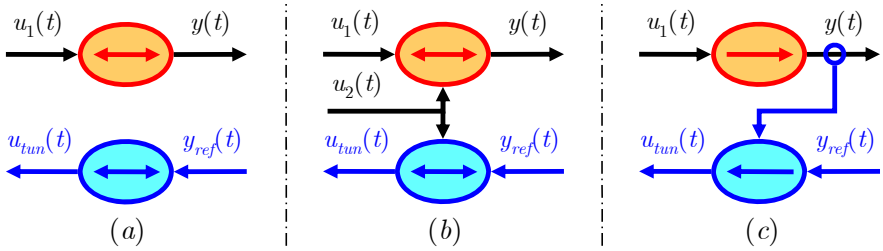

Figure 3 – 26 *: Basic inversions depicted using the COG description*

Other relationships: For non–linear or not well–defined rigid relationships, a direct inversion is not always possible. Controllers can be used then. Nevertheless, most relationships can be decomposed into the three basic relationships presented above.

Feedforward control structure: If the set point derivatives are also known, a feedforward control structure can be defined by direct inversion of the system's model. Then, the overall control structure of a system can be defined as,

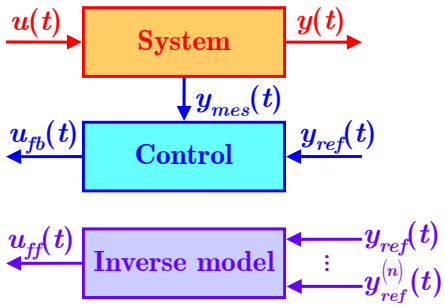

Figure 3 – 27 *: The inversion principle applied to the derivation of a feedforward and a feedback control structure*

Application to the COG description: In the COG description; all control sub–systems are depicted by oval pictograms; blue for the feed–back, purple for the feedforward. Pictograms describing direct inversions contain a double–headed arrow for they describe rigid relationships. Pictograms describing indirect inversions (controllers) contain a single–headed arrow. See **Figure 3 – 26**.

Application to the EMR description: In the EMR description; all control sub–systems are depicted by parallelograms; blue for the feed–back, purple for the feedforward. Parallelograms describing controllers contain an oblique bar, see **Figure 3 – 30**.

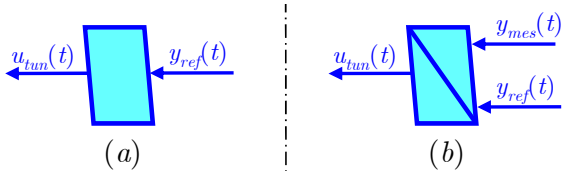

Figure 3 – 28 *: Control sub–systems depicted using the EMR description. Direct inversion (a). Controller (indirect inversion) (b)*

3.3.2 Causal Ordering Graph of the gantry stage

Among the many tools available to represent the dynamical model of the gantry stage, the Causal Ordering Graph (COG) is the chosen one. Based on the information flows within the system, i.e. force, velocity, etc.; this description allows evaluating graphically: the interactions between the elements composing the system and system properties such as structural Observability and Controllability (Gomand, 2008).

On the following, the motion equations of the gantry stage, (3.67) to (3.73), will be defined in terms of:

- The generalized coordinates $X(t)$, $\Theta(t)$, $Y(t)$, $q_1(t),\ldots,q_k(t)$, which are the outputs of the system.
- The input forces $F_1(t)$, $F_2(t)$, and $F_Y(t)$, which are the electromagnetic forces generated by the linear actuators X_1, X_2, and Y. The generalized forces, i.e. F_X, F_Θ, F_Y, $Q_1,\ldots,Q_k$, are functions of these forces.

a) Translation of the gantry stage (X–axis)

The translation is defined by the first row of matrix expressions (3.67) to (3.73). By reorganizing it, one obtains the linear acceleration of the cross–arm (3.95), and by successive integration, its velocity (3.96), and its position (3.97)

$$\ddot{X}=\frac{F_X-M_{X\Theta}\ddot{\Theta}-M_{XY}\ddot{Y}-\sum_{k=1}^{N}M_{Xk}\ddot{q}_k-H_{X\Theta}\dot{\Theta}-H_{XY}\dot{Y}}{M_{XX}};\quad \dot{X}=\int\ddot{X}dt;\quad X=\int\dot{X}dt \qquad (3.95),\ (3.96),\ (3.97)$$

b) Rotation of the gantry stage (Θ–axis)

The rotation is defined by the second row of matrix expressions (3.67) to (3.73). By reorganizing it, one obtains the angular acceleration of the cross–arm (3.98), and by successive integration, its angular velocity (3.99), and its yaw angle (3.100)

$$\ddot{\Theta}=\frac{F_\Theta-M_{X\Theta}\ddot{X}-M_{\Theta Y}\ddot{Y}-\sum_{k=1}^{N}M_{\Theta k}\ddot{q}_k-H_{\Theta\Theta}\dot{\Theta}-H_{\Theta Y}\dot{Y}-C_{\Theta\Theta}\dot{\Theta}-\sum_{k=1}^{N}C_{\Theta k}\dot{q}_k-K_{\Theta\Theta}\Theta-\sum_{k=1}^{N}K_{\Theta k}q_k}{M_{\Theta\Theta}} \qquad (3.98)$$

$$\dot{\Theta}=\int\ddot{\Theta}dt\,;\ \Theta=\int\dot{\Theta}dt \qquad (3.99),\ (3.100)$$

c) Motion of the payload (Y–axis)

The motion of the payload is defined by the third row of matrix expressions (3.67) to (3.73). By reorganizing it, one obtains the acceleration of the payload along the Y–axis (3.101), and by successive integration, its velocity (3.102), and position (3.103)

$$\ddot{Y}=\frac{F_Y-M_{XY}\ddot{X}-M_{\Theta Y}\ddot{\Theta}-\sum_{k=1}^{N}M_{Yk}\ddot{q}_k-H_{Y\Theta}\dot{\Theta}-H_{YY}\dot{Y}-C_{YY}\dot{Y}}{M_{YY}};\quad \dot{Y}=\int\ddot{Y}dt;\quad Y=\int\dot{Y}dt \qquad (3.101),\ (3.102),\ (3.103)$$

d) Flexible modes (q_1, q_2, q_3, …, q_N)

The vibration modes of the cross–arm are defined by the fourth and following rows of matrix expressions (3.67) to (3.73). By reorganizing each, one obtains the acceleration of the vibration mode $q_j(t)$ of the cross–arm (3.104), and by successive integration, its velocity (3.105), and its position (3.106)

$$\ddot{q}_j = \frac{Q_j - M_{Xj}\ddot{X} - M_{\Theta j}\ddot{\Theta} - M_{Yj}\ddot{Y} - \sum_{\substack{k=1 \\ k\neq j}}^{N} M_{jk}\ddot{q}_k - H_{j\Theta}\dot{\Theta} - H_{jY}\dot{Y} - C_{\Theta j}\dot{\Theta} - \sum_{k=1}^{N} C_{jk}\dot{q}_k - K_{\Theta j}\Theta - \sum_{k=1}^{N} K_{jk}q_k}{M_{jj}} \tag{3.104}$$

$$\dot{q}_j = \int \ddot{q}_j\,dt\,;\; q_j = \int \dot{q}_j\,dt \tag{3.105), (3.106}$$

e) Input forces $F_1(t)$, $F_2(t)$, and $F_Y(t)$

With exception of $F_Y(t)$, all the forces acting on the gantry stage are defined in terms of the equivalent forces $F_{b1}(t)$ and $F_{b2}(t)$. These forces are the result of the interaction between the actual input forces, i.e. the electromagnetic forces $F_1(t)$ and $F_2(t)$ generated by actuators X_1 and X_2, and the physical parameters of the actuators; namely, their respective inertias and static–viscous frictions.

To include the effects of the physical parameters of the actuators within the COG representation, their associated coordinates $X_1(t)$ and $X_2(t)$ are expressed in terms of the generalized coordinates $X(t)$ and $\Theta(t)$.

Such transformation is based on expressions (3.4) and (3.5)

$$F_{b1} = F_1 - m_1\ddot{X}_1 - c_{g1}\dot{X}_1 - c_{c1}\,\mathrm{sign}\left(\dot{X}_1\right) \quad \therefore \quad X_1(t) = X(t) + \left(\frac{y_2 - y_1}{2}\right)\sin(\Theta) \tag{3.107}$$

$$F_{b2} = F_2 - m_2\ddot{X}_2 - c_{g2}\dot{X}_2 - c_{c2}\,\mathrm{sign}\left(\dot{X}_2\right) \quad \therefore \quad X_2(t) = X(t) - \left(\frac{y_2 - y_1}{2}\right)\sin(\Theta) \tag{3.108}$$

f) Graphical representation

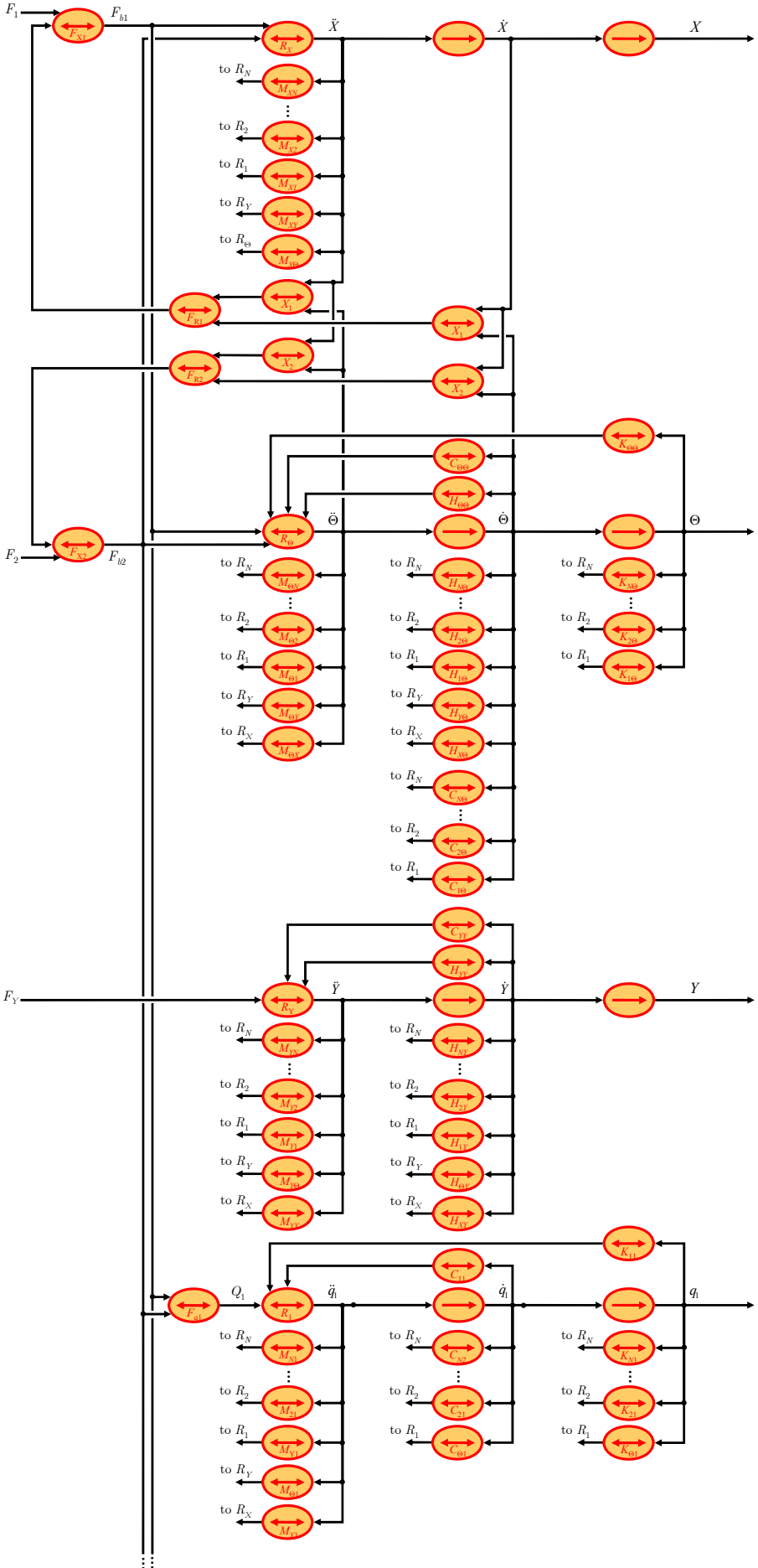

Figure 3 – 29 : *COG of the flexible gantry stage including N–flexible modes.*

As it can be appreciated on **Figure 3 – 29**, the objective of the COG representation is to put in evidence all the elements (or forces) interacting within the system. For the sake of clarity, most of the connections aren't shown. Instead, they are referred to the motion (or mode) they're connecting to. For example, the reference "to R_X" means that the studied motion is interacting with the motion $X(t)$. The reference "to R_N" means that the studied motion is interacting with the N–th flexible mode of the cross–arm. And so on.

As intended, the COG representation of **Figure 3 – 29** is general to all gantry stages. And, since it is derived from the general motion equations, it can be adapted to represent any type of gantry stage.

The next logical step is to obtain a control structure for the gantry stage using the inversion–based control methodology (§ 3.3.1.2). Nevertheless, the use of the COG description for this task may be unpractical regarding the implementation if one considers the number of measurements, estimations, and compensations to execute at each time step. To simplify the task, we move to the more compact representation provided by the Energetic Macroscopic Representation (EMR) description.

3.3.3 Energetic Macroscopic Representation of the gantry stage

The EMR description is aimed to represent multi–machine multi–converter and multi–physical systems in a concise manner. Its objective is to represent this kind of systems in terms of the exchanged power between the elements constituting them, and by using the inversion–based control methodology, to control such exchanges. The EMR description does not admit, however, the representation of mutual energy storage elements. This was put in evidence by (Kestelyn, 2003) when modeling the magnetic electrical coupling – which also stores energy – of multi–phase Permanent Magnet Synchronous Motor (PMSM) using the EMR description. For the gantry stage, this mutual energy storage is found in the form of the kinetic and potential elastic energy of the cross–arm connecting actuators X_1, X_2, and Y. In the case of (Kestelyn, 2003), the approach that was chosen to overcome this minor inconvenience was to represent the multi–phase PMSM on a decoupling basis, i.e. Park's transformation. The same approach will be adopted for the gantry stage.

To decouple the motion equations of the gantry stage, we apply a modal transformation. At this point, a first obstacle is encountered. Indeed, if expressions (3.67) to (3.73) are used to calculate a decoupling basis, we'll find that the eigenfrequencies of rigid motions X and Y are repeated[12]. As a result, the orthogonalization of the motion equations has to be force using an iterative method (such as Gramm–Schmidt, the Householder transformation, the Givens rotation, etc). Nevertheless, the use of these methods is contrary to the objective of passing from a COG to an EMR description, since, due to its nature, calculations grow quickly complex.

So, to overcome this obstacle, we'll take away the Y rigid motion from the motion equations of the gantry stage.

From experiment, it has been noticed that the effects related to the centripetal and coriolis accelerations are negligible in normal operation of the gantry stage; therefore, we'll make the H matrix (3.71) equal to zero. The motion equations of the gantry stage become then (3.109),

$$[M]\{\ddot{q}\}+[C]\{\dot{q}\}+[K]\{q\}=\{Q\} \quad \therefore \quad [H]=[0] \tag{3.109}$$

Also, from experiment, it has been noticed that the motion Y of the payload is only coupled with the yaw motion Θ of the cross–arm. That is, the motion of the payload has a negligible influence over the motions X, q_1,…, q_k,…, q_N and vice–versa. This coupling between Y and Θ is also

[12] Rigid modes have a vibration eigenfrequency of 0 Hz.

unidirectional. That is, the motion of the Y–axis ($M_{\Theta Y}\ddot{Y}$) can cause the cross–arm to yaw. The angular acceleration of the cross–arm ($M_{\Theta Y}\ddot{\Theta}$), on the other hand, has a negligible influence over the motion of the Y–axis.

Finally, to decouple the motion of the Y–axis from the system, the term $M_{\Theta Y}\ddot{Y}$ is added to the force vector Q and is considered as a perturbation. Then, the motion equations become (3.110) for the motions X, Θ, q_1,..., q_k,..., and q_N of the gantry stage

$$[M]\{\ddot{q}\}+[C]\{\dot{q}\}+[K]\{q\}=\{Q\} \tag{3.110}$$

With,

$$M=\begin{bmatrix} M_{XX} & M_{X\Theta} & M_{XY} & M_{X1} & M_{X2} & \cdots & M_{Xk} & \cdots & M_{XN} \\ M_{X\Theta} & M_{\Theta\Theta} & M_{\Theta Y} & M_{\Theta 1} & M_{\Theta 2} & \cdots & M_{\Theta k} & \cdots & M_{\Theta N} \\ M_{XY} & M_{\Theta Y} & M_{YY} & M_{Y1} & M_{Y2} & \cdots & M_{Yk} & \cdots & M_{YN} \\ M_{X1} & M_{\Theta 1} & M_{Y1} & M_{11} & M_{12} & \cdots & M_{1k} & \cdots & M_{1N} \\ M_{X2} & M_{\Theta 2} & M_{Y2} & M_{12} & M_{22} & \cdots & M_{2k} & \cdots & M_{2N} \\ \vdots & \vdots & \vdots & \vdots & \vdots & \ddots & & & \vdots \\ M_{Xk} & M_{\Theta k} & M_{Yk} & M_{1k} & M_{2k} & & M_{kk} & & M_{kN} \\ \vdots & \vdots & \vdots & \vdots & \vdots & & & \ddots & \vdots \\ M_{XN} & M_{\Theta N} & M_{YN} & M_{1N} & M_{2N} & \cdots & M_{kN} & \cdots & M_{NN} \end{bmatrix};\quad C=\begin{bmatrix} 0 & 0 & 0 & 0 & 0 & \cdots & 0 & \cdots & 0 \\ 0 & C_{\Theta\Theta} & 0 & C_{\Theta 1} & C_{\Theta 2} & \cdots & C_{\Theta k} & \cdots & C_{\Theta N} \\ 0 & 0 & C_{YY} & 0 & 0 & \cdots & 0 & \cdots & 0 \\ 0 & C_{\Theta 1} & 0 & C_{11} & C_{12} & \cdots & C_{1k} & \cdots & C_{1N} \\ 0 & C_{\Theta 2} & 0 & C_{12} & C_{22} & \cdots & C_{2k} & \cdots & C_{2N} \\ \vdots & \vdots & \vdots & \vdots & \vdots & \ddots & & & \vdots \\ 0 & C_{\Theta k} & 0 & C_{1k} & C_{2k} & & C_{kk} & & C_{kN} \\ \vdots & \vdots & \vdots & \vdots & \vdots & & & \ddots & \vdots \\ 0 & C_{\Theta N} & 0 & C_{1N} & C_{2N} & \cdots & C_{kN} & \cdots & C_{NN} \end{bmatrix} \tag{3.111), (3.112}$$

$$K=\begin{bmatrix} 0 & 0 & 0 & 0 & 0 & \cdots & 0 & \cdots & 0 \\ 0 & K_{\Theta\Theta} & 0 & K_{\Theta 1} & K_{\Theta 2} & \cdots & K_{\Theta k} & \cdots & K_{\Theta N} \\ 0 & 0 & 0 & 0 & 0 & \cdots & 0 & \cdots & 0 \\ 0 & K_{\Theta 1} & 0 & K_{11} & K_{12} & \cdots & K_{1k} & \cdots & K_{1N} \\ 0 & K_{\Theta 2} & 0 & K_{12} & K_{22} & \cdots & K_{2k} & \cdots & K_{2N} \\ \vdots & \vdots & \vdots & \vdots & \vdots & \ddots & & & \vdots \\ 0 & K_{\Theta k} & 0 & K_{1k} & K_{2k} & & K_{kk} & & K_{kN} \\ \vdots & \vdots & \vdots & \vdots & \vdots & & & \ddots & \vdots \\ 0 & K_{\Theta N} & 0 & K_{1N} & K_{2N} & \cdots & K_{kN} & \cdots & K_{NN} \end{bmatrix} \tag{3.113}$$

$$q=\begin{bmatrix} X \\ \Theta \\ Y \\ q_1 \\ q_2 \\ \vdots \\ q_k \\ \vdots \\ q_N \end{bmatrix};\quad Q=\begin{bmatrix} F_{b1}+F_{b2} \\ \left(F_{b1}-F_{b2}\right)\cos\left(\Theta\right)\left(y_2-y_1\right)/2+M_{\Theta Y}\ddot{Y} \\ F_Y \\ 0 \\ 0 \\ \vdots \\ 0 \\ \vdots \\ 0 \end{bmatrix} \tag{3.114), (3.115}$$

$$\therefore\quad \begin{aligned} F_{b1} &= F_1-m_1\ddot{X}_1-c_{g1}\dot{X}_1-c_{c1}\,\mathrm{sign}\left(\dot{X}_1\right) \\ F_{b2} &= F_2-m_2\ddot{X}_2-c_{g2}\dot{X}_2-c_{c2}\,\mathrm{sign}\left(\dot{X}_2\right) \\ F_Y &= F_y-c_{cy}\,\mathrm{sign}\left(\dot{Y}\right) \end{aligned}$$

And the independent motion equation (3.116) for the motion Y of the payload,

$$m_h\ddot{Y}+c_h\dot{Y}=F_y-c_{cy}\,\mathrm{sign}\left(\dot{Y}\right) \tag{3.116}$$

To take into account the unbalance between actuators X_1 and X_2 into the decoupling basis transformation, it is necessary to express the motion equations (3.110) in terms of the electromagnetic forces F_1 and F_2 generated by them. By doing so, the motion equations (3.110) become,

$$\left[M+M_{X_1X_2}\right]\{\ddot{q}\}+\left[C+C_{X_1X_2}\right]\{\dot{q}\}+[K]\{q\}=\left\{Q_{X_1X_2}\right\} \tag{3.117}$$

Where,

$$M_{X_1X_2}=\begin{bmatrix} m_1+m_2 & \left(m_1-m_2\right)\left(y_2-y_1\right)\cos\left(\Theta\right)/2 & 0 & 0 & 0 & \cdots & 0 & \cdots & 0 \\ \left(m_1-m_2\right)\left(y_2-y_1\right)\cos\left(\Theta\right)/2 & \left(m_1+m_2\right)\left(y_2-y_1\right)^2\cos^2\left(\Theta\right)/4 & 0 & 0 & 0 & \cdots & 0 & \cdots & 0 \\ 0 & 0 & 0 & 0 & 0 & \cdots & 0 & \cdots & 0 \\ 0 & 0 & 0 & 0 & 0 & \cdots & 0 & \cdots & 0 \\ 0 & 0 & 0 & 0 & 0 & \cdots & 0 & \cdots & 0 \\ \vdots & \vdots & \vdots & \vdots & \vdots & \ddots & & & \vdots \\ 0 & 0 & 0 & 0 & 0 & & 0 & & 0 \\ \vdots & \vdots & \vdots & \vdots & \vdots & & & \ddots & \vdots \\ 0 & 0 & 0 & 0 & 0 & \cdots & 0 & \cdots & 0 \end{bmatrix} \tag{3.118}$$

$$C_{X_1X_2}=\begin{bmatrix} c_{g1}+c_{g2} & \left(c_{g1}-c_{g2}\right)\left(y_2-y_1\right)\cos\left(\Theta\right)/2 & 0 & 0 & 0 & \cdots & 0 & \cdots & 0 \\ \left(c_{g1}-c_{g2}\right)\left(y_2-y_1\right)\cos\left(\Theta\right)/2 & \left(c_{g1}+c_{g2}\right)\left(y_2-y_1\right)^2\cos^2\left(\Theta\right)/4 & 0 & 0 & 0 & \cdots & 0 & \cdots & 0 \\ 0 & 0 & 0 & 0 & 0 & \cdots & 0 & \cdots & 0 \\ 0 & 0 & 0 & 0 & 0 & \cdots & 0 & \cdots & 0 \\ 0 & 0 & 0 & 0 & 0 & \cdots & 0 & \cdots & 0 \\ \vdots & \vdots & \vdots & \vdots & \vdots & \ddots & & & \vdots \\ 0 & 0 & 0 & 0 & 0 & & 0 & & 0 \\ \vdots & \vdots & \vdots & \vdots & \vdots & & & \ddots & \vdots \\ 0 & 0 & 0 & 0 & 0 & \cdots & 0 & \cdots & 0 \end{bmatrix} \tag{3.119}$$

$$Q_{X_1X_2}=\begin{bmatrix} \left(F_1+F_2\right)-\left[c_{c1}\,\mathrm{sign}\left(\dot{X}_1\right)+c_{c2}\,\mathrm{sign}\left(\dot{X}_2\right)\right] \\ \left\{\left(F_1-F_2\right)-\left[c_{c1}\,\mathrm{sign}\left(\dot{X}_1\right)-c_{c2}\,\mathrm{sign}\left(\dot{X}_2\right)\right]\right\}\cos\left(\Theta\right)\left(y_2-y_1\right)/2+M_{\Theta Y}\ddot{Y} \\ F_Y \\ 0 \\ 0 \\ \vdots \\ 0 \\ \vdots \\ 0 \end{bmatrix} \tag{3.120}$$

Now, a physical decoupling basis can be obtained from motion equations (3.117). To do so, it is assumed that the system is conservative, i.e. no damping, $[C+C_{X_1X_2}] = 0$, and no excitation, $\{Q_{X_1X_2}\} = 0$. The motion equations become then (3.121),

$$\left[M+M_{X_1X_2}\right]\left\{\ddot{q}\right\}+\left[K\right]\left\{q\right\}=\left\{0\right\} \tag{3.121}$$

We assume that the solution to (3.121) is the harmonic solution (3.122)

$$\left\{q\right\}=\mathrm{Re}\left[B\left\{\phi\right\}e^{i\omega t}\right] \tag{3.122}$$

Then, we have the eigenvalue problem (3.123),

$$\left(\left[K\right]-\omega^2\left[M+M_{X_1X_2}\right]\right)\cdot\left\{\phi\right\}=\left\{0\right\} \tag{3.123}$$

To obtain a non–trivial solution to $\{\phi\}$, the matrix $([K] - \omega^2[M+M_{X_1X_2}])$ must be non–invertible. In other words, its determinant must be zero.

$$\det\left(\left[K\right]-\omega^2\left[M+M_{X_1X_2}\right]\right)=0 \tag{3.124}$$

The values of ω that make valid expression (3.124) are the eigenvalues of the conservative system. In our case, we have $N + 2$ degrees–of–freedom; thus, we should find $N + 2$ positive eigenvalues. Remember, $N + 2$ is for the number of modeled flexible modes N plus the motions X and Θ.

The eigenvectors are calculated by replacing each of the found eigenvalues into (3.123). Then, the decoupling basis transformation is given by (3.125),

$$\left[\Phi\right]=\begin{bmatrix} 1 & \phi_{X\Theta} & \phi_{X1} & \phi_{X2} & \cdots & \phi_{Xk} & \cdots & \phi_{XN} \\ \phi_{\Theta X} & 1 & \phi_{\Theta 1} & \phi_{\Theta 2} & \cdots & \phi_{\Theta k} & \cdots & \phi_{\Theta N} \\ \phi_{1X} & \phi_{1\Theta} & 1 & \phi_{12} & \cdots & \phi_{1k} & \cdots & \phi_{1N} \\ \phi_{2X} & \phi_{2\Theta} & \phi_{21} & 1 & \cdots & \phi_{2k} & \cdots & \phi_{2N} \\ \vdots & \vdots & \vdots & \vdots & \ddots & & & \vdots \\ \phi_{kX} & \phi_{k\Theta} & \phi_{k1} & \phi_{k2} & & 1 & & \phi_{kN} \\ \vdots & \vdots & \vdots & \vdots & & & \ddots & \vdots \\ \phi_{NX} & \phi_{N\Theta} & \phi_{N1} & \phi_{N2} & \cdots & \phi_{Nk} & \cdots & 1 \end{bmatrix} \quad \therefore\ \phi_{ii}=1 \tag{3.125}$$

And the motion equations of the gantry stage on a decoupling basis are defined as (3.126),

$$\left[\Phi\right]^T\left[M+M_{X_1X_2}\right]\left[\Phi\right]\left\{\ddot{\eta}\right\}+\left[\Phi\right]^T\left[C+C_{X_1X_2}\right]\left[\Phi\right]\left\{\dot{\eta}\right\}+\left[\Phi\right]^T\left[K\right]\left[\Phi\right]\left\{\eta\right\}=\left[\Phi\right]^T\left\{Q_{X_1X_2}\right\} \tag{3.126}$$

Where,

$$\left[\Phi\right]^T\left[M+M_{X_1X_2}\right]\left[\Phi\right]=\begin{bmatrix} m_{tr} & 0 & 0 & 0 & \cdots & 0 & \cdots & 0 \\ 0 & J_{rot} & 0 & 0 & \cdots & 0 & \cdots & 0 \\ 0 & 0 & m_{\eta 1} & 0 & \cdots & 0 & \cdots & 0 \\ 0 & 0 & 0 & m_{\eta 2} & \cdots & 0 & \cdots & 0 \\ \vdots & \vdots & \vdots & \vdots & \ddots & & & \vdots \\ 0 & 0 & 0 & 0 & & m_{\eta k} & \ddots & 0 \\ \vdots & \vdots & \vdots & \vdots & & & \ddots & \vdots \\ 0 & 0 & 0 & 0 & \cdots & 0 & \cdots & m_{\eta N} \end{bmatrix};\ \left[\Phi\right]^T\left[C+C_{X_1X_2}\right]\left[\Phi\right]=\begin{bmatrix} c_{tr} & \times & \times & \times & \cdots & \times & \cdots & \times \\ \times & c_{rot} & \times & \times & \cdots & \times & \cdots & \times \\ \times & \times & c_{\eta 1} & \times & \cdots & \times & \cdots & \times \\ \times & \times & \times & c_{\eta 2} & \cdots & \times & \cdots & \times \\ \vdots & \vdots & \vdots & \vdots & \ddots & & & \vdots \\ \times & \times & \times & \times & & c_{\eta k} & \ddots & \times \\ \vdots & \vdots & \vdots & \vdots & & & \ddots & \vdots \\ \times & \times & \times & \times & \cdots & \times & \cdots & c_{\eta N} \end{bmatrix} \quad (3.127),\ (3.128)$$

$$\left[\Phi\right]^T\left[K\right]\left[\Phi\right]=\begin{bmatrix} 0 & 0 & 0 & 0 & \cdots & 0 & \cdots & 0 \\ 0 & k_{rot} & 0 & 0 & \cdots & 0 & \cdots & 0 \\ 0 & 0 & k_{\eta 1} & 0 & \cdots & 0 & \cdots & 0 \\ 0 & 0 & 0 & k_{\eta 2} & \cdots & 0 & \cdots & 0 \\ \vdots & \vdots & \vdots & \vdots & \ddots & & & \vdots \\ 0 & 0 & 0 & 0 & & k_{\eta k} & \ddots & 0 \\ \vdots & \vdots & \vdots & \vdots & & & \ddots & \vdots \\ 0 & 0 & 0 & 0 & \cdots & 0 & \cdots & k_{\eta N} \end{bmatrix};\ \left\{q\right\}=\begin{bmatrix} X \\ \Theta \\ q_1 \\ q_2 \\ \vdots \\ q_k \\ \vdots \\ q_N \end{bmatrix}=\left[\Phi\right]\begin{bmatrix} \eta_{tr} \\ \eta_{rot} \\ \eta_1 \\ \eta_2 \\ \vdots \\ \eta_k \\ \vdots \\ \eta_N \end{bmatrix};\ \left[\Phi\right]^T\left[Q\right]=\begin{bmatrix} F_{\eta_{tr}} \\ F_{\eta_{rot}} \\ F_{\eta_1} \\ F_{\eta_2} \\ \vdots \\ F_{\eta_k} \\ \vdots \\ F_{\eta_N} \end{bmatrix} \quad (3.129),\ (3.130),\ (3.131)$$

Expression (3.126) represents the motion of the flexible gantry stage using a physical decoupling basis. The non–diagonal terms of the modal damping matrix (3.128) are assumed to be negligible. The modal coordinates η_{tr} and η_{rot} represent the translation and the rotation of the gantry stage with respect to its center of mass (whose location varies in function of the payload's position). The modal coordinates η_1 to η_N represent the flexible modes of the cross–arm.

On a decoupling basis, the Energetic Macroscopic Representation (EMR) of the flexible gantry with N flexible modes is given by **Figure 3 – 30**. Note that the purple blocks are added to reconstruct the positions Y, X_1, X_2, q_1, …, and q_N from the decoupled coordinates Y, η_{tr}, η_{rot}, η_1, …, and η_N.

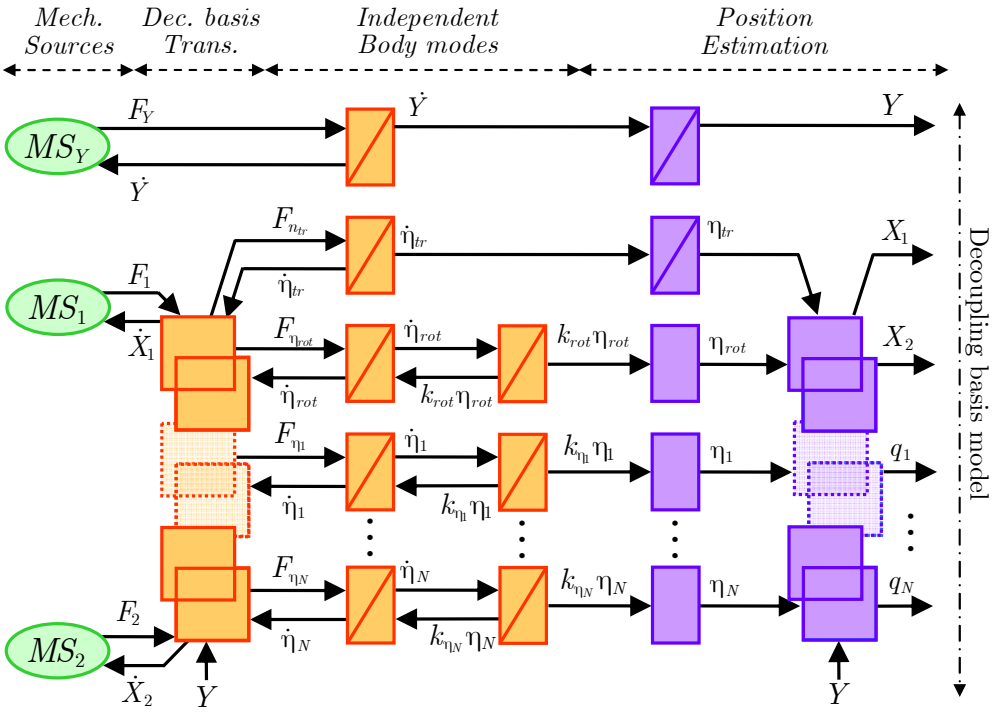

Figure 3 – 30 : *Energetic Macroscopic Representation of the flexible gantry*

As predicted, the EMR description of the gantry stage is far more synthetic that its COG counterpart. One advantage of this representation is that it allows a very quick evaluation of the interaction between the available actuators and the modes to be controlled.

"The available number of actuators is equal to the number of modes that can be controlled" (Meirovitch, 2001)

Thus, the proposed methodology allows identifying which modes we can control directly, which we can control indirectly, and which we can't control at all (at least with the available actuators).

The proposed methodology also allows:

- *Deduction of feedforward control structure*: based on the physical parameters of the system.
- *Deduction of feedback control structure*: and tuning based on the physical parameters of the system.

Additionally, as the model is now based on its modal representation, the precepts of modal control can be used to evaluate properties of the system such as Controllability and Observability. It also will serve as a perspective to merge model–based and optimal control techniques. See (Porter, et al., 1972).

3.3.4 Maximum Control Structure of the gantry stage

As aforementioned, the Energetic Macroscopic Representation (EMR) provides a compact alternative to represent graphically the dynamical model of the gantry stage. As it can be foreseen, each of the decoupled states is going to be controlled by an independent controller obtained by model inversion. As advanced on the state of the art (Tanquary, et al., 2000), the use of decoupled controllers allows improving the positioning performance of gantry stage thanks to the dissociation of the time constants associated to the pairs controller–linear actuator X_1 and X_2. The advantage of our approach is that it considers, along with the motions on the X and Θ, the payload's motion over the cross–arm and the flexible modes. While it is true that the available actuators cannot control the flexible modes without degrading the motion along the X or Θ, alternative passive or active control techniques can be used to minimize the influence of the flexible modes on the positioning performance of the gantry stage. The proposed model can be then used, for example, to estimate the optimal filter periods if trajectory planning techniques are used; or as an observer to generate the reference force for active compensation, as in (Stöppler, et al., 2008).

The Maximum Control Structure (MCS) of the flexible gantry is given on **Figure 3 – 31**.

3.3.5 Practical Control Structure of the gantry stage

Not all variables within a system are controllable or measurable. Therefore, its maximum control structure has to be simplified to take into consideration what can be measured (or estimated) and what can be controlled. This simplification can be organized in three stages:

(1) *Simplification of the control structure* by merging control blocs.

(2) *Estimation of non–measured variables* using a physical, statistical or stochastic model; or an observer.

(3) *Development of control strategies*. For example, to handle indirectly non–independent state variables/modes, to guarantee maximum efficiency or maximum power extraction, and so on.

In the case of the gantry stage, there are three actuators to control $N + 3$ mechanical modes. From the vector $\{Q\}$ (3.115) of generalized forces acting on the system, it can be easily deduced that the forces exciting the flexible modes are not linearly independent from the forces acting on the mechanical modes X, Θ, and Y. So, concerning the practical control structure of the gantry stage, we will simplify its maximum control structure to leave only the control, feedback and feedforward, of the decoupled motions η_{tr}, η_{rot}, and Y whose acting forces are linearly independent and are therefore fully controllable. Some of the flexible modes, notably the ones degrading the positioning performance, can be compensated indirectly by using, for example, trajectory planning

techniques (Biagiotti, et al., 2008). Residual modes are neglected. The Practical Control Structure of the gantry stage on a decoupling basis is presented on **Figure 3 – 32**.

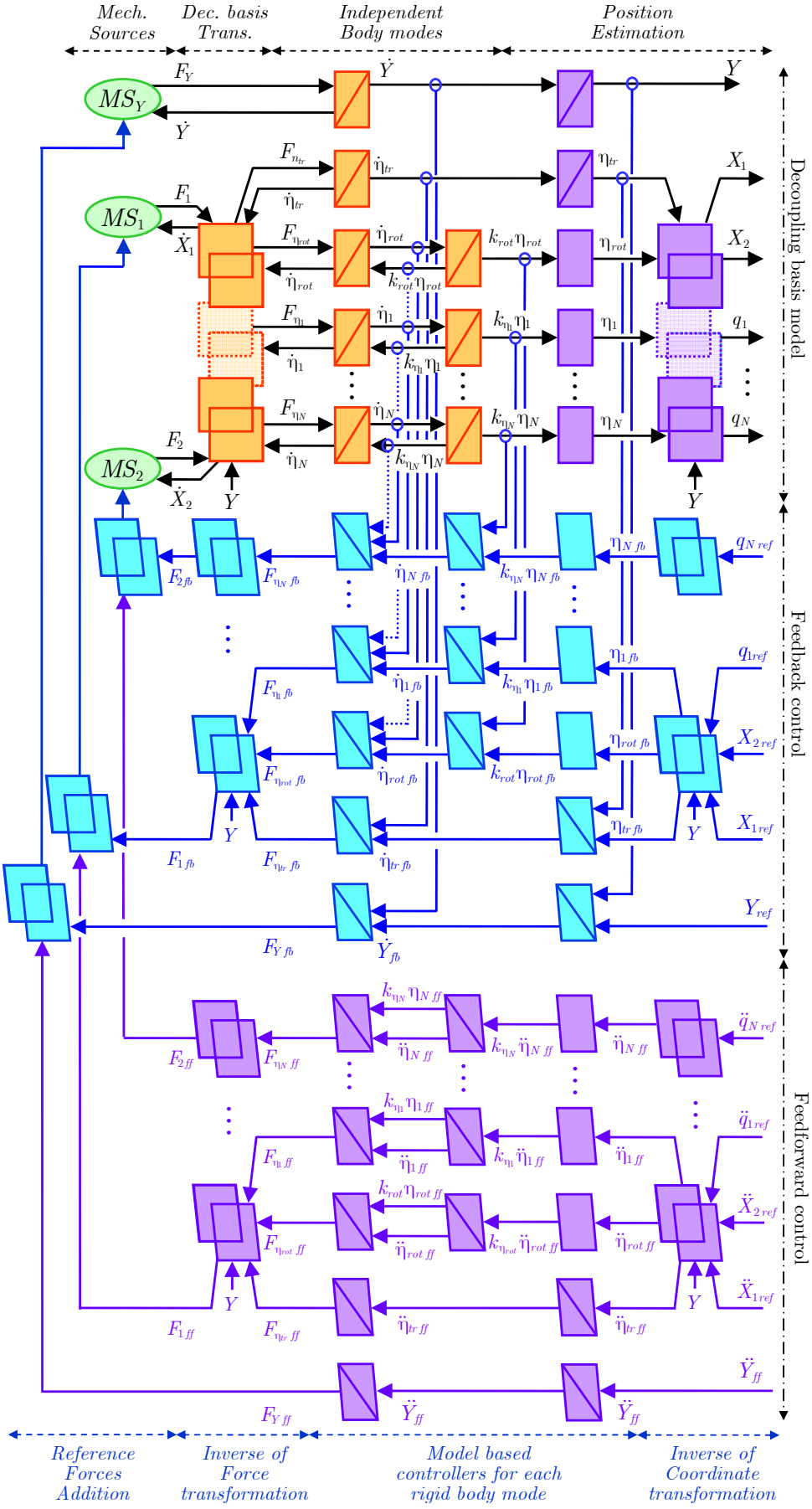

Figure 3 – 31 : *Maximum Control Structure of the flexible gantry (Feedback and Feedforward)*

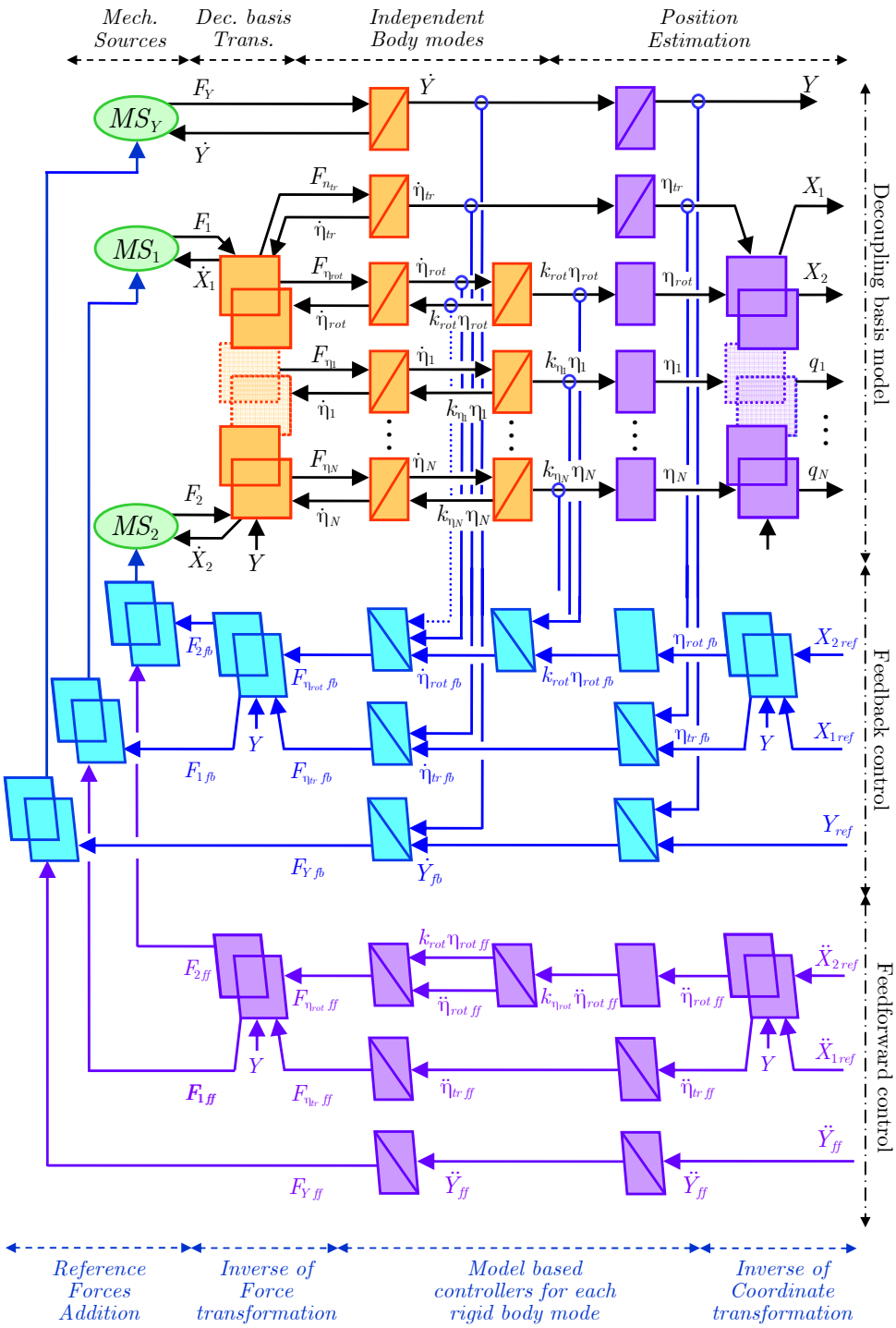

Figure 3 – 32 : *Practical Control Structure of the flexible gantry (Feedback and Feedforward)*

3.4 Conclusion

In the first two sections, based on a mechanical analysis of different types of gantry stages, a general model of the gantry stage is proposed. This model includes the translation $X(t)$, the yaw rotation $\Theta(t)$, and N flexible modes ($q_1(t)$, $q_2(t)$, $\dots q_N(t)$) of the cross–arm connecting actuators X_1, X_2, and Y. It also includes the translation $Y(t)$ of the payload. With respect to what is available in the literature, the main contributions of the proposed modeling approach are the consideration of:

- The effects of the payload's dynamics in the synchronization of actuators X_1 and X_2;
- The effects of the flexible cross–arm with variable eigenfrequencies in the overall positioning performance of the gantry stage.

Also, it is important to note that the parameters of the proposed model can be easily associated to physical parameters of the real system itself. This offers the implementation simplicity objective proposed at the beginning of the thesis. That is, physical modifications to the gantry machine can be easily taken into consideration into the modeling, and thus into the model–based control structure that is deduced from it. Finally, an original method to estimate the flexible parameters of the cross–arm is proposed.

The third section is consecrated to the development of a control structure based on the proposed modeling. To this purpose, we represented the gantry stage using the formalisms COG and EMR developed by the control team at the L2EP laboratory.

Initially, the motion equations of the gantry stage are decomposed and depicted using the three basic relationships (single–input rigid, multi–input rigid, and single–input causal) of the COG formalism. This representation makes easy to evaluate both the interactions of the elements constituting the system (inertias, frictions, and stiffnesses) and the evolution of the outputs, i.e. the coordinates X, Θ, Y, q_1, q_2, $\dots q_N$, in function of the inputs, i.e. the electromagnetic forces F_1, F_2, and F_Y generated by actuators X_1, X_2, and Y. All the simulation models that were used during this thesis were built based on the COG representation of the proposed gantry stage modeling.

A control structure can be deduced from the COG representation of the gantry stage. We chose not to because the large number of relationships contained within it would have made the deduced control structure quite unpractical from the implementation point of view. So, to obtain a simpler control structure, we decided to use the more global representation provided by the EMR formalism. That is, the motion equations of the system are decomposed and depicted using four types of elements (source, accumulation, conversion, and coupling). For example, an actuator can be represented as an accumulation element (as it stores kinetic energy). The terms associated to it, namely, its inertia and friction, are merged in one single element; leading to a simpler representation and thus to a simpler control structure.

There was, however, one inconvenience. For the sake of clarity, the EMR formalism does not allow mutual energy storage elements. This type of coupling is found in the gantry stage as the cross–arm connecting actuators X_1, X_2, and Y stores kinetic and potential elastic energy. Thus, in order to find a simplified representation of the proposed model and to conserve its physical aspects; we decided to orthogonalize it using a modal transformation. The drawback of this approach is that the gantry stage has two repeated eigenfrequencies; associated to the rigid motions of the gantry stage along the X–direction, and of the payload along the Y–direction. As a result, the orthogonalization has to be forced using a recursive algorithm such as the Gramm–Schmidt orthogonalization or similar. This was not an option providing that the objective is to produce a control structure that is simple both structurally and numerically.

To overcome this drawback, we decided to extract "manually" one of the repeated eigenfrequencies from the motion equations. This was facilitated by the particular configuration of the gantry stage itself. Indeed, thanks to the static friction of the Y–axis, the motion of the gantry

stage along the generalized coordinates X, Θ, q_1, q_2, ..., q_N has a negligible influence on the motion of the payload along the Y–direction. Similarly, the motion of the payload along the Y–direction has a negligible influence on the motions X, Θ, q_1, q_2, ..., q_N. Only the yaw rotation Θ of the cross–arm is significantly affected by the motion of the payload. To neglect this last coupling term between the motion Y of the payload and the motion equations of the gantry stage, we considered it as a perturbation that we reject by feedforward compensation. With the motion of the payload decoupled – and one of the repeated eigenfrequencies removed – it was then possible to apply a modal transformation to decouple the motions equations of the gantry stage. The advantage, and originality of this approach, is that decoupling the motion of the payload from the motion equations results in a decoupling basis transformation that is very simple to calculate.

With the model equations expressed on a decoupling basis, it was finally possible to represent them using the EMR formalism and to deduce a control structure by using the inversion–based control methodology. Initially, the deduced control structure has a maximum of measurements, compensations, and controllers. However, as not all variables are measurable or controllable, we have to reduce this control structure to what can be measured and controlled. This Practical Control Structure is the one that is implemented in real–time.

Representing the gantry stage on a decoupling basis puts in evidence that the flexible modes of the cross–arm are not directly controllable given the number and distribution of the gantry stage's actuators X_1, X_2, and Y. Nevertheless, the decoupled motion equations provide information in how the flexible modes are excited so that vibrations can be reduced by using, for example, trajectory planning techniques such as bang–bang jerk or input–shaping.

To validate the proposed approach; in the next chapter, we'll apply it to three different types of gantry stages. The results will be compared to the independent industrial axis controller structure provided by ETEL.

4. Application of the proposed methodology to the modeling and control of gantry stage industrial systems

The principal objective of this chapter is to show the capability of the proposed methodology to analyze, model, and control different types of gantry stages. To this purpose, it is divided in two sections.

(§ 4.1) ***Application to "rigid" gantry stages***

This section presents the application of the developed methodology to two different types of "rigid" gantry stages:

The first application example is the gantry stage that was used by J. Gomand on his thesis (Gomand, 2008). He studied the graphical properties of the COG formalism. As an application example of a complex system, he developed a model–based control structure of a gantry stage. He, however, did not take into account the dynamics of the payload; leading to a degraded positioning performance for path–tracking applications or for high–dynamics motions of the payload. To show the importance of a very accurate model, we compare our path–tracking results to the industrial control and to the results provided by J. Gomand.

The second application example is those of a large gantry stage. This type of system is used on the micro–electronics industry to manufacture and inspect flat–panel displays. To this intent, its cross–arm is built very rigid (and heavy). Once more, taking into account the mechanical coupling into the control of the large size gantry stage provides an improvement of its positioning performance. Also, as proposed on the introduction, the proposed methodology allows pointing out design issues and giving ideas to improve it.

(§ 4.2) ***Application to "flexible" gantry stages***

The second section concerns the application of the large–size gantry whose cross–arm has been replaced by a slender beam. This is done in order to intensify the effects of the cross–arm flexibility over the global positioning performance of the gantry machine. A dummy payload is used to emulate the effects of the actual payload.

In this case, using a physical model of the gantry stage provides the advantage of knowing precisely how the flexible modes of the cross-arm are excited and how they will vary in function of the payload's position. This information can be used, for example, to optimize the motion references so that it is possible to reduce their excitation.

4.1 Application to « rigid » gantry stages

This section presents the methodology of modeling and controlling gantry stages (Chapter 3) applied to two different types of "rigid" gantry stages.

Each application example is divided in three parts,

- *Experimental set–up*: The physical system is studied up–close. The objective of this study, as described on (§ 3.1.1), is to determine the configuration and the nature of the elements constituting the gantry stage.
- *Dynamical modeling*: Based on the system's analysis, we propose a dynamical model of the system based on the generic model presented on (§ 3.2.2). We identify its parameters using the method proposed on (§ 3.2.3)
- *Control on a decoupling basis*: We propose a decoupling controller based on the generic controller presented on (§ 3.3.4). In this section we'll present in detail the decoupling basis transformation for a rigid gantry stage.

4.1.1 Experimental set–up (Application Example No.1)

We have the gantry stage presented on **Figure 4 – 1**. This gantry stage was the same used by J. Gomand on his PhD. Thesis (Gomand, 2008) to validate the model–based control structure presented in (§ 2.4).

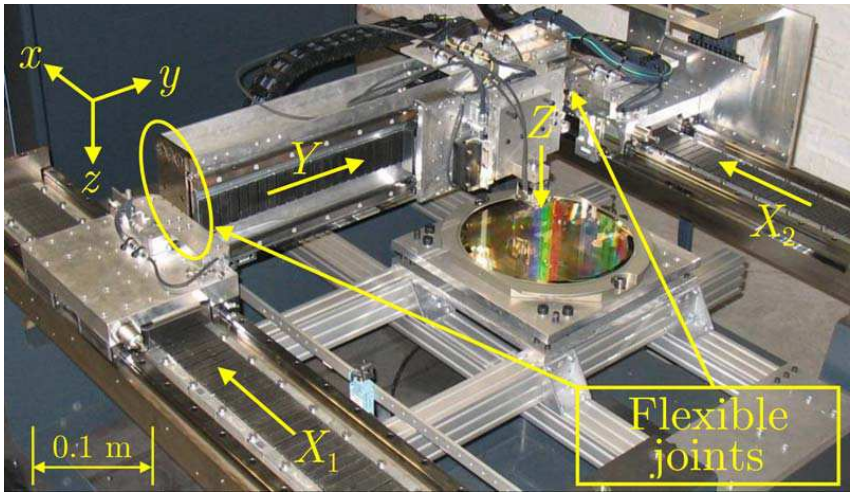

Figure 4 – 1 : *Dual–drive gantry stage* "Phoenix 2004" *provided by ETEL*

We'll apply the methodology proposed on Chapter 3. To this end, we start by analyzing the system. The gantry stage presented on **Figure 4 – 1** is classically used in the semi–conductor industry for pick and place applications such as surface chip mounting. This gantry stage is composed of a cross–arm (Y – axis), whose ends are mounted on two parallel linear actuators (axes X_1 and X_2) via flexible plate joints. The payload, which can be a placing or a soldering head, moves along the Y – and Z – axes using two orthogonal linear actuators. The overall system provides a 3 – DOF system.

As it was shown by (Gomand, 2008), except for the flexible plate joints, this system can be modeled using rigid elements. That is, the error induced by the deformation of the cross–arm is negligible in comparison to the experimental measurement error of ±1µm of the linear encoders associated to each actuator. Consequently, this gantry stage will be modeled using the hypothesis there are no flexible modes.

4.1.2 Dynamic Modeling (Application Example No.1)

To propose a model of the gantry stage presented on **Figure 4 – 1**, it is necessary to consider three points,

(1) The gantry stage is composed of:

- Four linear actuators (X_1, X_2, Y, and Z).
  - Two Permanent Magnet Linear Synchronous Machines (PMLSMs) (X_1 and X_2), which carry the cross–arm along the x–direction.
  - One PMLSM (Y) which is mounted on the cross–arm and carries the payload (actuator Z and tool–point) along the y–direction.
  - One actuator (Z) which carries the tool–point. Not considered in this study.
- A cross–arm which is considered rigid.
- Two flexible plate joints that connect the cross–arm to the actuators X_1 and X_2.
- A payload; which is the conjunction of the moving part of linear actuator Y, the linear actuator Z, and the tool–point.

(2) The gantry stage is one whose cross–arm is attached to the actuators at its ends,

(3) The deformation of the gantry stage along the z–axis is supposed negligible.

Based on these points, the following model is proposed:

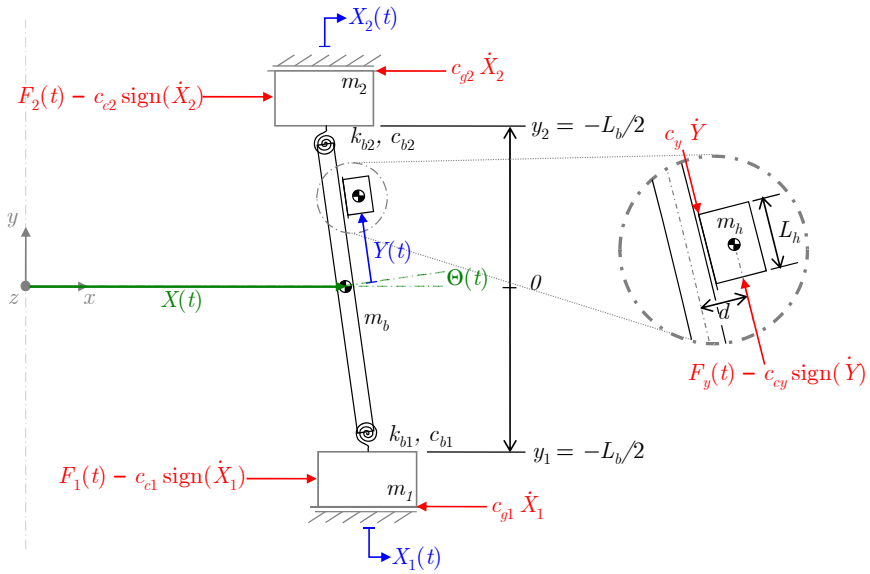

Figure 4 – 2 : *Dynamic model of the rigid gantry stage*

Where,

L_b is the length of the cross–arm;

y_1 is the location of the cross–arm to actuator joint No.1. $y_1 = -L_b/2$

y_2 is the location of the cross–arm to actuator joint No.2. $y_1 = +L_b/2$

d is the distance between the centers of mass of the cross–arm and of the payload

The motion equations of such system are defined by (3.67), with $N = 0$. N is the number of flexible modes to take into consideration into the general model of the gantry stage. Then,

$$[M]\{\ddot{q}\}+[H]\{\dot{q}\}+[C]\{\dot{q}\}+[K]\{q\}=\{Q\} \tag{4.1}$$

Where, M, C and K are the inertia (4.2), damping (4.3), and stiffness (4.4) matrices. H is the coriolis and centripetal acceleration matrix (4.5). Note that the motion equations are written in terms of the electromagnetic forces F_1 and F_2 generated by actuators X_1 and X_2 instead of the equivalent forces F_{b1} and F_{b2}, see (3.73).

$$M=\begin{bmatrix} M'_{XX} & M'_{X\Theta} & M'_{XY} \\ M'_{\Theta X} & M'_{\Theta\Theta} & M'_{\Theta Y} \\ M'_{YX} & M'_{Y\Theta} & M'_{YY} \end{bmatrix}=\begin{bmatrix} m_1+m_2+m_b+m_h & m_h d\sin(\Theta)-\left[m_h Y-(m_1-m_2)L_b/2\right]\cos(\Theta) & -m_h\sin(\Theta) \\ m_h d\sin(\Theta)-\left[m_h Y-(m_1-m_2)L_b/2\right]\cos(\Theta) & J_b+J_h+(m_1+m_2)\cos^2(\Theta)L_b^2/4+m_h d^2+m_h Y^2 & -m_h d \\ -m_h\sin(\Theta) & -m_h d & m_h \end{bmatrix} \tag{4.2}$$

$$C=\begin{bmatrix} c_{g1}+c_{g2} & \left[(c_{g1}-c_{g2})L_b/2\right]\cos(\Theta) & 0 \\ \left[(c_{g1}-c_{g2})L_b/2\right]\cos(\Theta) & c_{b1}+c_{b2}+(c_{g1}+c_{g2})\cos^2(\Theta)L_b^2/4 & 0 \\ 0 & 0 & c_y \end{bmatrix} \tag{4.3}$$

$$K=\begin{bmatrix} 0 & 0 & 0 \\ 0 & k_{b1}+k_{b2} & 0 \\ 0 & 0 & 0 \end{bmatrix};\quad H=\begin{bmatrix} 0 & \left\{m_h d\cos(\Theta)+\left[m_h Y-(m_1-m_2)L_b/2\right]\sin(\Theta)\right\}\dot{\Theta} & -2m_h\dot{\Theta}\cos(\Theta) \\ 0 & -\left[(m_1+m_2)\sin(\Theta)\cos(\Theta)L_b^2/4\right]\dot{\Theta} & 2m_h Y\dot{\Theta} \\ 0 & -m_h Y\dot{\Theta} & 0 \end{bmatrix} \tag{4.4, 4.5}$$

And there are, of course, the generalized coordinates (4.6), and the generalized forces (4.7),

$$q=\begin{bmatrix} X \\ \Theta \\ Y \end{bmatrix};\quad Q=\begin{bmatrix} \left\{(F_1+F_2)-\left[c_{c1}\,\mathrm{sign}(\dot{X}_1)+c_{c2}\,\mathrm{sign}(\dot{X}_2)\right]\right\} \\ \left\{(F_1-F_2)-\left[c_{c1}\,\mathrm{sign}(\dot{X}_1)-c_{c2}\,\mathrm{sign}(\dot{X}_2)\right]\right\}\cos(\Theta)L_b/2 \\ F_y-c_{cy}\,\mathrm{sign}(\dot{Y}) \end{bmatrix} \tag{4.6, 4.7}$$

The parameters of the dynamical model are estimated using the method presented on (§ 3.2.3) and are presented on TABLE II.

TABLE II
PHYSICAL PARAMETERS OF THE GANTRY STAGE "PHOENIX 2004"

Name	Value	Description
m_b	22.8 kg	Mass of the moving beam
m_h	10.1 kg	Mass of the head (Y–axis)
m_1	10.2 kg	Mass of actuator X_1
m_2	10.7 kg	Mass of actuator X_2
J_b	1.0 kg m²	Rotary inertia of the beam
J_h	0.05 kg m²	Rotary inertia of the head (Y–axis)
c_{g1}	14.5 N/(m/s)	Viscous friction of actuator X_1
c_{g2}	20.3 N/(m/s)	Viscous friction of actuator X_2
c_y	10 N/(m/s)	Viscous friction of the head (Y–axis)
$c_{b1} = c_{b2}$	9 Nm/(rad/s)	Viscous Friction of elastic joints 1 and 2
c_{c1}	16.8 N	Static friction of actuator X_1
c_{c2}	18.35 N	Static friction of actuator X_2
c_{cy}	11.6 N	Static friction of the head (Y–axis)
$k_{b1} = k_{b2}$	1987.5 Nm/rad	Stiffness of elastic joints 1 and 2
L_b	0.725 m	Length of the moving beam
L_h	0.25 m	Length of the head
d	0.1 m	Distance between beam and head

4.1.2.1 Comparison between model and experiment

The industrial independent axis control is reproduced on simulation. Experimental and simulation results are thus compared in order to validate the proposed model. The results presented in **Figure 4 – 3** are obtained with a simultaneous 0.4 m long displacement of X_1, X_2 and Y axes (diagonal displacement of the payload over the workspace).

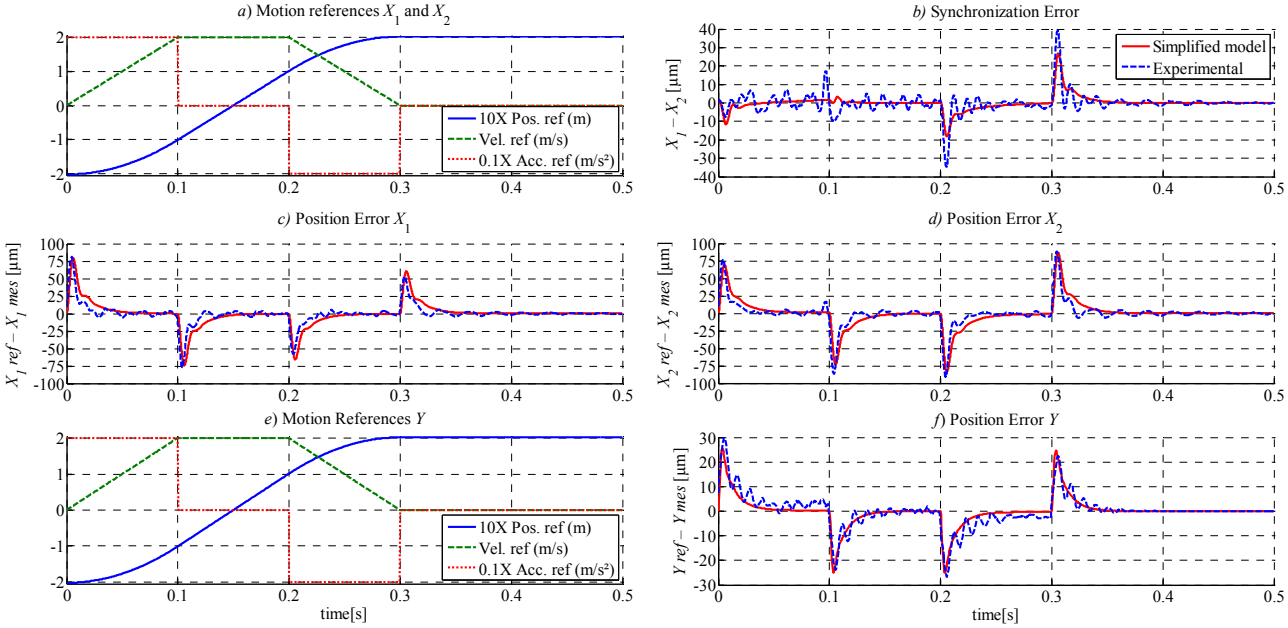

Figure 4 – 3 : *Experimental and simulation responses of a) Motion references X_1 and X_2; b) Synchronization Error; Position Error of c) X_1 axis, d) X_2 axis; e) Motion references Y; and f) position error of Y axis. Test realized using independent axis control for a displacement of* – 0.2 m *to* 0.2 m *for all axes, at a maximum speed of* 2 m/s, *and a maximum acceleration of* 20 m/s².

In comparison to the model, the experimental position errors X_1, X_2, and Y have additional oscillating components that can be explained as follows:

- The detent forces (Zhao, et al., 2004) of the PMLSMs. are not considered within the model. This is because the proposed approach is focused on the mechanical interaction between the elements composing the system and not into the electro–mechanical force transformations happening into the actuators.
- The vibration of the supporting structure along the X–direction. Indeed, concerning the installation, gantry stages can be mounted on different types of bases. For an increasing level of precision, the typical base types that are used are; welded, die–cast, and granite for very high–precision applications.

  The gantry stage presented on **Figure 4 – 1** is mounted on a die–cast base whose first vibration frequency along the X – direction is 37.5 Hz. This value is determined using experimental modal analysis (Schwarz, et al., 1999). This vibration can be compensated by adding jerk time to the motion references.
- The cross–arm vibrates between the flexible plates in which it is mounted. This vibration along the Y–direction is neglected as it is of small amplitude and it fades rapidly.

4.1.3 Control on a decoupling basis (Application Example No.1)

4.1.3.1 Transformation into a decoupling basis

The first stage to control the gantry stage on a decoupling basis is to transform its coupled motion equations (4.1) into a set of decoupled ones. As explained on (§ 3.3.3), this is done in two steps:

(1) The motion equations are simplified and the motion of the payload is decoupled from the rest of the motions by considering it as a disturbance.

(2) The simplified motion equations are transformed into a physical decoupling basis using a modal transformation

(1) *Model simplification*

Compared to the static friction of the Y – axis, both the linear and angular forces corresponding to the linear and angular accelerations of the beam, $\ddot{X}$ and $\ddot{\Theta}$, have a negligible influence over the motion of the payload. Consequently, the terms M'_{XY} and $M'_{\Theta Y}$ of the inertia matrix M (4.2) are neglected. Likewise, in comparison to the static friction of axes X_1 and X_2, the force due to the acceleration of the payload, $\ddot{Y}$, has negligible influence over the motion of the gantry stage along the X–direction. Thus, the term M'_{YX} is also neglected. By contrast, the term $M'_{Y\Theta}$ is not negligible. Indeed, the force generated by the moving payload can cause the cross–arm to yaw. To avoid an asymmetric inertia matrix M (4.2), this coupling term between Θ and Y is considered as a disturbance and moved to the generalized forces vector Q (4.7). This term will be later compensated by the feed–forward control.

Mechanically, the yaw angle Θ of the cross–arm is limited to 0.1 rad. What is more, in normal operation conditions, i.e. X_1 and X_2 moving in synchronization, the rotation Θ and the angular velocity $\dot{\Theta}$ of the cross–arm are limited, respectively, to several tens of micro–radians (μrad) and milli–radians per second (mrad/s). Because of this, the terms $M'_{X\Theta}$ and $M'_{\Theta X}$ of the inertia matrix M (4.2) can be reduced to,

$$M'_{X\Theta} = M'_{\Theta X} = -\left[m_h Y - \left(m_1 - m_2\right) L_b / 2\right] \cos\left(\Theta\right) \tag{4.8}$$

Assuming that,

$$\mathrm{abs}\left(-\left[m_h Y - \left(m_1 - m_2\right) L_b / 2\right] \cos\left(\Theta\right)\right) \gg \mathrm{abs}\left(m_h d \sin\left(\Theta\right)\right) \tag{4.9}$$

Also, since all the terms of the centripetal and coriolis acceleration matrix H (4.5) are proportional to the angular velocity of the cross–arm, $\dot{\Theta}$, it can be assumed that,

$$\left[M\right]\left\{\ddot{q}\right\} + \left[C\right]\left\{\dot{q}\right\} + \left[K\right]\left\{q\right\} \gg \left[H\right]\left\{\dot{q}\right\} \tag{4.10}$$

As aforementioned, for industrial gantry stages, the cross–arm's rotation Θ is mechanically limited to small–angles. This limitation allows applying the small–angle approximation to simplify the motion equations of the gantry stage. Indeed, at less than 10° (∼0.2 rad), the percentage error in the small–angle approximation is less than 1% for $\sin(\Theta) \approx \Theta$ and $\cos(\Theta) \approx 1$.

Finally, the simplified motion equations can be written as (4.11),

$$\left[M_s\right]\left\{\ddot{q}_s\right\} + \left[C_s\right]\left\{\dot{q}_s\right\} + \left[K_s\right]\left\{q_s\right\} = \left\{Q_s\right\} \tag{4.11}$$

Where M_s, C_s, and K_s are the simplified inertia (4.12), damping (4.13), and stiffness (4.14) matrices; q_s is the vector of coordinates X and Θ (4.15), and Q_s is the vector of simplified forces (4.16),

$$M_s=\begin{bmatrix} m_1+m_2+m_b+m_h & (m_1-m_2)L_b/2-m_hY \\ (m_1-m_2)L_b/2-m_hY & J_b+J_h+(m_1+m_2)L_b^2/4+m_hd^2+m_hY^2 \end{bmatrix} \tag{4.12}$$

$$C_s=\begin{bmatrix} c_{g1}+c_{g2} & (c_{g1}-c_{g2})L_b/2 \\ (c_{g1}-c_{g2})L_b/2 & c_{b1}+c_{b2}+(c_{g1}+c_{g2})L_b^2/4 \end{bmatrix};\quad K_s=\begin{bmatrix} 0 & 0 \\ 0 & k_{b1}+k_{b2} \end{bmatrix} \tag{4.13), (4.14}$$

$$q_s=\begin{bmatrix} X \\ \Theta \end{bmatrix};\quad Q_s=\begin{bmatrix} \{(F_1+F_2)-[c_{c1}\,\mathrm{sign}(\dot{X}_1)+c_{c2}\,\mathrm{sign}(\dot{X}_2)]\} \\ \{(F_1-F_2)-[c_{c1}\,\mathrm{sign}(\dot{X}_1)-c_{c2}\,\mathrm{sign}(\dot{X}_2)]\}L_b/2+m_hd\ddot{Y} \end{bmatrix} \tag{4.15), (4.16}$$

For the Y axis, we have the independent equation (4.17)

$$m_h\ddot{Y}+c_y\dot{Y}=F_y-c_{cy}\,\mathrm{sign}(\dot{Y}) \tag{4.17}$$

The inertia M_s (4.12) and the damping C_s (4.13) matrices' off–diagonal terms point out the unbalance between axes X_1 and X_2 due to the difference of mass and of friction between them, and to the payload's position along the cross–arm. The simplified forces vector Q_s (4.16) includes the remaining mechanical coupling term between the motion of the payload (i.e. the Y–axis) and the Θ–axis.

Modal transformation

The coupled coordinates X (3.4) and Θ (3.5) are transformed into the decoupled coordinates η_{tr} and η_{rot}. The new coordinate η_{tr} corresponds to the translation of the center of mass of the gantry stage. The coordinate η_{rot} corresponds to the rotation of the gantry stage about its center of mass. The deduction of such decoupling basis is done by means of the modal transformation (4.18).

$$q_s=\Phi\cdot\eta \tag{4.18}$$

q_s is defined by (4.15). η is the vector of modal coordinates (4.19). Φ is the modal transformation matrix (4.20). The payload's motion Y is considered independent and is described by (4.17).

$$\eta=\begin{bmatrix} \eta_{tr} \\ \eta_{rot} \end{bmatrix};\quad \Phi=\begin{bmatrix} 1 & \phi_{12} \\ 0 & 1 \end{bmatrix}\ \therefore\ \phi_{12}=[m_hY-(m_1-m_2)L_b/2]/(m_1+m_2+m_b+m_h) \tag{4.19), (4.20}$$

The decoupled motion equation is given by,

$$[\Phi]^T[M_s][\Phi]\{\ddot{\eta}\}+[\Phi]^T[C_s][\Phi]\{\dot{\eta}\}+[\Phi]^T[K_s][\Phi]\{\eta\}=[\Phi]^T\{Q_s\} \tag{4.21}$$

Where $[\Phi]^T[M_s][\Phi]$ is the modal inertia matrix (4.22); its diagonal terms correspond to the total moving mass and rotary inertia of the gantry stage. $[\Phi]^T[C_s][\Phi]$ is the modal damping matrix (4.23); its diagonal terms correspond to the friction opposing to the translation η_{tr} and rotation η_{rot}. $[\Phi]^T[K_s][\Phi]$ is the modal stiffness matrix (4.24). $[\Phi]^T\{Q_s\}$ is the vector of modal forces (4.25).

$$[\Phi]^T[M_s][\Phi]=\begin{bmatrix} m_1+m_2+m_b+m_h & 0 \\ 0 & J_b+J_h+(m_1+m_2)L_b^2/4+m_h(d^2+Y^2)-(m_1+m_2+m_b+m_h)\phi_{12}^2 \end{bmatrix} \tag{4.22}$$

$$[\Phi]^T[C_s][\Phi]=\begin{bmatrix} c_{g1}+c_{g2} & (c_{g1}+c_{g2})\phi_{12}+(c_{g1}-c_{g2})L_b/2 \\ (c_{g1}+c_{g2})\phi_{12}+(c_{g1}-c_{g2})L_b/2 & c_{b1}+c_{b2}+(c_{g1}+c_{g2})(L_b^2/4+\phi_{12}^2)+(c_{g1}-c_{g2})L_b\phi_{12} \end{bmatrix} \tag{4.23}$$

$$[\Phi]^T[K_s][\Phi]=\begin{bmatrix} 0 & 0 \\ 0 & k_{b1}+k_{b2} \end{bmatrix} \tag{4.24}$$

$$[\Phi]^T\{Q_s\}=\begin{bmatrix} \{(F_1+F_2)-[c_{c1}\,\mathrm{sign}(\dot{X}_1)+c_{c2}\,\mathrm{sign}(\dot{X}_2)]\} \\ \{(F_1-F_2)-[c_{c1}\,\mathrm{sign}(\dot{X}_1)-c_{c2}\,\mathrm{sign}(\dot{X}_2)]\}L_b/2+m_hd\ddot{Y}+\{(F_1+F_2)-[c_{c1}\,\mathrm{sign}(\dot{X}_1)+c_{c2}\,\mathrm{sign}(\dot{X}_2)]\}\phi_{12} \end{bmatrix} \tag{4.25}$$

To have a full decoupling basis, the off–diagonal terms in (4.23) are neglected considering that,

$$c_{g1}+c_{g2} \gg \left(c_{g1}+c_{g2}\right)\phi_{12}+\left(c_{g1}-c_{g2}\right)L_b/2 \quad \because \quad \phi_{12} \ll 1 \tag{4.26}$$

$$c_{b1}+c_{b2}+\left(c_{g1}+c_{g2}\right)\left(L_b^2/4+\phi_{12}^2\right)+\left(c_{g1}-c_{g2}\right)L_b\phi_{12} \gg \left(c_{g1}+c_{g2}\right)\phi_{12}+\left(c_{g1}-c_{g2}\right)L_b/2 \tag{4.27}$$

4.1.3.2 Decoupling control

The decoupling basis control structure is divided in three parts:

(1) *A feedforward control structure* (bottom of **Figure 4 – 5**), which is obtained by direct inversion of the decoupling basis model (4.21). The feedforward control starts from the reference positions, velocities, and accelerations X_{1ref}, X_{2ref}, and Y_{ref}. These references are transformed into the equivalent decoupling basis references $\eta_{tr\ ref}$, $\eta_{rot\ ref}$ and Y_{ref}, using (4.28). Each of the decoupled references is fed into its respective feed–forward controllers $C_{\eta_{tr}ff}$, $C_{\eta_{rot}ff}$, and C_{yff}. The calculated feedforward forces $F_{\eta_{tr}ff}$ (4.29), $F_{\eta_{rot}ff}$ (4.30), and F_{yff} (4.31) are transformed into the reference forces F_{1ff}, F_{2ff}, and F_{yff} using (4.32). The compensation of the payload's motion (Y–axis) is performed by transforming the acceleration reference $\ddot{Y}_{ref}$, into the forces $F_{1anticipation}$ and $F_{2anticipation}$ using (4.33). These compensation forces are then added to the feedforward forces F_{1ff} and F_{2ff}.

$$\begin{bmatrix}\eta_{tr}\\ \eta_{rot}\\ Y\end{bmatrix}=\Phi^{-1}q \quad \therefore \quad \Phi=\begin{bmatrix}1 & \phi_{12} & 0\\ 0 & 1 & 0\\ 0 & 0 & 1\end{bmatrix};\ q=\begin{bmatrix}X\\ \Theta\\ Y\end{bmatrix}=T\cdot\begin{bmatrix}X_1\\ X_2\\ Y\end{bmatrix}=\begin{bmatrix}1/2 & 1/2 & 0\\ 1/L_b & -1/L_b & 0\\ 0 & 0 & 1\end{bmatrix}\begin{bmatrix}X_1\\ X_2\\ Y\end{bmatrix} \tag{4.28}$$

$$F_{\eta_{tr}ff}=C_{\eta_{tr}ff}\cdot\begin{bmatrix}\ddot{\eta}_{tr\,ref}\\ \dot{\eta}_{tr\,ref}\\ \eta_{tr\,ref}\end{bmatrix} \ \therefore\ C_{\eta_{tr}ff}=\begin{bmatrix}m_1+m_2+m_b+m_h\\ c_{g1}+c_{g2}\\ 0\end{bmatrix}^T \tag{4.29}$$

$$F_{\eta_{rot}ff}=C_{\eta_{rot}ff}\cdot\begin{bmatrix}\ddot{\eta}_{rot\,ref}\\ \dot{\eta}_{rot\,ref}\\ \eta_{rot\,ref}\end{bmatrix} \ \therefore\ C_{\eta_{rot}ff}=\begin{bmatrix}J_b+J_h+\left(m_1+m_2\right)L_b^2/4+m_h\left(d^2+Y^2\right)-\left(m_1+m_2+m_b+m_h\right)\phi_{12}^2\\ c_{b1}+c_{b2}+\left(c_{g1}+c_{g2}\right)\left(L_b^2/4+\phi_{12}^2\right)+\left(c_{g1}-c_{g2}\right)L_b\phi_{12}\\ k_{b1}+k_{b2}\end{bmatrix}^T \tag{4.30}$$

$$F_{yff}=C_{yff}\cdot\begin{bmatrix}\ddot{Y}_{ref}\\ \dot{Y}_{ref}\\ Y_{ref}\end{bmatrix} \ \therefore\ C_{yff}=\begin{bmatrix}m_h\\ c_h\\ 0\end{bmatrix}^T\ ;\ \begin{bmatrix}F_1\\ F_2\\ F_Y\end{bmatrix}=P^{-1}\cdot\left(\Phi^T\right)^{-1}\cdot\begin{bmatrix}F_{\eta_{tr}}\\ F_{\eta_{rot}}\\ F_Y\end{bmatrix} \ \therefore\ P=\begin{bmatrix}1 & 1 & 0\\ L_b/2 & -L_b/2 & 0\\ 0 & 0 & 1\end{bmatrix} \tag{4.31), (4.32}$$

$$\begin{bmatrix}F_{1\,anticipation}\\ F_{2\,anticipation}\end{bmatrix}=\ddot{Y}_{ref}\frac{2m_hd}{L_b}\begin{bmatrix}1\\ -1\end{bmatrix} \tag{4.33}$$

(2) *A feedback control structure* (middle of **Figure 4 – 5**). The decoupling basis feedforward control provides most of the dynamic response of the gantry stage (i.e. coarse positioning). In the same way, it compensates for most of the unbalance and the mechanical coupling between actuators. However, it does not compensate for un–modeled disturbances, uncertainties on the model parameters, and other neglected phenomena. Therefore, to improve the fine positioning of the gantry stage, a decoupling basis feedback control is proposed. It starts from the reference positions $X_{1\ ref}$, $X_{2\ ref}$ and Y_{ref}, which are transformed into the decoupled references $\eta_{tr\ ref}$, $\eta_{rot\ ref}$ and Y_{ref} using (4.28). These references are then fed into classical industrial PID controllers. They generate the feedback decoupling forces $F_{\eta_{tr}fb}$, $F_{\eta_{rot}fb}$, and F_{yfb}, which are the transformed into the reference forces F_{1fb}, F_{2fb} and F_{yfb} using (4.32).

(3) *Control strategy* (Trajectory planning) To cancel residual vibrations of the support structure, a jerk time (Chang, et al., 2010) (Olabi, et al., 2010) of 26.5 ms is added to the references $X_{1\ ref}$ and $X_{2\ ref}$. This reduces the solicitation of the first vibration mode (37 Hz) of the supporting structure along the X–direction. Along the Y–direction no jerk time is added. This is because, on this direction, the vibrations are of small amplitude and they disappear rapidly.

Finally, the reference forces from the feedback and feedforward controls are added and fed into the drives controlling actuators X_1, X_2 and Y (top of **Figure 4 – 5**).

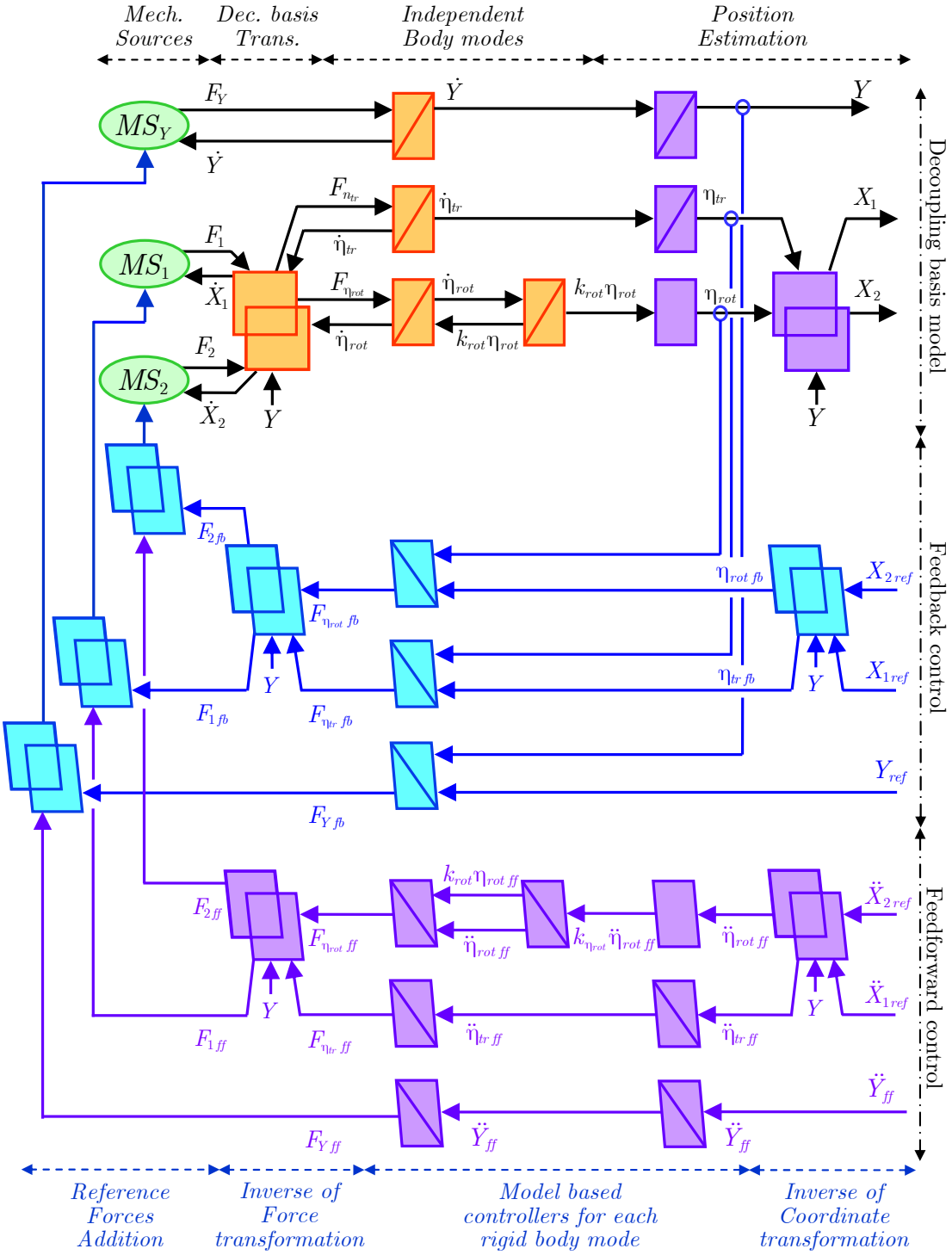

Figure 4 – 4 : *Feedback–feedforward decoupling basis control structure*
(Energetic Macroscopic Representation)

We can also represent the feedback–feedforward control structure of the gantry stage using the more classical representation provided by a block–diagram.

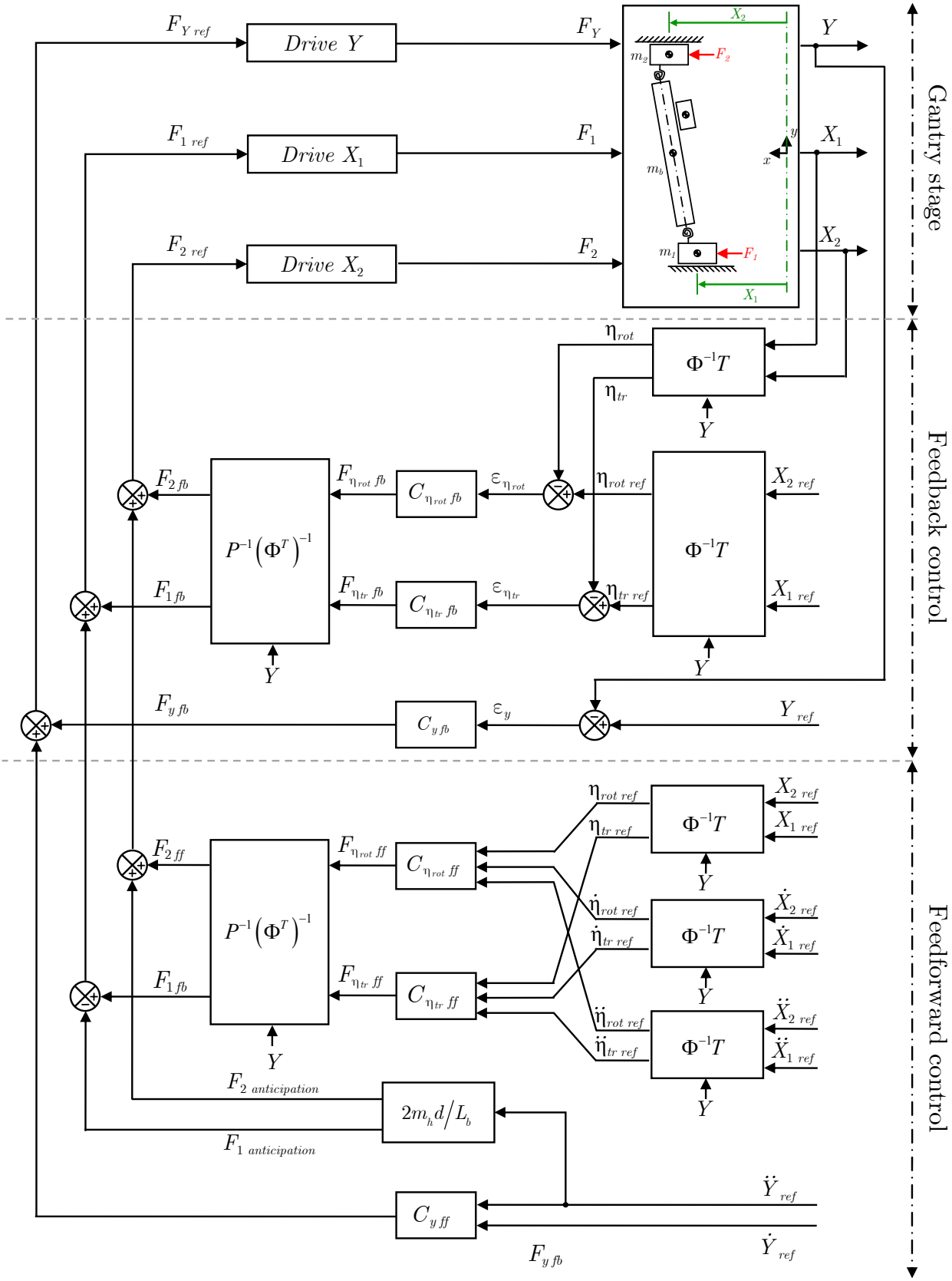

Figure 4 – 5 : *Feedback–feedforward decoupling basis control structure.* (Block diagram)

4.1.3.3 Experimental Validation

In this section, independent axis control and the proposed decoupling basis control are compared. First, two point–to–point motion examples are presented. Next, a path–tracking motion test is presented.

Point–to–point motion tests

This first test consists in synchronously displacing X_1 and X_2 from –0.2 m to +0.2 m at a maximum velocity of 2 m/s and acceleration of 20 m/s². For the first example, see **Figure 4 – 6**, position references are generated with a 26.5 ms jerk time, the payload is kept immobile at 0.2 m. In this configuration of the Y–axis (payload), the unbalance between actuators X_1 and X_2 is at its maximum value.

The second example consists in displacing the payload along a diagonal over the workspace. The reference trajectories for axes X_1, X_2, and Y are identical. They move from –0.2 m to +0.2 m, at a maximum velocity of 2 m/s and an acceleration of 20 m/s². During this motion, the gantry stage goes from an extreme unbalance condition to the other. Due to the acceleration of the payload, the dynamical coupling between actuator Y and actuators X_1 and X_2 is considerable. To exacerbate this phenomenon, the jerk time has been set to zero for all axes, see **Figure 4 – 7**.

Figures 4 – 6 and **4 – 7** allow verifying that controlling the gantry stage on a decoupling basis results in an improved synchronization of actuators X_1 and X_2 and in a reduction of more that 50% of their position errors with respect to the independent axis control scheme. This reduction of 50% of the position error is uniform in both X and Y motions thanks to the feedforward compensation added to the control of actuator Y. Moreover, when jerk time is well tuned (**Figure 4 – 6**), the settling time is significantly reduced, i.e. a reduction of about 10% with respect to independent axis control. This way, the production capacity of the system can be increased by 10%. The remaining oscillations on position tracking errors are mostly due to the detent forces of the PMLSMs.

Another advantage of the decoupling basis approach is a reduction of about 12% of the peak force of actuators X_1 and X_2, as shown on force plots in **Figures 4 – 6** and **4 – 7**. So, future versions of the gantry stage using the decoupling basis approach could be designed with less powerful actuators for X_1 and X_2 axes. This is an economical advantage for manufacturers insofar as gantry stages will be more efficient at reduced production costs.

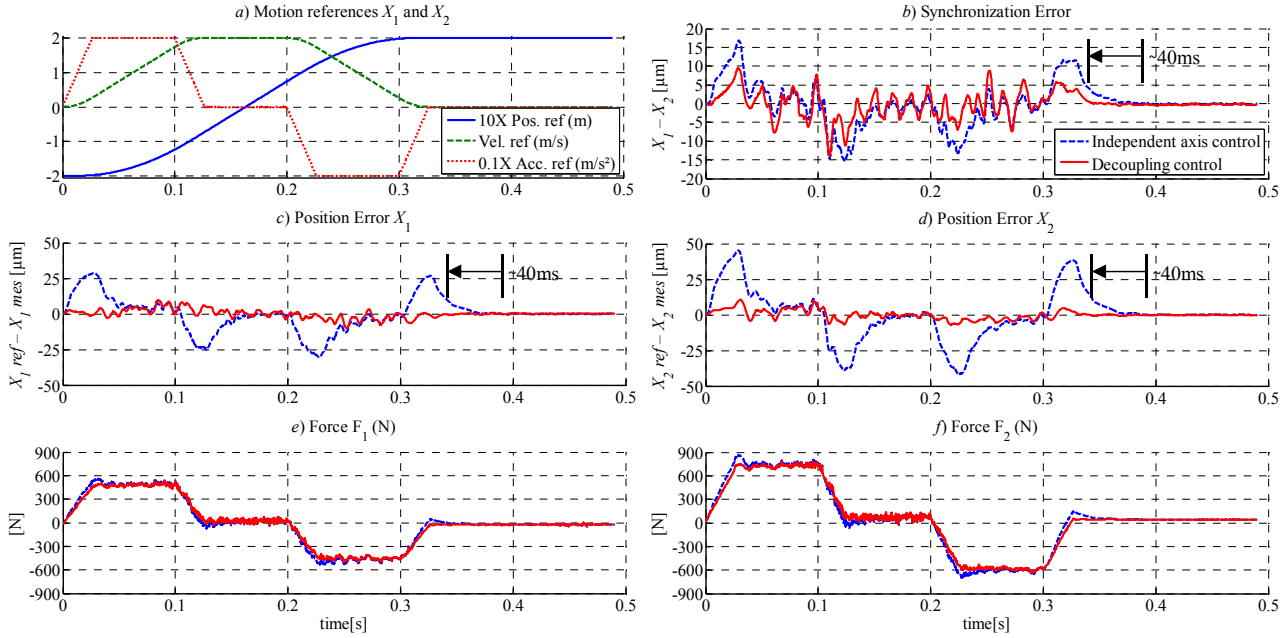

Figure 4 – 6 : *Independent axis control vs. decoupling basis control, point–to–point X_1 and X_2 synchronized motions (from* –0.2 *to* +0.2 m*) at a maximum velocity of* 2 m/s *and a maximum acceleration of* 20 m/s²*; the position of the payload is kept at* 0.2 m *(i.e. maximum unbalance).*

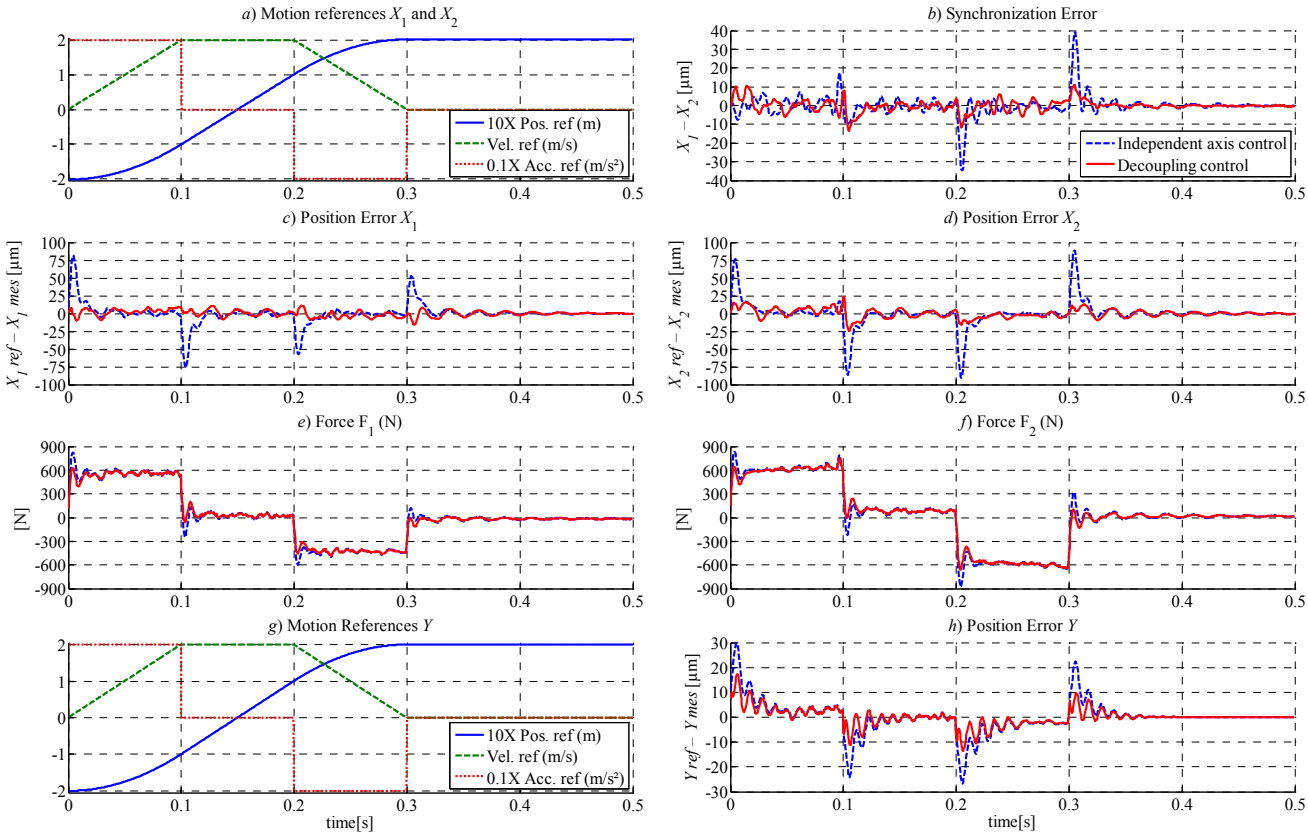

Figure 4 – 7 : *Independent axis control vs. decoupling basis control, point–to–point diagonal movement* (X_1, X_2, *and* Y *from* –0.2 *to* +0.2 m) *at a maximum velocity of* 2 m/s *and a maximum acceleration of* 20 m/s².

Path–tracking motion test

The path–tracking motion test consists in tracing clockwise three concentric circles of radius $R = 100$ mm, see **Figure 4 – 8**. This test, commonly known as a Ballbar test, is extensively used to assess the positioning performance of machine tools. The solid green circle represents the reference (a circle of radius $R = 100$ mm). The path–tracking error is amplified a million times. The first circle is traced (clockwise) during the tangential acceleration cycle of the payload; the peak acceleration of actuators X_1, X_2, and Y is 16 m/s². At the end of this first cycle, the payload has reached a constant tangential velocity of 1.3 m/s. The second circle is traced at this velocity. The third and final circle is traced during the deceleration cycle. The measurement precision is ±1µm.

The Ballbar plots are presented as follows:

a) *Independent axis control*: Actuators X_1, X_2, and Y are controlled independently. The effects of the mechanical coupling are exacerbated during the acceleration and deceleration phases; see **Figure 4 – 8** (*a*).

b) *Compensation of the mechanical coupling by feedforward* (Gomand, 2008): As commented on the introduction, this research project is the third collaboration between the L2EP and ETEL. The two previous collaborations were those of (Remy, 2007), who worked on the modeling and control of linear synchronous machines; and those of (Gomand, 2008), who studied the properties of the Causal Ordering Graph formalism. As a validation example, (Gomand, 2008) proposed a model–based control structure for the gantry stage presented on **Figure 4 – 1**, see (§ 2.4).

The model of the gantry stage proposed by (Gomand, 2008) is presented on **Figure 2 – 16** (*c*). This model neither takes into account the motion of the payload nor the distance between the centers of mass of the payload and the cross–arm. The control structure presented on **Figure 2 – 17** is derived from such model.

As it can be appreciated on **Figure 4 – 8** (b), the positioning performance is improved with respect to the independent axis control. This is due to the compensation of the mass and viscous friction unbalance between actuators X_1 and X_2. Nevertheless, ignoring the payload's dynamics and the distance between its center of mass and those of the cross–arm has a penalizing effect over the positioning performance; notably, at the beginning and at the end of the motion.

c) *Decoupling basis control*: The gantry stage is controlled using the decoupling basis control structure derived from the methodology proposed on Chapter 3. As it can be appreciated on **Figure 4 – 8** (c), taking into account the unbalance and the mechanical coupling between actuators within the control structure results in a minimization of 33% of the maximum radius error (in comparison to independent axis control) and in a global minimization of the mean error, i.e. better shape preservation.

Note that, for all Ballbar plots, the path–tracking error is repeatable and independent of the payload's velocity. This error is due to the detent forces of actuators X_1, X_2, and Y (PMLSMs) and to their static friction (lobes appearing along the vertical and horizontal axes of the plots).

a) Independent Axis Control : R=100 mm, ΔR *max* = 16 µm

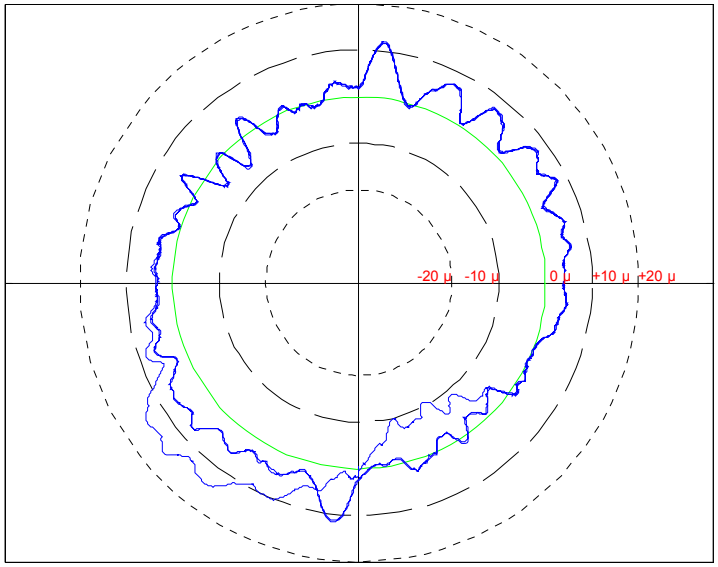

b) Cross-coupling Control : R=100 mm, ΔR *max* = 14 µm

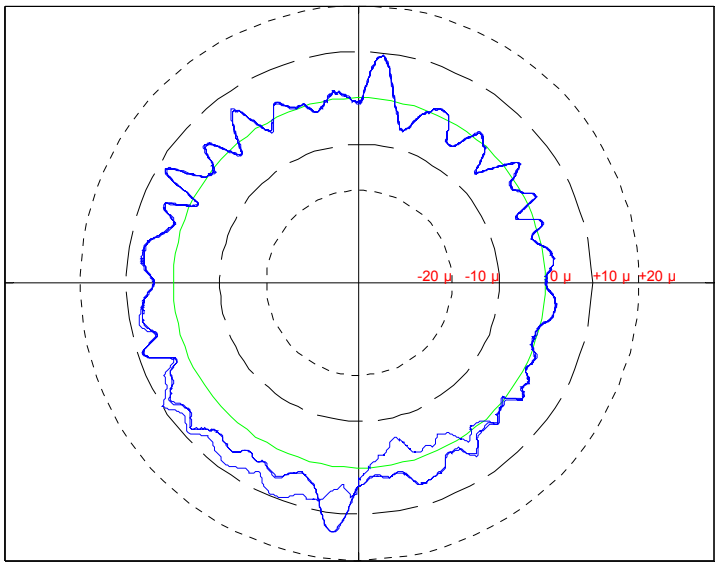

c) Decoupling Basis Control : R=100 mm, ΔR *max* = 11 µm

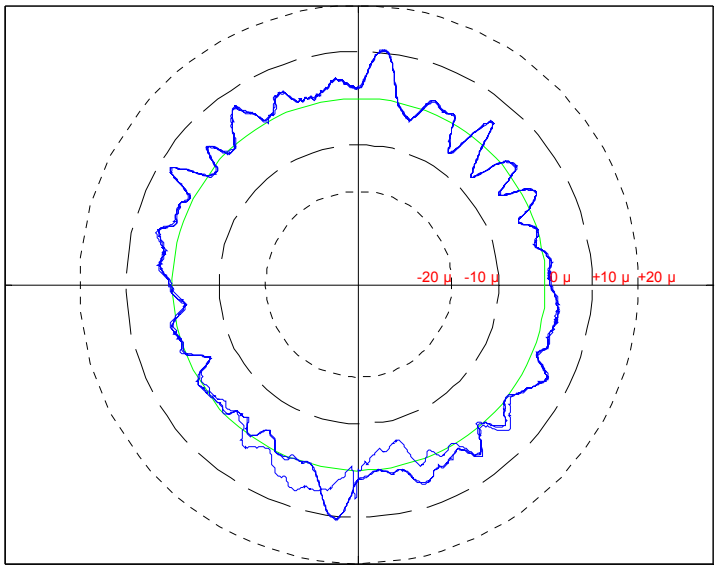

Figure 4 – 8 : *Independent axis control vs. cross–coupling control vs. decoupling basis control. Ballbar tests realized with three* 100 mm *radius circles at a maximum tangential velocity of* 1.3 m/s *and acceleration of* 16 m/s^2.

4.1.4 Experimental set–up (Application Example No.2)

The gantry stage presented on **Figure 4 – 9** is classically used in the micro–electronics industry for Flat Panel Display (FPD) fabrication and inspection. This gantry stage is composed of a cross–arm (Y – axis), which is mounted on two parallel linear actuators (X_1 and X_2) at intermediate positions via a flexible plate joint on one side and a pivot joint on the other. The payload, which can be a printing head or an inspection camera, moves along the Y – and Z – axes using two orthogonal linear actuators. The overall system provides a 3 – DOF system.

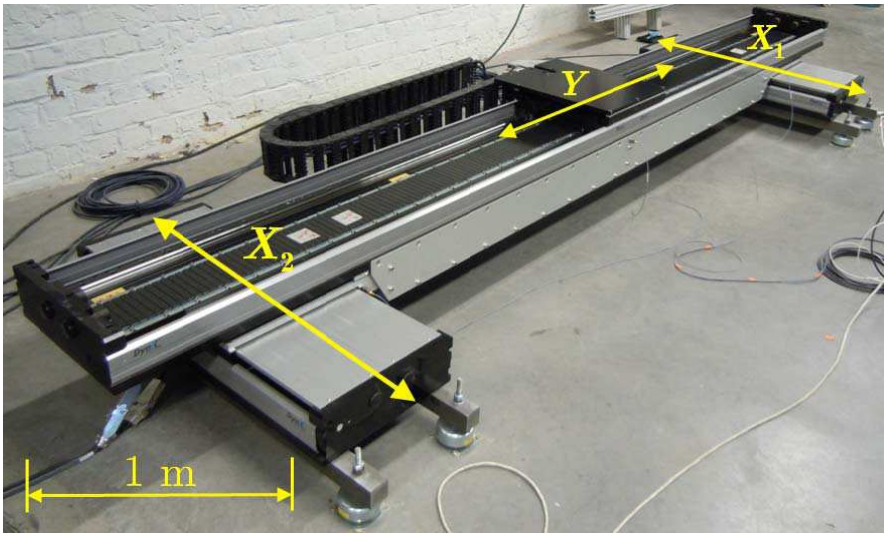

Figure 4 – 9 : *Dual–drive gantry stage "Andromeda" provided by ETEL*

Before start modeling the gantry stage, it is necessary to determine whether the cross–arm behaves as a rigid or flexible body. This can be done via a very simple experiment: by using the build–in independent axis controllers, we move actuators X_1 and X_2 in synchronization at several different velocities and accelerations; the payload is located at the middle of the cross–arm. We measure the acceleration of actuators X_1, X_2, and of the middle of the cross–arm. If all acceleration signals are in phase, as in **Figure 4 – 10**; we can conclude that the cross–arm can be modeled as being rigid.

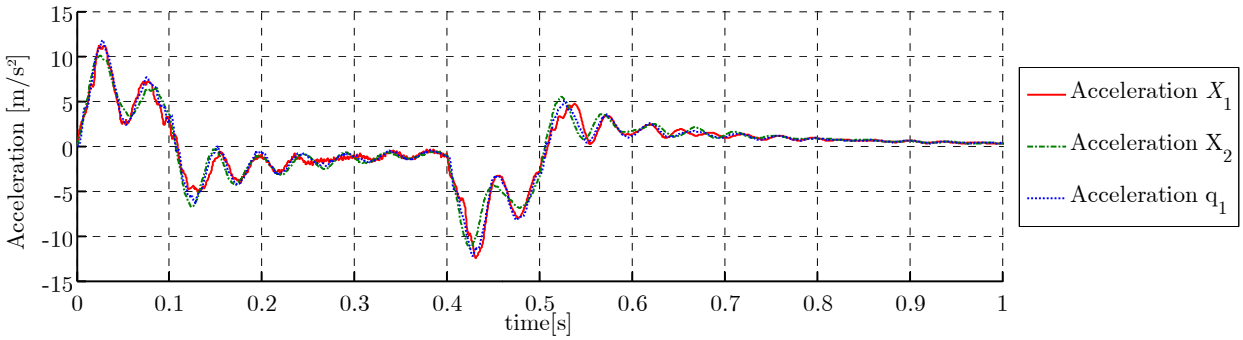

Figure 4 – 10 : *Acceleration measurements taken at actuator X_1, actuator X_2, and middle of the cross–arm for a displacement from* –0.15 m *to* +0.15 m. *Maximum velocity,* 0.75 m/s. *Maximum acceleration,* 7.5 m/s².

The oscillations that are observed in acceleration signals X_1, X_2, and q_1 in **Figure 4 – 10** are the combined result of four vibrating elements: (1) the vibration of actuator X_1 on its support; (2) the vibration of actuator X_2 on its support; (3) the vibration of the cable carrier attached to the cross–arm; and (4) the pitch vibration of the cross–arm (the cross–arm oscillates as an inverse pendulum with respect to actuators X_1 and X_2). The motion of this "pendulum" is produced by the moment of force created by the acceleration imposed by actuators X_1 and X_2 on the cross–arm times the distance separating their centers of mass along the Z–axis (normal to the ground in **Figure 4 – 9**). The stiffness of this "pendulum" is those of the mechanical joints about the pitch axis.

By now, we will model the gantry stage "Andromeda" as being rigid using the proposed methodology. A comparison between model and experiment will allow assessing the impact of these un–modeled phenomena on the quality of the proposed modeling.

4.1.5 Dynamic Modeling (Application Example No.2)

To propose a general model of the gantry stage on **Figure 4 – 9**, it is necessary to consider three points,

(1) The gantry stage is composed of:

- Three linear actuators (X_1, X_2, and Y).
  - Two Permanent Magnet Linear Synchronous Machines (PMLSMs) (X_1 and X_2), which carry the cross–arm along the x–direction.
  - One PMLSM (Y) which is mounted on the cross–arm and carries the payload (tool–point) along the y–direction.
- A cross–arm which is considered rigid.
- A flexible plate joint connecting the cross–arm to actuator X_1.
- A pivot joint connecting the cross–arm to actuator X_2.
- A payload; which is the conjunction of the moving part of linear actuator Y and the tool–point.

(2) The gantry stage is one whose cross–arm is attached to the actuators at intermediate positions,

(3) The deformation of the gantry stage along the z–axis is supposed negligible.

Based these points, the following model is proposed:

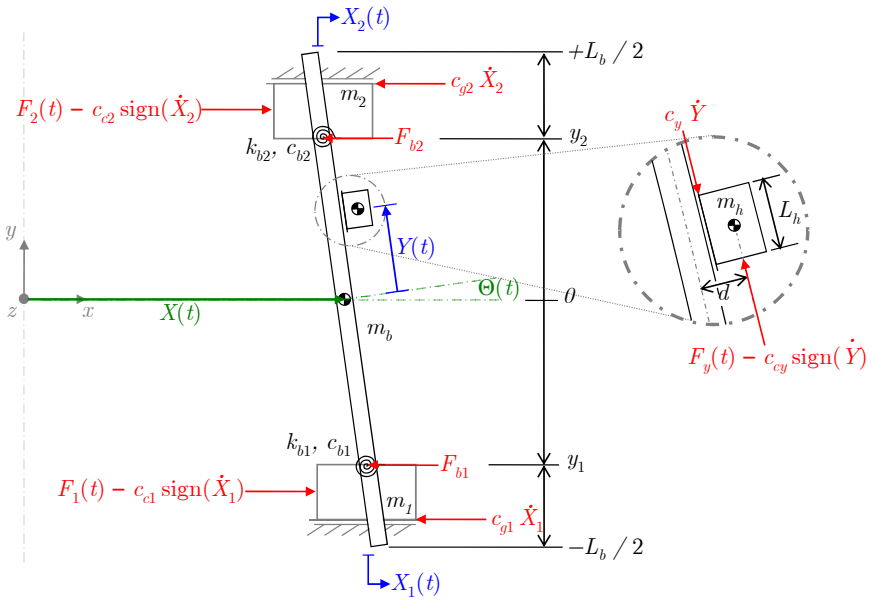

Figure 4 – 11 : *Dynamic model of the rigid gantry stage "Andromeda"*

Where,

L_b is the length of the cross–arm;

y_1 is the location of the flexible plate joint;

y_2 is the location of the pivot joint;

d is the distance between the centers of mass of the cross–arm and of the payload

The motion equations of such system are defined by (3.67), with $N = 0$. N is the number of flexible modes to take into consideration into the general model of the gantry stage. Then,

$$\left[M\right]\left\{\ddot{q}\right\}+\left[H\right]\left\{\dot{q}\right\}+\left[C\right]\left\{\dot{q}\right\}+\left[K\right]\left\{q\right\}=\left\{Q\right\} \tag{4.34}$$

Where, M, C and K are the inertia (4.35), damping (4.36), and stiffness (4.37) matrices. H is the coriolis and centripetal acceleration matrix (4.38).

$$M=\begin{bmatrix} M_{XX} & M_{X\Theta} & M_{XY} \\ M_{X\Theta} & M_{\Theta\Theta} & M_{Y\Theta} \\ M_{XY} & M_{Y\Theta} & M_{YY} \end{bmatrix}=\begin{bmatrix} m_b+m_h & m_h d\sin(\Theta)-m_h Y\cos(\Theta) & -m_h\sin(\Theta) \\ m_h d\sin(\Theta)-m_h Y\cos(\Theta) & J_b+J_h+m_h d^2+m_h Y^2 & -m_h d \\ -m_h\sin(\Theta) & -m_h d & m_h \end{bmatrix} \tag{4.35}$$

$$C=\begin{bmatrix} 0 & 0 & 0 \\ 0 & C_{\Theta\Theta} & 0 \\ 0 & 0 & C_{YY} \end{bmatrix}=\begin{bmatrix} 0 & 0 & 0 \\ 0 & c_{b1}+c_{b2} & 0 \\ 0 & 0 & c_y \end{bmatrix};\quad K=\begin{bmatrix} 0 & 0 & 0 \\ 0 & K_{\Theta\Theta} & 0 \\ 0 & 0 & 0 \end{bmatrix}=\begin{bmatrix} 0 & 0 & 0 \\ 0 & k_{b1}+k_{b2} & 0 \\ 0 & 0 & 0 \end{bmatrix} \tag{4.36), (4.37}$$

$$H=\begin{bmatrix} 0 & H_{X\Theta} & H_{XY} \\ 0 & H_{\Theta\Theta} & H_{\Theta Y} \\ 0 & H_{Y\Theta} & H_{YY} \end{bmatrix}=\begin{bmatrix} 0 & m_h\left\{d\cos(\Theta)+Y\sin(\Theta)\right\}\dot{\Theta} & -2m_h\dot{\Theta}\cos(\Theta) \\ 0 & 0 & 2m_h Y\dot{\Theta} \\ 0 & -m_h Y\dot{\Theta} & 0 \end{bmatrix} \tag{4.38}$$

q and Q are the generalized coordinates (4.39), and the generalized forces (4.40),

$$q=\begin{bmatrix} X \\ \Theta \\ Y \end{bmatrix}\quad\therefore\quad \begin{matrix} X(t)=\left[X_1(t)+X_2(t)\right]/2 \\ \Theta(t)=\sin^{-1}\left\{\left[X_1(t)-X_2(t)\right]/(y_2-y_1)\right\} \end{matrix} \tag{4.39}$$

$$Q=\begin{bmatrix} F_X \\ F_\Theta \\ F_Y \end{bmatrix}=\begin{bmatrix} F_{b1}+F_{b2} \\ (F_{b1}-F_{b2})\cos(\Theta)(y_2-y_1)/2 \\ F_Y \end{bmatrix}\quad\therefore\quad \begin{matrix} F_{b1}=F_1-m_1\ddot{X}_1-c_{g1}\dot{X}_1-c_{c1}\,\mathrm{sign}(\dot{X}_1) \\ F_{b2}=F_2-m_2\ddot{X}_2-c_{g2}\dot{X}_2-c_{c2}\,\mathrm{sign}(\dot{X}_2) \\ F_Y=F_y-c_{cy}\,\mathrm{sign}(\dot{Y}) \end{matrix} \tag{4.40}$$

The parameters of the dynamical model are estimated using the method presented on (§ 3.2.3) and are presented on TABLE III.

TABLE III
PHYSICAL PARAMETERS OF THE GANTRY STAGE "ANDROMEDA"

Name	Value	Description
m_b	173.35 kg	Mass of the moving cross–arm
m_h	24.89 kg	Mass of the payload (Y–axis)
m_1	30.4 kg	Mass of actuator X_1
m_2	26.6 kg	Mass of actuator X_2
J_b	129 kg m^2	Rotary inertia of the beam
J_h	0.23 kg m^2	Rotary inertia of the head (Y–axis)
c_{g1}	352.6 N/(m/s)	Viscous friction of actuator X_1
c_{g2}	360.3 N/(m/s)	Viscous friction of actuator X_2
c_y	476.23 N/(m/s)	Viscous friction of the payload (Y–axis)
c_{b1}	0.32 Nm/(rad/s)	Viscous Friction of mechanical joint No.1
c_{b2}	0.9 Nm/(rad/s)	Viscous Friction of mechanical joint No.2
k_{b1}	1550 Nm/rad	Stiffness of mechanical joint No.1
k_{b2}	0 Nm/rad	Stiffness of mechanical joint No.2
c_{cy}	126.6 N	Static friction of the payload (Y–axis)
c_{c1}	111 N	Static friction of actuator X_1
c_{c2}	104 N	Static friction of actuator X_2
L_b	3.00 m	Length of the moving beam
L_h	0.32 m	Length of the payload
d	–0.01 m	Distance between beam and head
y_1	–1.00 m	Distance between beam's center and mechanical joint No.1
y_2	1.00 m	Distance between beam's center and mechanical joint No.2

4.1.5.1 Comparison between model and experiment

The industrial independent axis control is reproduced on simulation. Experimental and simulation results are thus compared in order to validate the proposed model. The results presented in **Figure 4 – 12** are obtained with a simultaneous 0.3 m long displacement of X_1, X_2 and Y axes (diagonal displacement of the payload over the workspace).

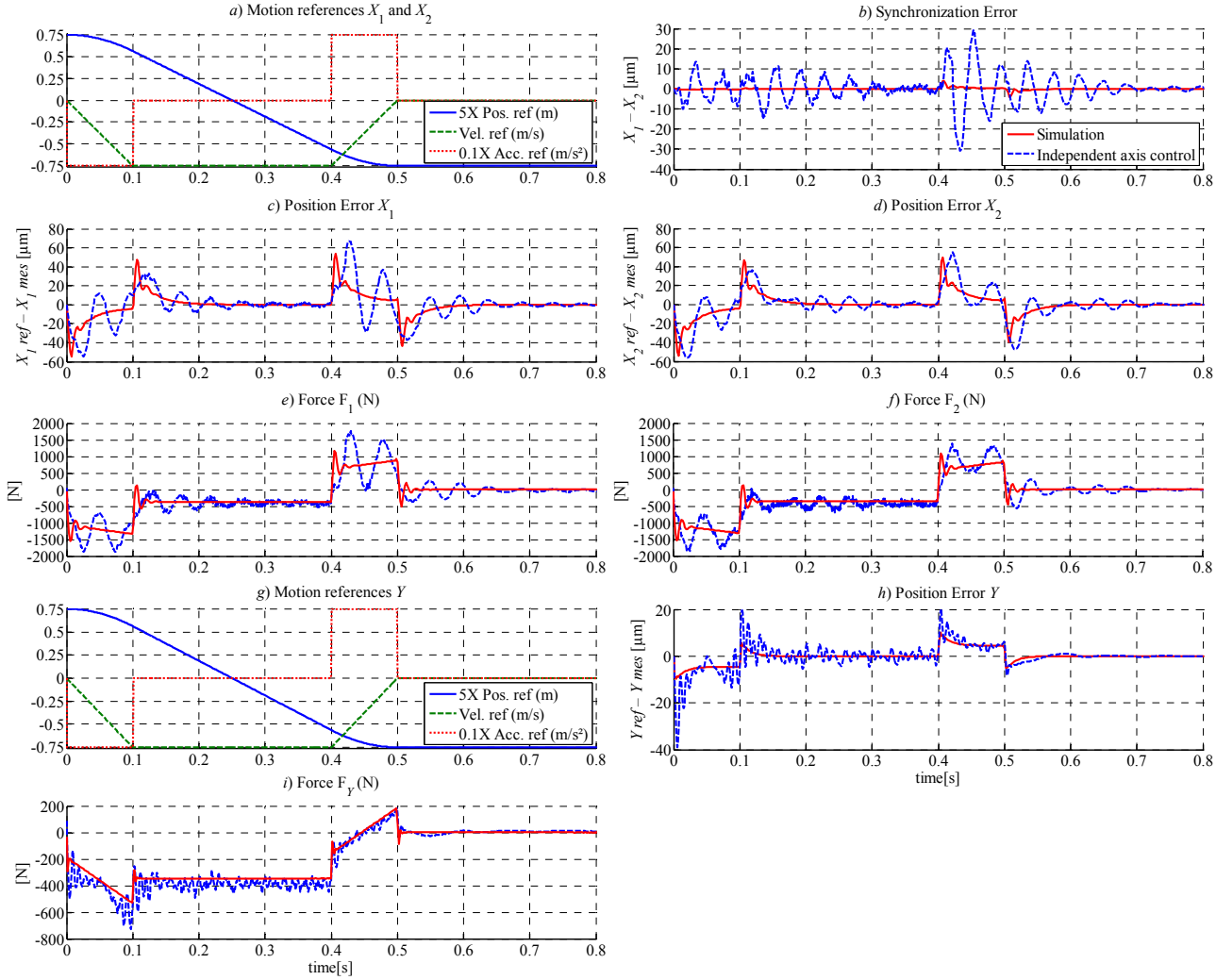

Figure 4 – 12 : *Experimental and simulation responses. Test realized using independent axis control. Displacement from* – 0.15 m *to* + 0.15 m *for all axes at a maximum velocity,* 0.75 m/s *and a maximum acceleration,* 7.5 m/s².

As commented on the description of the experimental setup (§ 4.1.4), even if the cross–arm behaves as a rigid body, other sources of vibration may have a detrimental influence on its positioning performance. For the gantry stage "Andromeda", we have associated these sources to four specific factors:

- The vibration of actuators X_1 and X_2 on its respective supporting structures.
- The vibration of the cable carrier attached to the cross–arm.
- The pitch vibration of the cross–arm.

From several experimental measurements, we have identified the pitch vibrations of the cross–arm as being the most influent of these factors. This can be noted, for example, at the measured forces F_1 and F_2 of actuators X_1 and X_2 in **Figure 4 – 12** (dash blue). From 0.0 to 0.1 seconds, the motion references X_1 and X_2 impose a constant acceleration and a linearly increasing velocity. Hence, the measured forces should have a constant and a linearly increasing component; as shown

by the simulation plots (solid red). Nevertheless, in addition to these, the measured forces have a strong oscillating component; namely, the perturbation induced by the cross–arm's pitch vibration on the actuators. This perturbation acts as follows: at the beginning of the motion, the cross–arm is "left behind" by the actuators; pulling them backwards. Then, when it starts moving, it passes the actuators pulling them onwards and forcing them to brake (at about 0.05s).

To take this phenomenon into consideration, we propose a modification to the proposed model. This modification is based on the following modeling hypotheses:

(1) As the pitch motion is small (several tens of μrad), we assume that the oscillating motion of the cross–arm is planar along the x–direction.

(2) We assume that the flexibility of the mechanical joints 1 and 2 can be modeled as the linear stiffnesses k_{l1} and k_{l2} with associated linear viscous frictions c_{l1} and c_{l2}.

(3) We assume that these stiffnesses are decoupled from the already modeled torsional stiffnesses of the mechanical joints 1 and 2.

The model of the rigid gantry becomes then,

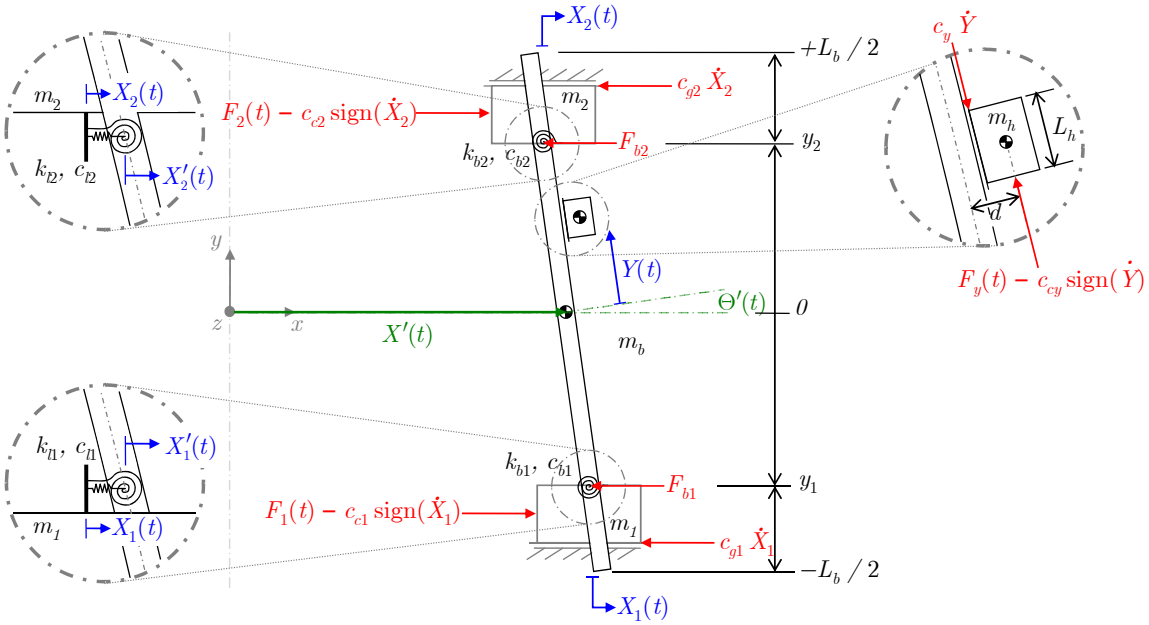

Figure 4 – 13 : *Corrected Dynamic model of the rigid gantry stage "Andromeda"*

Since the structure of the model is essentially the same, the motion equations are not modified by this adjustment, see (4.41)

$$\begin{bmatrix} M_{XX} & M_{X\Theta} & M_{XY} \\ M_{X\Theta} & M_{\Theta\Theta} & M_{Y\Theta} \\ M_{XY} & M_{Y\Theta} & M_{YY} \end{bmatrix} \begin{bmatrix} \ddot{X}' \\ \ddot{\Theta}' \\ \ddot{Y} \end{bmatrix} + \begin{bmatrix} 0 & H_{X\Theta} & H_{XY} \\ 0 & H_{\Theta\Theta} & H_{\Theta Y} \\ 0 & H_{Y\Theta} & H_{YY} \end{bmatrix} \begin{bmatrix} \dot{X}' \\ \dot{\Theta}' \\ \dot{Y} \end{bmatrix} + \begin{bmatrix} 0 & 0 & 0 \\ 0 & C_{\Theta\Theta} & 0 \\ 0 & 0 & C_{YY} \end{bmatrix} \begin{bmatrix} \dot{X}' \\ \dot{\Theta}' \\ \dot{Y} \end{bmatrix} + \begin{bmatrix} 0 & 0 & 0 \\ 0 & K_{\Theta\Theta} & 0 \\ 0 & 0 & 0 \end{bmatrix} \begin{bmatrix} X' \\ \Theta' \\ Y \end{bmatrix} = \begin{bmatrix} F_{b1} + F_{b2} \\ \left(F_{b1} - F_{b2}\right)\cos\left(\Theta\right)\left(y_2 - y_1\right)/2 \\ F_Y \end{bmatrix} \tag{4.41}$$

$$\therefore \quad \begin{aligned} F_{b1} &= F_1 - m_1\ddot{X}_1 - c_{g1}\dot{X}_1 - c_{c1}\,\mathrm{sign}\left(\dot{X}_1\right) \\ F_{b2} &= F_2 - m_2\ddot{X}_2 - c_{g2}\dot{X}_2 - c_{c2}\,\mathrm{sign}\left(\dot{X}_2\right); \\ F_Y &= F_y - c_{cy}\,\mathrm{sign}\left(\dot{Y}\right) \end{aligned} \qquad \begin{aligned} F_{b1} &= k_{l1}\left(X_1' - X_1\right) + c_{l1}\left(\dot{X}_1' - \dot{X}_1\right) \\ F_{b2} &= k_{l2}\left(X_2' - X_2\right) + c_{l2}\left(\dot{X}_2' - \dot{X}_2\right); \end{aligned}$$

The generalized coordinates X' and Θ' are, respectively, the position of the geometric center and the yaw angle of the pitching cross–arm. They are defined by (4.42)

$$\begin{aligned} X'(t) &= \left[X_1'(t) + X_2'(t)\right]/2 \\ \Theta'(t) &= \sin^{-1}\left\{\left[X_1'(t) - X_2'(t)\right]/\left(y_2 - y_1\right)\right\} \end{aligned} \tag{4.42}$$

X_1' and X_2' are the relative displacement of the cross–arm at positions y_1 and y_2 with respect to the measured positions of actuators X_1 and X_2.

The new added parameters k_{li} and c_{li} (with $i = 1, 2$) are the linear stiffness and viscous friction of the mechanical joints 1 and 2. They are estimated using the optimization algorithm *fmincon*(), provided by Matlab®. Their values are given by (4.43),

$$\begin{aligned} k_{l1} &= 1396512 \text{ N/m}; & k_{l2} &= 2268004 \text{ N/m}; \\ c_{l1} &= 3448 \text{ N/(m/s)}; & c_{l2} &= 775 \text{ N/(m/s)}; \end{aligned} \tag{4.43}$$

If we compare once more model and experiment; we'll be available to appreciate that using a physical modeling approach allows to quickly take into consideration un–modeled phenomena.

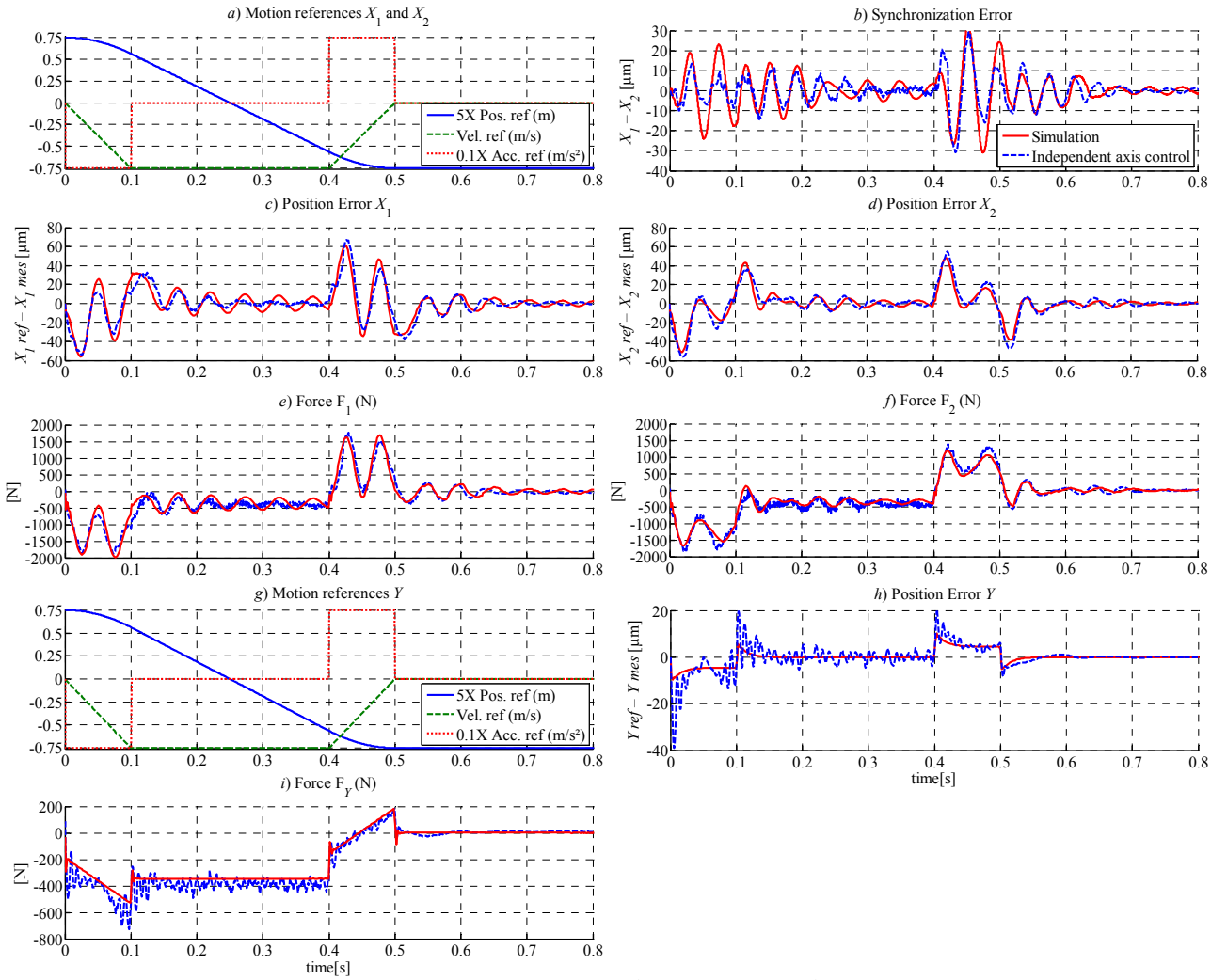

Figure 4 – 14 : *Experimental and simulation responses (corrected model). Test realized using independent axis control. Displacement from* – 0.15 m *to* + 0.15 m *for all axes at a maximum velocity,* 0.75 m/s *and a maximum acceleration,* 7.5 m/s².

4.1.6 Control on a decoupling basis (Application Example No.2)

Deducing a control structure from the adjusted model is a little bit more complicated. Indeed, by adding the linear stiffness of joints 1 and 2 to the modeling, we have modified the model's physical causality by adding additional energy storage elements. Because of this, its causal graphical representation and thus its control structure have to be modified. Since this is out of the scope of this research project, the development of such control structure will be reserved for the short term perspectives.

By the moment, we will control the gantry stage "Andromeda" using the decoupling basis controller proposed on Chapter 3. As it will be appreciated, taking into account the mechanical coupling into the control of the gantry stage provides a significant improvement on its positioning performance.

4.1.6.1 Transformation into a decoupling basis

Same as (§ 4.1.3.1)

4.1.6.2 Decoupling control

Same as (§ 4.1.3.2)

4.1.6.3 Experimental Validation

In this section, independent axis control and the proposed decoupling basis control are compared. First, two point–to–point motion examples are presented, then a Ballbar test is proposed.

Point–to–point motion tests

The first test consists in synchronously displacing X_1 and X_2 from +0.15 m to –0.15 m at a maximum velocity of 0.75 m/s and acceleration of 7.5 m/s², see **Figure 4 – 15**. The position references are generated with a 50 ms jerk time; this way, the effects of the oscillation of the cross–arm with respect to actuators X_1 and X_2 on the positioning performance are minimized. The payload is kept immobile at 1.2 m. In this configuration of the Y–axis, the unbalance between X_1 and X_2 actuators is at its maximum value.

The second test consists in displacing the payload along a diagonal over the machine workspace. Trajectories for axes X_1, X_2, and Y are identical, from +0.15 m to –0.15 m, at a maximum velocity of 0.75 m/s and acceleration of 7.5 m/s². The jerk time is set to 50 ms for all axes, see **Figure 4 – 16**.

From **Figures 4 – 15** and **4 – 16**, it can be noticed that the proposed decoupling basis control provides a slight improvement of the gantry stage's positioning performance with respect to the industrial independent axis control. Still, it is difficult to talk about an actual improvement; since, for point–to–point applications the main interest is the positioning performance at the end of the motion, which both for independent axis and decoupling basis control is detrimentally affected by the oscillations of the rigid cross–arm with respect to the moving parts actuators X_1 and X_2, the oscillations of the cable carrier attached to it, and by the oscillation of actuators X_1 and X_2 along with their respective supporting structures. We have identified the oscillations of the rigid cross–arm with respect to the moving parts actuators X_1 and X_2 as the principal source of disturbance to the positioning performance, see **Figure 4 – 12**. We have partially overcome this drawback by adding jerk time to the motion references of actuators X_1 and X_2; but despite that, this vibration mode is still excited by the cable carrier during the deceleration phase.

To address this problem, there are two possible solutions. One solution is to improve the mechanical design of the gantry stage by increasing the stiffness of the flexible plate joint attaching the cross–arm to actuator X_1, which, as it can be appreciated on **Figures 4 – 15 (*c*)** and **4 – 16 (*c*)** is a major source of oscillations; and by improving the design of the cable carrier. Other solution, it is to modify the modeling of the gantry stage to take into consideration the oscillation of the rigid cross–arm, as presented on (§ 4.1.5.1), and based on such a model, to derive a control structure capable compensating it.

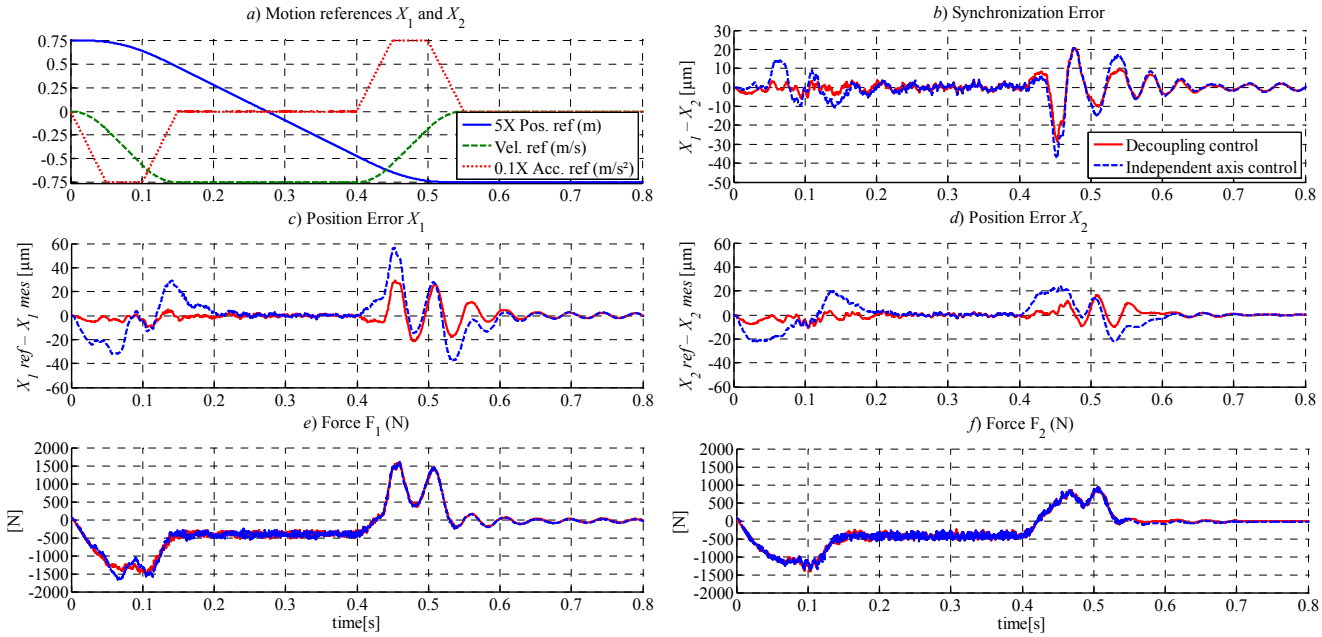

Figure 4 – 15 : *Independent axis control vs. decoupling basis control, point–to–point* X_1 *and* X_2 *synchronized motions (from* +0.15 *to* –0.15 m*) at a maximum velocity of* 0.75 m/s *and a maximum acceleration of* 7.5 m/s²*; the position of the payload is kept at* 1.2 m *(i.e. maximum unbalance).*

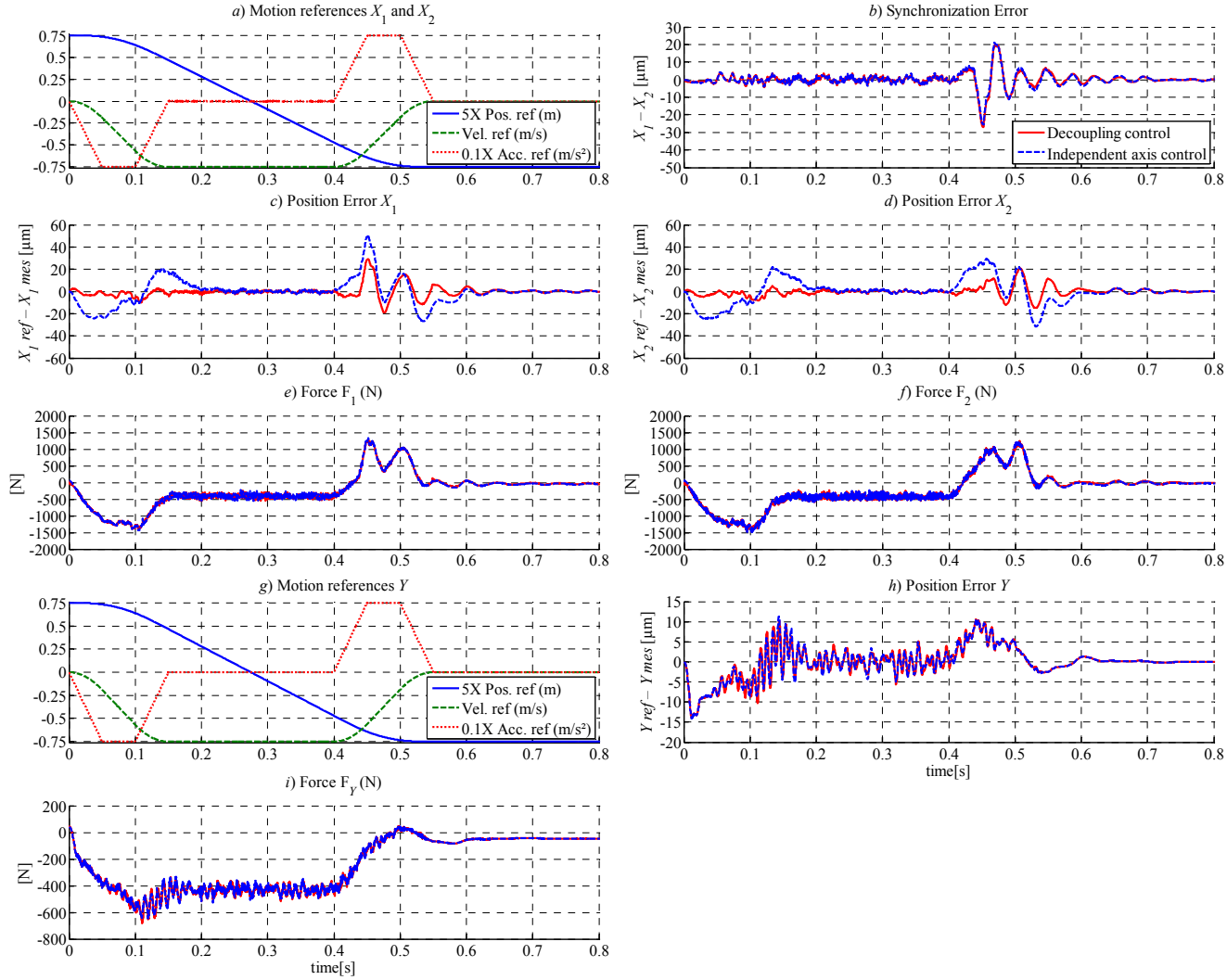

Figure 4 – 16 : *Independent axis control vs. decoupling basis control, point–to–point diagonal movement (*X_1*,* X_2*, and* Y *from* +0.15 *to* –0.15 m*) at a maximum velocity of* 0.75 m/s *and a maximum acceleration of* 7.50 m/s²*.*

Path–tracking motion test

The path–tracking motion test consists in tracing clockwise three concentric circles of radius $R = 100$ mm, see **Figure 4 – 17**. This test, commonly known as a Ballbar test, is extensively used to assess the positioning performance of machine tools. The dash light green circle represents the reference, i.e. a circle of radius $R = 100$ mm. The plotted radius error is amplified a million times. The first circle is traced during the tangential acceleration cycle of the payload; the peak acceleration of actuators X_1, X_2, and Y is $6\,\mathrm{m/s^2}$. At the end of this first cycle, the payload has reached a constant tangential velocity of $0.8\,\mathrm{m/s}$. The second circle is traced at this velocity. The third and final circle is traced during the deceleration cycle. The measurement precision is ±1μm.

The effect of the mechanical coupling and the unbalance between actuators on the tracking precision is easy to identify by comparing the two Ballbar plots presented on **Figure 4 – 17**. This is specially highlighted when the direction of the motion along the X–direction changes, i.e. transition at the vertical axis. The vibration of the rigid cross–arm with respect to actuators X_1 and X_2 is not particularly excited by the motion of actuators X_1 and X_2 since the acceleration transitions are quite smooth, i.e. sinusoidal signal. It is however slightly excited by the vibrations of the cable carrier when the direction of the motion along the X–direction changes from positive to negative. Even then, to take into account the unbalance and the mechanical coupling between actuators within the control structure results in a minimization of 22% of the maximum radius error and in a global minimization of the mean error. As commented before; the remaining error, which is quite repeatable, is mostly due to the detent forces of the PMLSMs.

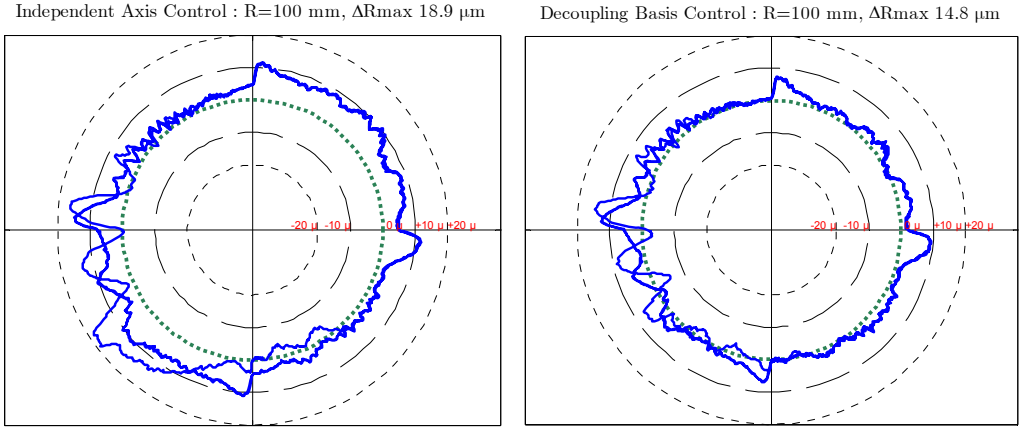

Figure 4 – 17 : *Independent axis control vs. decoupling basis control. Ballbar tests realized with three* 100 mm *radius circles at a maximum tangential velocity of* 0.8 m/s *and acceleration of* 6 m/s².

The lobes in **Figure 4 – 17** at the horizontal and vertical axes are principally due to the static friction of axes X_1, X_2, and Y. If their values are compensated, the positioning performance of the gantry stage can be improved even more.

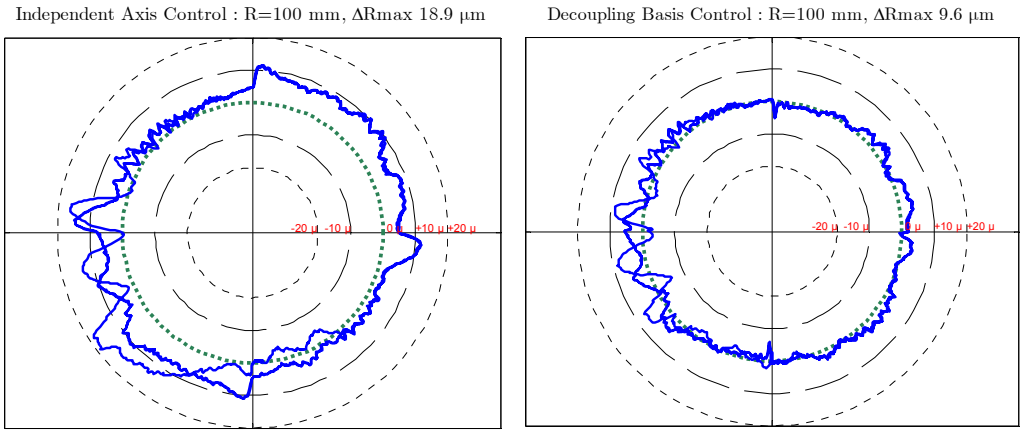

Figure 4 – 18 : *Independent axis control vs. decoupling basis control with compensation of the static friction of actuators X_1, X_2, and Y. Ballbar tests realized with three* 100 mm *radius circles at a maximum tangential velocity of* 0.8 m/s *and acceleration of* 6 m/s².

4.2 Application to a « flexible » gantry

This section presents the methodology of modeling and controlling gantry stages (Chapter 3) applied to a "flexible" gantry stage. It is divided in three parts,

- *Experimental set–up*: The physical system is studied up–close. The objective of this study, as described on (§ 3.1.1), is to determine the configuration and the nature of the elements constituting the gantry stage.
- *Dynamical modeling*: Based on the system's analysis, we propose a dynamical model of the system based on the generic model presented on (§ 3.2.2). We identify its parameters using the method proposed on (§ 3.2.3).
- *Control on a decoupling basis*: We propose a decoupling controller based on the generic controller presented on (§ 3.3.4). In this section we'll present in detail the decoupling basis transformation for a flexible gantry stage with one flexible mode.

4.2.1 Experimental set–up

One of the principal objectives of this research project is to take into consideration the flexibility of the cross–arm into the modeling and into the development of an adapted control structure. To this purpose, the gantry stage "Andromeda" presented on (§ 4.1.4) has been modified. Its rigid cross–arm has been replaced by a slender, flexible beam, see **Figure 4 – 19**. To emulate the effects of a moving payload, a dummy payload is used.

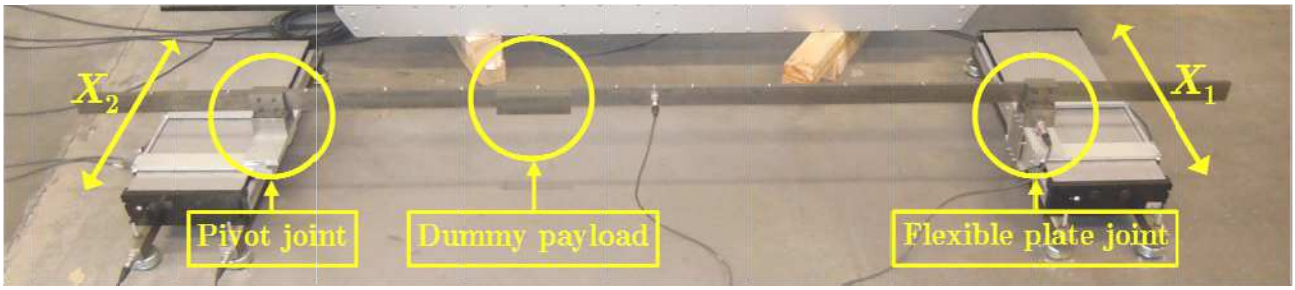

Figure 4 – 19 : *Modified dual–drive gantry stage*

We know that the cross–arm is flexible. We need however to determine how many of its flexible modes are excited due to the synchronous motion of actuators X_1 and X_2, and the variable position of the dummy payload. As explained on (§ 3.2.3.2), this can be done by imposing a series of motions on actuators X_1 and X_2 (using the build–in independent axis controllers) and by measuring either their forces or their tracking errors for each motion. For example, in **Figure 4 – 20**, we can see the measured forces and tracking errors of actuators X_1 and X_2 for an imposed motion (see figure legend).

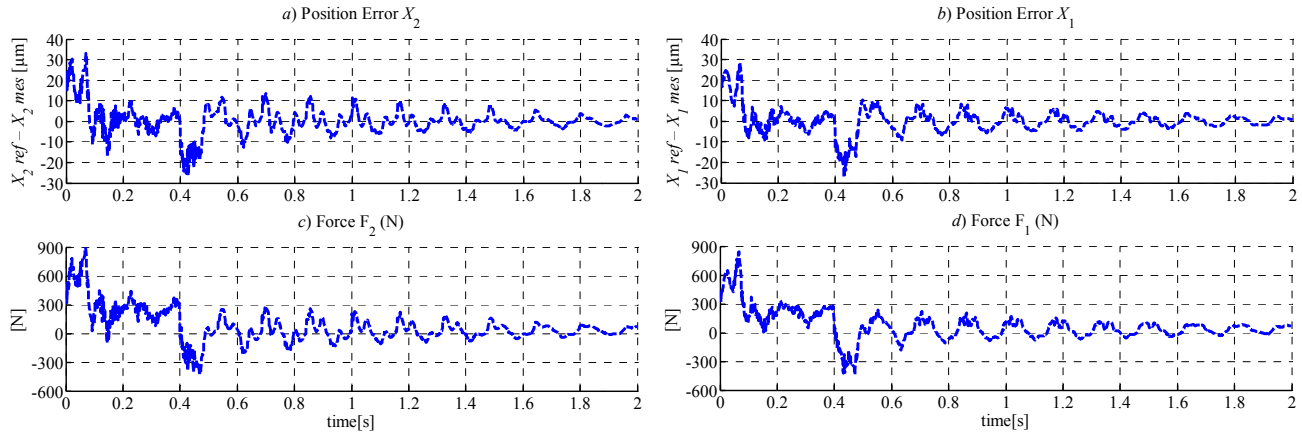

Figure 4 – 20 : *influence of the flexibility of the cross–arm on the reaction forces and tracking errors of actuators X_1 and X_2. Motion from* –0.15 *to* +0.15 m *at a maximum velocity of* 0.75 m/s *and a maximum acceleration of* 10 m/s². *The dummy payload is located at* Y =–0.1 m.

From the force plots (c) and (d) in **Figure 4 – 20**, we can recognize a constant acceleration cycle (0 to 0.1 s); a constant velocity cycle (0.1 to 0.4 s); and a constant deceleration cycle (0.4 to 0.5 s). At 0.5 s, actuators X_1 and X_2 have arrived to the target position and their motion should have stopped. This is however not the case from what we can appreciate on the position error plots (a) and (b). The oscillations that appear are due to two factors. The first factor is the pitch motion of the cross–arm, which this time is less important with respect to the example presented on (§ 4.1.4) due to the reduced cross–arm's weight. Nonetheless, it is important to note that its effects are more pronounced on actuator X_2 due to important backlash at the junction "cross–arm – actuator X_2". The second factor is the first flexible mode of the cross–arm, which pulls actuators X_1 and X_2 back and forth from the target position. The oscillating forces F_1 and F_2 are the forces imposed by the independent controllers in order to hold actuators X_1 and X_2 at the target position.

4.2.2 Dynamic Modeling

To propose a model of the flexible gantry stage presented on **Figure 4 – 21**, it is necessary to consider three elements,

(1) The gantry stage is composed of:

- Three linear actuators (X_1 and X_2).
  - Two Permanent Magnet Linear Synchronous Machines (PMLSMs) (X_1 and X_2), which carry the cross–arm along the x–direction.
- A cross–arm which is considered having one flexible mode, the first for instance.
- A flexible plate joint connecting the cross–arm to actuator X_1.
- A pivot joint connecting the cross–arm to actuator X_2.
- A dummy payload.

(2) The gantry stage is one whose cross–arm is attached to the actuators at intermediate positions,

(3) The deformation of the gantry stage along the z–axis is supposed negligible.

Based on elements (1) to (3), the following model is proposed:

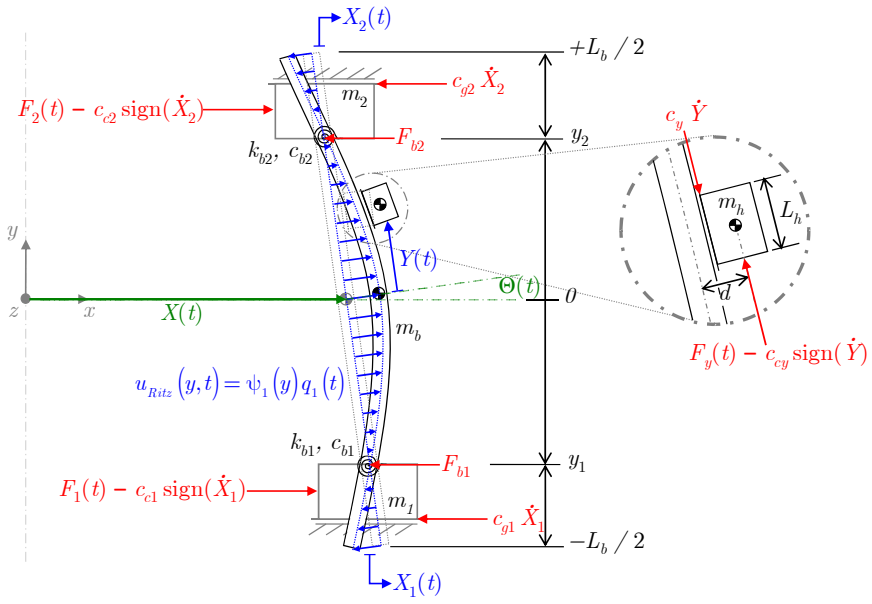

Figure 4 – 21 : *Dynamic model of the flexible gantry stage*

Where,

L_b is the length of the cross–arm;

y_1 is the location of the flexible plate joint;

y_2 is the location of the pivot joint;

d is the distance between the centers of mass of the cross–arm and of the payload

The motion equations of such system are defined by (3.67), with $N = 1$. N is the number of flexible modes to take into consideration into the general model of the gantry stage. Then,

$$[M]\{\ddot{q}\}+[H]\{\dot{q}\}+[C]\{\dot{q}\}+[K]\{q\}=\{Q\} \tag{4.44}$$

Where, M, C and K are the inertia (4.45), damping (4.46), and stiffness (4.47) matrices. H is the coriolis and centripetal acceleration matrix (4.48),

$$M=\begin{bmatrix} M_{XX} & M_{X\Theta} & M_{XY} & M_{X1} \\ M_{X\Theta} & M_{\Theta\Theta} & M_{\Theta Y} & M_{\Theta 1} \\ M_{XY} & M_{\Theta Y} & M_{YY} & M_{Y1} \\ M_{X1} & M_{\Theta 1} & M_{Y1} & M_{11} \end{bmatrix} \quad \therefore \quad \begin{aligned} M_{XX} &= m_b + m_h \\ M_{X\Theta} &= -\mathrm{Sin}(\Theta)\left\{q_1\int_{-L_b/2}^{L_b/2}\mu\psi_1(y)dy + m_h\left[d+q_1\psi_1(Y)\right]\right\} - m_h Y\mathrm{Cos}(\Theta) \\ M_{XY} &= m_h\left[\mathrm{Cos}(\Theta)q_1\psi_1'(Y) - \mathrm{Sin}(\Theta)\right] \\ M_{X1} &= \mathrm{Cos}(\Theta)\left[m_h\psi_1(Y) + \int_{-L_b/2}^{L_b/2}\mu\psi_1(y)dy\right] \\ M_{\Theta\Theta} &= q_1^2\int_{-L_b/2}^{L_b/2}\mu\psi_1^2(y)dy + J_b + J_h + m_h Y^2 + m_h\left[d+\psi_1(Y)q_1\right]^2 \\ M_{\Theta Y} &= m_h\left[d+\psi_1(Y)q_1\right] - Y m_h q_1\psi_1'(Y) + J_h\psi_1''(Y)q_1 \\ M_{\Theta 1} &= -Y m_h\psi_1(Y) + J_h\psi_1'(Y) - \mu\int_{-L_b/2}^{L_b/2} y\psi_1(y)dy \\ M_{YY} &= m_h + m_h\psi_1'^2(Y)q_1^2 + J_h\psi_1''^2(Y)q_1^2 \\ M_{Y1} &= m_h\psi_1(Y)\psi_1'(Y)q_1 + J_h\psi_1'(Y)\psi_1''(Y)q_1 \\ M_{11} &= m_h\psi_1^2(Y) + J_h\psi_1'^2(Y) + m_{11} \quad \therefore \quad m_{11} = \int_{-L_b/2}^{L_b/2}\mu\psi_1^2(y)dy \end{aligned} \tag{4.45}$$

$$C=\begin{bmatrix} 0 & 0 & 0 & 0 \\ 0 & C_{\Theta\Theta} & 0 & C_{\Theta 1} \\ 0 & 0 & C_{YY} & 0 \\ 0 & C_{\Theta 1} & 0 & C_{11} \end{bmatrix} = \begin{bmatrix} 0 & 0 & 0 & 0 \\ 0 & c_{b1}+c_{b2} & 0 & c_{b1}\psi_1'(y_1)+c_{b2}\psi_1'(y_2) \\ 0 & 0 & c_y & 0 \\ 0 & c_{b1}\psi_1'(y_1)+c_{b2}\psi_1'(y_2) & 0 & c_{11}+c_{b1}\psi_1'^2(y_1)+c_{b2}\psi_1'^2(y_2) \end{bmatrix} \quad \therefore \quad c_{11} = \int_{-L_b/2}^{L_b/2}\gamma EI\,\psi_1''^2(y)dy \tag{4.46}$$

$$K=\begin{bmatrix} 0 & 0 & 0 & 0 \\ 0 & K_{\Theta\Theta} & 0 & K_{\Theta 1} \\ 0 & 0 & 0 & 0 \\ 0 & K_{\Theta 1} & 0 & K_{11} \end{bmatrix} = \begin{bmatrix} 0 & 0 & 0 & 0 \\ 0 & k_{b1}+k_{b2} & 0 & k_{b1}\psi_1'(y_1)+k_{b2}\psi_1'(y_2) \\ 0 & 0 & 0 & 0 \\ 0 & k_{b1}\psi_1'(y_1)+k_{b2}\psi_1'(y_2) & 0 & k_{11}+k_{b1}\psi_1'^2(y_1)+k_{b2}\psi_1'^2(y_2) \end{bmatrix} \quad \therefore \quad k_{11} = \int_{-L_b/2}^{L_b/2}EI\,\psi_1''^2(y)dy \tag{4.47}$$

$$H=\begin{bmatrix} 0 & H_{X\Theta} & H_{XY} & 0 \\ 0 & H_{\Theta\Theta} & H_{\Theta Y} & 0 \\ 0 & H_{Y\Theta} & H_{YY} & 0 \\ 0 & H_{1\Theta} & H_{1Y} & 0 \end{bmatrix} \quad \therefore \quad \begin{aligned} H_{X\Theta} &= -\left\{\begin{aligned} &2\left(\mathrm{Sin}(\Theta)\left(\dot{q}_1\int_{-L_b/2}^{L_b/2}\mu\psi_1(y)dy + m_h\frac{d}{dt}\left[q_1\psi_1(Y)\right]\right) + \mathrm{Cos}(\Theta)m_h\dot{Y}\right) + \\ &+\left(\mathrm{Cos}(\Theta)\left(q_1\int_{-L_b/2}^{L_b/2}\mu\psi_1(y)dy + m_h\left[d+q_1\psi_1(Y)\right]\right) - \mathrm{Sin}(\Theta)m_h Y\right)\dot{\Theta}\end{aligned}\right\} \\ H_{XY} &= \left[2m_h\dot{q}_1\psi_1'(Y) + m_h q_1\psi_1''(Y)\dot{Y}\right]\mathrm{Cos}(\Theta) \\ H_{\Theta\Theta} &= 2\left\{q_1\dot{q}_1\int_{-L_b/2}^{L_b/2}\mu\psi_1^2(y)dy + m_h\left[d+\psi_1(Y)q_1\right]\left[\psi_1(Y)\dot{q}_1\right]\right\} \\ H_{\Theta Y} &= \left\{\begin{aligned} &\left\{-2Y m_h\psi_1'(Y)\dot{q}_1 + 2\dot{\Theta}\left\{m_h\left[Y+\left(d+\psi_1(Y)q_1\right)\psi_1'(Y)q_1\right]\right\} + 2J_h\psi_1''(Y)\dot{q}_1\right\} + \\ &+\dot{Y}\left[J_h\psi_1''(Y)q_1 - Y m_h\psi_1''(Y)q_1\right]\end{aligned}\right\} \\ H_{Y\Theta} &= m_h\left\{2\psi_1(Y)\dot{q}_1 - \dot{\Theta}\left[Y+\left(d+\psi_1(Y)q_1\right)\psi_k'(Y)q_k\right]\right\} \\ H_{YY} &= \left\{2\left[m_h\psi_1'^2(Y)q_1\dot{q}_1 + J_h\psi_1''^2(Y)q_1\dot{q}_1\right] + \dot{Y}\psi_1''(Y)q_1\left[m_h\psi_1'(Y)q_1 + J_h\psi_1''(Y)q_1\right]\right\} \\ H_{1\Theta} &= -\dot{\Theta}\left[q_1\int_{-L_b/2}^{L_b/2}\mu\psi_1^2(y)dy + m_h\psi_1(Y)\left(d+\psi_1(Y)q_1\right)\right] \\ H_{1Y} &= 2\left\{m_h\psi_1(Y)\left[\psi_1'(Y)\dot{q}_1 - \dot{\Theta}\right] + J_h\psi_1'(Y)\psi_1''(Y)\dot{q}_1\right\} + \dot{Y}\left[m_h\psi_1(Y)\psi_1''(Y)q_1 + J_h\psi_1'(Y)\psi_1''(Y)q_1\right] \end{aligned} \tag{4.48}$$

The generalized coordinates and the generalized forces are defined, respectively, by (4.49) and (4.50),

$$q=\begin{bmatrix} X \\ \Theta \\ Y \\ q_1 \end{bmatrix};\ Q=\begin{bmatrix} F_X \\ F_\Theta \\ F_Y \\ Q_1 \end{bmatrix}=\begin{bmatrix} F_{b1}+F_{b2} \\ \left(F_{b1}-F_{b2}\right)\cos\left(\Theta\right)\left(y_2-y_1\right)/2 \\ F_Y \\ F_{b1}\psi_1\left(y_1\right)+F_{b2}\psi_1\left(y_2\right) \end{bmatrix} \quad \therefore \quad \begin{aligned} F_{b1} &= F_1-m_1\ddot{X}_1-c_{g1}\dot{X}_1-c_{c1}\,\mathrm{sign}\left(\dot{X}_1\right) \\ F_{b2} &= F_2-m_2\ddot{X}_2-c_{g2}\dot{X}_2-c_{c2}\,\mathrm{sign}\left(\dot{X}_2\right) \\ F_Y &= F_y-c_{cy}\,\mathrm{sign}\left(\dot{Y}\right) \\ \psi_1\left(y_1\right) &= \psi_1\left(y_2\right)=0 \end{aligned} \qquad (4.49),\ (4.50)$$

The parameters of the dynamical model are estimated using the method presented on (§ 3.2.3) and are presented on TABLE IV.

TABLE IV
PHYSICAL PARAMETERS OF THE "FLEXIBLE" GANTRY STAGE

Name	Value	Description
$\boldsymbol{\mu}$	6.4 kg/m	Cross–arm's linear density
$\boldsymbol{m_b}$	19.2 kg	Mass of the moving cross–arm
$\boldsymbol{m_h}$	3.1 kg	Mass of the payload (Y–axis)
$\boldsymbol{m_1}$	30.4 kg	Mass of actuator X_1
$\boldsymbol{m_2}$	26.6 kg	Mass of actuator X_2
$\boldsymbol{m_{11}}$	9.6 kg	Modal mass (cross–arm's 1st flexible mode)
$\boldsymbol{J_b}$	14.382 kg m²	Rotary inertia of the beam
$\boldsymbol{J_h}$	0.0058 kg m²	Rotary inertia of the head (Y–axis)
$\boldsymbol{c_{g1}}$	352.6 N/(m/s)	Viscous friction of actuator X_1
$\boldsymbol{c_{g2}}$	360.3 N/(m/s)	Viscous friction of actuator X_2
$\boldsymbol{c_y}$	476.23 N/(m/s)	Viscous friction of the payload (Y–axis)
$\boldsymbol{c_{11}}$	34.90 N/(m/s)	Modal damping (cross–arm's 1st flexible mode)
$\boldsymbol{c_{b1}}$	0.32 Nm/(rad/s)	Viscous Friction of mechanical joint No.1
$\boldsymbol{c_{b2}}$	0.9 Nm/(rad/s)	Viscous Friction of mechanical joint No.2
$\boldsymbol{k_{b1}}$	1550 Nm/rad	Stiffness of mechanical joint No.1
$\boldsymbol{k_{b2}}$	0 Nm/rad	Stiffness of mechanical joint No.2
$\boldsymbol{k_{11}}$	22248 N/m	Modal Stiffness (cross–arm's 1st flexible mode)
$\boldsymbol{c_{cy}}$	126.6 N	Static friction of the payload (Y–axis)
$\boldsymbol{c_{c1}}$	111 N	Static friction of actuator X_1
$\boldsymbol{c_{c2}}$	104 N	Static friction of actuator X_2
$\boldsymbol{L_b}$	3.00 m	Length of the moving beam
$\boldsymbol{L_h}$	0.32 m	Length of the payload
$\boldsymbol{d}$	0.0 m	Distance between beam and head
$\boldsymbol{y_1}$	–1 m	Location of the flexible plate joint
$\boldsymbol{y_2}$	1 m	Location of the flexible plate joint
$\boldsymbol{\psi_1(y_1)}$	0 m	Value of the 1st mode shape at y_1
$\boldsymbol{\psi_1(y_2)}$	0 m	Value of the 1st mode shape at y_2
$\boldsymbol{\psi_1\,(Y)}$	$-0.137y^5-0.055y^4+0.528y^3+1.1y^2-0.29y-1.1$	1st mode shape

4.2.2.1 Comparison between model and experiment

Validation tests are executed at various positions Y of the dummy payload. The motion of axes X_1 and X_2 is always from –0.15m to +0.15m at various velocities and accelerations.

Payload at Y = –1.1 m. Max. Acceleration = 2.5 m/s². Max. Velocity = 0.25 m/s

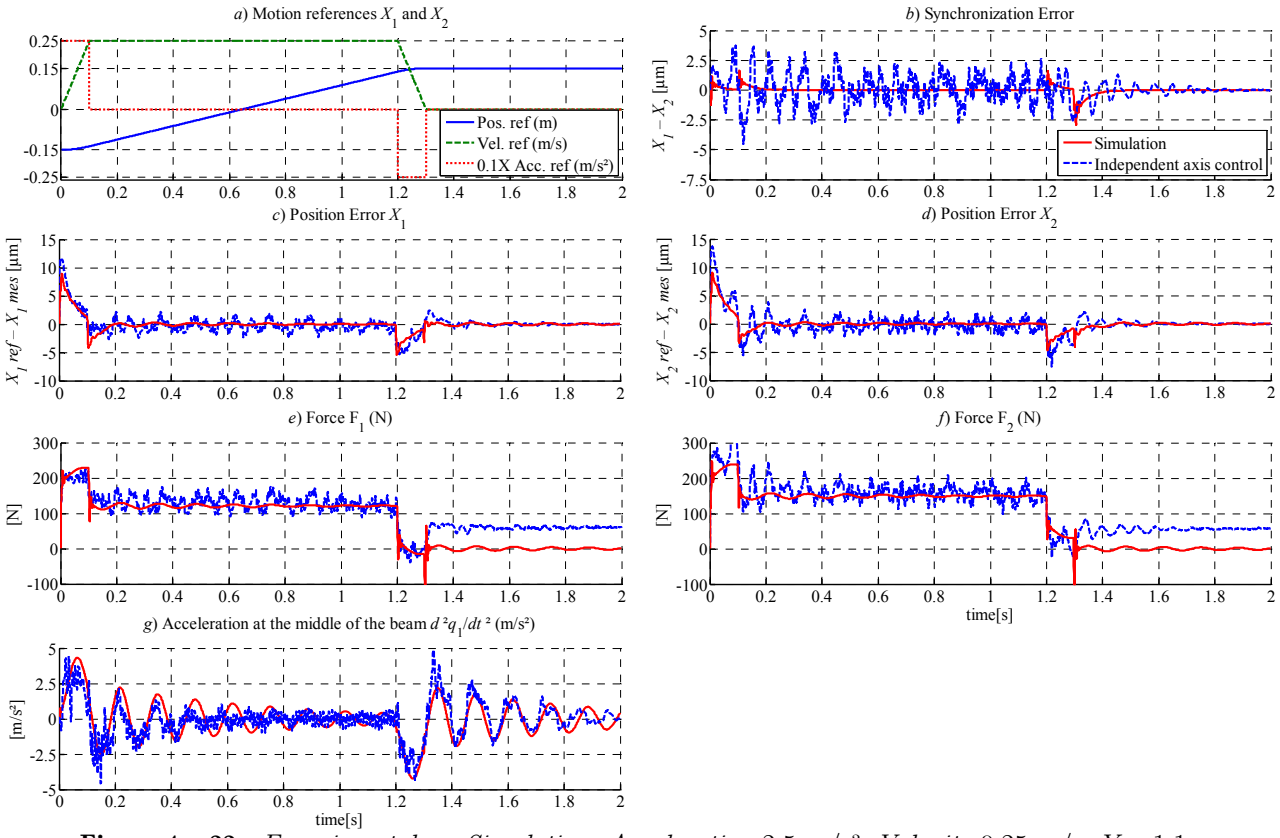

Figure 4 – 22 : *Experimental vs. Simulation. Acceleration* 2.5 m/s²; *Velocity* 0.25 m/s; *Y*=–1.1 m.

Head at Y = –0.7 m. Max. Acceleration = 7.5 m/s². Max. Velocity = 0.50 m/s

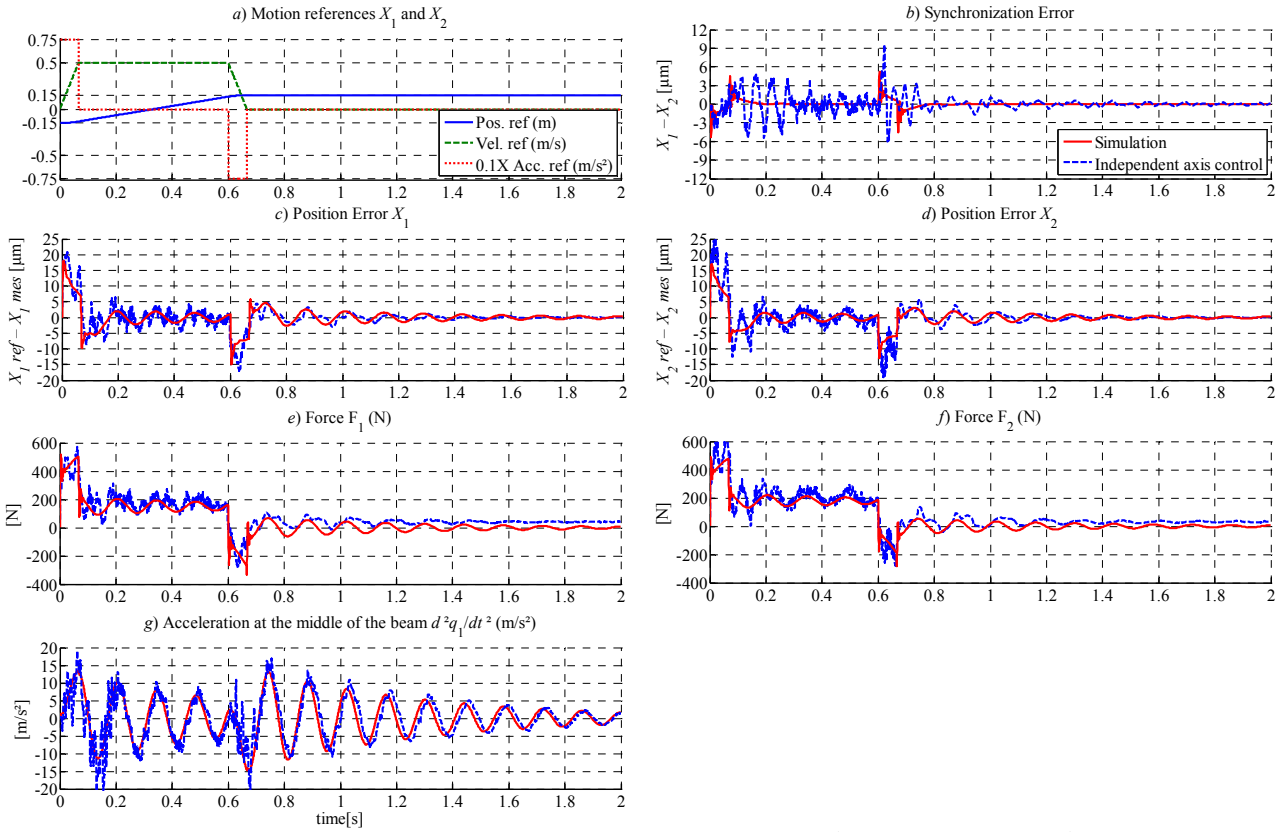

Figure 4 – 23 : *Experimental vs. Simulation. Acceleration* 7.5 m/s²; *Velocity* 0.50 m/s; *Y*=–0.7 m.

Payload at Y = –0.1 m. Max. Acc. = 10 m/s². Max. Vel. = 0.75 m/s

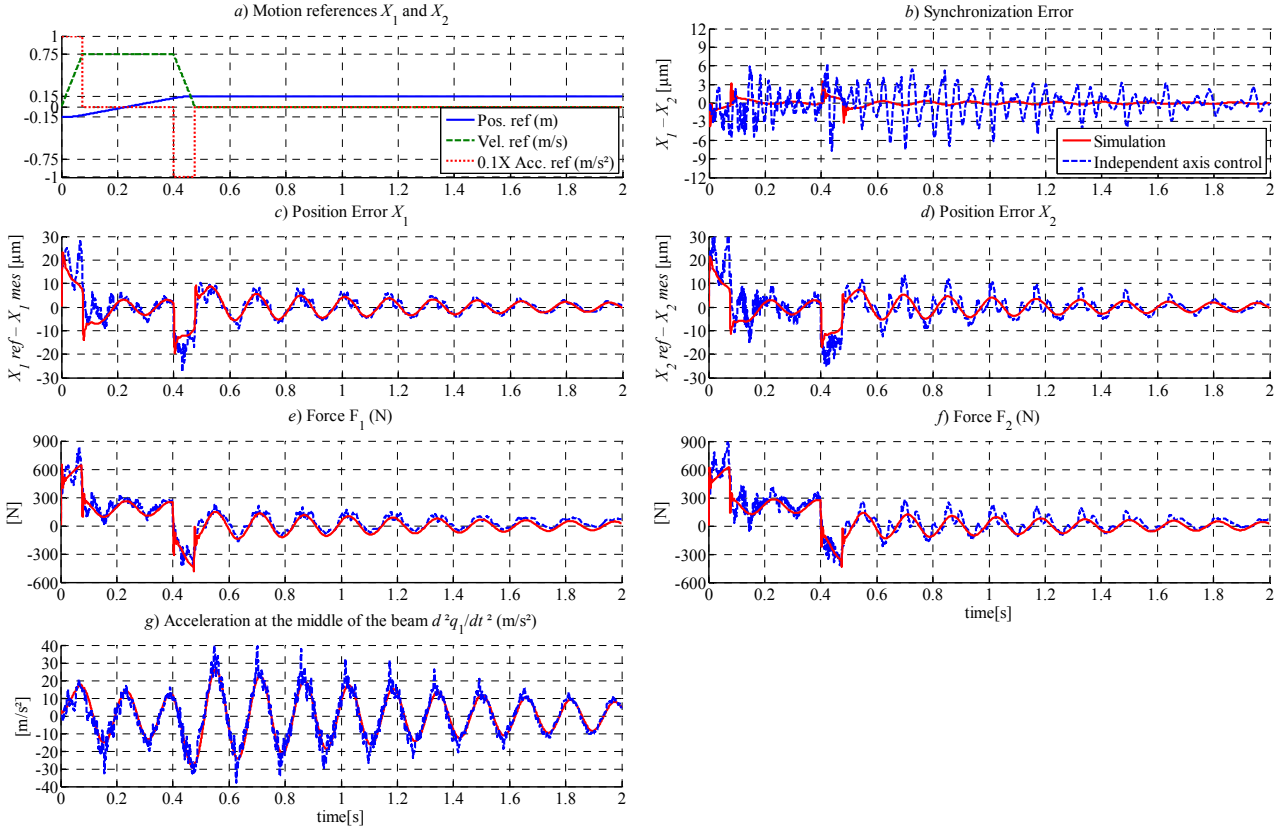

Figure 4 – 24 : *Experimental vs. Simulation. Acceleration* 10.0 m/s²; *Velocity* 0.75 m/s; *Y*=–0.1 m.

Payload at Y = 0.0 m. Max. Acc. = 10 m/s². Max. Vel. = 1.00 m/s

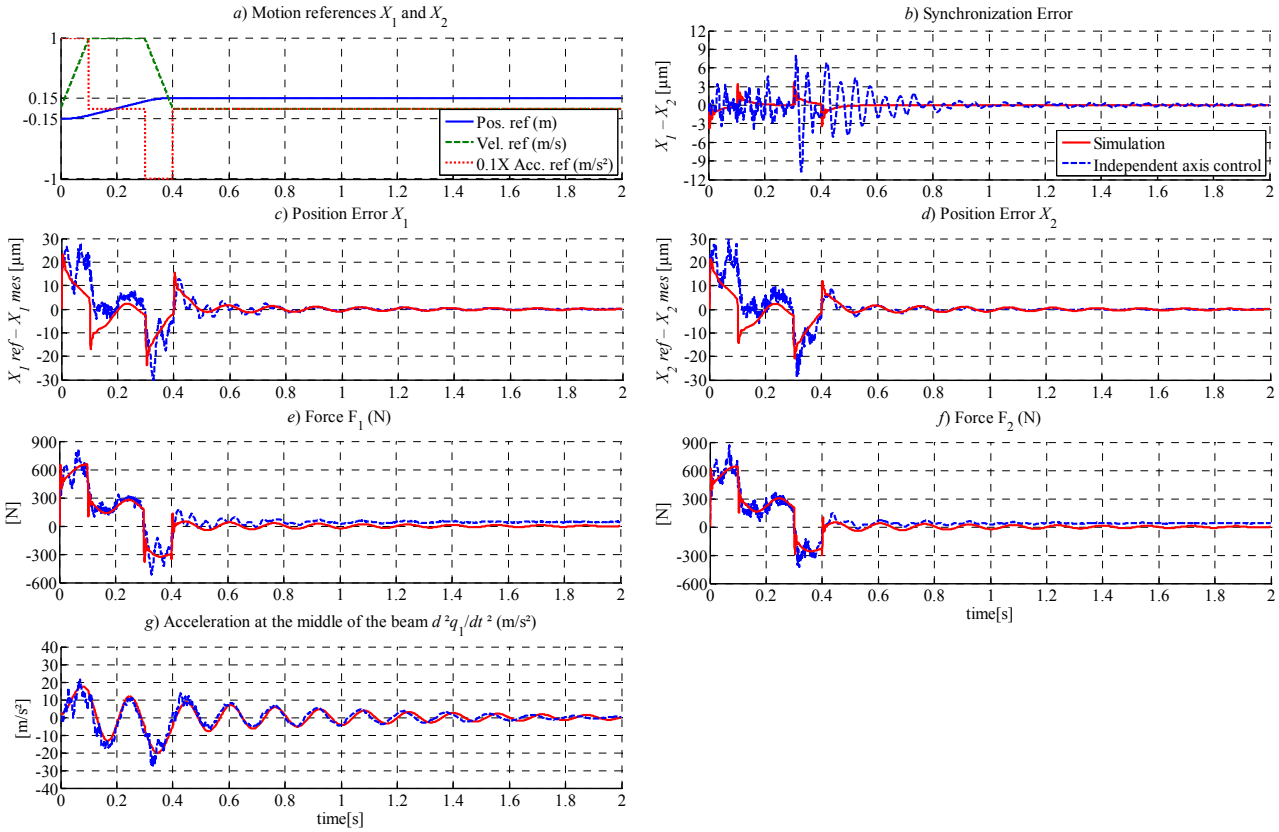

Figure 4 – 25 : *Experimental vs. Simulation. Acceleration* 10.0 m/s², *Velocity* 1.00 m/s, *Y*=0.0 m.

Payload at Y = 0.3 m. Max. Acc. = 5.0 m/s². Max. Vel. = 1.00 m/s

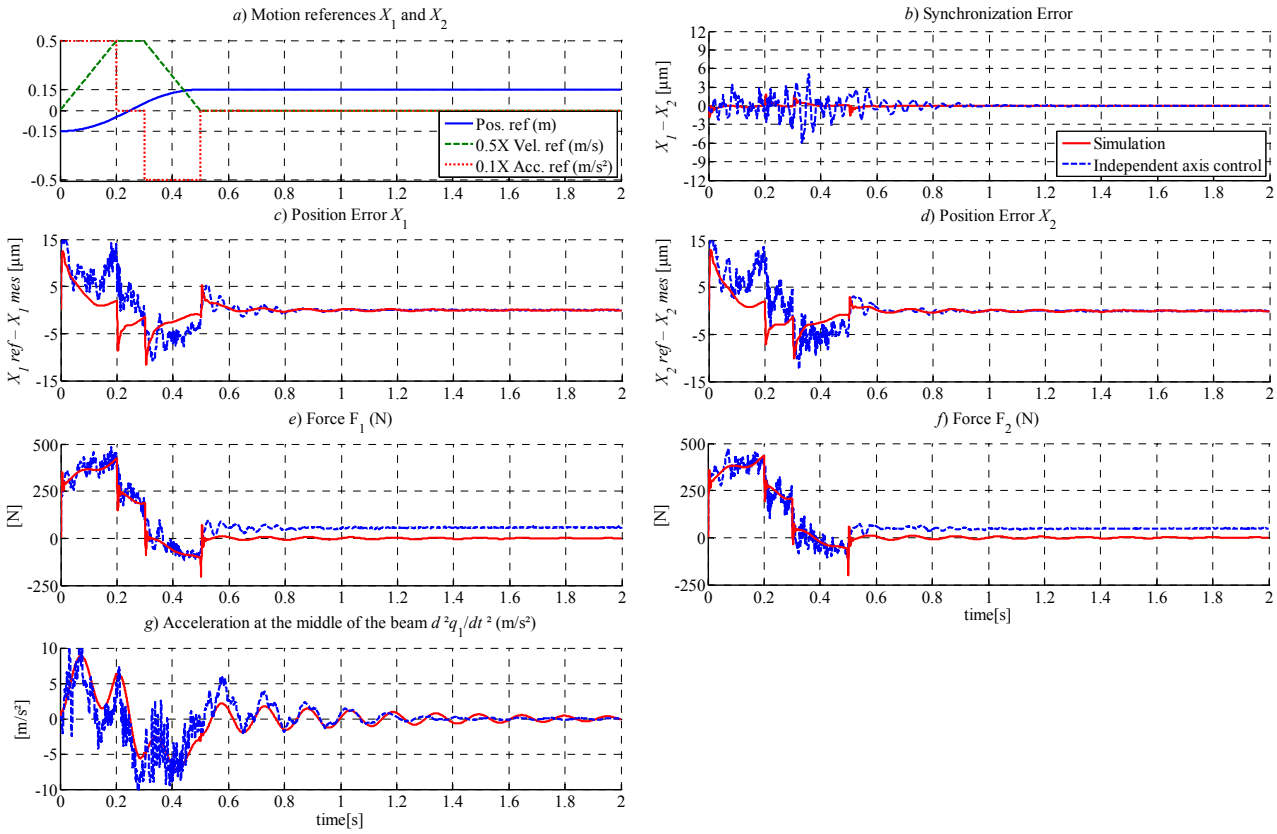

Figure 4 – 26 : *Experimental vs. Simulation. Acceleration* 5.0 m/s²; *Velocity* 1.00 m/s; *Y*=0.3.

Payload at Y = 0.5 m. Max. Acc. = 2.5 m/s². Max. Vel. = 0.75 m/s

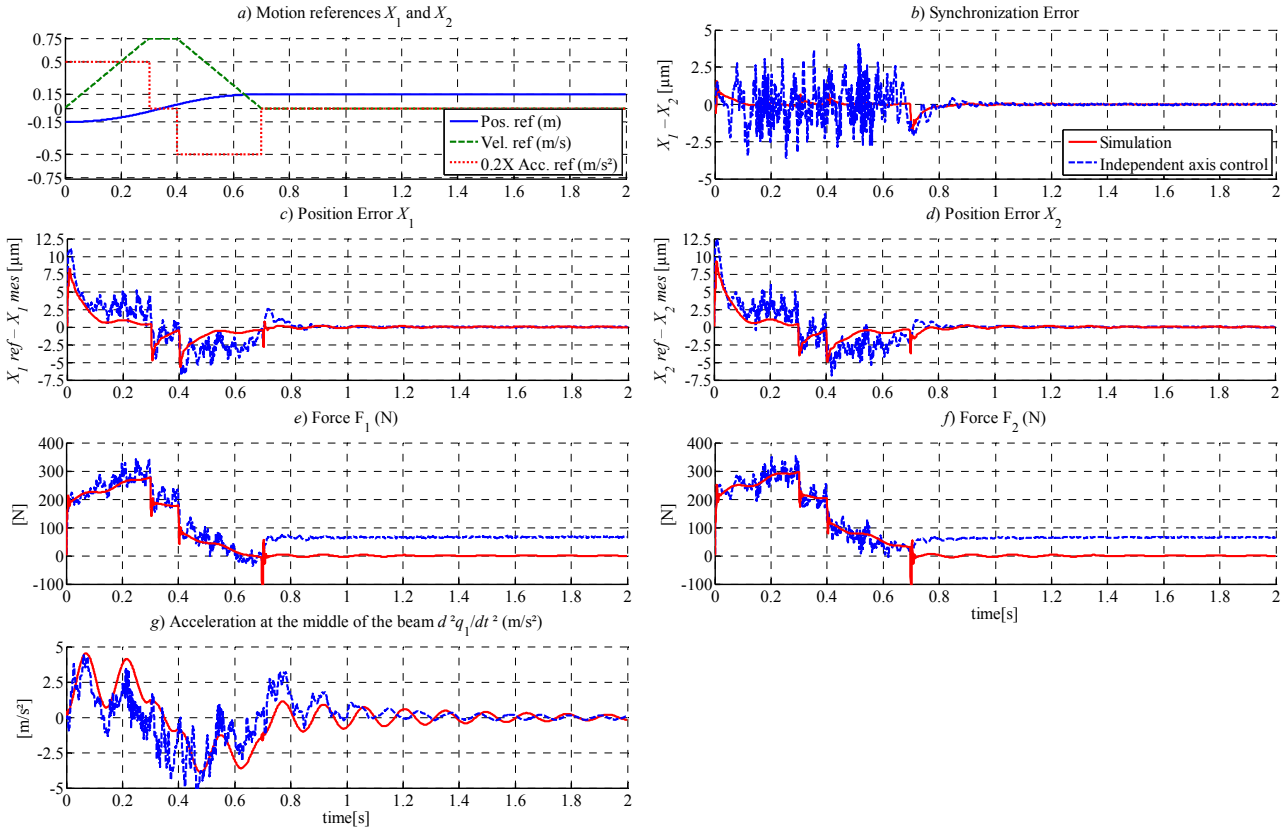

Figure 4 – 27 : *Experimental vs. Simulation. Acceleration* 2.5 m/s²; *Velocity* 0.75 m/s; *Y*=0.5 m.

Payload at Y = 0.9 m. Max. Acc. = 5.0 m/s². Max. Vel. = 1.00 m/s

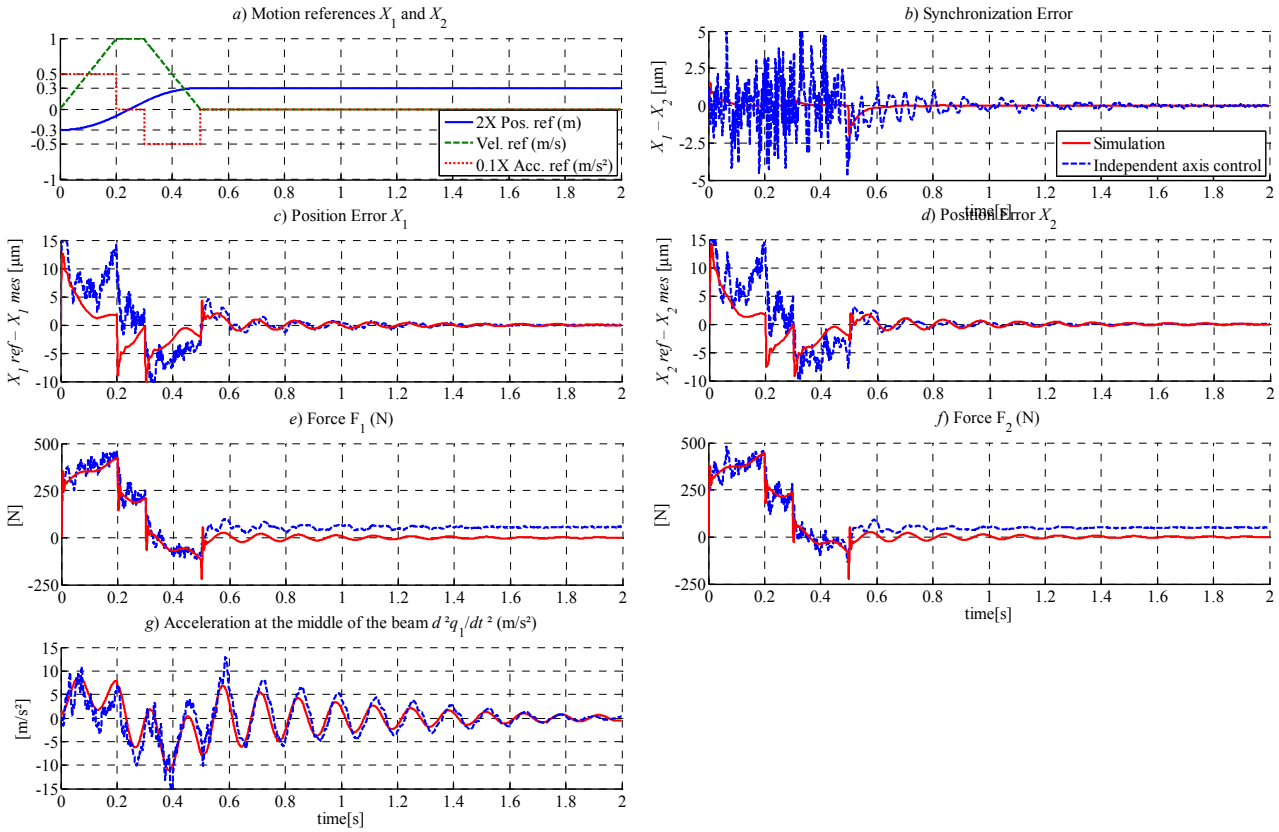

Figure 4 – 28 : *Experimental vs. Simulation. Acceleration* 5.0 m/s²; *Velocity* 1.00 m/s; ; *Y*=0.5 m.

Payload at Y = 1.3 m. Max. Acc. = 10 m/s². Max. Vel. = 0.5 m/s

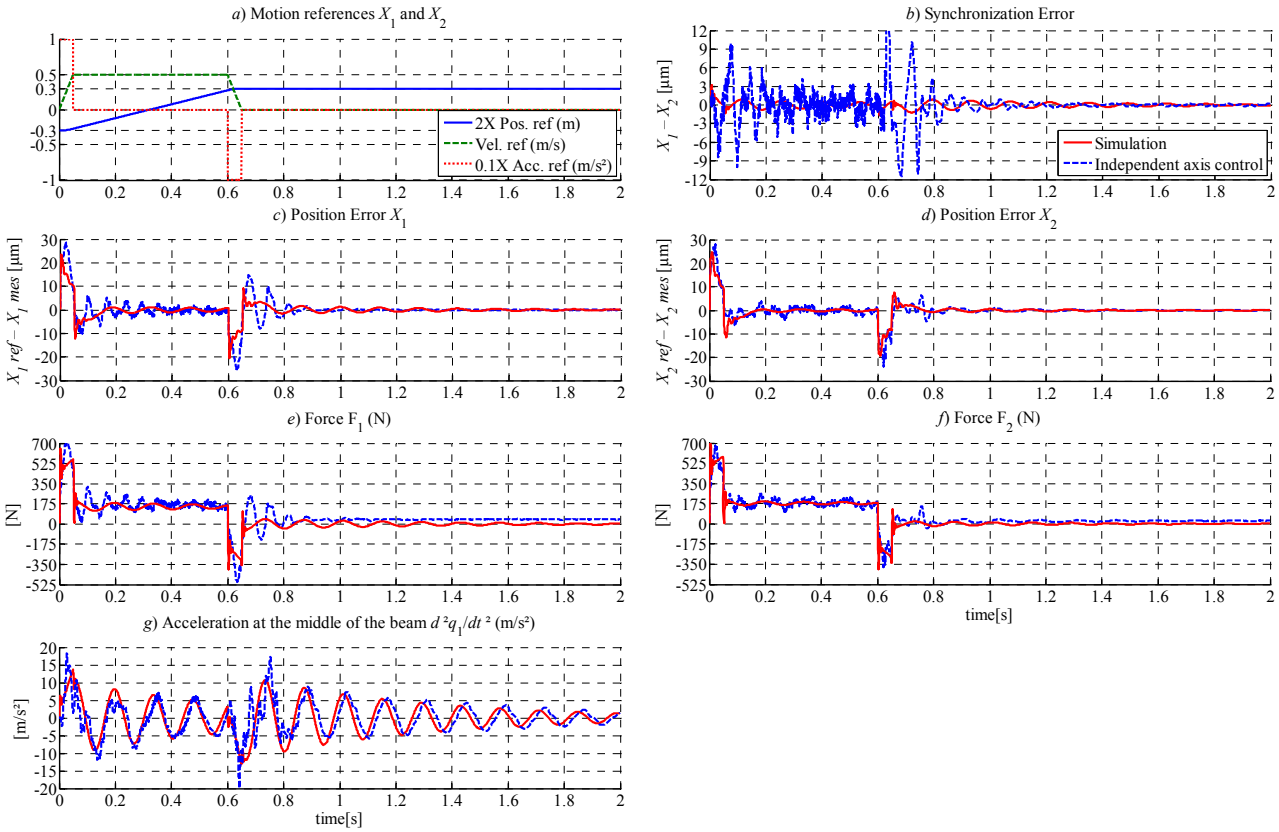

Figure 4 – 29 : *Experimental vs. Simulation. Acceleration* 10.0 m/s², *Velocity* 0.5 m/s, $Y = 1.3$ m

There are several observations to take into consideration for the validation of the proposed model and to better understand the experimental response of the system.

1. *Thermal behavior*: the cross–arm is made of steel; it is slender, homogeneous and sensitive to temperature variations. Giving this, the eigenfrequencies are likely to shift in function of the internal forces acting on the cross–arm and the boundary conditions (also sensitive to temperature).

   In consequence, taking into consideration that the measurements were carried out at different dates and that the temperature was slightly different, the estimated value of the fundamental (headless) eigenfrequency may vary.

2. *Backlash*: Besides vibrating, the beam has also tendency to swing back and forth. This is because of backlash at the beam to actuator supports (notably at X_2 which is a pivot joint), which is excited due to the fact that the center of mass of the beam and of the actuators are misaligned. A good analogy to this phenomenon is an inverse pendulum.

   A good example of this can be appreciated on **Figure 4 – 24**. Note that the peaks in force and tracking error are accentuated for actuator X_2 and that the vibration has a particular triangular shape due to the combination deformation + swing. This phenomenon is greatly accentuated for high–deformation amplitudes (system in resonance).

   Another consequence of this phenomenon is the frequency shift that can also be noticed on **Figure 4 – 24**. Indeed, as the beam swings during the motion, the overall moving mass is modified. Thus, the fundamental eigenfrequency of the beam is shifted.

   A final observation to this phenomenon is that if the actuators' and beam + head's centers of mass are aligned, it won't be excited.

3. *Miscalculation of* $\psi(Y)$: As commented before, the system is sensitive to thermal variations. In consequence the estimated mode shape may not be suitable to fit all the measurements done at different temperatures.

A quick conclusion to this section is that, as it can be appreciated on **Figure 4 – 22** to **Figure 4 – 29**, the proposed model is representative of the actual behavior of the physical system, and it's therefore suitable to develop a model–based control structure taking into account the flexibility of the system.

4.2.3 Control on a decoupling basis

4.2.3.1 Transformation into a decoupling basis

To transform the motion equations (4.44) of the flexible gantry stage into a decoupling basis, we apply the steps presented on (§ 3.3.3). First, we simplify the motion equations (4.44). Then, we decouple the motion of the payload from the rest of the system; which is now considered as a disturbance that will be compensated by the feedforward control.

Then motion equations of the flexible gantry stage are now defined by,

$$[M]\{\ddot{q}\}+[C]\{\dot{q}\}+[K]\{q\}=\{Q\} \tag{4.51}$$

Where,

$$M=\begin{bmatrix} M_{XX} & M_{X\Theta} & M_{XY} & M_{X1} \\ M_{X\Theta} & M_{\Theta\Theta} & M_{\Theta Y} & M_{\Theta 1} \\ M_{XY} & M_{\Theta Y} & M_{YY} & M_{Y1} \\ M_{X1} & M_{\Theta 1} & M_{Y1} & M_{11} \end{bmatrix};\ C=\begin{bmatrix} 0 & 0 & 0 & 0 \\ 0 & C_{\Theta\Theta} & 0 & C_{\Theta 1} \\ 0 & 0 & C_{YY} & 0 \\ 0 & C_{\Theta 1} & 0 & C_{11} \end{bmatrix};\ K=\begin{bmatrix} 0 & 0 & 0 & 0 \\ 0 & K_{\Theta\Theta} & 0 & K_{\Theta 1} \\ 0 & 0 & 0 & 0 \\ 0 & K_{\Theta 1} & 0 & K_{11} \end{bmatrix} \tag{4.52), (4.53), (4.54}$$

q_s and Q_s are the generalized coordinates and the generalized forces and are defined, respectively, by (4.55)(4.56),

$$q=\begin{bmatrix}X\\ \Theta\\ Y\\ q_1\end{bmatrix};\ Q=\begin{bmatrix}F_X\\ F_\Theta\\ F_Y\\ Q_1\end{bmatrix}=\begin{bmatrix}F_{b1}+F_{b2}\\ \left\{\left(F_{b1}-F_{b2}\right)\cos\left(\Theta\right)\left(y_2-y_1\right)/2\right\}-M_{\Theta Y}\ddot{Y}\\ F_Y\\ F_{b1}\psi_1\left(y_1\right)+F_{b2}\psi_1\left(y_2\right)\end{bmatrix}\quad\therefore\quad\begin{matrix}F_{b1}=F_1-m_1\ddot{X}_1-c_{g1}\dot{X}_1-c_{c1}\operatorname{sign}\left(\dot{X}_1\right)\\ F_{b2}=F_2-m_2\ddot{X}_2-c_{g2}\dot{X}_2-c_{c2}\operatorname{sign}\left(\dot{X}_2\right)\\ F_Y=F_y-c_{cy}\operatorname{sign}\left(\dot{Y}\right)\\ \psi_1\left(y_1\right)=\psi_1\left(y_2\right)=0\end{matrix}\qquad(4.55),\ (4.56)$$

The motion of the payload (Y – axis) is now defined by the independent equation (4.57)

$$m_h\ddot{Y}+c_h\dot{Y}=F_y-c_{cy}\operatorname{sign}\left(\dot{Y}\right)\tag{4.57}$$

To take into account the unbalance between actuators X_1 and X_2 into the decoupling basis transformation; the motion equations (4.51) are expressed in terms of the electromagnetic forces F_1 and F_2 generated by actuators X_1 and X_2. The motion equations (4.51) become,

$$\left[M+M_{X_1X_2}\right]\left\{\ddot{q}\right\}+\left[C+C_{X_1X_2}\right]\left\{\dot{q}\right\}+\left[K\right]\left\{q\right\}=\left\{Q_{X_1X_2}\right\}\tag{4.58}$$

Where $M+M_{X_1X_2}$, $C+C_{X_1X_2}$ and K are the inertia (4.59), damping (4.60), and stiffness (4.61) matrices defined in terms of the electromagnetic forces F_1 and F_2.

$$M+M_{X_1X_2}=\begin{bmatrix}M_{XX}+\left(m_1+m_2\right) & M_{X\Theta}+\left(m_1-m_2\right)\left(y_2-y_1\right)\cos\left(\Theta\right)/2 & M_{X1}\\ M_{X\Theta}+\left(m_1-m_2\right)\left(y_2-y_1\right)\cos\left(\Theta\right)/2 & M_{\Theta\Theta}+\left(m_1+m_2\right)\left(y_2-y_1\right)^2\cos^2\left(\Theta\right)/4 & M_{\Theta1}\\ M_{X1} & M_{\Theta1} & M_{11}\end{bmatrix}=\begin{bmatrix}M'_{XX} & M'_{X\Theta} & M_{X1}\\ M'_{X\Theta} & M'_{\Theta\Theta} & M_{\Theta1}\\ M_{X1} & M_{\Theta1} & M_{11}\end{bmatrix}\tag{4.59}$$

$$C+C_{X_1X_2}=\begin{bmatrix}c_{g1}+c_{g2} & \left(c_{g1}-c_{g2}\right)\left(y_2-y_1\right)\cos\left(\Theta\right)/2 & 0\\ \left(c_{g1}-c_{g2}\right)\left(y_2-y_1\right)\cos\left(\Theta\right)/2 & C_{\Theta\Theta}+\left(c_{g1}+c_{g2}\right)\left(y_2-y_1\right)^2\cos^2\left(\Theta\right)/4 & 0\\ 0 & 0 & C_{11}\end{bmatrix}=\begin{bmatrix}C'_{XX} & C'_{X\Theta} & 0\\ C'_{X\Theta} & C'_{\Theta\Theta} & 0\\ 0 & 0 & C_{11}\end{bmatrix}\tag{4.60}$$

$$K=\begin{bmatrix}0 & 0 & 0\\ 0 & K_{\Theta\Theta} & 0\\ 0 & 0 & K_{11}\end{bmatrix}\tag{4.61}$$

And q and $Q_{X_1X_2}$ are the generalized coordinates (4.62), and the generalized forces (4.63),

$$q=\begin{bmatrix}X\\ \Theta\\ q_1\end{bmatrix};\ Q_{X_1X_2}=\begin{bmatrix}F'_X\\ F'_\Theta\\ Q_1\end{bmatrix}=\begin{bmatrix}\left\{\left(F_1+F_2\right)-\left[c_{c1}\operatorname{sign}\left(\dot{X}_1\right)+c_{c2}\operatorname{sign}\left(\dot{X}_2\right)\right]\right\}\\ \left\{\left(F_1-F_2\right)-\left[c_{c1}\operatorname{sign}\left(\dot{X}_1\right)-c_{c2}\operatorname{sign}\left(\dot{X}_2\right)\right]\right\}\cos\left(\Theta\right)\left(y_2-y_1\right)/2-M_{\Theta Y}\ddot{Y}\\ 0\end{bmatrix}\qquad(4.62),\ (4.63)$$

Now, a physical decoupling basis can be obtained from the motion equations (4.58). To do so, it is assumed that the system is conservative, i.e. no damping, $[C+C_{X_1X_2}]=0$, and no excitation, $\{Q_{X_1X_2}\}=0$. The motion equations become then (4.64),

$$\left[M+M_{X_1X_2}\right]\left\{\ddot{q}\right\}+\left[K\right]\left\{q\right\}=\left\{0\right\}\tag{4.64}$$

We assume that the solution to (4.64) is the harmonic solution (4.65)

$$\left\{q\right\}=\operatorname{Re}\left[B\left\{\phi\right\}e^{i\omega t}\right]\tag{4.65}$$

So that, we have an eigenvalue problem (4.66),

$$\left(\left[K\right]-\omega^2\left[M+M_{X_1X_2}\right]\right)\cdot\left\{\phi\right\}=\left\{0\right\}\tag{4.66}$$

To obtain a non–trivial solution to $\{\phi\}$, the matrix $([K']-\omega^2[M'])$ must be non–invertible. In other words, its determinant must be zero.

$$\det\left(\left[K\right]-\omega^2\left[M+M_{X_1X_2}\right]\right)=0\tag{4.67}$$

The values of ω that make (4.67) valid are the eigenvalues of the system. In our case, we have three DOFs, therefore, we should find three positive eigenvalues

$$\omega_{tr}^2=0;\qquad \omega_{rot}^2=K_{\Theta\Theta}\Big/\Big[M'_{\Theta\Theta}-\Big(M'^2_{X\Theta}\Big/M'_{XX}\Big)\Big];\qquad \omega_1^2=K_{11}\Big/\Big[M_{11}-\Big(M^2_{X1}\Big/M'_{XX}\Big)\Big] \tag{4.68), (4.69), (4.70}$$

The eigenvectors are calculated by replacing each of the found eigenvalues into (4.66). Then, the decoupling basis transformation is given by (4.71),

$$[\Phi]=\begin{bmatrix}1 & \phi_{12} & \phi_{13}\\ 0 & 1 & 0\\ 0 & 0 & 1\end{bmatrix}=\begin{bmatrix}1 & -M'_{X\Theta}\big/M'_{XX} & -M_{X1}\big/M'_{XX}\\ 0 & 1 & 0\\ 0 & 0 & 1\end{bmatrix} \tag{4.71}$$

And the motion equations of the gantry stage on a decoupling basis are defined as (4.72),

$$[\Phi]^T\left[M+M_{X_1X_2}\right][\Phi]\{\ddot{\eta}\}+[\Phi]^T\left[C+C_{X_1X_2}\right][\Phi]\{\dot{\eta}\}+[\Phi]^T[K][\Phi]\{\eta\}=[\Phi]^T\left\{Q_{X_1X_2}\right\} \tag{4.72}$$

Where,

$$[\Phi]^T\left[M+M_{X_1X_2}\right][\Phi]=\begin{bmatrix}M'_{XX} & 0 & 0\\ 0 & M'_{\Theta\Theta}-M'^2_{X\Theta}\big/M'_{XX} & 0\\ 0 & 0 & M_{11}-M^2_{X1}\big/M'_{XX}\end{bmatrix} \tag{4.73}$$

$$[\Phi]^T\left[C+C_{X_1X_2}\right][\Phi]=\begin{bmatrix}C'_{XX} & \times & \times\\ \times & C'_{\Theta\Theta}+M'_{X\Theta}\left(C'_{XX}M'_{X\Theta}-2C'_{X\Theta}M'_{XX}\right)\big/M'^2_{XX} & \times\\ \times & \times & C_{11}+C'_{XX}M^2_{X1}\big/M'^2_{XX}\end{bmatrix} \tag{4.74}$$

$$[\Phi]^T[K][\Phi]=\begin{bmatrix}0 & 0 & 0\\ 0 & K_{\Theta\Theta} & 0\\ 0 & 0 & K_{11}\end{bmatrix};\ \{q\}=\begin{bmatrix}X\\ \Theta\\ q_1\end{bmatrix}=[\Phi]\begin{Bmatrix}\eta_{tr}\\ \eta_{rot}\\ \eta_1\end{Bmatrix}=\begin{bmatrix}\eta_{tr}-\eta_{rot}M'_{X\Theta}\big/M'_{XX}-\eta_1M_{X1}\big/M'_{XX}\\ \eta_{rot}\\ \eta_1\end{bmatrix} \tag{4.75), (4.76}$$

$$[\Phi]^T\left[Q_{X_1X_2}\right]=\begin{bmatrix}F_{\eta_{tr}}\\ F_{\eta_{rot}}\\ F_{\eta_1}\end{bmatrix}=\begin{bmatrix}F'_X\\ F'_\Theta-\left(F'_XM'_{X\Theta}\big/M'_{XX}\right)\\ -F'_XM_{X1}\big/M'_{XX}\end{bmatrix} \tag{4.77}$$

Expressions (4.73) to (4.77) represent the motion of the flexible gantry stage on a physical decoupling basis. The non–diagonal terms of the modal damping matrix are neglected. The modal coordinates η_{tr}, η_{rot}, and η_1 represent the translation of, rotation about, and oscillation of the center of mass of the gantry stage. Given the number and distribution of the system's DOFs, the modes η_{tr} and η_1 cannot be controlled independently as they share the same input, and are, therefore, not linearly independent.

4.2.3.2 Decoupling control

Feedforward control

It has been demonstrated that the modes η_{tr} and η_{rot} cannot be controlled independently given the available DOFs. Thus, we shall look for alternative strategies to control simultaneously the motion and the vibration/oscillation of the gantry machine along the longitudinal/X–direction.

For the deduction of the references (in a pseudo–decoupling basis) of the feed–forward structure, we start from the known references X_{1ref}, X_{2ref} and Y_{ref}.

Note: the Y – axis is not treated in detail since its dynamics is of no influence on the decoupling transformation.

$$\begin{bmatrix}X_1\\ X_2\\ q_1\end{bmatrix}=[T]\begin{bmatrix}X\\ \Theta\\ q_1\end{bmatrix}=[T][\Phi]\begin{bmatrix}\eta_{tr}\\ \eta_{rot}\\ \eta_1\end{bmatrix}\ \therefore\ [T]=\begin{bmatrix}1 & \left(y_2-y_1\right)\big/2 & 0\\ 1 & -\left(y_2-y_1\right)\big/2 & 0\\ 0 & 0 & 1\end{bmatrix};\ [\Phi]=\begin{bmatrix}1 & -M'_{X\Theta}\big/M'_{XX} & -M_{X1}\big/M'_{XX}\\ 0 & 1 & 0\\ 0 & 0 & 1\end{bmatrix} \tag{4.78}$$

Then, we can modify (4.78) in order to obtain the motion references on a pseudo–decoupling basis (4.79)

$$\begin{bmatrix}\eta_{tr\,ref}\\ \eta_{rot\,ref}\\ \eta_{1\,ref}\end{bmatrix}=\left([T][\Phi]\right)^{-1}\begin{bmatrix}X_{1\,ref}\\ X_{2\,ref}\\ q_{1\,ref}\end{bmatrix}=\begin{bmatrix}\left[\frac{1}{2}+\left(\frac{1}{y_2-y_1}\right)\frac{M'_{X\Theta}}{M'_{XX}}\right] & \left[\frac{1}{2}-\left(\frac{1}{y_2-y_1}\right)\frac{M'_{X\Theta}}{M'_{XX}}\right] & \frac{M_{X1}}{M'_{XX}}\\ \left(y_2-y_1\right)^{-1} & -\left(y_2-y_1\right)^{-1} & 0\\ 0 & 0 & 1\end{bmatrix}\begin{bmatrix}X_{1\,ref}\\ X_{2\,ref}\\ q_{1\,ref}\end{bmatrix} \tag{4.79}$$

With the new references defined, we multiply them by the parameters of the system on a pseudo–decoupling basis. This way, the feed–forward decoupled forces (4.80) for a given motion can be calculated,

$$\begin{bmatrix}F_{\eta_{tr}\,ff}\\ F_{\eta_{rot}\,ff}\\ F_{\eta_1 ff}\end{bmatrix}=[\Phi]^T[M][\Phi]\begin{bmatrix}\ddot{\eta}_{tr\,ref}\\ \ddot{\eta}_{rot\,ref}\\ \ddot{\eta}_{1\,ref}\end{bmatrix}+[\Phi]^T[C][\Phi]\begin{bmatrix}\dot{\eta}_{tr\,ref}\\ \dot{\eta}_{rot\,ref}\\ \dot{\eta}_{1\,ref}\end{bmatrix}+[\Phi]^T[K][\Phi]\begin{bmatrix}\eta_{tr\,ref}\\ \eta_{rot\,ref}\\ \eta_{1\,ref}\end{bmatrix} \tag{4.80}$$

Finally, we transform the decoupled reference forces to the machine reference frame. This is done as follows,

$$\begin{bmatrix}F_X\\ F_\Theta\\ Q_1\end{bmatrix}=[P]\begin{bmatrix}F_1\\ F_2\\ 0\end{bmatrix}-\begin{bmatrix}0\\ M_{\Theta Y}\\ 0\end{bmatrix}\ddot{Y}\quad\therefore\quad[P]=\begin{bmatrix}1 & 1 & 0\\ \left(y_2-y_1\right)/2 & -\left(y_2-y_1\right)/2 & 0\\ 0 & 0 & 1\end{bmatrix} \tag{4.81}$$

The transpose of the pseudo–decoupling transformation, $[\Phi]^T$, times the force vector on the reference frame X, Θ, and q_1 (4.81) gives the expression of the decoupled forces,

$$\begin{bmatrix}F_{\eta_{tr}\,ff}\\ F_{\eta_{rot}\,ff}\\ F_{\eta_1 ff}\end{bmatrix}=[\Phi]^T\begin{bmatrix}F_{X\,ff}\\ F_{\Theta ff}\\ Q_{1ff}\end{bmatrix}=[\Phi]^T[P]\begin{bmatrix}F_{1ff}\\ F_{2ff}\\ Q_{1ff}\end{bmatrix}-[\Phi]^T\begin{bmatrix}0\\ M_{\Theta Y}\\ 0\end{bmatrix}\ddot{Y}_{ref} \tag{4.82}$$

From (4.82), we can extract the feed–forward forces on the machine reference frame; i.e. F_{1ff} and F_{2ff}, in terms of the decoupled forces,

$$\begin{bmatrix}F_{1ff}\\ F_{2ff}\\ Q_{1ff}\end{bmatrix}=\left([\Phi]^T[P]\right)^{-1}\left(\begin{bmatrix}F_{\eta_{tr}\,ff}\\ F_{\eta_{rot}\,ff}\\ F_{\eta_1 ff}\end{bmatrix}+[\Phi]^T\begin{bmatrix}0\\ M_{\Theta Y}\\ 0\end{bmatrix}\ddot{Y}_{ref}\right)=\begin{bmatrix}\left(\frac{1}{y_2-y_1}\right)\left\{\left[\left(\frac{y_2-y_1}{2}\right)+\frac{M'_{X\Theta}}{M'_{XX}}\right]F_{\eta_{tr}\,ff}+F_{\eta_{rot}\,ff}+M_{\Theta Y}\ddot{Y}_{ref}\right\}\\ \left(\frac{1}{y_2-y_1}\right)\left\{\left[\left(\frac{y_2-y_1}{2}\right)-\frac{M'_{X\Theta}}{M'_{XX}}\right]F_{\eta_{tr}\,ff}-F_{\eta_{rot}\,ff}-M_{\Theta Y}\ddot{Y}_{ref}\right\}\\ F_{\eta_1 ff}+F_{\eta_{tr}\,ff}\frac{M_{X1}}{M'_{XX}}\end{bmatrix}\quad\therefore\quad F_{\eta_1 ff}=-F_{\eta_{tr}\,ff}\frac{M_{X1}}{M'_{XX}} \tag{4.83}$$

Once again, expression (4.83) confirms that indeed there is no possible way of acting directly on the flexible modes given the number and distribution of available DOFs.

Feedback control

An advantage of the decoupling basis approach is that it allows easily tuning the feedback decoupled controllers based on the already known independent axis control parameters. This goes as follows:

The decoupling forces $F_{\eta tr}$ and $F_{\eta rot}$ can be expressed as a linear combination of the forces generated by actuators X_1 and X_2 and the perturbation induced by the dynamics of the Y – axis, as in (4.84)

$$\begin{bmatrix}F_{\eta_{tr}}\\ F_{\eta_{rot}}\end{bmatrix}=\begin{bmatrix}F_1+F_2\\ \left(F_1-F_2\right)\left[\left(y_2-y_1\right)/2\right]-M_{\Theta Y}\ddot{Y}-\left(F_1+F_2\right)M'_{X\Theta}/M'_{XX}\end{bmatrix}\quad\therefore\quad\begin{matrix}F_{\eta_{tr}}=\varepsilon_{\eta_{tr}}C_{\eta_{tr}}\\ F_{\eta_{rot}}=\varepsilon_{\eta_{rot}}C_{\eta_{rot}}\end{matrix};\quad\begin{matrix}F_1=\varepsilon_1 C_1\\ F_2=\varepsilon_2 C_2\end{matrix} \tag{4.84}$$

We know that, on a control scheme, the generated reference forces are the product of the error and the value of the controllers. Therefore, it is possible to express the parameters of the decoupling basis controllers in terms of the independent ones, as in (4.85)

$$\begin{bmatrix} C_{\eta_{tr}} \\ C_{\eta_{rot}} \end{bmatrix} = \begin{bmatrix} \dfrac{\varepsilon_1 C_1 + \varepsilon_2 C_2}{\varepsilon_{\eta_{tr}}} \\ \dfrac{\left(\varepsilon_1 C_1 - \varepsilon_2 C_2\right)\left[\left(y_2 - y_1\right)/2\right] - M_{\Theta Y}\ddot{Y} - \left(\varepsilon_1 C_1 + \varepsilon_2 C_2\right) M'_{X\Theta}/M'_{XX}}{\varepsilon_{\eta_{rot}}} \end{bmatrix} \therefore \begin{matrix} \varepsilon_{\eta_{tr}} = \left[\dfrac{1}{2} + \left(\dfrac{1}{y_2 - y_1}\right)\dfrac{M'_{X\Theta}}{M'_{XX}}\right]\varepsilon_1 + \left[\dfrac{1}{2} - \left(\dfrac{1}{y_2 - y_1}\right)\dfrac{M'_{X\Theta}}{M'_{XX}}\right]\varepsilon_2 \\ \varepsilon_{\eta_{rot}} = \dfrac{\varepsilon_1 - \varepsilon_2}{y_2 - y_1} \end{matrix} \tag{4.85}$$

To find the value of the decoupling basis controllers, we apply the following simplifying hypotheses:

- The values associated to the asymmetry of the system, i.e. $M'_{X\Theta}/M'_{XX}$, are compensated by the feedforward control. Therefore, $M'_{X\Theta}/M'_{XX} = 0$.
- The perturbation associated to the dynamics of the payload is also compensated by the feedforward control. Thus, $M_{\Theta Y}\ddot{Y} = 0$.
- The values of independent controllers C_1 and C_2 are equal, i.e. $C_1 = C_2$

Finally, the values of the decoupling basis controllers are defined by,

$$\begin{bmatrix} C_{\eta_{tr}} \\ C_{\eta_{rot}} \end{bmatrix} = \begin{bmatrix} 2C_1 \\ 2\left[\left(y_2 - y_1\right)/2\right]^2 C_1 \end{bmatrix} \tag{4.86}$$

4.2.3.3 Experimental Validation

To this point, we have seen that the flexible mode(s) are not directly controllable given the number and distribution of the gantry stage's DOFs. Despite this, the proposed methodology allows identifying the interaction between the available DOFs, i.e. the actuators X_1 and X_2, and the flexible modes. This makes possible to control the flexible modes indirectly using trajectory planning techniques.

On **Figures 4 – 30** and **4 – 31**, for the same motion, with and without jerk time, we compare the industrial independent axis control (dash blue) and the proposed decoupling basis control (solid red). Because of the very flexible beam, there is virtually no coupling between actuators X_1 and X_2. Hence, independent axis and decoupling basis controls shall perform the same. Yet, in terms of mean tracking error, the decoupling control performs about 50% better than the independent axis control. This is because of the feedforward control structure which is derived and tuned using the proposed methodology. If taken away, the performance is the same in both cases.

As it can be appreciated on **Figure 4 – 31**, a well tuned jerk time provides a significant improvement on the settling time of the point–tool.

One of the biggest challenges of the flexible gantry stage is that its vibration eigenfrequencies vary non–linearly in function of the payload's position. Because of this, the use of single jerk trajectory planners may be an issue. To this purpose and since we don't have a prototype of a flexible gantry stage with a functional Y–axis, on the next section; we propose, on simulation, a point–to–point motion of the flexible gantry using a double jerk trajectory planner which will be compared to the positioning performances provided by a single jerk one. For the double jerk trajectory planner, the initial jerk time is those corresponding to starting configuration; the second jerk is those corresponding to the final configuration. For the single jerk trajectory planner, the jerk time is those corresponding to the final configuration.

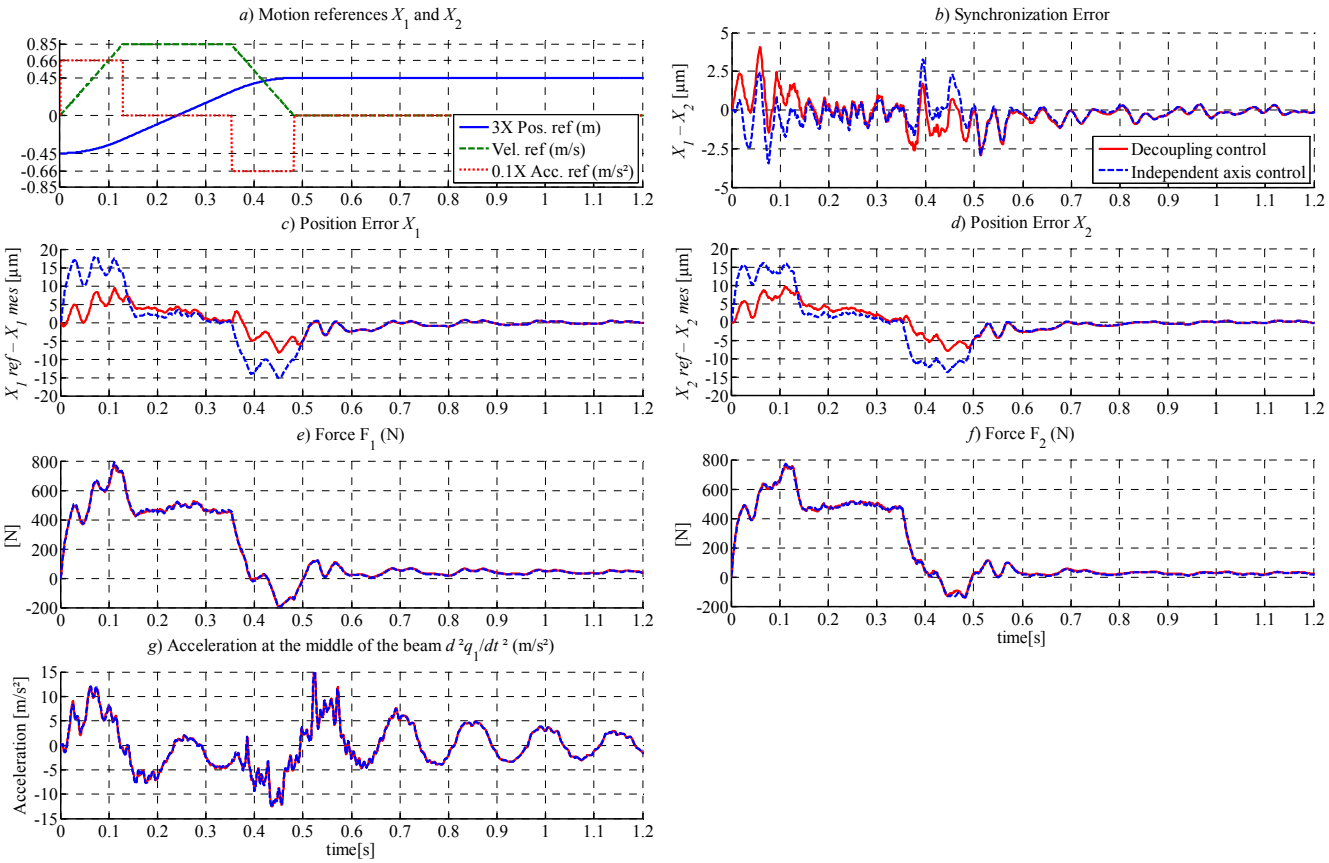

Figure 4 – 30 : *Independent Axis vs. Decoupling Basis Control. Acceleration* 6.6 m/s², *Velocity* 0.85 m/s, *position* –0.15 m to +0.15 m. $Y = 0.3$ m.

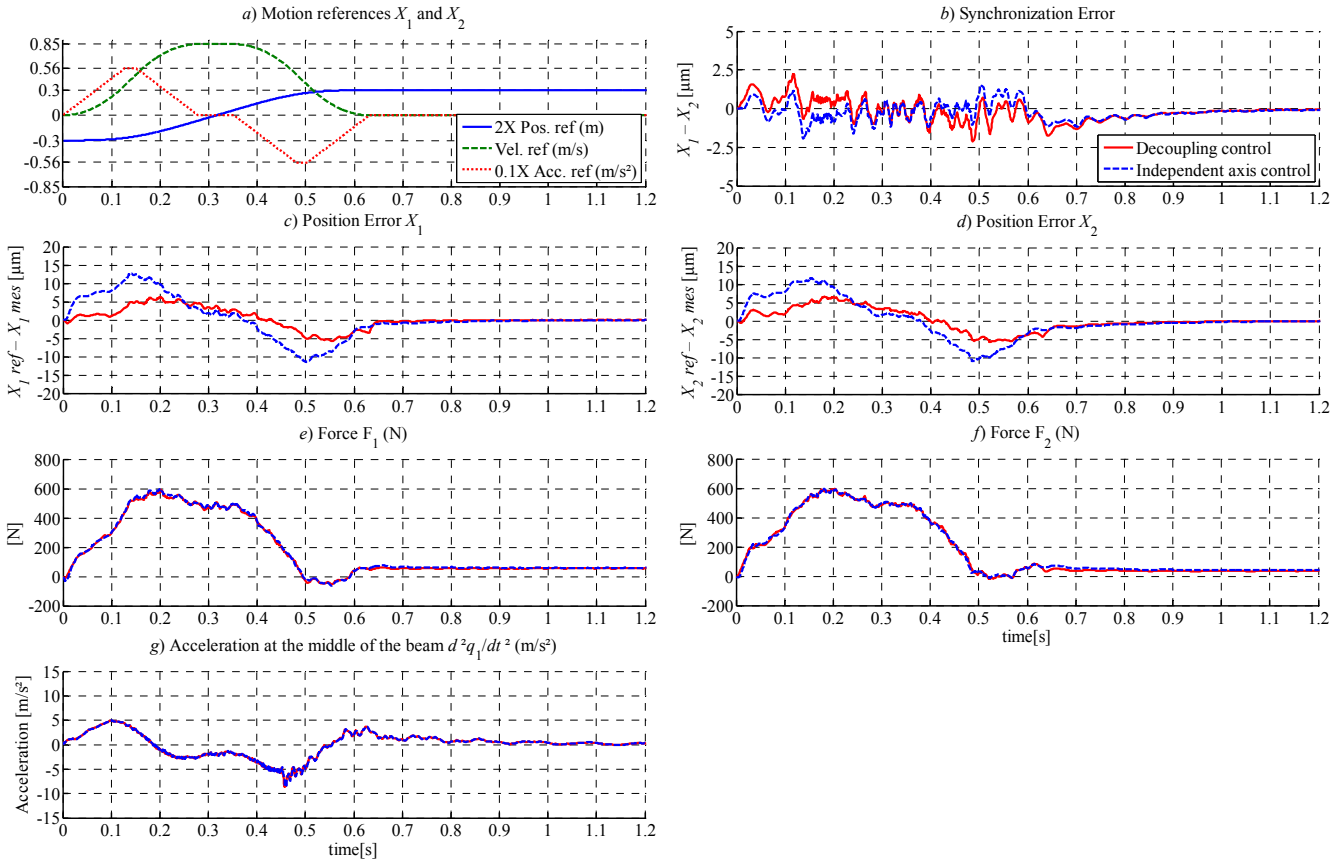

Figure 4 – 31 : *Independent Axis vs. Decoupling Basis Control with Jerk. Acceleration* 6.6 m/s², *Velocity* 0.85 m/s, *position* –0.15 m to +0.15 m. $Y = 0.3$ m.

4.2.4 Improving the positioning performance of the flexible gantry stage: Trajectory planning techniques

As we know, it is not possible to act directly on the flexible mode(s) given the number and distribution of the system's DOFs without degrading the positioning performance of the translation rigid mode and vice versa. Nevertheless, trajectory planning techniques allow minimizing the vibration(s) associated to flexible mode(s) while guaranteeing the positioning performance of the translation rigid mode. The principle is simple, it consists in eliminating the vibrations that may appear during and after the motion by generating a counter vibration by "hitting" the system strategically (Singhose, 1997) for Bang–bang and input–shaping techniques, see **Figure 4 – 32**, Or by minimizing the derivatives of the position for smooth motion planning techniques (Colas, 2006).

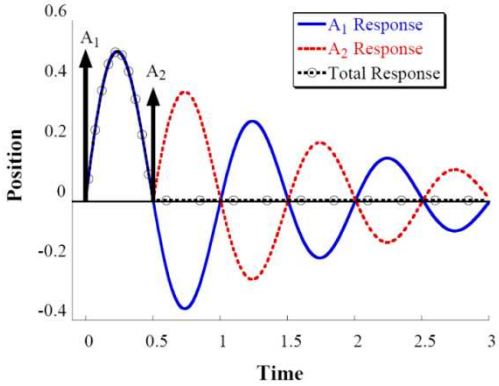

Figure 4 – 32 : *Two impulses input shaping command* **(Singhose, 1997)**. *The* A_2 *response cancels the vibration of the* A_1 *response.*

By the moment, we will interest ourselves to the bang–bang jerk techniques (Béarée, 2005) since industrially, they are widely used. The difficulty in our case is that the gantry stage is a system of variable configuration, which means that the eigenfrequencies of the flexible modes are variable as well. In consequence, classical bang–bang jerk planners are inadequate since they generate the same jerk time at both the beginning and the end of the motion. To overcome this drawback, a trajectory planner capable of generating two different jerk times is necessary.

In practical terms, the motion references of a variable jerk are presented on **Figure 4 – 33**,

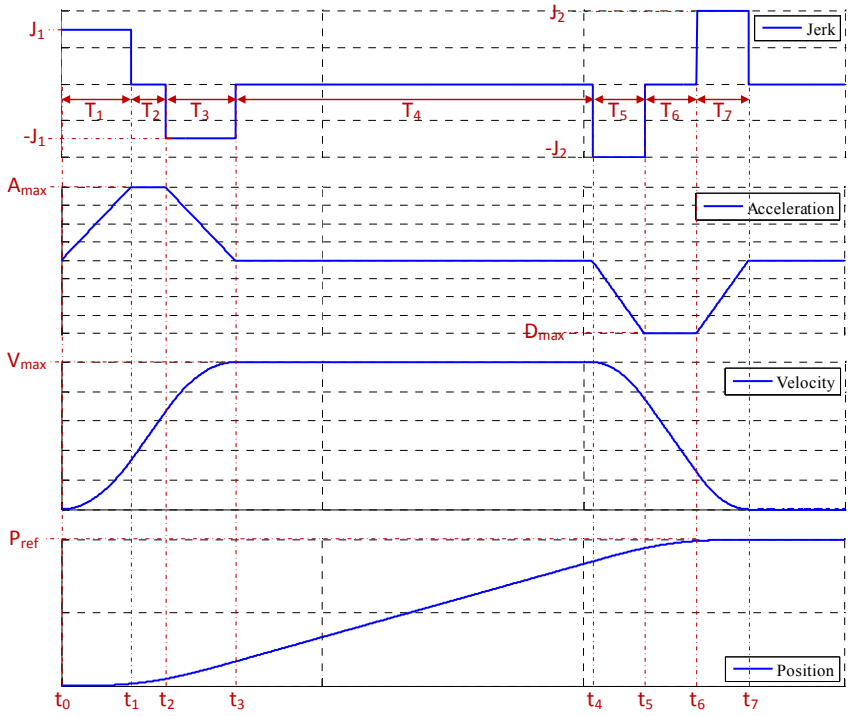

Figure 4 – 33 : *Variable Jerk motion Law*

The equation defining the variable jerk references is (4.87),

$$Jerk \rightarrow \dddot{X}(t) = J_1\left[u(t-t_0) - u(t-t_1) - u(t-t_2) + u(t-t_3)\right] - J_2\left[u(t-t_4) - u(t-t_5) - u(t-t_6) + u(t-t_7)\right] \tag{4.87}$$

Then, by successive integration, it is possible to find the acceleration (4.88), velocity (4.89), and position (4.90) references:

$$Acceleration \rightarrow \ddot{X}(t) = \begin{Bmatrix} J_1\left[(t-t_0)u(t-t_0) - (t-t_1)u(t-t_1) - (t-t_2)u(t-t_2) + (t-t_3)u(t-t_3)\right] - \\ J_2\left[(t-t_4)u(t-t_4) - (t-t_5)u(t-t_5) - (t-t_6)u(t-t_6) + (t-t_7)u(t-t_7)\right] \end{Bmatrix} \tag{4.88}$$

$$Velocity \rightarrow \dot{X}(t) = \frac{1}{2}\begin{Bmatrix} J_1\left[(t-t_0)^2 u(t-t_0) - (t-t_1)^2 u(t-t_1) - (t-t_2)^2 u(t-t_2) + (t-t_3)^2 u(t-t_3)\right] - \\ J_2\left[(t-t_4)^2 u(t-t_4) - (t-t_5)^2 u(t-t_5) - (t-t_6)^2 u(t-t_6) + (t-t_7)^2 u(t-t_7)\right] \end{Bmatrix} \tag{4.89}$$

$$Position \rightarrow X(t) = \frac{1}{6}\begin{Bmatrix} J_1\left[(t-t_0)^3 u(t-t_0) - (t-t_1)^3 u(t-t_1) - (t-t_2)^3 u(t-t_2) + (t-t_3)^3 u(t-t_3)\right] - \\ J_2\left[(t-t_4)^3 u(t-t_4) - (t-t_5)^3 u(t-t_5) - (t-t_6)^3 u(t-t_6) + (t-t_7)^3 u(t-t_7)\right] \end{Bmatrix} \tag{4.90}$$

Now, what we want to do, based on expressions (4.87) to (4.90), is to determine periods T_2, T_4 ,T_6 and Jerk amplitudes J_1 and J_2 in function of constraints: initial ($T_1 = T_3$) and final ($T_5 = T_7$) jerk time; maximum acceleration A_{max}, deceleration D_{max}, velocity V_{max}; and reference position P_{ref}.

To do so, we evaluate (4.87) to (4.90) at each instant t_0 to t_7 in order to find the unknown values T_2, T_4, T_6, J_1 and J_2,

For $t = t_0$,

$$\dddot{X}(t_0) = J_1; \quad \ddot{X}(t_0) = 0; \quad \dot{X}(t_0) = 0; \quad X(t_0) = 0 \tag{4.91}$$

For $t = t_1$,

$$\dddot{X}(t_1) = 0; \quad \ddot{X}(t_1) = J_1 T_1 = A_{\max}; \quad \dot{X}(t_1) = J_1 T_1^2/2; \quad X(t_1) = J_1 T_1^3/6 \tag{4.92}$$

For $t = t_2$,

$$\dddot{X}(t_2) = -J_1; \quad \ddot{X}(t_2) = J_1 T_1; \quad \dot{X}(t_2) = J_1 T_1 (T_1 + 2T_2)/2; \quad X(t_2) = J_1 T_1 (T_1^2 + 3T_1 T_2 + 3T_2^2)/6 \tag{4.93}$$

For $t = t_3$,

$$\dddot{X}(t_3) = 0; \quad \ddot{X}(t_3) = 0; \quad \dot{X}(t_3) = J_1 T_3 (T_2 + T_3) = V_{\max}; \quad X(t_3) = J_1 T_3 (T_2^2 + 3T_2 T_3 + 2T_3^2)/2 \tag{4.94}$$

For $t = t_4$,

$$\dddot{X}(t_4) = -J_2; \quad \ddot{X}(t_4) = 0; \quad \dot{X}(t_4) = J_1 T_3 (T_2 + T_3) = V_{\max}; \quad X(t_4) = J_1 T_3 (T_2 + T_3)\left[T_2 + 2(T_3 + T_4)\right] \tag{4.95}$$

For $t = t_5$,

$$\dddot{X}(t_5) = 0; \ \ddot{X}(t_5) = -J_2 T_5 = -D_{\max}; \ \dot{X}(t_5) = J_1 T_3 (T_2 + T_3) - J_2 T_5^2/2; \ X(t_5) = \left\{J_1 T_3 (T_2 + T_3)\left[T_2 + 2(T_3 + T_4 + T_5)\right]/2\right\} - (J_2 T_5^3/6) \tag{4.96}$$

For $t = t_6$,

$$\begin{array}{ll} \dddot{X}(t_6) = J_2; & \ddot{X}(t_6) = -J_2 T_5; \\ \dot{X}(t_6) = J_1 T_3 (T_2 + T_3) - \left[J_2 T_5 (T_5 + 2T_6)/2\right]; & X(t_6) = \left\{J_1 T_3 (T_2 + T_3)\left[T_2 + 2(T_3 + T_4 + T_5 + T_6)\right]/2\right\} - \left[J_2 T_5 (T_5^2 + 3T_5 T_6 + 3T_6^2)/6\right]; \end{array} \tag{4.97}$$

For $t = t_7$,

$$\begin{array}{ll} \dddot{X}(t_7) = 0; & \ddot{X}(t_7) = 0; \\ \dot{X}(t_7) = J_1 T_3 (T_2 + T_3) - J_2 T_7 (T_6 + T_7) = 0; & X(t_7) = \left\{J_1 T_3 (T_2 + T_3)\left[T_2 + 2(T_3 + T_4 + T_6 + 2T_7)\right] - J_2 T_7 (T_6^2 + 3T_6 T_7 + 2T_7^2)\right\}/2 = P_{ref} \end{array} \tag{4.98}$$

From (4.92) and (4.96) is possible to calculate, respectively, the jerk amplitudes J_1 (4.99) and J_2 (4.100),

$$J_1 = A_{\max} / T_1 \; ; \qquad J_2 = D_{\max} / T_5 \qquad (4.99), (4.100)$$

In the same manner, T_2 (4.101) and T_6 (4.102) can be calculated, respectively, from (4.94) and (4.98)

$$T_2 = \frac{V_{\max}}{J_1 T_3} - T_3 \rightarrow \; T_2 = \frac{V_{\max}}{A_{\max}} - \frac{A_{\max}}{J_1} \; ; \qquad T_6 = \frac{V_{\max}}{J_2 T_7} - T_7 \; \rightarrow \; T_6 = \frac{V_{max}}{D_{\max}} - \frac{D_{\max}}{J_2} \qquad (4.101), (4.102)$$

If we want T_2 and T_6 equal to zero (optimal time for a bang–bang jerk motion), then $A_{\max}$ and $D_{\max}$ must be equal, respectively, to (4.103) and (4.104)

$$A_{\max} = V_{\max} / T_3 \qquad D_{\max} = V_{\max} / T_7 \qquad (4.103), (4.104)$$

Finally, T_4 is isolated from the position expression in (4.98)

$$T_4 = \frac{2P_{ref} + \overbrace{J_2 T_7 \left(T_6 + T_7\right)}^{V_{\max}} \left(T_6 + 2T_7\right) - \overbrace{J_1 T_3 \left(T_2 + T_3\right)}^{V_{\max}} \left[T_2 + 2\left(T_3 + T_6 + 2T_7\right)\right]}{2\underbrace{J_1 T_3 \left(T_2 + T_3\right)}_{V_{\max}}} \; \therefore \; J_1 T_3 \left(T_2 + T_3\right) = J_2 T_7 \left(T_6 + T_7\right) = V_{\max}$$

And written in terms of $A_{\max}$, $D_{\max}$, $V_{\max}$, J_1 and J_2

$$T_4 = \frac{P_{ref}}{V_{\max}} - \frac{1}{2}\left(\frac{V_{\max}}{A_{\max}} + \frac{V_{\max}}{D_{\max}} + \frac{A_{\max}}{J_1} + \frac{D_{\max}}{J_2}\right) \qquad (4.105)$$

The total duration of the motion is given by (4.106),

$$T = \sum_{i=0}^{7} T_i = \frac{P_{ref}}{V_{\max}} + \frac{1}{2}\left(\frac{V_{\max}}{A_{\max}} + \frac{V_{\max}}{D_{\max}} + \frac{A_{\max}}{J_1} + \frac{D_{\max}}{J_2}\right) \qquad (4.106)$$

4.2.4.1 Simulation results

The proposed double jerk and classical single jerk approaches are compared. The former uses the jerk time corresponding to the final configuration; the latter, as aforementioned, takes into account the jerk times of both the initial and final configurations just as well as it calculates the optimal values of $A_{\max}$ and $D_{\max}$ in order to execute the motion in minimum time. The used control scheme is the one proposed on (§ 3.2.1.1).

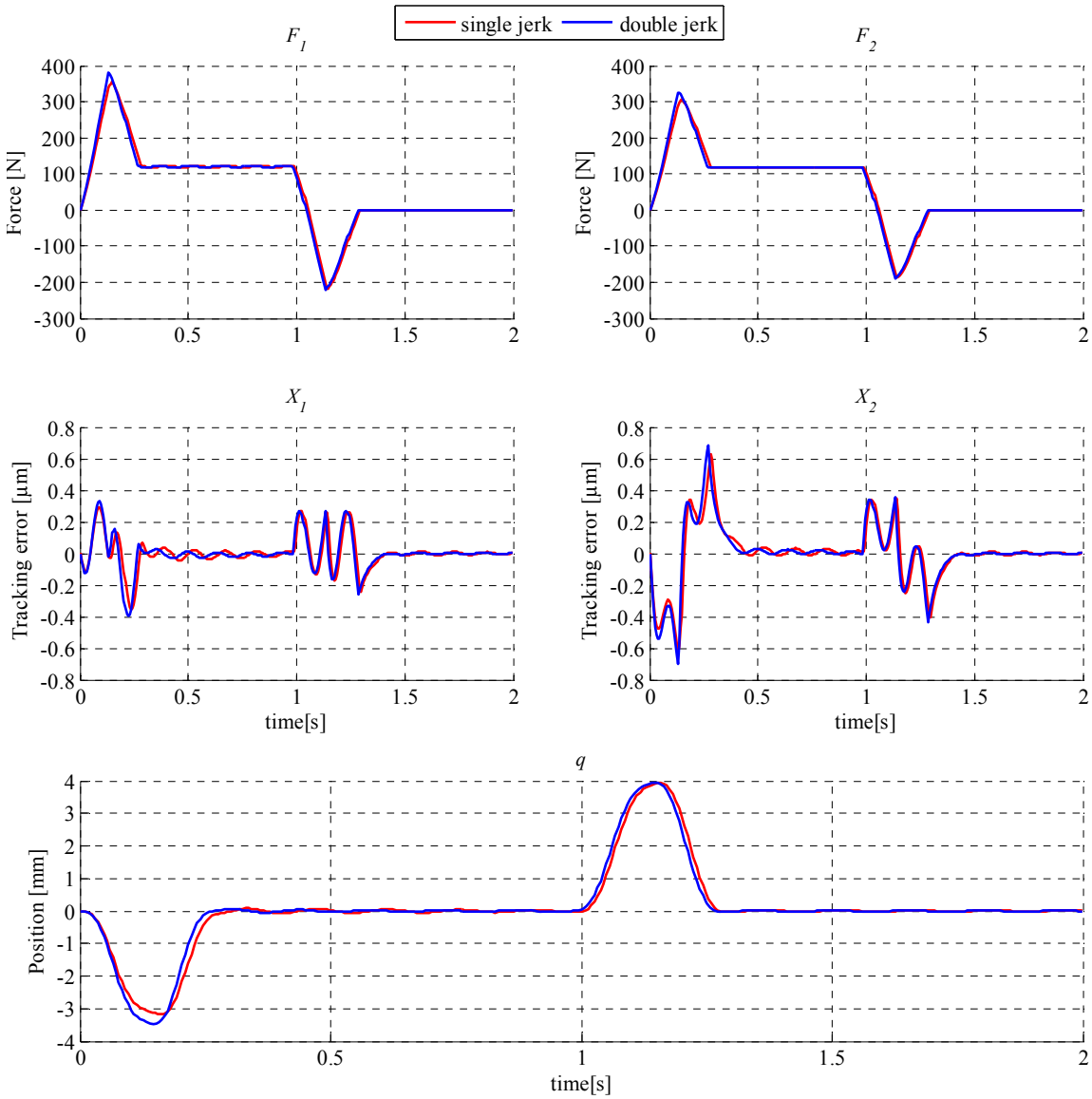

Figure 4 – 34 : *Single Jerk vs. double jerk trajectory planner. Simulation results for*: *Acceleration max* 6.6 m/s², *Velocity* 1.00 m/s, *Position* $X = 0.0$ to $+1.0$ m. *Position* $Y = -1.1$ to -0.3 m. *Top*, *Forces* F_1 and F_2 , *middle*, *Tracking error of actuators* X_1 *and* X_2, *bottom*, *Displacement* q_1 *at the middle of the cross–arm.*

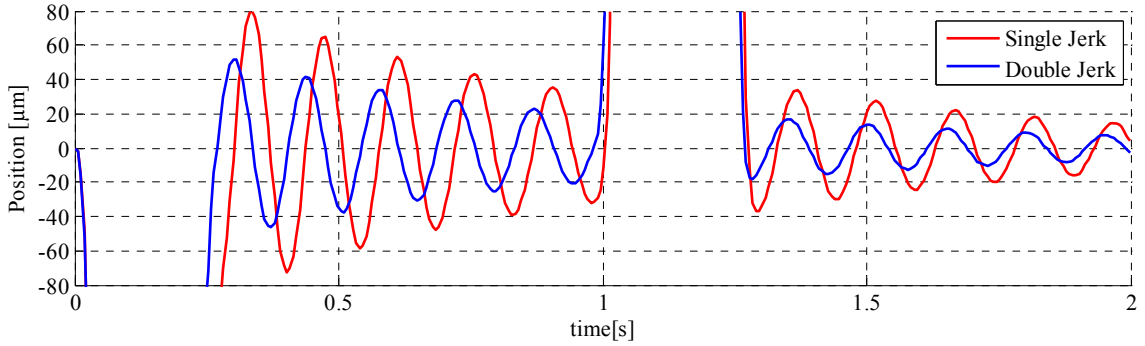

Figure 4 – 35 : *Single Jerk vs. double jerk trajectory planner. Zoom on the displacement* q_1 *at the middle of the cross–arm.*

4.2.5 Comparison between the rigid and the flexible gantry

A principal objective of this research project is to prove that it is possible to build lighter gantry stages capable of attaining similar positioning performances than its stiffer counterparts thanks to improved control algorithms. To this purpose, we compare, on **Figure 4 – 36**, for the same motion, the rigid gantry "Andromeda", presented on **Figure 4 – 9**, and the flexible gantry, presented on **Figure 4 – 19**. Both systems are controlled using decoupling basis control.

As it can be appreciated on **Figure 4 – 36** (b), (c), and (d); for the rigid gantry (dash blue), its positioning performance is degraded due to the oscillation of the rigid cross–arm with respect to actuators X_1 and X_2, see (§ 4.1.5.1). This phenomenon is less pronounced on the flexible gantry (solid red) thanks to its lighter cross–arm. Concerning the energy consumption of actuators X_1 and X_2, see **Figure 4 – 36** (e) and (f), it can be appreciated that, for the flexible gantry, it is reduced by half during the acceleration cycles. For the constant velocity cycle located between 0.2 and 0.4 seconds; the energy consumption is the same providing that actuators X_1 and X_2 are the same for both the flexible and the rigid gantry stage.

Concerning the oscillations of the cross–arm, we have measured the acceleration $\ddot{q}_1$ at the middle of the cross–arm. As it can be appreciated on **Figure 4 – 36** (g), during the motion, the measured acceleration for both systems is equivalent. At the end of the motion, see **Figure 4 – 36** (g), there is a residual oscillation of the cross–arm that appears. This is due to the estimation of the jerk time, which is done based upon the identified parameters of the flexible gantry and it is not exact. This residual oscillation can be eliminated by increasing, for example, the stiffness of the flexible plate joint connecting the cross–arm to actuator X_1.

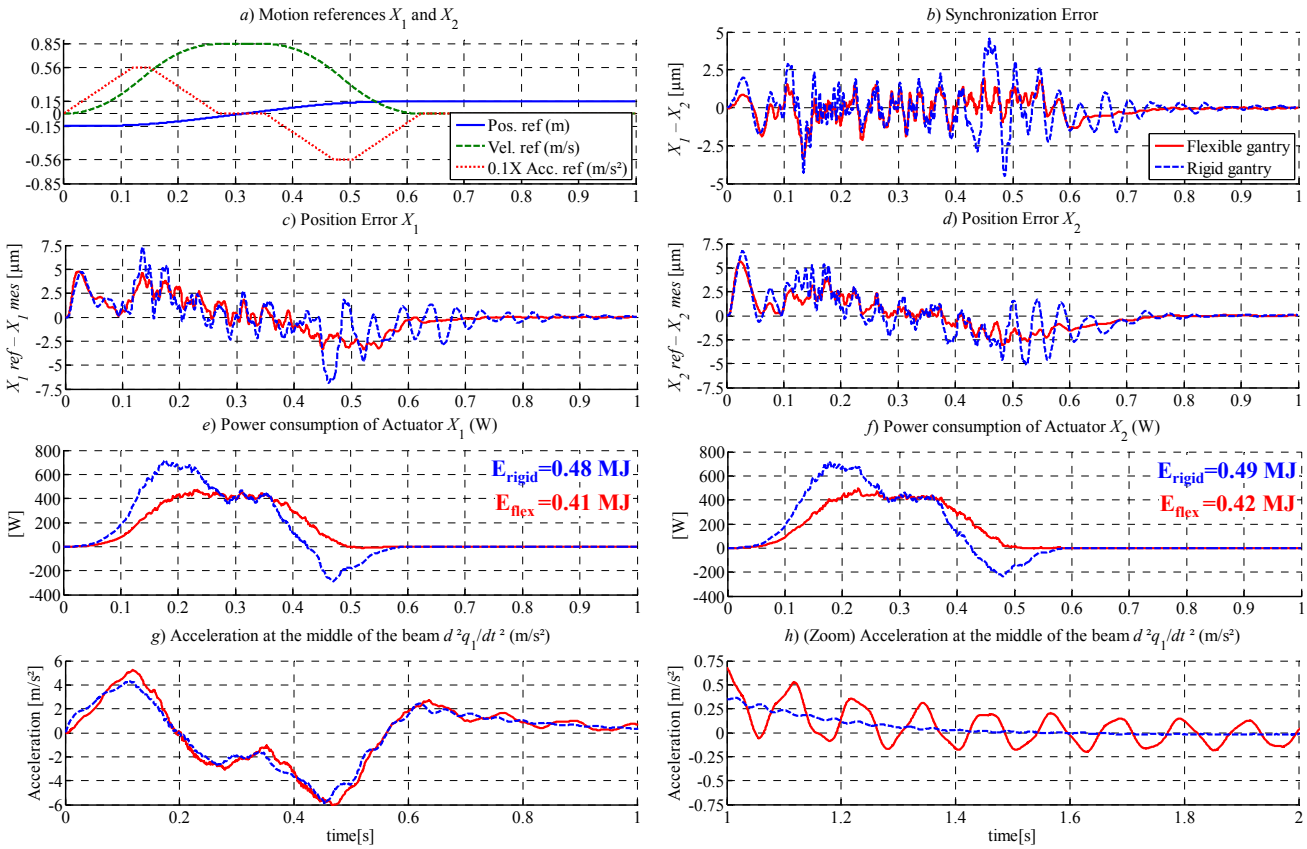

Figure 4 – 36 : *Rigid vs. flexible gantry. Decoupling Basis Control with Jerk; Acceleration* 5.6 m/s², *Velocity* 0.85 m/s, *position* –0.15 m to +0.15 m. $Y = 0.3$ m.

4.3 Conclusion

To validate experimentally the proposed methodology for modeling and controlling gantry stages, we confronted it to three different types of gantry stages; two rigid and one flexible.

The first section (§ 4.1) is devoted to the application of the proposed methodology to two different types of rigid gantry stages.

The first rigid gantry stage that was used, was the same used by J. Gomand on its thesis (Gomand, 2008). As a recall, based on a physical model of the gantry stage (represented using the COG formalism), Gomand deduced a control structure allowing a feedforward compensation of the coupling between the parallel actuators; leading to an improved positioning performance with respect to the independent axis control scheme. Gomand, however, didn't take into account the dynamics of the payload on the proposed control structure; leading to less important improvements regarding path–tracking applications.

Concerning rigid systems, the methodology proposed in this thesis allows going one step beyond by taking into account not only the effects of the mechanical coupling between the parallel actuators but also the effects of the payload dynamics on the positioning performance of the gantry stage. The proposed decoupling control allows handling each control objective independently. The motion of the gantry stage as a whole is handled by a pair of independent feedback–feedforward controllers; the feedforward handles the coarse positioning while the feedback handles the fine positioning. The synchronization (or the rotation) is also handled by a pair of single feedback–feedforward controllers; the feedforward control handles the changes on the mass distribution due to the motion of the payload while the feedback handles the residual coupling (due to un–modeled phenomena and/or uncertainties on the parameters of the model). Finally, the motion of the payload is also handled by a single controller and the effect of its dynamics on the overall system performance is rejected by feedforward compensation.

The main contribution of the proposed methodology is that by using a systematic approach, we are capable of finding a conjunction of control actions allowing an improved management of the system's DOFs (the actuators). This improvement can be particularly appreciated on the path–tracking tests, where the effects of the actuator coupling and the dynamics of the payload are almost totally removed with respect to both the control structure proposed by Gomand and by the independent axis control. As commented; the remaining error is repeatable and is principally due to the detent forces of the actuators. Phenomena that we did not take into consideration as we were most interested on the interaction between the elements constituting the gantry stage and not in phenomena associated to the actuator itself.

The second type of gantry stage that was used was a large–size gantry stage. As it has been shown, the search for a stiffer – and consequently heavier – cross–arm, leads to the appearance of unwanted flexibilities of the mechanical joints connecting it to the parallel actuators. A contribution of the proposed methodology is that it was possible to quickly point out this drawback and associate it to the mechanical joints through the modeling. The control structure that is derived from the proposed methodology provides an improvement of the system performances with respect to the initial industrial controllers. The remaining error is mostly due to the detent forces of the actuators, the pitch motion of the cross–arm (it can be reduced by reinforcing the joints), and the static friction of the actuators. A compensation of the static friction results in a further improvement in the positioning performance for path–tracking applications.

The second part of the chapter (§ 4.2) is dedicated to the main interest of this thesis. The modeling and the control of a gantry stage with a flexible cross–arm.

We have shown that it is not possible to act directly on the flexible modes given the number and distribution of the system's DOFs (or the actuators). We can however act indirectly on the flexible modes via trajectory planning techniques. A contribution of the proposed methodology is that we

are capable of estimating, using the physical model, the jerk times (assuming a bang–bang compensation) necessary to minimize the excitation of the flexible modes during and after the motion, thus providing a reduction of the settling time for each operation.

To sum up, we have validated experimentally the proposed methodology on three different types of gantry stages. However, we do not dare to claim that the method is valid to all gantry machines because, as it was well put in evidence by the large size gantry stage, there are always un–modeled phenomena that may be well specific to the system under study. Nevertheless, the understanding of the gantry dynamics plus the inversion based control methodology, provided by the proposed methodology, shall allow an easy adaptation to each case.

5. Conclusions Générales et Perspectives

Cette thèse avait deux objectifs intimement liés:

- Un objectif industriel consistant à développer des lois de commande adaptées à des applications de type suivi de trajectoire pour des axes en gantry bi–actionnés de grande taille dont la flexibilité du bras transversal dit « en gantry » ne peut plus être ignorée.
- Un objectif scientifique consistant à développer un outil méthodologique de modélisation et de commande pour des systèmes de positionnement multi–actionnés de type axe en gantry. Le but étant de rendre le travail réalisé dans cette thèse applicable au plus grand nombre d'axes en gantry ainsi que de pouvoir créer un échange entre les concepteurs des structures électromécaniques et ceux des systèmes de commande.

Ces objectifs, essentiellement tournés vers l'amélioration des performances dynamiques de positionnement des axes multi-actionnés, sont en adéquation avec le projet du $7^{ième}$ Programme–Cadre de Recherche et Développement (PCRD) Européen qui fixe comme objectif une réduction des temps de cycles de production d'un facteur 3 à 5 et une réduction de 30 à 40 % de la consommation énergétique.

5.1 Synthèse des travaux réalisés et résultats marquants

Le premier chapitre de ce mémoire avait pour objectif de préciser le contexte de l'étude. Il décrit l'évolution des axes en gantry dans l'industrie et leurs problématiques spécifiques selon le degré de rigidité du bras transversal dit en « gantry » et des liaisons l'attachant aux actionneurs permettant de le déplacer le long de l'espace de travail.

Ces problématiques dégradant les performances en positionnement de l'axe en gantry peuvent se classer en deux catégories :

- Perturbations induites par le couplage entre les actionneurs portant le bras transversal
- Perturbations induites par l'excitation de la flexibilité structurelle du bras transversal lors de déplacements à grande dynamique.

Dans le deuxième chapitre nous avons présenté la façon dont la solution à ces problématiques est abordée dans la littérature. Trois types de commande sont essentiellement trouvés :

1. Commandes à axes indépendants
2. Commandes synchronisantes
3. Commandes par compensation de couplage.

Pour ces trois types de commande, le critère d'évaluation de la performance de positionnement de l'axe en gantry est la synchronisation entre les actionneurs qui portent le bras transversal.

La commande à axes indépendants est la commande industrielle de base. Chaque actionneur est contrôlé indépendamment l'un de l'autre et le couplage entre les actionneurs déplaçant le bras transversal est ignoré. Les asservissements indépendants sont réglés « au mieux » afin d'obtenir la meilleure dynamique possible tout en minimisant la désynchronisation entre les axes parallèles. Les oscillations du bras transversal sont évitées par une solution mécanique qui consiste à fabriquer un bras très rigide (et lourd) en dépit du coût énergétique que son déplacement implique.

Les commandes synchronisantes sont basées sur la commande à axes indépendants et consistent à insérer un troisième asservissement, qui agit entre les asservissements indépendants des actionneurs portant le bras transversal afin de forcer leur synchronisation. Le problème de ce type de commande est que l'on cherche à contrôler indépendamment une combinaison de variables (associées aux actionneurs portant le bras transversal) qui sont déjà contrôlées par des contrôleurs indépendants.

Les commandes par compensation de couplage cherchent à anticiper les effets du couplage afin d'alléger la tâche des contrôleurs indépendants. L'inconvénient majeur de ces commandes est que le couplage est considéré comme invariant et présenté d'une façon difficilement généralisable à des paramètres physiques de la machine.

Dans la mesure où elles exécutent l'objectif établi, les commandes citées ci-dessus sont, en effet, très performantes. Nonobstant, des critères de performance plus subjectifs (tels que la facilité d'implémentation, la simplicité algorithmique, ou même la consommation énergétique) sont laissés-pour-compte en raison de l'absence de compréhension de la technologie et du comportement du système. Ce manque de compréhension du problème mène à ce que les résultats obtenus ne soient pas toujours réalistes ou appropriés à un travail pratique (contrôleurs structurellement complexes, complexité de réglage, contresens physiques, difficultés d'identification, etc.). Prenons comme exemple les commandes synchronisantes; si elles améliorent la synchronisation, ceci est fait au détriment des performances énergétiques.

Afin de pallier ce manque de compréhension des phénomènes physiques existants au sein du système, la suite du chapitre est consacrée aux approches de modélisation existantes pour les axes en gantry. Comme pour la commande, un manque d'intérêt pour la prise en compte des phénomènes globaux affectant les performances de positionnement de l'axe en gantry est remarqué. Les modélisations proposées, soit ne correspondent pas à la réalité (*Ex* : le couplage entre les actionneurs est ignoré, les actionneurs se déplacent en synchronisation parfaite), soit modélisent le comportement de l'axe en gantry de façon incomplète (*Ex* : couplage invariant, le bras transversal et la charge qu'il porte sont modélisés mais alors les actionneurs les portant sont négligés, ou encore, la flexibilité du bras transversal est représentée d'une façon très élémentaire; modèle 3 masses – 2 ressorts).

La prise en compte de la flexibilité du bras transversal des axes en gantry dans leur modélisation et commande est très peu développée dans la littérature. Un état de l'art étendu à la modélisation et commande des systèmes flexibles en général n'a pas donné des résultats plus encourageants. Ce qui a été trouvé peut s'inscrire dans le cadre suivant : des structures de commande structurellement complexes associées à des modèles simples (ou pas de modèle du tout), ou bien des modèles très élaborés mais qui ne donnent aucune information pertinente vis–à–vis du développement d'une commande.

Cette conjonction entre modélisation et commande est finalement trouvée dans l'approche des formalismes de représentation à causalité intégrale imposée, développés par l'équipe commande du L2EP de Lille : Graphe Informationnel Causal (GIC) et Représentation Energétique Macroscopique (REM). Ces formalismes permettent d'en déduire des architectures de commande, par le biais d'une inversion de leur représentation d'un système donné. Par exemple, l'application du GIC par J. GOMAND (Gomand, 2008) pour représenter un modèle mécanique simple de l'axe en gantry a permis d'obtenir une structure de commande du type compensation du couplage avec prise en compte de la distribution de masse inégale du bras transversal due à la position variable de la charge. L'avantage principal de ce type de démarche réside dans la méthodologie de déduction d'architectures de commande par inversion de modèle qu'elle permet. Cette démarche permet en effet une bonne compréhension du comportement physique du système à contrôler, limitant ainsi tout contresens physique. Les architectures de commande auxquelles elle conduit sont en effet basées sur la structure d'un modèle physique, et donc du système, ce qui permet d'établir des procédures de réglage également en rapport avec les éléments physiques qui le constituent. Ces architectures de commande sont par conséquent industriellement viables.

Comme il peut être apprécié, peu d'aspects de la dynamique de l'axe en gantry sont pris en compte dans la littérature, notamment ceux concernant la dynamique de la charge se déplaçant au long du bras transversal ainsi que le comportement vibratoire de ce dernier. L'objectif de cette thèse est cependant plus vaste qu'une simple adaptation d'une loi de commande pour la prise en

compte de ces phénomènes. Ce qu'on a développé est une méthodologie de modélisation et de commande des axes en gantry servant d'outil de travail commun entre les concepteurs des structures électromécaniques et ceux des systèmes de commande. Le développement de cet outil méthodologique fait l'objet du troisième chapitre qui se divise en deux parties. Une partie modélisation, qui débute par une analyse de la structure mécanique des axes en gantry et des éléments le composant. L'objectif de cette analyse a été de développer un modèle qui soit facilement généralisable à divers types d'axes en gantry. Par rapport à ce que l'on peut trouver dans la littérature, les principales contributions de cette démarche de modélisation sont :

- La prise en compte de la dynamique de la charge dans le modèle dynamique de l'axe en gantry.
- La prise en compte de la flexibilité du bras transversal (avec des fréquences de résonance variables en fonction de la position de la charge) dans le modèle dynamique de l'axe en gantry.

Cette démarche de modélisation physique permet également d'associer facilement les paramètres du modèle obtenu aux paramètres du système physique (masses réelles, raideurs réelles, frictions réelles). Ce qui donne les avantages suivants :

- Les paramètres identifiés sont indépendants de la configuration du système. Ce qui permet de gagner en temps de calcul pour des applications temps réel car leurs valeurs sont estimées une fois pour toutes.
- Si des modifications sont apportées au système physique (par exemple changement du point–outil), celles–ci peuvent être rapidement prises en compte dans le modèle sans affecter la valeur des paramètres déjà identifiés.

Finalement, en ce qui concerne l'identification des paramètres associés à la flexibilité du bras transversal, une méthode simple et originale a été proposée. La déformation du bras transversal peut être estimée à partir de la mesure de la force (ou de l'erreur de positionnement) des actionneurs le portant. Elle ne requiert donc pas de moyens de mesure autres que ceux déjà présents dans la commande industrielle de l'axe en gantry.

L'avantage des formalismes de représentation à causalité intégrale imposée GIC et REM a déjà été discuté. La deuxième partie du troisième chapitre concernait donc la représentation du modèle général de l'axe en gantry à l'aide de ces formalismes afin de déduire une architecture de commande adaptée à leur contrôle. Dans un premier temps, une représentation du modèle général de l'axe en gantry est faite à l'aide du GIC, qui permet de décrire en détail les interactions entre les éléments du système. C'est d'ailleurs cette représentation qui a été choisie pour construire les modèles de simulation utilisés dans ce mémoire. Toutefois, dans la mesure où un modèle devient grand ou complexe, déduire une structure de commande à partir de sa représentation GIC devient peu pratique en termes d'implémentation. Ceci à cause du grand nombre de mesures, estimations et compensations à exécuter à chaque pas de calcul. Alors, dans un esprit d'applicabilité, il a été décidé de passer à la représentation complémentaire fournie par la REM qui permet une représentation plus concaténée et donc plus allégée.

Par souci de clarté, on s'est interdit dans ce mémoire de représenter un stockage d'énergie mutuel par la REM. Dans l'axe en gantry, on trouve ce type de stockage dans les énergies cinétique et potentielle élastique associées au bras transversal connectant les actionneurs X_1, X_2 et Y. Alors, afin de pouvoir représenter les équations de mouvement de l'axe en gantry avec ce formalisme, on les a transformées dans une base de pseudo–découplage. L'avantage de cette base de pseudo–découplage est qu'elle est très simple à calculer car elle est basée sur les paramètres physiques du système et donc très intéressante pour une application en temps réel. Basée sur cette représentation, une structure de commande générique a été définie pour l'axe en gantry.

Afin de valider l'approche proposée, son application à trois axes en gantry différents a été présentée dans le quatrième chapitre.

La première partie du quatrième chapitre concernait l'application de la méthodologie à deux différents types d'axes en gantry dits rigides. Comme il peut être apprécié dans (§ 4.1.3.3), dans la mesure où tous les degrés de liberté de la machine sont contrôlables, pour des systèmes rigides, la méthodologie proposée permet d'atteindre des niveaux de performance très intéressants. Elle permet également de mettre en évidence des points problématiques du système et de réaliser un retour d'expérience sur sa conception. Ceci est particulièrement mis en évidence pour l'axe en gantry « Andromeda » qui, à cause de son très lourd bras transversal, excite un mode de vibrations des liaisons mécaniques l'attachant aux actionneurs parallèles. Ce qui a un impact considérable sur les performances de positionnement de la machine. Grâce à la modélisation physique détaillée, on a su identifier rapidement les liaisons mécaniques à l'origine du problème. On a pu également adapter la modélisation physique pour prendre en compte ce phénomène. Cependant, l'ajout de cette nouvelle variable modifie la structure de la représentation graphique causale du système et donc de sa structure de commande. Cette nouvelle structure de commande fera l'objet d'une étude projetée à court terme.

La deuxième partie du quatrième chapitre concernait l'application de la méthodologie proposée pour modéliser, identifier et commander un axe en gantry constitué d'un bras transversal très flexible.

La première chose qui a été montrée, c'est la facilité avec laquelle la méthodologie proposée peut être adaptée pour la prise en compte de la flexibilité du bras transversal. Celle-ci peut en effet être facilement identifiée et associée aux paramètres physiques de la machine grâce à la méthode d'identification qui lui est dédiée en (§ 3.2.3.2). Un des avantages principaux d'une modélisation basée sur les paramètres physiques de la machine est le gain de temps qu'elle représente en termes d'identification des paramètres. Pour l'axe en gantry flexible, on a remplacé le bras transversal de l'axe en gantry « Andromeda » utilisé en (§ 4.1.4) par un bras plus léger (et plus flexible). Comme les éléments de ce nouveau gantry (à exception de ceux associés au bras transversal) étaient les mêmes que pour le gantry précédent, Il n'a pas été nécessaire d'identifier à nouveau la totalité des paramètres du système modélisé mais seulement ceux qui étaient associés au nouveau bras transversal.

En ce qui concerne la commande du gantry flexible, dans le Chapitre 3, il a été montré qu'une modélisation physique détaillée de l'axe en gantry permet de voir directement la contrôlabilité des modes mécaniques de l'axe en gantry. On sait donc que les modes flexibles ne peuvent pas être contrôlés directement par les degrés de liberté (actionneurs) disponibles car ceux-ci sont utilisés pour commander les modes rigides. On sait cependant qu'on peut agir indirectement sur les modes flexibles si on contrôle d'une façon intelligente les modes rigides, notamment avec des techniques de planification de trajectoire. Il est alors montré qu'une meilleure gestion des degrés de liberté de la machine combinée à des algorithmes de planification de trajectoire peut mener un axe en gantry très flexible à atteindre des niveaux de performance similaires à ceux d'un axe en gantry rigide à moindre coût énergétique.

5.2 Perspectives

La méthodologie de modélisation et de commande des axes en gantry proposée dans ce document apporte des solutions de commande performantes et industriellement viables en raison du caractère physique des méthodes qui lui sont associées. Elle permet également d'ouvrir de nombreuses perspectives pour la poursuite des travaux de recherche sur la thématique des systèmes de positionnement multi–actionnés de type axe en gantry.

5.2.1 Perspectives à court terme

Ces perspectives sont issues des observations faites lors de l'application de la méthodologie de modélisation et de commande à des systèmes réels.

La première perspective consiste à adapter la structure de commande proposée afin de prendre en compte le degré de liberté supplémentaire induit par les oscillations longitudinales des liaisons mécaniques qui apparaissent dans des axes en gantry ayant un bras transversal très lourd. Comme pour l'axe en gantry présenté dans (§ 4.1.5). Cette adaptation permettra notamment d'améliorer les performances de positionnement des systèmes présentant ce phénomène.

La structure de commande avec prise en compte du degré de liberté supplémentaire cité ci–dessus peut, par la suite, être adaptée à une compensation active de la force agissant sur les liaisons mécaniques (conditions limitées) d'un bras transversal flexible pour limiter ses vibrations.

La commande de l'axe en gantry n'est pas limitée à la structure de commande proposée dans ce mémoire. Elle n'est qu'une alternative. En effet, en revenant sur la modélisation physique de l'axe en gantry, et en l'associant aux formalismes de représentation graphique causale GIC et REM, d'autres types de commande ou de stratégies de commande peuvent être déduites. A ce propos, quelques voies d'amélioration sont possibles :

- Amélioration du degré de précision de la méthode d'identification des paramètres de l'axe en gantry, notamment ceux associés aux paramètres des modes flexibles. Ces derniers servent à estimer les temps de jerk nécessaires pour la planification de trajectoires (dans le cas d'une compensation du type bang–bang).
- Intégration des forces de détente dans la modélisation des actionneurs linéaires afin de compenser leurs effets.
- Utilisation d'un modèle de frottement plus évolué que celui déjà utilisé afin d'améliorer leur compensation en boucle ouverte.
- Construction d'un observateur à partir des mesures de position et de courant des actionneurs portant le bras transversal afin d'amortir les oscillations de ce dernier (les courants mesurés sont une image des forces de réaction du bras transversal sur les actionneurs).

5.2.2 Perspectives à moyen terme

La fabrication d'un prototype d'axe en gantry flexible ayant un axe Y fonctionnel permettrait de valider expérimentalement les hypothèses concernant les méthodes de planification de trajectoires à fréquences de résonance variables.

La modélisation physique détaillée de l'axe en gantry a donné des pistes intéressantes pour la compensation active des oscillations du bras transversal. En effet, le modèle physique de l'axe en gantry peut être utilisé pour générer les références des actionneurs de compensation active, comme présenté par (Stöppler, et al., 2008). A la différence que ce dernier a utilisé un observateur d'état pour générer la référence de force de la boucle de compensation active.

Une dernière perspective, ou série de perspectives, concerne l'association de la méthodologie développée dans ce mémoire à d'autres méthodologies de commande (requérant elles aussi une modélisation détaillée du système à contrôler). A ce propos, on pense à la commande MPC (Model Predictive Control) afin d'améliorer la commande en boucle ouverte de l'axe en gantry. Notamment pour la modification des trajectoires de référence afin de prendre en compte la déformation élastique de l'axe transversal lors des applications de type suivi de trajectoire. Cette déformation élastique sera estimée grâce au modèle physique de l'axe en gantry proposé dans ce mémoire. On pense également à des commandes du type backstepping et de type synthèse de correcteur par approche paramétrique afin de formaliser une méthode de réglage des contrôleurs en boucle fermée.

Appendix A: Theoretical background

A.1: Euler–Bernoulli Beam Theory (EBBT)

There are several beam theories: *Euler–Bernoulli, Timoshenko, Shear, Rayleigh, Levinson, Reddy–Bickfort, etc*; see (Wang, et al., 2000). Among them, the *Euler–Bernoulli beam theory* (EBBT) is the most used. It is simple and provides reasonable engineering approximations for many problems. Its main drawback is that it tends to overestimate the natural frequencies of higher modes. Also the prediction is better for slender beams than for non–slender beams (Han, et al., 1999).

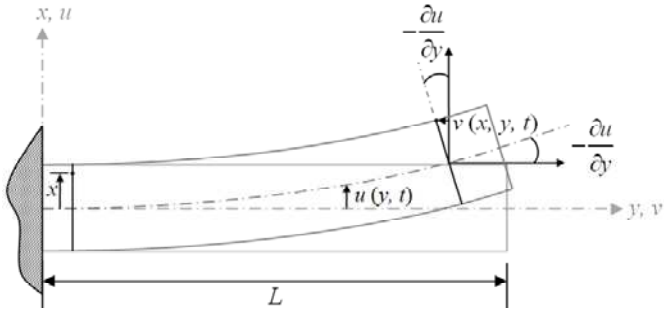

Figure A – 1 : *Schematic representation of a beam under planar deflection using the Euler–Bernoulli beam theory*

The displacement field of the beam is defined by an axial displacement along the y–axis (A.1) and by a *transverse displacement* $u\ (y,\ t)$ along the x – axis.

$$v(x,y,t) = -x\sin(u_{,y}) \cong -xu_{,y} \tag{A.1}$$

The motion equations of the beam can be obtained using energy principles (Reddy, 2002); which of course requires knowing the energy expressions for the beam. The potential energy of an Euler–Bernoulli beam (A.3) can be obtained by developing the general expression of elastic potential energy (A.2)

$$U = \int_V \left(\int_0^{\varepsilon} \sigma d\varepsilon \right) dV \tag{A.2}$$

$$U = \int_0^L \left[\int_A \left(\int_0^{\varepsilon} \sigma_{yy} d\varepsilon_{yy} \right) dA \right] dy \ \ \therefore\ \sigma_{yy} = E_{yy}\varepsilon_{yy}$$

$$U = \int_0^L \left(\int_A \frac{1}{2} E_{yy} \varepsilon_{yy}^2 dA \right) dy \ \ \therefore\ \varepsilon_{yy}^2 = v_{,y}^{\ 2} = x^2 u_{,yy}^{\ 2}$$

$$U = \int_0^L \left(\frac{1}{2} E_{yy} I_{yy} u_{,yy}^{\ 2} \right) dy \ \ \therefore\ I_{yy} = \int_A x^2 dA \tag{A.3}$$

The kinetic energy of the beam (A.4) can be obtained by considering the beam made of slices of mass $\mu = \rho A\ (kg/m)$ moving with a velocity $u_{,t}\ (m/s)$. Then, by integration of the contribution kinetic energy of every section over the span of the beam, we obtain

$$T = \int_0^L \left(\frac{1}{2} \mu u_{,t}^{\ 2} \right) dy \tag{A.4}$$

A.2: Flexure of an Euler–Bernoulli Beam (Mounted in gantry)

A.2.1: Dynamic Model

Let's consider the hybrid lumped–distributed parameters model of **Figure A – 2** to model a flexible beam mounted in gantry. The model is based upon the following hypotheses.

- The beam is considered homogeneous.
- The actuators are considered rigid.
- The electromechanical transformation is considered perfect.
- The beam is modeled using the EBBT, i.e. the rotary inertia of the infinitesimal section is neglected. Indeed, the *Timoshenko beam theory* (TBT) reveals that the rotary inertia is unimportant for low–frequency vibrations (Han, et al., 1999).
- The actuators to beam junctions are considered as discrete torsion stiffnesses with proportional damping.
- The static friction is neglected.

The governing equations of the system can be derived using either vector mechanics or energy and variational principles. In vector mechanics, the forces and moments are summed to obtain the equilibrium equations. In energy methods, the principles of virtual work or their derivatives are used to obtain the equations. While both methods can give the same equations, the energy methods have the advantage of providing information on the boundary conditions (Reddy, 2002). The later imply, however, a prior knowledge of the energy expressions of the studied system. For the model in **Figure A – 2**, these expressions are given in (A.5) to (A.12). To include the effect of forces that are not derived from a potential, i.e. the forces generated by the actuators and the forces due to the friction, the virtual work done by potential less forces (A.13) is included on the variational equation describing *Hamilton's principle* (A.14).

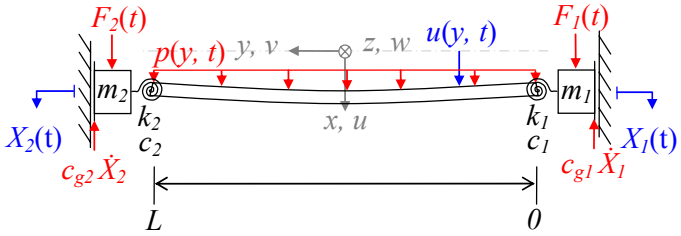

Figure A – 2 : *A flexible beam mounted in gantry*

- *Kinetic Energy*
  - *Kinetic Energy of linear actuator No.1* $$T_1 = \frac{1}{2} m_1 \dot{X}_1^2 = \frac{1}{2} m_1 u_{,t}^2 \Big|_{y=0} \quad \text{(A.5)}$$
  - *Kinetic Energy of linear actuator No.2* $$T_2 = \frac{1}{2} m_2 \dot{X}_2^2 = \frac{1}{2} m_2 u_{,t}^2 \Big|_{y=L} \quad \text{(A.6)}$$
  - *Kinetic Energy stored on the beam* $$T_b = \int_0^L \left(\frac{1}{2} \mu u_{,t}^2 \right) dy \quad \text{(A.7)}$$
  - *Total kinetic energy stored by the system* $$T = T_1 + T_2 + T_b \quad \text{(A.8)}$$
- *Potential Energy*
  - *Potential Energy of Elastic Joint No.1* $$V_1 = \frac{1}{2} k_1 u_{,y}^2 \Big|_{y=0} \quad \text{(A.9)}$$
  - *Potential Energy of Elastic Joint No.2* $$V_2 = \frac{1}{2} k_2 u_{,y}^2 \Big|_{y=L} \quad \text{(A.10)}$$

- *Potential Elastic Energy stored by the beam* $$V_b = \int_0^L \left(\frac{1}{2} EI\, u_{,yy}^2 \right) dy \tag{A.11}$$

- *Total potential elastic energy of the system* $$V = V_1 + V_2 + V_b \tag{A.12}$$

- *Virtual Work done by Potential–less forces*

  As described before, this expression is given by forces acting on the system that are not derived from a potential, i.e. the overall work is different than zero. Among them, the forces and moments generated by the actuators and their opposing forces due to the friction. In the case of the gantry, all these forces act at the boundaries of the system. The forces derived from the static friction are not considered.

$$\delta W = p(y,t)\delta u + \left[F_1 - c_{g1}\, u_{,t}\big|_{y=0} \right] \delta u\big|_{y=0} + \left[F_2 - c_{g2}\, u_{,t}\big|_{y=L} \right] \delta u\big|_{y=L} - c_1\, u_{,yt}\big|_{y=0}\, \delta u_{,y}\big|_{y=0} - c_2\, u_{,yt}\big|_{y=L}\, \delta u_{,y}\big|_{y=L} \tag{A.13}$$

To obtain the motion equations of the flexible gantry, the generalized *Hamilton's principle* (A.14) is used. It includes the action of potential–less forces acting on the system on the form of a virtual work δW.

$$\delta \int_{t_1}^{t_2} (T - V)\, dt + \int_{t_1}^{t_2} \delta W dt = 0 \tag{A.14}$$

To bring up the variation of X_1, X_2 and u, each member of (A.14) is integrated by parts. The expressions that are defined at the boundaries, i.e. at $y = 0$ and $y = L$, cannot be further developed. Likewise, initial and final configurations of the trajectory $u(y, t)$ do not vary. Hence, $\delta u(y,t_1) = \delta u(y,t_2) = 0$

$$\begin{aligned} \delta \int_{t_1}^{t_2} T_1 dt = \delta \int_{t_1}^{t_2} \frac{1}{2} m_1 \dot{X}_1^{\,2} dt = \int_{t_1}^{t_2} \underbrace{m_1 \dot{X}_1}_{u} \underbrace{\delta \dot{X}_1 dt}_{dv} &= \cancel{\left[m_1 \dot{X}_1 \delta X_1 \right]_{t_1}^{t_2}} - \int_{t_1}^{t_2} m_1 \ddot{X}_1 \delta X_1 dt \\ &= -\int_{t_1}^{t_2} m_1 \ddot{X}_1 \delta X_1 dt \quad \therefore \quad X_1 = \left[u(y,t) \right]_{y=0},\ \delta X_1(t_1) = \delta X_1(t_2) = 0 \end{aligned} \tag{A.15}$$

$$\begin{aligned} \delta \int_{t_1}^{t_2} T_2 dt = \delta \int_{t_1}^{t_2} \frac{1}{2} m_2 \dot{X}_2^{\,2} dt = \int_{t_1}^{t_2} \underbrace{m_2 \dot{X}_2}_{u} \underbrace{\delta \dot{X}_2 dt}_{dv} &= \cancel{\left[m_2 \dot{X}_2 \delta X_2 \right]_{t_1}^{t_2}} - \int_{t_1}^{t_2} m_2 \ddot{X}_2 \delta X_2 dt \\ &= -\int_{t_1}^{t_2} m_2 \ddot{X}_2 \delta X_2 dt \quad \therefore \quad X_2 = \left[u(y,t) \right]_{y=L},\ \delta X_2(t_1) = \delta X_2(t_2) = 0 \end{aligned} \tag{A.16}$$

$$\begin{aligned} \delta \int_{t_1}^{t_2} T_b dt = \int_{t_1}^{t_2} \int_0^L \frac{1}{2} \mu\, \delta u_{,t}^2\, dy\, dt = \int_0^L \int_{t_1}^{t_2} \underbrace{\mu\, u_{,t}}_{u} \underbrace{\delta u_{,t}\, dt}_{dv} dy &= \int_0^L \left\{ \cancel{\left[\mu\, u_{,t} \delta u \right]_{t_1}^{t_2}} - \int_{t_1}^{t_2} \mu\, u_{,tt} \delta u\, dt \right\} dy \\ &= -\int_{t_1}^{t_2} \int_0^L \mu\, u_{,tt} \delta u\, dy\, dt \ \therefore\ u = u(y,t),\ \delta u(y,t_1) = \delta u(y,t_2) = 0 \end{aligned} \tag{A.17}$$

$$-\delta \int_{t_1}^{t_2} V_1 dt = -\delta \int_{t_1}^{t_2} \frac{1}{2} k_1 u_{,y}^2 dt = -\int_{t_1}^{t_2} k_1 u_{,y} \delta u_{,y} dt \ \ \therefore\ \ u_{,y} = u_{,y}(0,t) \tag{A.18}$$

$$-\delta \int_{t_1}^{t_2} V_2 dt = -\delta \int_{t_1}^{t_2} \frac{1}{2} k_2 u_{,y}^2 dt = -\int_{t_1}^{t_2} k_2 u_{,y} \delta u_{,y} dt \ \ \therefore\ \ u_{,y} = u_{,y}(L,t) \tag{A.19}$$

$$\begin{aligned} -\delta \int_{t_1}^{t_2} V_b dt = -\delta \int_{t_1}^{t_2} \left[\int_0^L \left(\frac{1}{2} EI\, u_{,yy}^2 \right) dy \right] dt &= -\int_{t_1}^{t_2} \int_0^L \underbrace{EI\, u_{,yy}}_{u} \underbrace{\delta u_{,yy}\, dy}_{dv}\, dt \\ &= -\int_{t_1}^{t_2} \left\{ \left[EI u_{,yy} \delta u_{,yy} \right]_{y=0}^{y=L} - \int_0^L \underbrace{EI\, u_{,yyy}}_{u} \underbrace{\delta u_{,y}\, dy}_{dv} \right\} dt \\ &= -\int_{t_1}^{t_2} \left\{ \left[EI u_{,yy} \delta u_{,y} \right]_{y=0}^{y=L} - \left[EI u_{,yyy} \delta u \right]_{y=0}^{y=L} + \int_0^L EI\, u_{,yyyy} \delta u\, dy \right\} dt \end{aligned} \tag{A.20}$$

Rewriting the *Hamilton's principle* for the beam mounted in gantry as the superposition of the *virtual work done by potential–less forces* (A.13), the first variation of the *total kinetic energy* (A.15) to (A.17), and of the *total potential energy* (A.18) to (A.20). And, by factorization of terms, the general expression (A.21) of the motion equations and boundary conditions of the flexible beam mounted in gantry is obtained

$$\int_{t_1}^{t_2}\int_0^L\left[-\mu\, u_{,tt}-EI\,u_{,yyyy}+p(y,t)\right]\delta u\,dy\,dt+\int_{t_1}^{t_2}\left[\left(F_1-c_{g1}u_{,t}-m_1u_{,tt}-EIu_{,yyy}\right)\delta u\right]_{y=0}dt+\int_{t_1}^{t_2}\left[\left(F_2-c_{g2}u_{,t}-m_2u_{,tt}+EIu_{,yyy}\right)\delta u\right]_{y=L}dt$$
$$+\int_{t_1}^{t_2}\left[\left(-k_1u_{,y}+EIu_{,yy}-c_1u_{,yt}\right)\delta u_{,y}\right]_{y=0}dt+\int_{t_1}^{t_2}\left[\left(-k_2u_{,y}-EIu_{,yy}-c_2u_{,yt}\right)\delta u_{,y}\right]_{y=L}dt=0 \tag{A.21}$$

The *fundamental lemma of the calculus of variations* (Reddy, 2002) tells us that the integrant of the first term in (A.21) must vanish. Thus,

$$\mu\, u_{,tt}+EI\,u_{,yyyy}=p(y,t) \tag{A.22}$$

This is the equation of motion of an *Euler–Bernoulli* beam. Finally the remaining integrals vanish, for example, if

$$\left[F_1-c_{g1}u_{,t}-m_1u_{,tt}-EIu_{,yyy}\right]_{y=0}=0\,, \qquad \text{or} \qquad \delta u(0,t)=0 \tag{A.23}$$

$$\left[F_2-c_{g2}u_{,t}-m_2u_{,tt}+EIu_{,yyy}\right]_{y=L}=0\,, \qquad \text{or} \qquad \delta u(L,t)=0 \tag{A.24}$$

$$\left[-k_1u_{,y}+EIu_{,yy}-c_1u_{,yt}\right]_{y=0}=0\,, \qquad \text{or} \qquad \delta u_{,y}(0,t)=0 \tag{A.25}$$

$$\left[-k_2u_{,y}-EIu_{,yy}-c_2u_{,yt}\right]_{y=L}=0\,, \qquad \text{or} \qquad \delta u_{,y}(L,t)=0 \tag{A.26}$$

These relations yield the possible boundary conditions of the problem. Note, however, that *Hamilton's principle* only requires the *sum* of all the boundary terms to vanish, and not necessarily the different boundary terms individually (Hagedorn, et al., 2007). This idea will be clarified on the next section when analyzing the properties of the boundary conditions of the flexible beam mounted in gantry. By now, the solution of the equation of motion (A.22) along with the boundary conditions (A.23) – (A.26) yields the successive configurations of the system at any time instant starting from any arbitrary initial condition.

A.2.2: Comments on the Boundary Conditions of a beam mounted in gantry

For a continuum, there are two types of boundary conditions, *geometric* and *natural*. The *geometric* boundary conditions are related to a displacement, or a displacement field, of the boundary. The *natural* boundary conditions are related to forces acting on the boundary.

> *"A fundamental concept of mechanics is that in any system, either the value of a generalized coordinate may be specified, or the value of the associated generalized force may be specified, but not both."* (Ginsberg, 2001).

For an *Euler–Bernoulli* beam, the *geometric* boundary conditions are defined by the *transverse displacement* (δu) and the *neutral fiber slope*[13] ($\delta u_{,y}$).

> *"A geometric boundary condition, in which either u or ∂u/∂y is known, requires the generation of a constraint force that is sufficient to impose that motion."* (Ginsberg, 2001).

For an *Euler–Bernoulli* beam, the *natural* boundary conditions are defined by the *shear force* ($S = EI\, u_{,yyy}$) and the *bending moment* ($M = EI\, u_{,yy}$), see **TABLE A – 1**

TABLE A – 1
BOUNDARY CONDITIONS OF AN EULER – BERNOULLI BEAM

	Natural		***Geometric***
Bending moment (M)	$M = EI\, u_{,yy}$	***Neutral fiber slope***	$\delta u_{,y}$
Shear stress (S)	$S = EI\, u_{,yyy}$	***Transverse displacement***	δu

When there are external forces over the beam, or at the boundaries, appropriate forcing terms can be added, respectively, to (A.22), or to the natural boundary conditions. The standard boundary conditions associated with an *Euler–Bernoulli beam* mounted in gantry are given on **TABLE A – 2**.

When the geometric boundary condition is time independent, we say that it is *homogeneous*, because the only variable is the associated displacement. Time dependent boundary conditions may be imposed by large machines or through servo control (Ginsberg, 2001).

As it is true for geometric boundary conditions, the natural boundary conditions may be time dependent. This would correspond to a situation where the internal force resultant at a boundary must match a specified external force or couple, rendering the boundary condition *non–homogeneous*. However, a time–dependent force may also be considered to be an external load applied very close to the end. This approach allows considering the external force affecting any natural condition to be zero, so we only need to consider homogeneous natural boundary conditions. The simplest conditions are those in which no springs of masses are attached at an end, in which case, the internal force variable must be zero (Ginsberg, 2001).

Conversely, a spring (*non–homogeneous* BC) complicates the situation, because displacement of the end leads to deformation of the spring, which, in turn, produces to an internal force. Possible ways in which a spring may act at the ends are depicted in **TABLE A – 2**. A method to deal with non–homogeneous time–dependent boundary conditions is presented on **Appendix C**.

[13] Or rotation of the cross–section, which is perpendicular to the neutral fiber slope

TABLE A – 2

DIFFERENT BOUNDARY CONDITIONS FOR AN EULER – BERNOULLI BEAM

Type	*Example*	*Boundary conditions*
Clamped	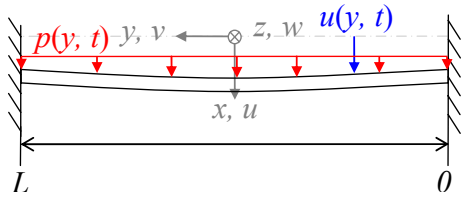	$EI\,u_{,yy}(0,t)\neq 0 \;\because\; \delta u_{,y}(0,t)=0$ $EI\,u_{,yy}(L,t)\neq 0 \;\because\; \delta u_{,y}(L,t)=0$ $EI\,u_{,yyy}(0,t)\neq 0 \;\because\; \delta u(0,t)=0$ $EI\,u_{,yyy}(L,t)\neq 0 \;\because\; \delta u(L,t)=0$
pinned	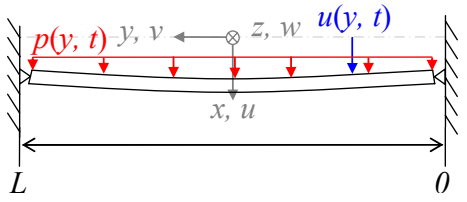	$EI\,u_{,yy}(0,t)=0 \;\because\; \delta u_{,y}(0,t)\neq 0$ $EI\,u_{,yy}(L,t)=0 \;\because\; \delta u_{,y}(L,t)\neq 0$ $EI\,u_{,yyy}(0,t)\neq 0 \;\because\; \delta u(0,t)=0$ $EI\,u_{,yyy}(L,t)\neq 0 \;\because\; \delta u(L,t)=0$
Free	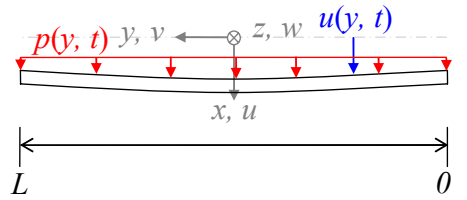	$EI\,u_{,yy}(0,t)=0 \;\because\; \delta u_{,y}(0,t)\neq 0$ $EI\,u_{,yy}(L,t)=0 \;\because\; \delta u_{,y}(L,t)\neq 0$ $EI\,u_{,yyy}(0,t)=0 \;\because\; \delta u(0,t)\neq 0$ $EI\,u_{,yyy}(L,t)=0 \;\because\; \delta u(L,t)\neq 0$
Sliding	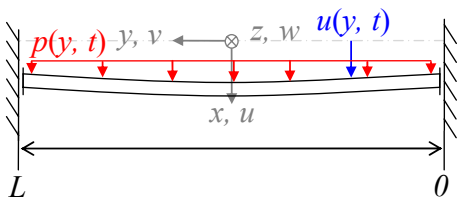	$EI\,u_{,yy}(0,t)\neq 0 \;\because\; \delta u_{,y}(0,t)=0$ $EI\,u_{,yy}(L,t)\neq 0 \;\because\; \delta u_{,y}(L,t)=0$ $EI\,u_{,yyy}(0,t)=0 \;\because\; \delta u(0,t)\neq 0$ $EI\,u_{,yyy}(L,t)=0 \;\because\; \delta u(L,t)\neq 0$
Linear spring	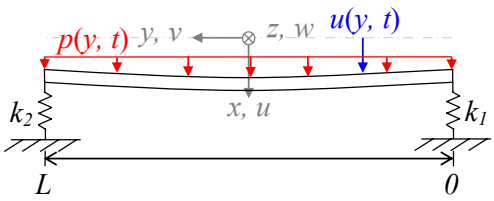	$EI\,u_{,yy}(0,t)=0 \;\because\; \delta u_{,y}(0,t)\neq 0$ $EI\,u_{,yy}(L,t)=0 \;\because\; \delta u_{,y}(L,t)\neq 0$ $-EI\,u_{,yyy}(0,t)-k_1 u(0,t)=0 \;\because\; \delta u(0,t)\neq 0$ $EI\,u_{,yyy}(L,t)-k_2 u(L,t)=0 \;\because\; \delta u(L,t)\neq 0$
Linear spring (Sliding)	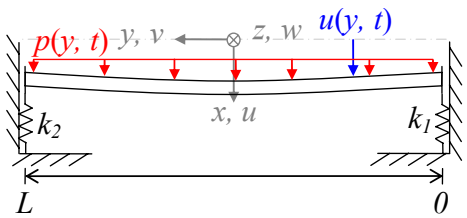	$EI\,u_{,yy}(0,t)\neq 0 \;\because\; \delta u_{,y}(0,t)=0$ $EI\,u_{,yy}(L,t)\neq 0 \;\because\; \delta u_{,y}(L,t)=0$ $-EI\,u_{,yyy}(0,t)-k_1 u(0,t)=0 \;\because\; \delta u(0,t)\neq 0$ $EI\,u_{,yyy}(L,t)-k_2 u(L,t)=0 \;\because\; \delta u(L,t)\neq 0$
Torsion spring	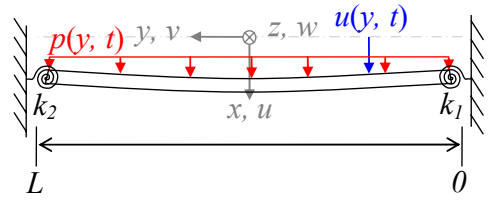	$EI\,u_{,yy}(0,t)-k_1 u_{,y}(0,t)=0 \;\because\; \delta u_{,y}(0,t)\neq 0$ $-EI\,u_{,yy}(L,t)-k_2 u_{,y}(L,t)=0 \;\because\; \delta u_{,y}(L,t)\neq 0$ $-EI\,u_{,yyy}(0,t)\neq 0 \;\because\; \delta u(0,t)=0$ $EI\,u_{,yyy}(L,t)\neq 0 \;\because\; \delta u(L,t)=0$
gantry	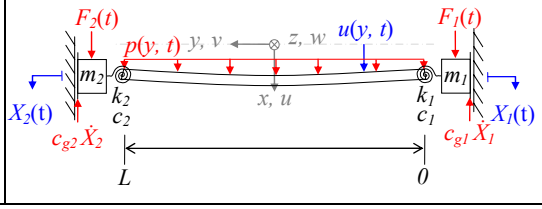	$\left[-k_1 u_{,y}+EIu_{,yy}-c_1 u_{,yt}\right]_{y=0}=0 \because \delta u_{,y}(0,t)\neq 0$ $\left[-k_2 u_{,y}-EIu_{,yy}-c_2 u_{,yt}\right]_{y=L}=0 \because \delta u_{,y}(L,t)\neq 0$ $\left[F_1-c_{g1}u_{,t}-m_1 u_{,tt}-EIu_{,yyy}\right]_{y=0}=0 \because \delta u(0,t)\neq 0$ $\left[F_2-c_{g2}u_{,t}-m_2 u_{,tt}+EIu_{,yyy}\right]_{y=L}=0 \because \delta u(L,t)\neq 0$

Appendix B: Closed–form solution method

B.1. Motion Equation of the headless gantry

The motion equation and boundary conditions for the model presented in **Figure B – 1** are obtained on § A.2. The objective of this model is to put in evidence the rigid and flexible modes of the beam and evaluate the influence of the boundary conditions over these modes.

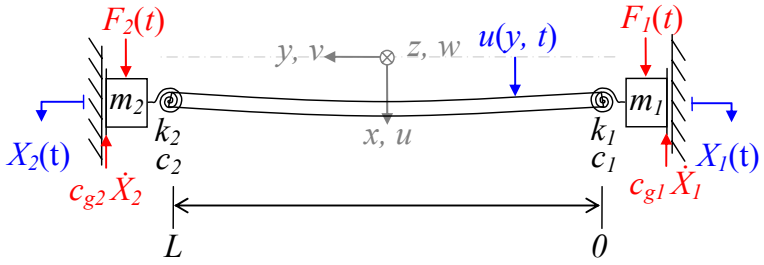

Figure B – 1 : *Head–less the gantry stage.*

The governing equation (B.1) of the system can be derived using either vector mechanics (Newton) or energy and variational principles (Hamilton, Lagrange–Euler, Power balance, etc). Hamilton's principle is used since it allows determining the boundary conditions (B.2) and (B.3) automatically.

$$\mu\frac{\partial^2 u(y,t)}{\partial t^2}+EI\frac{\partial^4 u(y,t)}{\partial y^4}=0 \tag{B.1}$$

$$\begin{aligned} F_{b1}(t)-EI\frac{\partial^3 u(0,t)}{\partial y^3}=0 \quad &\therefore \quad F_{b1}(t)=F_1(t)-c_{g1}\dot{X}_1(t)-m_1\ddot{X}_1(t)-c_{c1}sign\left[\dot{X}_1(t)\right] \\ F_{b2}(t)+EI\frac{\partial^3 u(L,t)}{\partial y^3}=0 \quad &\therefore \quad F_{b2}(t)=F_2(t)-c_{g2}\dot{X}_2(t)-m_2\ddot{X}_2(t)-c_{c2}sign\left[\dot{X}_2(t)\right] \end{aligned} \tag{B.2}$$

$$\begin{aligned} -k_1\frac{\partial u(0,t)}{\partial y}-c_1\frac{\partial^2 u(0,t)}{\partial y\partial t}+EI\frac{\partial^2 u(0,t)}{\partial y^2}=0 \\ -k_2\frac{\partial u(L,t)}{\partial y}-c_2\frac{\partial^2 u(L,t)}{\partial y\partial t}-EI\frac{\partial^2 u(L,t)}{\partial y^2}=0 \end{aligned} \tag{B.3}$$

B.2. The free–vibration problem

The equation of motion, boundary conditions, and initial conditions form a boundary value problem (BVP) that can be solved using the method of *modal analysis*.

B.2.1 Separation of variables

If we consider the solution $u(y, t)$ of (B.1) as a product of two functions of independent variable (Polyanin, 2002), i.e. $u(y, t) = q(t)\ \psi(y)$. Then, (B.1) can be rewritten as

$$\mu\,\psi(y)\frac{d^2 q(t)}{dt^2}+EI\,q(t)\frac{d^4\psi(y)}{dy^4}=0 \tag{B.4}$$

We can separate (B.4) into an equality (B.5). Each side of the equality is a function of a single and independent variable, namely, y and t. To be true, this equality, regardless of the value of y and t, must be constant. So, the constant ω^2 is introduced.

$$-\frac{1}{q(t)}\frac{d^2 q(t)}{dt^2}=\frac{EI}{\mu}\frac{1}{\psi(y)}\frac{d^4\psi(y)}{dy^4}=\omega^2 \tag{B.5}$$

Using (B.5) we can split (B.1) in two independent ODEs,

$$\frac{d^2q(t)}{dt^2}+\omega^2 q(t)=0 \tag{B.6}$$

$$\frac{d^4\psi(y)}{dy^4}-\frac{\alpha^4}{L^4}\psi(y)=0 \;\;\therefore\;\; \alpha^4=\frac{\mu L^4}{EI}\omega^2 \tag{B.7}$$

The solutions to (B.6) and (B.7) are, respectively,

$$q(t)=A_1\sin(\omega t)+A_2\cos(\omega t) \tag{B.8}$$

$$\psi(y)=C_1\sin\left(\alpha\frac{y}{L}\right)+C_2\cos\left(\alpha\frac{y}{L}\right)+C_3\sinh\left(\alpha\frac{y}{L}\right)+C_4\cosh\left(\alpha\frac{y}{L}\right) \tag{B.9}$$

By using the variable separation method $u(y,\,t) = q(t)\,\psi(y)$; the BCs (B.2) and (B.3) are also modified.

$$\begin{aligned} &F_{b1}(t)-EI\frac{d^3\psi(0)}{dy^3}=0 \quad\therefore\quad F_{b1}(t)=F_1(t)-c_{g1}\dot{X}_1(t)-m_1\ddot{X}_1(t)-c_{c1}\,\mathrm{sign}\left[\dot{X}_1(t)\right] \\ &F_{b2}(t)+EI\frac{d^3\psi(L)}{dy^3}=0 \quad\therefore\quad F_{b2}(t)=F_2(t)-c_{g2}\dot{X}_2(t)-m_2\ddot{X}_2(t)-c_{c2}\,\mathrm{sign}\left[\dot{X}_2(t)\right] \end{aligned} \tag{B.10}$$

$$\begin{aligned} &-k_1\frac{d\psi(0)}{dy}+EI\frac{d^2\psi(0)}{dy^2}=0 \quad\therefore\quad c_1=0 \\ &-k_2\frac{d\psi(L)}{dy}-EI\frac{d^2\psi(L)}{dy^2}=0 \quad\therefore\quad c_2=0 \end{aligned} \tag{B.11}$$

Assumptions are made to redefine the BCs. The shear stress BCs (B.10) are equal to the resultant forces $F_{b1}(t)$ and $F_{b2}(t)$ derived from the electromechanical transformation of actuators X_1 and X_2 acting on the beam. The bending moment BCs (B.11) are equal to the moment induced by the torsion springs k_1 and k_2. The damping c_1 and c_2 associated to the torsion springs are neglected to avoid coupling terms.

Yet, (B.10) is a set of non–homogeneous BCs. This makes the system non–self–adjoint and therefore unsolvable using modal analysis. To overcome this, one approach is proposed on the literature.

This method consists in reformulating the problem to make the system self–adjoint and therefore solvable using modal analysis (Meirovitch, 2001). The problem defined by the homogeneous PDE (B.1) and the non–homogeneous BCs (B.2) is transformed into a problem defined by the non–homogeneous PDE (B.12) and the homogeneous BCs (B.13) and (B.14),

$$\mu\frac{\partial^2u(y,t)}{\partial t^2}+EI\frac{\partial^4u(y,t)}{\partial y^4}=p(y,t) \quad\therefore\quad p(y,t)=F_{b1}(t)\boldsymbol{\delta}(y-0)+F_{b2}(t)\boldsymbol{\delta}(y-L) \tag{B.12}$$

$$-EI\frac{\partial^3u(0,t)}{\partial y^3}=0; \qquad EI\frac{\partial^3u(L,t)}{\partial y^3}=0 \tag{B.13}$$

$$-k_1\frac{\partial u(0,t)}{\partial y}+EI\frac{\partial^2u(0,t)}{\partial y^2}=0 \qquad -k_2\frac{\partial u(L,t)}{\partial y}-EI\frac{\partial^2u(L,t)}{\partial y^2}=0 \tag{B.14}$$

In other words, this method consists in considering the forces $F_{b1}(t)$ and $F_{b2}(t)$ not acting at the boundary but very close to it. Even if it seems insignificant, this allows to supposing the shear stress BCs (B.2) equal to zero, as in (B.13). It is important to note that such boundary conditions are characteristic of a sliding–sliding beam.

Again, if the variable separation method $u(y,\,t) = q(t)\,\psi(y)$ is applied. One obtains,

$$-EI\frac{\partial^3\psi(0)}{\partial y^3}=0; \qquad EI\frac{\partial^3\psi(L)}{\partial y^3}=0\,, \tag{B.15}$$

$$-k_1\frac{\partial\psi(0)}{\partial y}+EI\frac{\partial^2\psi(0)}{\partial y^2}=0; \qquad -k_2\frac{\partial\psi(L)}{\partial y}-EI\frac{\partial^2\psi(L)}{\partial y^2}=0\,, \tag{B.16}$$

There is a second method (Hagedorn, et al., 2007), which is quite similar. It consists in converting the non–homogeneous BCs into homogeneous ones, along with appropriate forcing in the equation of motion.

B.2.2. Eigenvalues, Eigenvectors and Eigenfunctions

B.2.2.1. Introduction

To determine the unknown coefficients C_1 to C_4 of (B.9), we apply the corresponding sets of BCs (B.15) and (B.16) to it. We find a four equation four unknown system of equations. Using a matrix notation, this system has the form

$$\left[F(\alpha)\right]\left\{C\right\}=\left\{0\right\} \tag{B.17}$$

$\{C\}$ is the vector of unknown coefficients C_1 to C_4. $[F(\alpha)]$ contains trigonometric and hyperbolic functions evaluated at the boundaries. For arbitrary values of α, the solution to (B.17) is trivial, i.e. $\{C\} = \{0\}$. To obtain a non–trivial solution, $[F(\alpha)]$ must be non invertible. In linear algebra, this means that its determinant must be zero, leading to the characteristic equation, also called the frequency equation.

$$\left|F(\alpha)\right|=0 \tag{B.18}$$

Whenever α is an Eigenvalue, the rank of $[F(\alpha)]\{C\} = \{0\}$ is reduced by one. Hence, one of the corresponding coefficients C may be considered arbitrary. Arbitrariness that will be removed when we normalize the modes based on their orthogonality properties. The values of the remaining coefficients are defined as amplitude ratios to the arbitrary coefficient. These ratios are better known as *Eigenvectors*.

So the solution to (B.7) or the Eigenfunctions may be rewritten as

$$\psi_k(y)=C_{1k}\left[\sin\left(\alpha_k\frac{y}{L}\right)+\frac{C_{2k}}{C_{1k}}\cos\left(\alpha_k\frac{y}{L}\right)+\frac{C_{3k}}{C_{1k}}\sinh\left(\alpha_k\frac{y}{L}\right)+\frac{C_{4k}}{C_{1k}}\cosh\left(\alpha_k\frac{y}{L}\right)\right] \tag{B.19}$$

B.2.2.2. Eigenvalues of the headless gantry

In the case of the headless gantry, its characteristic equation (B.20) is obtained from evaluating (B.9) at the boundaries (B.15) and (B.16). The eigenvalues are the roots of the characteristic equation.

Note: Here, we introduce the stiffness ratios $\beta_1 = k_1 / EI$ and $\beta_2 = k_2 / EI$.

$$\alpha\left\{L\alpha\left(\beta_1+\beta_2\right)\left[\mathrm{Cosh}(\alpha)\mathrm{Sin}(\alpha)+\mathrm{Cos}(\alpha)\mathrm{Sinh}(\alpha)\right]+2L^2\beta_1\beta_2\mathrm{Sin}(\alpha)\mathrm{Sinh}(\alpha)+\alpha^2\left[\mathrm{Cos}(\alpha)\mathrm{Cosh}(\alpha)-1\right]\right\}=0 \tag{B.20}$$

Now, if $\beta_1 \to \infty$ and $\beta_2 \to \infty$. The characteristic equation becomes those of a sliding–sliding beam (B.21). Similarly, if $\beta_1 \to 0$ and $\beta_2 \to 0$. The characteristic equation becomes then those of a free–free beam (B.22).

$$\mathrm{Sin}(\alpha)\mathrm{Sinh}(\alpha)=0 \tag{B.21}$$

$$\mathrm{Cos}(\alpha)\mathrm{Cosh}(\alpha)-1=0 \tag{B.22}$$

Since the values β_1 and β_2 are yet to be determined experimentally for the headless gantry. We present a possible evolution of the first four Eigenvalues α_k of the gantry in function of the values of β_1 and β_2.

TABLE B – 1

EVOLUTION OF THE EIGENVALUES OF THE HEADLESS GANTRY WHEN $\beta_1 = \beta_2$

β1=β2	Translation mode	Rotation Mode	1st mode	2nd mode	3rd mode	Type of Boundary conditions
0	0	0	4,730	7,853	10,995	free-free beam
0,001	0	0,504	4,731	7,854	10,996	
0,01	0	0,896	4,741	7,860	11,001	
0,1	0	1,570	4,832	7,919	11,043	
1	0	2,500	5,362	8,334	11,375	
10	0	3,035	6,082	9,137	12,202	
100	0	3,130	6,260	9,391	12,521	
1000	0	π	2π	3π	4π	sliding-sliding beam

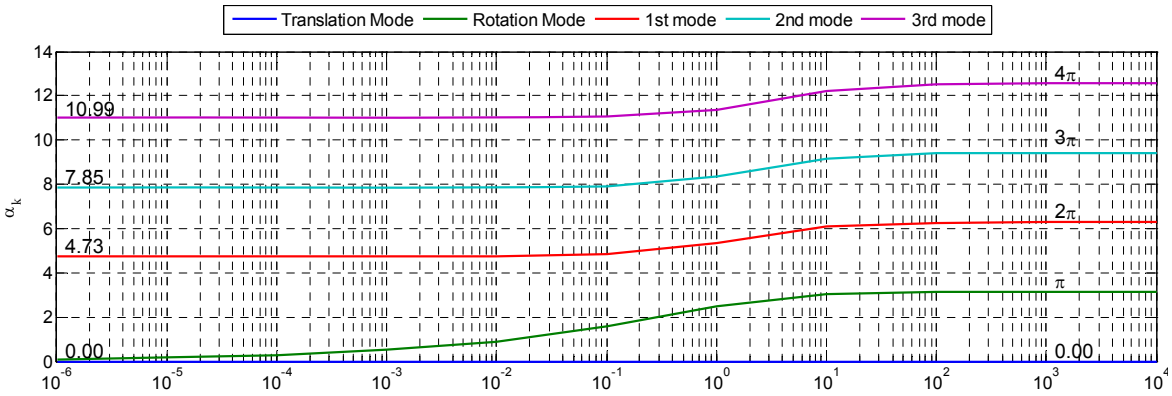

Figure B – 2: *Evolution of the Eigenvalues of the headless gantry when* $\beta_1 = \beta_2$. *The numeric values present at both the beginning and the end of each curve are the asymptotic values of* α_k.

TABLE B – 2

EVOLUTION OF THE EIGENVALUES OF THE HEADLESS GANTRY WHEN $\beta_1 \neq 0$ and $\beta_2 = 0$

β1≠0, β2=0	Translation mode	Rotation Mode	1st mode	2nd mode	3rd mode	Type of Boundary conditions
0	0	0	4,730	7,853	10,995	free-free beam
0,001	0	0,424	4,731	7,854	10,996	
0,01	0	0,753	4,736	7,857	10,998	
0,1	0	1,310	4,782	7,886	11,020	
1	0	2,001	5,055	8,099	11,188	
10	0	2,313	5,408	8,504	11,606	
100	0	2,360	5,488	8,624	11,760	
1000	0	2,365	5,498	8,639	11,781	free-sliding beam

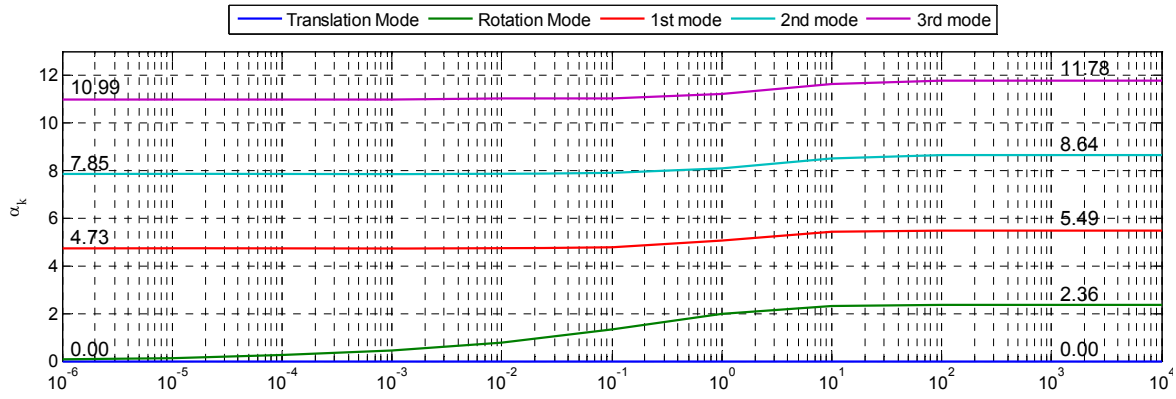

Figure B – 3: *Evolution of the Eigenvalues of the headless gantry when* $\beta_1 \neq 0$ *and* $\beta_2 = 0$. *The numeric values present at both the beginning and the end of each curve are the asymptotic values of* α_k

The natural frequency associated to each Eigenvalue is given by

$$\omega_k = \alpha_k^2 \sqrt{\frac{EI}{\mu L^4}} \tag{B.23}$$

One can conclude that if the ratios β_1 and β_2 are much less than one. The beam can be considered rigid with respect to the elastic joints k_1 and k_2 and therefore elastically decoupled from them.

B.2.2.3. Eigenvectors of the headless gantry

To determine the amplitude ratios of the system, we first select the arbitrary constant. In our case, we have chosen C_1 as the arbitrary constant. From evaluating (B.9) at the boundaries (B.15) and (B.16) we known that $C_1 = C_3$. Then, the amplitude ratios to be determined are C_2 / C_1 and C_4 / C_1. They are defined by

$$\frac{C_2}{C_1}=\frac{\alpha^2\left[\mathrm{Sinh}(\alpha)-\mathrm{Sin}(\alpha)\right]+\beta_2\alpha L\mathrm{Cos}(\alpha)+\alpha L\left(\beta_2+2\beta_1\right)\mathrm{Cosh}(\alpha)+2L^2\beta_1\beta_2\mathrm{Sinh}(\alpha)}{\alpha^2\left[\mathrm{Cos}(\alpha)-\mathrm{Cosh}(\alpha)\right]+\beta_2\alpha L\left[\mathrm{Sin}(\alpha)-\mathrm{Sinh}(\alpha)\right]} \tag{B.24}$$

$$\frac{C_4}{C_1}\rightarrow\frac{\alpha^2\left[\mathrm{Sinh}(\alpha)-\mathrm{Sin}(\alpha)\right]+\beta_2\alpha L\mathrm{Cosh}(\alpha)+\alpha L\left(\beta_2+2\beta_1\right)\mathrm{Cos}(\alpha)+2L^2\beta_1\beta_2\mathrm{Sin}(\alpha)}{\alpha^2\left[\mathrm{Cos}(\alpha)-\mathrm{Cosh}(\alpha)\right]+\beta_2\alpha L\left[\mathrm{Sin}(\alpha)-\mathrm{Sinh}(\alpha)\right]} \tag{B.25}$$

Considering that for the headless gantry $\beta_2 = 0$, then, the amplitude ratios become,

$$\frac{C_2}{C_1}=\frac{\alpha\left[\mathrm{Sinh}(\alpha)-\mathrm{Sin}(\alpha)\right]+2L\mathrm{Cosh}(\alpha)\beta_1}{\alpha\left[\mathrm{Cos}(\alpha)-\mathrm{Cosh}(\alpha)\right]} \tag{B.26}$$

$$\frac{C_4}{C_1}=\frac{\alpha\left[\mathrm{Sinh}(\alpha)-\mathrm{Sin}(\alpha)\right]+2L\mathrm{Cos}(\alpha)\beta_1}{\alpha\left[\mathrm{Cos}(\alpha)-\mathrm{Cosh}(\alpha)\right]} \tag{B.27}$$

B.2.2.4. Eigenfunctions of the headless gantry

With the arbitrary constant chosen and the amplitude ratios calculated. The next thing to be done is to replace them inside (B.19). So, for the headless gantry, the Eigenfunctions or Eigensolutions $\psi_k(y)$ to the spatial equation (B.7) are given by

$$\psi_k(y)=C_{1k}\left\{\mathrm{Sin}\left(\alpha_k\frac{y}{L}\right)+\mathrm{Sinh}\left(\alpha_k\frac{y}{L}\right)+\left[\frac{\mathrm{Sinh}(\alpha_k)-\mathrm{Sin}(\alpha_k)}{\mathrm{Cos}(\alpha_k)-\mathrm{Cosh}(\alpha_k)}\right]\left[\mathrm{Cos}\left(\alpha_k\frac{y}{L}\right)+\mathrm{Cosh}\left(\alpha_k\frac{y}{L}\right)\right]+R_k\right\} \tag{B.28}$$

Where,

$$R_k=\frac{2L\beta_1}{\alpha_k\left[\mathrm{Cos}(\alpha_k)-\mathrm{Cosh}(\alpha_k)\right]}\left[\mathrm{Cos}(\alpha_k)\mathrm{Cosh}\left(\alpha_k\frac{y}{L}\right)+\mathrm{Cosh}(\alpha_k)\mathrm{Cos}\left(\alpha_k\frac{y}{L}\right)\right] \tag{B.29}$$

Note that, if we neglect R_k, (B.28) are the Eigensolutions of the free–free beam (Han, et al., 1999). This confirms the conclusion to § B.2.2.2. "If the stiffness ratios β_1 and β_2 are much less than one, the beam can be considered elastically decoupled from the elastic joints k_1 and k_2". See Figure B – 4.

For the gantry Andromeda, $\beta_2 = 0$, since the beam to actuator junction is assured by a pivot articulation, i.e. $k_2 = 0$. The junction corresponding to k_1 is assured by a thin plate. Therefore, β_1 is presumed to be small if we compare the stiffness of the beam to those of the plate, i.e. $\beta_1 << 1$. Its approximate value will be determined experimentally using *finite element modal analysis* and *experimental modal analysis*.

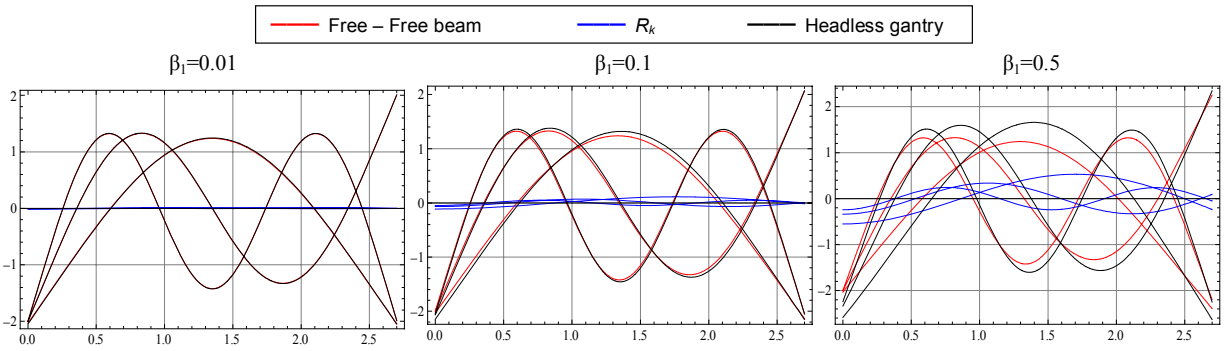

Figure B – 4: *Influence of* β_1 *on the response of the first three eigenfunctions of the headless gantry.*

A zero Eigenvalue ($\alpha_k = 0$, and thus $\omega_k = 0$) as solution to the characteristic equation (B.20) indicates the existence of rigid–body modes. For the headless gantry, there are three possible cases.

1. **$\beta_1 \approx 0$ and $\beta_2 = 0$.**

In this particular case, there are two possible situations.

a. The stiffness of the torsion spring is negligible, i.e. $k_1 \approx 0$.

b. The stiffness of the beam is much larger than those of the torsion spring $EI >> k_1$.

In both cases, the headless gantry behaves as a Free–Free beam and therefore it has two rigid body modes. It *translates* along the x–axis and the desynchronization between drives X_1 and X_2 forces the beam to *rotate* about its own center of mass. The verification of the existence of such rigid body modes or eigenfunctions is given next.

Analytically, when $\alpha_k = 0$ is a solution to (B.20), an eigenfunction verifying (B.30) must exists.

$$d^4\psi(y)/dy^4 = 0 \tag{B.30}$$

The general solution to (B.30) is given by (B.31)

$$\psi(y) = C_0 + C_1 y + C_2 y^2 + C_3 y^3 \tag{B.31}$$

A condition for the beam to move as a rigid body implies that the flexural deformation is zero everywhere. This implies that,

$$d^2\psi(y)/dy^2 = 0 \qquad \text{And} \qquad d^3\psi(y)/dy^3 = 0 \tag{B.32), (B.33}$$

Reducing the possible solution to (B.34),

$$\psi(y) = C_0 + C_1 y \tag{B.34}$$

The contribution of C_0 to the displacement field is constant, corresponding to a displacement in the transverse direction. In contrast, C_1 is associated to a displacement that increases linearly with y. Such a displacement is characteristic of a rotation about $y = 0$. Because C_0 and C_1 may be selected arbitrarily, we accordingly define the eigenfunctions describing the rigid body modes of the headless gantry as (B.35) for translation, and (B.36) for rotation.

$$\psi_{tr}(y) = 1 \tag{B.35}$$

$$\psi_{rot}(y) = \frac{L}{2} - y \tag{B.36}$$

Eigenfunctions (B.35) and (B.36) are valid for cases a and b, however, for case b, as we consider the beam as being much stiffer than the torsion spring, i.e. $EI >> k_1$, we are obtaining

a zero Eigenvalue ($\alpha = 0$, and thus $\omega = 0$) from the characteristic equation (B.20). This is indeed not true, since the hypothesis of the rigid beam requires a different approach. We know that the eigenfrequency corresponding to the rotation of a beam with a torsion spring on one end is defined by (B.37).

$$\omega_{\text{rot}} = \sqrt{k_1 / J} \tag{B.37}$$

2. $\mathbf{0 < \beta_1 < 1}$ **and** $\boldsymbol{\beta_2 = 0}$.

There is a unique rigid body mode in translation. The rotation of the beam is now a flexible mode, it is calculated using (B.28) with the corresponding eigenvalue α_k, see **Figure B – 3**. However, if $\beta_1 << 1$ (because $EI >> k_1$), However, the eigenfunction defining the rotation of the beam can be approximated using (B.36) and (B.37).

3. $\mathbf{\beta_1 \geq 1}$ **and** $\boldsymbol{\beta_2 = 0}$.

Translation rigid body mode only, the beam behaves as a sliding–free beam.

B.2.2.5. Orthogonality of the Eigenfunctions of the headless gantry

One of the interesting properties of the eigenfunctions of self–adjoint systems in that they are orthogonal, thus, the response can be expressed using the *expansion theorem*.

In general, a physical system governed by a differential operator L on a spatial coordinate frame is self–adjoint if the system satisfies the law of conservation of energy. In other words, if the governing equations are derived from a Lagrangian function representing the total energy of the system, then, the differential operator L is self–adjoint (Hayek, 2001).

Mathematically, a system is said to be self–adjoint if identities (B.38) and (B.39) are valid (Han, et al., 1999) (Hayek, 2001),

$$\int_0^L \left[\psi_m L(\psi_n) - \psi_n L(\psi_m)\right] dy = 0 \tag{B.38}$$

$$\int_0^L \left[\psi_m M(\psi_n) - \psi_n M(\psi_m)\right] dy = 0 \tag{B.39}$$

In the case of the headless gantry, the operator L is the fourth–order differential operator of the spatial equation (B.40). M is a rigid operator. $\psi_n(y)$ and $\psi_m(y)$ are the eigensolutions (B.28), (B.35) and (B.36).

$$\frac{d^4\psi_m(y)}{dy^4} - \frac{\alpha_m{}^4}{L^4}\psi_m(y) = 0 \;\therefore\; \alpha_m{}^4 = \frac{\mu L^4}{EI}\omega_m{}^2 \tag{B.40}$$

By using operators L and M, (B.40) can be rewritten as follows

$$L(\psi_m) = \omega_m{}^2 M(\psi_m) \;\therefore\; L(\psi_m) = \frac{d^4\psi_m(y)}{dy^4},\; M(\psi_m) = \frac{\mu}{EI}\psi_m(y) \tag{B.41}$$

As we can see, (B.39) is automatically verified since M is a rigid operator. (B.38) is also verified with a little development. Numerically, we have also have verified that the eigenfunctions are indeed orthogonal. Also, as it was commented previously, the system equations were derived using an energetic approach and the order of the differential operator L is an even integer, so, this is more a formality rather than verification.

As a comment, if the order of the operator L is an odd integer, the system is not self–adjoint and therefore unsolvable using modal analysis. This is the reason why the non–conservative terms, such as the damping, are usually neglected. They are more easily included (approximately) once the system has been decomposed using modal analysis. See (Hayek, 2001) and (Meirovitch, 2001).

Appendix C: The Ritz method

C.1 Time–dependent boundary conditions

Several methods considering time–dependent boundary conditions on distributed parameter systems are presented on the literature. Namely, Mindlin–Goodman's decomposition (Ginsberg, 2001) (Chandra, 1979), William's (Walter, 1971) (Chandra, 1979), boundary operator (Fisher, et al., 1979) and quasi–comparison functions (Meirovitch, et al., 1994) methods. All of these methods concentrate in finding a set of eigenfunctions satisfying all the boundary conditions of non–self adjoint systems.

The approach we use is derived from the Mindlin–Goodman method. **It is focused on including the time–dependent boundary conditions into the model instead of trying to find a suitable eigenfunction.** First, the displacement field u is divided in two parts (C.1). u_{bc} accounts for the time–dependent boundary conditions. u_{Ritz} is a Ritz series accounting for any know excitations and compensation for artifices introduced by the fact that u_{bc} does not satisfy the equation of motion (B.1).

$$u(y,t) = u_{bc}(y,t) + u_{Ritz}(y,t) \;\; \therefore \;\; u_{Ritz}(y,t) = \sum_{j=1}^{N} \psi_j(y) q_j(t) \tag{C.1}$$

By definition, u_{Ritz}, satisfy the homogeneous boundary conditions associated with immobile supports. This means that the base functions $\psi_j(y)$ are the same as the set of admissible functions used if the boundary conditions did not depend on time.

In flexure, a time–dependent boundary condition may be (C.2)

$$u(y,t) = f(t) \quad \text{or} \quad u_{,y}(y,t) = f(t) \tag{C.2}$$

By definition u_{Ritz} is zero when substituted into (C.2). This way, (C.1) will satisfy (C.2) it u_{bc} satisfies it. We observe that all other boundary conditions will be satisfied by u_{Ritz}. Hence, u_{bc} must evaluate to zero when substituted into any time–invariant boundary condition.

Now, let's denote J as the total number of geometric boundary conditions. Let the operator $B_n = 1$ or $\partial/\partial y$ as appropriated to a geometric boundary conditions n evaluated at $y = y_n$. We therefore must find a function $u_{bc}(y, t)$ that satisfies (C.3)

$$\mathscr{B}_n\left[u_{bc}(y_n,t)\right] = f(t)\delta_{nj} \;\; \therefore \;\; n = 1,\ldots,J \tag{C.3}$$

Any function u_{bc} satisfying (C.3) would be acceptable. We shall use an approach that resembles the Ritz series. We select a set of J independent functions $g_j(y)$ which are used to represent u_{bc} as in (C.4)

$$u_{bc}(y,t) = \sum_{j=1}^{J} g_j(y)\alpha_j(t) \;\; \therefore \;\; J = \#\text{ of time dependent BCs} \tag{C.4}$$

Usually, the $g_j(y)$ functions are usually selected from power series or harmonic functions. The $\alpha_j(t)$ are determined by satisfying the geometric boundary conditions. When (C.4) is replaced in (C.3), the dependence on y is replaced by an evaluation of $g_j(y)$ at the boundary. Thereby J algebraic equations for the $\alpha_j(t)$ coefficients are obtained, see (C.5)

$$\sum_{j=1}^{J} \mathscr{B}_n\left[g_j(y_n)\right]\alpha_j(t) = f(t)\delta_{nj} \;\; \therefore \;\; n = 1,\ldots,J \tag{C.5}$$

In order for (C.5) to be solvable, the terms $B_n(g_j)$ evaluated at y_n cannot all vanish. This condition will be met if the g_j functions are not admissible for the case where the supports are stationary.

C.1.1 Evaluation of the time–dependent boundary conditions of the gantry

For the gantry, there are two time–dependent geometric boundary conditions. They are defined by (C.6). Therefore, $J = 2$. As they are boundary conditions in displacement, the operators B_1 and B_2 are equal to one.

$$u(y_1,t)=X_1(t); \quad u(y_2,t)=X_2(t) \tag{C.6}$$

We replace (C.6) in (C.5) and we evaluate

$$\begin{aligned}
&\sum_{j=1}^{J}\mathscr{B}_1\left[g_j(y_1)\right]\alpha_j(t)=X_1(t) \;\therefore\; n=1; \quad \mathscr{B}_1\left[g_j(y_1)\right]=g_j(y_1)\\
&g_1(y_1)\alpha_1(t)+g_2(y_1)\alpha_2(t)=X_1(t) \;\therefore\; g_1(y)=1;\; g_2(y)=(L/2)-y\\
&\alpha_1(t)+\alpha_2(t)\frac{y_1}{L}=X_1(t)\\
&\sum_{j=1}^{J}\mathscr{B}_2\left[g_j(y_2)\right]\alpha_j(t)=X_2(t) \;\therefore\; n=2; \quad \mathscr{B}_2\left[g_j(y_2)\right]=g_j(y_2)\\
&g_1(y_2)\alpha_1(t)+g_2(y_2)\alpha_2(t)=X_2(t)\\
&\alpha_1(t)+\alpha_2(t)\frac{y_2}{L}=X_2(t)
\end{aligned} \tag{C.7}$$

Finally, we obtain $\alpha_1(t)$ and $\alpha_2(t)$ from (C.7), by evaluating $y_1 = L/6$ and $y_2 = 5L/6$.

$$\begin{bmatrix}1 & y_1/L\\ 1 & y_2/L\end{bmatrix}\begin{bmatrix}\alpha_1(t)\\ \alpha_2(t)\end{bmatrix}=\begin{bmatrix}X_1(t)\\ X_2(t)\end{bmatrix} \Rightarrow \alpha_1(t)=\frac{X_1(t)+X_2(t)}{2}=X(t);\; \alpha_2(t)=\frac{3}{2}\frac{X_1(t)-X_2(t)}{L}=\Theta(t) \tag{C.8}$$

We can note that we actually have obtained the generalized coordinates X and Θ describing the rigid motion of the headless gantry from the time–dependent BCs.

C.2 The Ritz method for a beam in flexure

The energy expressions of the flexible beam are defined in (C.9) for kinetic energy and (C.10) for elastic potential energy.

$$T_b=\int_0^L\left(\frac{1}{2}\mu u_{,t}^2\right)dy; \quad V_b=\int_0^L\left(\frac{1}{2}EI\,u_{,yy}^2\right)dy \tag{C.9), (C.10}$$

Now, let's suppose that there are other elements attached to the beam, see Figure B – 1.

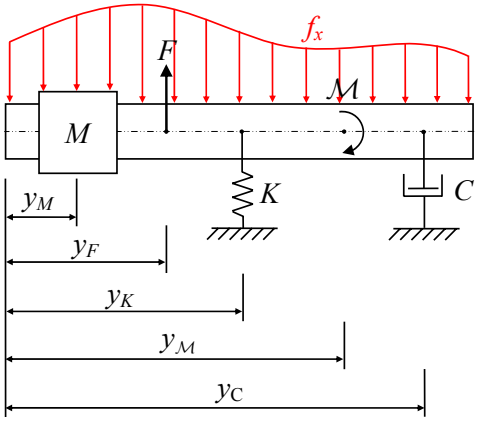

Figure B – 1 : *a flexible beam with different intermediate loads*

The acting power on the beam in Figure B – 1 is given by

$$P_{in}=\int_0^L f_x u_{,t}(y,t)dy+\sum F u_{,t}(y_F,t)+\sum \mathcal{M} u_{,yt}(y_{\mathcal{M}},t) \tag{C.11}$$

Attached masses, springs, dashpots also exert transverse forces and couples on the beam. We describe their effects in terms of kinetic (T) and potential energy (V) and dissipated power (P_{dis}). The total kinetic energy is given by (C.12). The total potential energy is given by (C.13), where κ is a rotary spring located at y_κ.

$$T=\frac{1}{2}\int_0^L\left[\mu u_{,t}^2(y,t)\right]dy+\frac{1}{2}\sum M u_{,t}^2(y_M,t) \tag{C.12}$$

$$V=\frac{1}{2}\int_0^L\left[EI\,u_{,yy}^2(y,t)\right]dy+\frac{1}{2}\sum K u^2(y_K,t)+\frac{1}{2}\sum\kappa u_{,y}^2(y_\kappa,t) \tag{C.13}$$

In flexure, the transverse motion of the bar can generate air resistance. A simple model is to consider it to be proportional to the transverse velocity with factor of proportionality c_v. In addition, visco–elastic effects are presented by a term like the strain energy of the bar, with $u_{,yy}$ replaced by $u_{,yyt}$. Adding these effects to the power dissipated by extensional and torsional dashpots, C and χ we can calculate the dissipated power, as in (C.14)

$$P_{\text{dis}}=\int_0^L\left[\gamma EI\,u_{,yyt}^2(y,t)+c_v u_{,t}^2(y,t)\right]dy+\sum C u^2(y_C,t)+\sum\chi u_{,yt}^2(y_\chi,t) \tag{C.14}$$

We say that the solution $u(y,\,t)$ has the form of a series (C.15)

$$u_{Ritz}(y,t)=\sum_{j=1}^{N}\psi_j(y)q_j(t) \tag{C.15}$$

The power balance method requires expressions for the mechanical energies and power in terms of the generalized coordinates. We obtain these by substituting the Ritz series (C.15) into the expressions for T, V, P_{in} and P_{dis}. The expressions featuring squares of displacement; In order to account for all combinations when the series expansion is substituted into these products, different indices j and n are used to form each term. For the kinetic energy (C.12), it gives

$$T=\frac{1}{2}\int_0^L\mu\left[\sum_{\text{j}=1}^{N}\psi_{\text{j}}(y)\dot{q}_{\text{j}}(t)\right]\left[\sum_{n=1}^{N}\psi_n(y)\dot{q}_n(t)\right]dy+\frac{1}{2}\sum M\left[\sum_{\text{j}=1}^{N}\psi_{\text{j}}(y_M)\dot{q}_{\text{j}}(t)\right]\left[\sum_{n=1}^{N}\psi_n(y_M)\dot{q}_n(t)\right] \tag{C.16}$$

We simplify this expression by extracting the $\dot{q}_{\text{j}}(t)$ and $\dot{q}_n(t)$ terms and bringing the summations of j and n outside the products.

$$T=\frac{1}{2}\sum_{\text{j}=1}^{N}\sum_{n=1}^{N}M_{jn}\dot{q}_j(t)\dot{q}_n(t)\ \therefore\ M_{nj}=M_{jn}=\int_0^L\mu\psi_{\text{j}}(y)\psi_n(y)dy+\sum M\psi_{\text{j}}(y_M)\psi_n(y_M) \tag{C.17}$$

Similarly, we can describe the potential energy V as in (C.18)

$$\begin{aligned}V&=\frac{1}{2}\sum_{\text{j}=1}^{N}\sum_{n=1}^{N}K_{jn}q_j(t)q_n(t)\\ \therefore\ K_{nj=jn}&=\int_0^L EI\frac{d^2\psi_{\text{j}}(y)}{dy^2}\frac{d^2\psi_n(y)}{dy^2}dy+\sum K\psi_{\text{j}}(y_K)\psi_n(y_K)+\sum\kappa\frac{d\psi_{\text{j}}(y_\kappa)}{dy}\frac{d\psi_n(y_\kappa)}{dy}\end{aligned} \tag{C.18}$$

The dissipated power P_{dis} and the input power P_{in} are defined by (C.19) and (C.20) respectively

$$\begin{aligned}P_{dis}&=\frac{1}{2}\sum_{\text{j}=1}^{N}\sum_{n=1}^{N}C_{jn}\dot{q}_j(t)\dot{q}_n(t)\ \therefore\\ C_{nj=jn}&=\int_0^L\left[EI\frac{d^2\psi_{\text{j}}(y)}{dy^2}\frac{d^2\psi_n(y)}{dy^2}+c_v\psi_{\text{j}}(y)\psi_n(y)\right]dy+\sum C\psi_{\text{j}}(y_C)\psi_n(y_C)+\sum\chi\frac{d\psi_{\text{j}}(y_\chi)}{dy}\frac{d\psi_n(y_\chi)}{dy}\end{aligned} \tag{C.19}$$

$$P_{in}=\frac{1}{2}\sum_{\text{j}=1}^{N}Q_j\dot{q}_j(t)\ \therefore\ Q_j=\int_0^L f_x\psi_{\text{j}}(y)dy+\sum F\psi_{\text{j}}(y_F)+\sum\mathcal{M}\frac{d\psi_{\text{j}}(y_{\mathcal{M}})}{dy} \tag{C.20}$$

For expressions (C.17) to (C.20), ψ_j and ψ_n are the basis functions (or eigenfunctions) yet to be defined, however, they must always respect the boundary conditions.

Once we have calculated ψ_j and ψ_n, we are able to evaluate the coefficients M_{jn}, K_{jn}, C_{jn}, and Q_j. Then, the motion equations of the system can be written in form of the matrix equation (C.21)

$$[M]\{\ddot{q}\}+[C]\{\dot{q}\}+[K]\{q\}=\{Q\} \tag{C.21}$$

So far, we have specified u_{bc}, now we must find the associated basis functions coefficients appearing in u_{Ritz}. A time dependent system is one in which the position depends explicitly on time, as well as the current values of the generalized coordinates. This is the situation described by (C.1) . The standard power balance equations of motion (C.21) apply only for time invariant systems. Consequently, we have to reformulate the equations of motion by turning to the Lagrange–Euler formalism (C.22)

$$\frac{d}{dt}\left(\frac{\partial L}{\partial \dot{q}_j}\right)-\frac{\partial L}{\partial q_j}+\frac{\partial D}{\partial \dot{q}_j}=Q_j \;\;\therefore\;\; j=1,..,N;\;\; D=\frac{1}{2}P_{dis} \tag{C.22}$$

The first quantities we shall evaluate are the generalized forces, in order to understand how we excite the modes. This requires consideration of the virtual work. Taking the time derivative of (C.1), the velocity field gives (C.23)

$$\dot{u}(y,t)=\dot{u}_{bc}(y,t)+\sum_{j=1}^{N}\psi_j(y)\dot{q}_j(t) \tag{C.23}$$

The virtual work δW is defined in (C.24), F is the applied force and δu is a virtual displacement of (C.1) and its defined in (C.25).

$$\delta W = F\cdot\delta u \tag{C.24}$$

$$\begin{aligned}\delta u(\psi_j,q_j)&=\delta_{\psi_j}u+\delta_{q_j}u\\&=\frac{\partial u}{\partial \psi_j}\delta\psi_j+\frac{\partial u}{\partial q_j}\delta q_j\\&=\cancel{q_j\delta\psi_j}+\psi_j\delta q_j \;\;\because\;\; \delta\psi_j=0\end{aligned} \tag{C.25}$$

In (C.25), $\delta\psi_j$ does not vary at a fixed y. δq_j on the other hand may be arbitrary for a fixed t, See (Reddy, 2002) for further information. u_{bc} is not considered because it is function of independent variables. As a result, the virtual displacement at any y is given by

$$\delta u=\sum_{j=1}^{N}\psi_j(y)\delta q_j(t) \tag{C.26}$$

Note that the coefficients $\dot{q}_j(t)$ in (C.23) match the corresponding coefficients of δq_j in (C.26). So that, δu and $\dot{u}$ have similar forms when $u_{bc} = 0$. However, $u_{bc} = 0$ corresponds to the time independent situation considered in (C.21). It follows then that the generalized forces for the system with time dependent BCs are the same as those for a system whose constraints are invariant in time.

So, as a conclusion, to form the motion equations of the system taking into account the time dependent BCs, we only have to replace (C.1) into the expressions of input power (C.11), kinetic energy (C.12), potential energy(C.13) and dissipated power (C.14).

Références Bibliographiques

Agbli K.S. Multiphysics simulation of a PEM electroliser: Energetic Macroscopic Representation approach [Revue] // International Journal of Hydrogen Energy. - 2011. - 2 : Vol. 36. - pp. 1382-1398.

Barre P.J. Inversion-based control of electromechanical systems using causal graphical descriptions [Conférence] // IEEE-IECON'06 - 32nd Annual Conference on Industrial Electronics. - 2006. - pp. 5276-5281.

Barre P.J. Commande et entraînement des machines-outils à dynamique élevée: Formalismes et Applications // Habilitation à Diriger des Recherches. - Lille : [s.n.], 2004.

Béarée Richard Prise en compte des phénomenènes vibratoires dans la génération de la commande des machines-outils à dynamique élevée // Thèse. - Lille : [s.n.], 2005.

Biagiotti Luigi and Melchiorri Claudio Trajectory Planning for Automatic Machines and Robots [Livre]. - [s.l.] : Springer, 2008. - ISBN 978-3-540-85628-3.

Borne P. Modélisation et identification des processus [Livre]. - Paris : Editions Technip, 1992.

Bouscayrol A. Weighted control of traction drives with parallel-connected AC machines [Revue] // IEEE Transactions on Industrial Electronics. - 2006. - 6 : Vol. 53. - pp. 1799-1806.

Bouscayrol A. Formalismes de représentation et de commande appliqués aux systèmes électromécaniques multi-machines multi-convertisseurs // Habilitation à Diriger des Recherches. - Lille : [s.n.], 2003.

Chandra S. Some comments on the Mindlin-Goodman method of solving vibration problems with time-dependent boundary conditions [Revue] // Journal of sound and Vibration. - 1979. - 2 : Vol. 67. - pp. 275-277.

Chang Y.F., Nguyen T.G. et Wang C.P. Design and Implementation of look-ahead linear jerk filter for a computerized numerical controller machine [Revue] // Control Engineering Practice. - 2010. - Vol. 18. - pp. 1399-1405.

Chu B. Optimal cross-coupled synchronizing control of dual-drive gantry system for a SMD assembly machine [Revue] // JSME International Journal. - 2004. - 3 : Vol. 47. - pp. 939-945.

Colas Frédéric Synthèse et réglage de lois de commande adaptées aux axes souples en translation: application aux robots cartesiens 3 axes // Thèse. - 2006.

Corsi Nicolas, Coleman Ralph and Piaget Denis Status and New Development of Linear Drives and Subsystems [Conference] // LDIA (Linear Drives for Industrial Applications). - Lille : [s.n.], 2007.

Ding H. and Xiong Z.H. Motion stages for electronics packaging design and control [Revue] // IEEE Robot Automation Magazine. - 2006. - 4 : Vol. 13. - pp. 51-61.

Fisher H.D., Cepkauskas M.M. et Chandra S. Solution of time dependent boundary value problems by the boundary operator method [Revue] // International Journal of Solids and Structures. - 1979. - Vol. 15. - pp. 607-614.

Frýba Ladislav Vibration of solids and structures under moving loads [Livre]. - [s.l.] : Thomas Telford, 1999. - 3e édition. - ISBN 0-7277-2741-9.

Fu K.S. Robotics [Livre]. - [s.l.] : McGraw-Hill International Editions, 1987. - ISBN 0-07-022625-3.

Fung Y.C. Classical and Computational Solid Mechanics [Livre]. - [s.l.] : World Scientific, 2001. - ISBN 981-02-3912-2.

Gawronski W. Dynamics and Control of Structures: A Modal Approach [Livre]. - [s.l.] : Springer, 2004. - ISBN 0-387-98527-1.

Ginsberg J. Mechanical and Structural Vibrations [Livre]. - [s.l.] : Wiley, 2001. - ISBN 0-471-12808-2.

Gomand Julien Analyse de systèmes multi-actionneurs parallèles par un approche graphique causale. - Lille : [s.n.], 2008. - PhD. Thesis memory.

Gomand Julien, Kestelyn Xavier et Barre Pierre-Jean Système de regulation d'un portique à double moyen d'entraînement [Brevet]. - France, 13 11 2009.

Guibert N., Paris H. et Rech J. A numerical simulator to predict the dynamical behavior of the self-vibratory drilling head [Revue] // International Journal of Machine Tools & Manufacture. - 2008. - Vol. 48. - pp. 644-655.

Hagedorn Peter et Dasgupta Anirvan Vibrations and Waves in continous mechanical systems [Livre]. - [s.l.] : Wiley, 2007. - ISBN 978-0470-051738-3.

Han Seon M., Benayora Haym et Wei Timothy Dynamics of transversely vibrating beams using four engineering theories [Revue] // Journal of sound and vibration. - [s.l.] : Academic press, 1999. - pp. 935-988.

Harris Cyril M. et Piersol Allan G. Harris' shock and vibration handbook [Livre]. - [s.l.] : McGraw-Hill, 2002. - 5th. - ISBN 0-07-137081-1.

Harrison et Nettleton Advanced Engineering Dynamics [Livre]. - 1997.

Hautier J.P. et Faucher J. Le graphe informationnel causal [Revue] // Bulletin de l'Union des Physiciens. - 1996. - Vol. 90. - pp. 167-189.

Hayek S.I. Advanced mathematical methods in science and engineering [Livre]. - [s.l.] : Marcel Dekker Inc., 2001. - ISBN 0-8247-0466-5.

Hayes Monson H. Statistical digital signal processing and modelling [Livre]. - [s.l.] : John Wiley & Sons, Inc., 1996. - ISBN 0-471-59463-8.

Kelly Rafael, Santibañez Victor et Loria Antonio Control of Robot Manipulators in Joint Space [Livre]. - [s.l.] : Springer, 2005. - ISBN-10 1852339942.

Kestelyn Xavier Modélisation vectorielle multi-machines pour la commande des ensembles convertisseurs-machines polyphasés // Thèse. - 2003.

Kim Sungsoo Synchronizing Dual-Drive Gantry of Chip Mounter with LQR Approach [Revue] // Proceeding of the 2003 IEEE/ASME International conference on Advance Intelligence Mechatronics / éd. IEEE. - 2003. - 0-7803-7759-1. - pp. 838-843.

Kung Y.S. Design and implementation of a high-performance PMLSM drive using DSP chip [Revue] // IEEE Transactions on Industrial Electronics. - 2008. - 3 : Vol. 55. - pp. 1341-1351.

Kwan Yimbun Patrick Positioning apparatus and lithograghic apparatus comprising the same [Brevet] : EP 1107067. - Deuschland, France, Great Britain, Italy, the Netherlands, 12 27, 2006.

Lampaert Vincent, Swevers Jan et Al-Bender Farid Comparison of model and non-model based friction compensation techniques in the neighbourdhood of pre-sliding friction [Conférence] // Proceedings of the 2004 American Control Conference. - Boston, Massachusetts : [s.n.], 2004. - pp. 1121-1126.

Lin Faa-Jeng DSP-Based Cross-Coupled Synchronous Control for Dual Linear Motors via Intelligent [Revue] // IEEE Transactions on Industrial Electronics. - 2011. - Early access paper.

Ljung Lennart System Identification: Theory for the User [Livre]. - [s.l.] : Prentice Hall, 1987. - ISBN 0-13-881640-9.

Meirovitch Leonard Dynamics and Control of Structures [Livre]. - [s.l.] : John Wiley & Sons, Inc., 1990. - ISBN 0-471-62858-1.

Meirovitch Leonard et Hagedorn Peter A new-approach to the modeling of distributed non-self-adjoint systems [Revue] // Journal of Sound and Vibration. - 1994. - 2 : Vol. 178. - pp. 227-241.

Meirovitch Leonard Fundamentals of vibrations [Livre] / éd. Education McGraw-Hill Higher. - 2001. - ISBN 0-470-01051-7.

Olabi A. Feedrate planning for machining with industrial six-axis robots [Revue] // Control Engineering Practice. - 2010. - 5 : Vol. 18. - pp. 471-482.

Parent Thomas Conception d'un Bras de Robot en Matériau Composite [Rapport] : Rapport Projet Fin d'Etudes / Arts et Métiers ParisTech. - 2009.

Park Heung-Keun Dynamics of Dual-Drive Servo Mechanism [Conference] // ISIE 2001. - Pusan : [s.n.], 2001. - pp. 1996 - 2000.

Park S. Motion analysis of a moving elastic beam with a moving mass [Conference] // Proceedings of the 1999 IEEE/ASME International Conference on Advanced Intelligent Mechatronics. - Atlanta : [s.n.], 1999.

Paynter H. Analysis and design of engineering systems [Livre]. - [s.l.] : MIT Press, 1961.

Polyanin Andrei Handbook of Linear PDEs for Engineers and scientists [Livre] / ed. Hall/CRC Chapman &. - 2002. - 1st.. - ISBN 1-58488-299-9.

Porter Brian and Crossley Roger Modal Control: Theory and Applications [Livre]. - [s.l.] : Taylor & Francis Ltd., 1972. - ISBN 0-85066-057-2.

Preumont A. Vibration Control of Active Structures [Livre]. - Brussels, Belgium : Springer-Verlag, 2011. - ISBN 978-94-007-2032-9.

Rao Anil Vithala Dynamics of Particles and Rigid Bodies: A systematic Approach [Livre]. - [s.l.] : Cambridge University Press, 2006. - ISBN 0-521-85811-9.

Reddy Junuthula Narashima Energy Principles and Variational Methods in Applied Mechanics [Livre]. - [s.l.] : John Wiley & Sons, Inc, 2002. - ISBN 0-471-17985-X.

Remy Ghislain Commande optimisée d'un actionneur lineaire synchrone pour un axe de positionnement rapide // Thèse. - 2007.

Rieber Jochen M. and Taylor David G. Gain-Scheduled L2-Gain Based Control of a Flexible Parameter-Varying Robot Link [Conference] // IECON'01: The 27th Annual Conference of the IEEE Industrial Electronics Society. - 2001. - pp. 552-557.

Schwarz B.J. and Richardson M.H. Experimental Modal Analysis [Conference] // CSI reliability week. - Orlando, FL : [s.n.], 1999.

Singhose William Earl Command Generation for Flexible Systems [Livre]. - 1997. - PhD. Thesis.

Smith James, Rajaraman Devarajan and Ambaji Patil Sachchit Damping stabilization for linear motor stage [Brevet]. - United States, 05 05, 2009.

Stöppler Guido and Douglas Steve Adaptronic gantry machine tool with piezo-electric actuator for active error compensation of structural oscillations at the tool centre point [Revue] // Mechatronics. - [s.l.] : Elsevier, 2008. - 18. - pp. 426-433.

Tan K.K. Coordinated motion control of moving gantry stages for precision applications based on an observer-augmented composite controller [Revue] // IEEE Transactions on Control Systems Technology. - November 2004. - 6 : Vol. 12. - pp. 984-991.

Tanquary Mark, Singer Neil and Rappole Whitney Method and apparatus for the control of gantry machines [Brevet] : 6,163,116. - United States, December 19, 2000.

Teo C.S. Dynamic modeling and adaptative control of a H-type gantry stage [Revue] // Mechatronics. - 2007. - 7 : Vol. 17. - pp. 361-367.

Timoshenko Stephen Strength of Materials [Livre]. - [s.l.] : D. Van Nostrand Company, 1940. - 2 : Vol. 1 : 2.

Verhoeven S.L.H. Robust Control of Flexible Systems [Report] : Bibliographic Research. - Eindhoven, The Netherlands : [s.n.], 2009.

Walter W.W. The forced motion of a non-conservatively loaded elastic system [Revue] // Journal of Sound and Vibration. - 1971. - 3 : Vol. 18. - pp. 297-310.

Wang C.M., Reddy J.N. and Lee K.H. Shear Deformable Beams and Plates: Relationships with Classical Solutions [Livre]. - [s.l.] : Elsevier Science, 2000. - ISBN 0-08-043784-2.

Wang Limei and Tang Yaping Fuzzy Cross-coupling Control for Dual Linear Motors based on Preview Feedforward Compensation [Conference] // Proceedings of the 2009 IEEE International Conference on Mechatronics and Automation. - Changchun, China : [s.n.], 2009.

Whittaker Edmund Taylor and McCrea William A treatise on the Analytical Dynamics of Particles and Rigid Bodies [Livre]. - [s.l.] : Cambrigde University Press, 1988. - ISBN 0521358833.

Ximei Zhao and Quingding Guo Synchronous Control of Gantry Moving Type Boring-Milling Machining Centers Based-on Disturbance Observer [Conference] // Electrical Machines and Systems, 2005. ICEMS 2005. Proceedings of the Eighth International Conference on . - Nanjing : [s.n.], 2006. - Vol. 2. - pp. 1573-1575.

Yang J.X., Tsai M.C. and Hsieh M.F. Identification and Control of a Linear Sevo System [Conference] // Proc. 4th International Symposium on Linear Drives for Industry Applications, LDIA 2003. - 2003.

Yoshikawa T. Trajectory control of cartesian type industrial manipulators with flexible joints [Conference] // IEEE/RSJ International Conference on Intelligent Robots and Systems. - 1993.

Yousefi H. Application of neural network in suppressing mechanical vibration of a permanent magnet linear motor [Revue] // Control Engineering Practice. - 2008. - 7 : Vol. 16. - pp. 787-797.

Yu D., Guo Q. and Lili Q.H. "Position synchronized control of dual linear motors servo system using fuzzy logic [Conference] // IEEE Proc. of the 36th World Congress on Intelligent Control and Automation. - 2006. - pp. 8041-8044.

Yu D., Guo Q. et Hu Q. Study on Synchronous Drive Technique of Biaxial Linear Servo Motor Based on Decoupling Control and Internal Model Control with two Degree of Freedom [Conférence] // Sixth International Conference on Electrical Machines and Systems, 2003, ICEMS 2003 Proceedings. - 2003.

Zhao S. et Tan K.K. Adaptative feedforward compensation of force ripples in linear motors [Revue] // Control Engineering Practice. - 2004. - 4 : Vol. 13. - pp. 1081-1092.

MÉTHODE DE MODÉLISATION ET DE COMMANDE DES SYSTÈMES DE POSITIONNEMENT MULTI–ACTIONNÉS DE TYPE « AXE EN GANTRY »

RESUME : Un manipulateur cartésien dit « axe en gantry » peut être utilisé pour des applications requérant une dynamique élevée et une grande précision. Le type d'axe en gantry étudié dans ce mémoire consiste en un axe transversal porté par deux actionneurs linéaires balayant la direction longitudinale de l'espace de travail. Un troisième actionneur, monté sur le bras transversal, permet de déplacer la charge le long de la direction transversale de l'espace de travail. La problématique de ces systèmes réside dans la dégradation des performances de positionnement due au couplage mécanique existant entre les actionneurs et aux vibrations du bras transversal. La solution industrielle, consistant à minimiser les vibrations en rigidifiant (et en alourdissant) le bras transversal et à contrôler indépendamment les axes parallèles, mène à une consommation d'énergie importante qui ne sera plus acceptable à long terme. Un état de l'art sur la commande des axes en gantry met en évidence un manque d'analyse des phénomènes physiques responsables des couplages mécaniques et des vibrations du bras transversal. Ceux–ci sont en effet considérés comme des perturbations compensées par des méthodes mathématiques dérivées de l'automatique avancée. L'approche proposée dans ce mémoire se veut une alternative à ces méthodes. Elle est basée sur une modélisation physique détaillée de l'axe en gantry comprenant la flexibilité du bras transversal. Cette modélisation, associée à des méthodes d'identification expérimentale et de représentation causale, est exploitée afin de déduire des structures de commande et des méthodes de réglage adaptées. Des résultats expérimentaux montrent que cette méthodologie mène à une amélioration des performances de positionnement des axes en gantry par rapport à la commande industrielle et permet par exemple d'envisager l'allégement du bras transversal.

Mots clés : Modélisation dynamique, Commande par inversion, Identification expérimentale, asservissement de position, contrôle des vibrations, commande modale

METHOD OF MODELING AND CONTROLLING MULTI–ACTUATED POSITIONING SYSTEMS OF TYPE "DUAL–DRIVE GANTRY STAGES"

ABSTRACT : Gantry stages are used for high–speed high–precision motion control applications such as wafer and flat panel display manufacturing and inspection. A gantry stage is a type of Cartesian manipulator that is composed of three linear actuators on its basic configuration. Two actuators move in tandem a cross–arm along the longitudinal direction of the work–space. The third actuator, mounted on the cross–arm, carries the payload along the transverse direction of the workspace. The positioning performance of the gantry stage is principally degraded by the mechanical coupling between actuators and by the vibrations of the cross–arm along the longitudinal direction. To solve the vibration problem, the current solution is to make the cross–arm very rigid. The drawback of this solution is that rigidity is generally synonym of heaviness, which leads to the use of more powerful actuators and higher energy consumption. To solve the coupling problem, the current industrial solution is independent axis control. That is, the coupling between actuators is ignored, leading to a degraded position performance. State of the art solutions put in evidence a general lack of interest in considering the physical causes of the coupling and vibration problems into the controller design, leading to complex control architectures derived from advanced control techniques. The approach presented in this PhD. Thesis is meant to be an alternative to such techniques by proposing a methodology that is based on a detailed physical modeling of gantry stages (flexibility of the cross–arm included). This physical modeling, associated to experimental identification methods, is exploited to obtain adapted control structures and tuning methods allowing to enhance the system's performance by improving the management of its degrees of freedom. Experimental results show that the proposed methodology leads to an improved motion control of the point–tool, even for very flexible systems.

Keywords : Model–based control, Modal Control, Physical modeling, Distributed parameter systems, Motion control, path–planning, Vibration control, System identification.

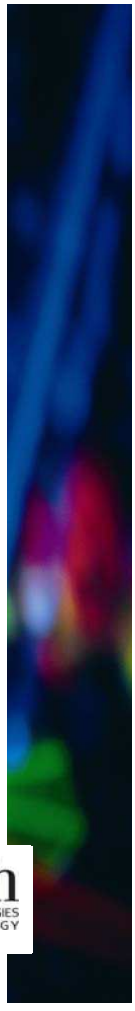

ARTS ET MÉTIERS ParisTech

ParisTech INSTITUT DES SCIENCES ET TECHNOLOGIES PARIS INSTITUTE OF TECHNOLOGY